Theoretical Analyses of Wedge Cutting Through Metal Plates

by

Zi-Ming Zheng, P.E.

Submitted to the Department of Civil and Environmental Engineering in partial fulfillment of the requirements for the degree of

Doctor of Philosophy

at the

MASSACHUSETTS INSTITUTE OF TECHNOLOGY

September 30, 1994

Author .....
Department of Civil and Environmental Engineering
October 15, 1994

Certified by .....
Prof. Tomasz Wierzbicki (Thesis Supervisor)
Department of Ocean Engineering

Certified by .....
Prof. Jerome Connor (Chairman of Thesis Committee)
Department of Civil and Environmental Engineering

Certified by .....
Prof. Eduardo A. Kausel (Thesis Committee Member)
Department of Civil and Environmental Engineering

Accepted by .....
Prof. Joseph M. Sussman
Chairman, Departmental Committee on Graduate Studies
Department of Civil and Environmental Engineering

Theoretical Analyses of Wedge Cutting Through Metal Plates

by

Zi-Ming Zheng, P.E.

Submitted to the Department of Civil and Environmental Engineering on September 30, 1994, in partial fulfillment of the requirements for the degree of Doctor of Philosophy

Abstract

The process of wedge "clean" cutting through metal plates is analyzed in this dissertation by studying the experimental results and developing simple and realistic mathematical models of the problem. Two stages of wedge indentation process are considered: transient and steady-state cutting processes.

For the transient indentation process, two characteristic deformation zones are identified: (i) plastic zone at a wedge tip, and (ii) transient flap bending. For the steady-state cutting process, an additional deformation zone to that of the transient stage is identified: (iii) flap first stretching then compression deformation in the transition zone. Under each stage of cutting process, the internal plastic work is calculated, and the minimum energy postulate is applied to derive the closed-form solutions of wedge indentation force and the corresponding optimum flap rolling radius.

Frictional effects are studied and included in the final wedge force equations. Two distinct frictional forces are identified in the analysis: machining friction near a wedge tip and sliding friction between the interface of transient flap and wedge attack surface.

Transient cutting force analysis is performed by assuming an instantaneous cylindrical flap model with increasing rolling radius. In the steady-state wedge cutting process, two kinematic models are proposed: curling and upright flap models. Both models have their merits depending on the magnitude of controlling parameters involved, e.g. wedge angle and B/t ratio. A simplified solution for the steady-state wedge cutting process using curling flap model is also derived and its accuracy compared with its original form is determined in a wide range of the controlling parameters.

The closed-form solutions for both transient and steady-state cutting processes are verified with small and large scale experimental results. Good correlations are reported and the scaling law is proved to be valid in the current theory.

Thesis Supervisor: Tomasz Wierzbicki
Title: Professor of Applied Mechanics

Acknowledgments

I wish to express my appreciation first and foremost to my wife, Lei Li, and my son, Da-Cheng, for their love, support, and endurance in the past five years so I would fulfill my academic goal at M.I.T. Also, I would like to thank my parents and parents-in-law who have always been a source of love, encouragement, and strength. It is greatly appreciated to my family's long-time friends, Mr. and Mrs. Hua, who have given me lots of help and guidance in the path of my educational success.

I would like to express my sincere gratitude and appreciation to my research and thesis advisor, Prof. Tomasz Wierzbicki of Ocean Engineering Department, M.I.T., for his dedicated guidance, advice, encouragement, and moral and theoretical support with all aspects of the work over the years. The entire research process has been a valuable learning experience to me, and Prof. Tomasz Wierzbicki's lead has been the key to the success of this work. Thanks are also due to Prof. Jerome Connor and Prof. Eduardo A. Kausel who have presided over my thesis committee meeting and have given me extensive guidance and thought-provoking discussion throughout the process of this dissertation.

I would like to acknowledge the diligence and hard work of the Joint MIT-Industry Program on Tanker Safety experimental team. They are Mohammed Yahiaoui, Mark Bracco, Pat Little, Leonard M. Maxwell, Katherine Trauth, and Neil Best. Most of the valuable experimental results presented in this dissertation are from their devotion and genius work. I am also very grateful for Dr. Ole Astrup of DnV for providing me very important experimental results used to conform the validity of the theory for wedge cutting through the actual hull plating

Lastly, but certainly not least, special thanks to the Joint MIT-Industry Consortium on Tanker Safety for the support of this research work.

Table of Contents

List of figures

List of tables

NOTATION

a	rectangular plate length
b	rectangular plate width
B	half wedge shoulder width
d	maximum stretch in transition zone (distance between points A and B in Fig. 3-6)
D_o	plate flexural rigidity, $= \frac{E\, t_o^3}{12\,(1-\mu^2)}$
E	Young's modulus
$\dot{E}_b$	bending energy rate
$\dot{E}_m$	membrane energy rate
F	wedge cutting force
F_b	wedge cutting force contributed by bending deformation only
F_{conc}	concertina tearing force
F_f	wedge cutting force including friction
F_{fm}	machining frictional force
F_{fs}	sliding frictional force
F_s	simplified wedge force
F'_t	total force needed for stable flap to buckle
H	width of buckled stable flap
K	compressive buckling coefficient
l	plastic hinge length for transient flap or stable flap buckled wave length
l^*	wedge indentation depth under transient indentation process
l_p	depth of plastic zone in front of a wedge tip
M_o	fully plastic bending moment per unit length

N compressive force

N_o maximum compressive force

R rolling radius

R_f rolling radius including frictional effects

R_s rolling radius for the simplified curling flap model solution

t plate thickness

t_o plate thickness at the thicker end of a non-uniform plate

u opening in transition zone for a given rolling angle ϕ or a given coordinate ξ (Fig. 3-5)

V wedge advancing velocity projected on the cut plate

v_y separation velocity in the near-tip plastic zone along y-axis

w out-of-plane deflection due to stable flap buckling

w_o maximum w located in the middle of a buckled stable flap

x coordinate along x-axis with the origin at the intersection of two inclined (transient) plastic hinges

β coefficient of plate thickness non-uniformity

δ_t crack tip opening displacement (CTOD) parameter

$\bar{\delta}_t$ normalized CTOD parameter, $= \delta_t / t$

ε tensile strain

ε_{xx} compressive buckling strain

γ ratio of total *vs.* stretching energies in transition zone

θ wedge semi-angle

λ plate aspect ratio

ν Poisson's ratio

μ_m frictional coefficient for machining

μ_s frictional coefficient for sliding friction

σ_o flow stress of plate material

σ_{xx} uniaxial compressive buckling stress

ϕ rolling angle measured along the stable flap curling direction

ϕ_{max} maximum ϕ

ζ ratio of rake face length and plate thickness for machining friction

ξ, η local coordinate systems in the flaps

Chapter 1

Introduction

1.1. Background

Throughout the maritime history, waterborne transportation encounters potential accidents including grounding upon undersea reef or rock. Recent oil supertanker grounding accidents have made mass media and public awareness of the environmental protection against oil spillage disasters. For example, the March 1989 grounding of the supertanker, *Exxon Valdez*, resulted in the loss of nearly 11 million gallons of crude oil! Strict laws have been imposed by jurisdictions around the world to eliminate the possible massive oil spillage at sea in the future. In the United States, the Congress passed the *Oil Pollution Act of 1990* (OPA 90) mandating that petroleum product cargo ships operating in U.S. waters be double hull construction and/or designs providing equivalent protections by January 1, 2015.

In the pass several decades, research efforts were made mainly to improve the ship collision protection. It has only been in the recent fifteen years or so that hull grounding damage has been investigated. Early work in grounding failure prediction was concentrated in plate cutting experiments and formulation of empirical equations correlating wedge force with controlling parameters such as wedge attack angle and plate thickness. One of the most important contributions in this direction was made by Lu and Calladine [1] who were first to correctly apply the dimensional analysis method into the interpretation of wedge cutting test results which clarified the long lasting confusions and questions of how to apply the experimental results and the corresponding empirical equations into the real world cutting failure predictions. Recently, Wierzbicki and Thomas [2] pioneered the application of energy postulation into the grounding failure prediction. This approach has been proved to

be very effective and have initiated the whole new school of research. (This dissertation is actually an extension of such a research activity.) The advantages of applying analytical methods in the hull grounding failure study are obvious: it can provide an insight towards the understanding of wedge cutting failure mechanism and will produce theoretical solutions valid in a wide range of wedge cutting scenarios. The latter is especially important because it opens a new way to solve such a complicated wedge cutting problem efficiently and economically. In order to provide for the ship building industry the most up-to-date academic research results about hull grounding damage prediction and to apply such knowledge into the designs of a new generation oil tanker, a joint MIT-Industry Program on Tanker Safety was started in 1992 and continues up until now. The primary goal of such an ambitious project is to develop a state-of-art computer program used to predict the extent of structural damage due to grounding accident and, at the same time, to provide an expert guidance on how to increase hull rupture resistance through the improved hull design and fabrication techniques. This dissertation plays an important role in the project aimed to expand the existing grounding failure knowledge into the area of steady-state hull grounding analysis.

1.2. Goals of the present research

The ultimate goal of present research is to solve the problem of plate failure under wedge indentation analytically and to apply the theoretical solutions into the ship grounding computer program, *DAMAGE*, to be developed in M.I.T. A set of closed-form solutions are derived covering both transient and steady-state wedge indentation situations.

The present study of transient indentation process is an extension of the existing theory developed by Wierzbicki and Thomas [2]. The major difference between the two theories lies on the basic assumptions about cutting initiation. Wierzbicki and Thomas assumes that

there exists a fracture or tearing in front of a wedge tip whereas the current theory adopts an alternative hypothesis in which a wedge tip has a direct contact with plate material. The correct application of such assumptions depends on what plate material and wedge shape are used in an actual cutting situation. For example, Lu and Calladine [1] observed a crack developing in front of a wedge tip for a dural plate cutting, but no crack was observed for all other metals tested. Also, a crack was seen running ahead of a semi-circular wedge head during a wedge indentation experiment even though a mild steel specimen was tested [14]. But, for the majority of wedge cutting results, a wedge tip has been observed to have a direct contact with a plate. So, both theories will be incorporated into the newly developed computer program, *DAMAGE*, which will have an automatic check routine executed internally in order to determine which theory will give a good and reasonable estimation to the real problem.

The study of steady-state wedge cutting through a metal plate is a relatively new research area which requires constructing kinematically admissible models and formulating closed-form wedge force solutions. Due to a great complexity of the problem, two kinematic models are proposed simulating the two typical cutting failure modes observed from experimental results, i.e. failure modes with curling and upright flap deformation patterns (Fig. 3-4). As we shall see in Chapter 3, both models have their merits and should be included in the computer program - *DAMAGE*. In the steady-state cutting analysis, it is always assumes that a wedge tip has a direct contact with plate material.

Validation of the theoretical solutions by the typical experimental results is performed which shows a good correlation and proves the correctness of the theory.

1.3. Grounding scenarios

A brief overview of a tanker grounding situation will be helpful to gain an insight of the current research context. Wierzbicki *et al.* [3] proposed a model for a ship grounding sce-

nario as follows. Consider a ship of mass M travelling with a forward velocity V which strikes an undersea rock. If a hull damage cannot be prevented, the structure failure is assumed to start at the bow or forward part of a ship, and proceeds toward the stern. The kinetic energy of the ship, i.e. $\frac{1}{2} M \cdot V^2$, is dissipated through any combination of the following four possible failure modes during the progress of a ship grounding:

- global uplifting of the ship's front part due to riding over upon an undersea obstacle,
- frictional forces between the hull bottom and rock surface,
- initiation of local hull damage, and
- steady-state cutting through hull plating with an interaction between overall ship motion.

During a grounding accident, a ship is first lifted and rides over a rock underneath with a good possibility of local hull denting damage. If the hull plating resistance towards the vertical punching force from the ship's self-weight has been overcome, hull rupture or cutting will begin. Initial indention process is confined in an area comparable to the size of the rock. The force required to have an initial penetration through a hull plating is larger than that of a steady-state cutting process. Once the steady-state cutting process initiates, damage towards a hull structure will have a relatively regular pattern with a constant rate of energy dissipation. Most of the kinetic energy of a ship before grounding is exhausted at the steady-state grounding stage. The first failure mode, i.e. ship global lifting and riding over upon a rock without hull rupture, is considered as an esthetical and/or minor structural damage without losing the oil cargo of a tanker, which is studied as a separate project in M.I.T. The remaining three grounding failure modes are studied in detail in this dissertation because they are hazardous and dangerous towards both the ship structure and the environment.

1.4. Review of previous work

The study of ship damage started as early as 1959 by Minorsky who pioneered the path-finding work in the area of structural damage prediction due to ship collisions [4]. By correlating data obtained from twenty-six relevant ship collision accidents, he hypothesized that the resistance of a ship to collision was proportional to the volume of the deformed material during collision. After using the momentum conservation law and energy principles of rigid body mechanics, Minorsky developed a linear empirical relationship between the kinetic energy lost, K_T, and the structural resistant factor, R_T, (relating directly to the damaged material volume) as follows:

$$K_T = 414.5R_T + 121900\,, \tag{1-1}$$

where K_T has a unit of $lton\text{-}knot^2$, and R_T has a unit of $ft^2\text{-}in$. This equation holds quite accurately for the collisions when K_T is large. However, it does not give satisfactory results for minor collisions where K_T is small. This can be easily explained nowadays: the reason that the above equation is not valid for a wide range of application is because that it lacks the dimensional consistency on both sides of the equation so that it is correct only to the same size of the ships and the same amount of the damages investigated.

Vaughan extended Minorsky's theory to include ship grounding as well as collision damages into his empirical equations [5]. After studying the behaviors of plate penetration by a rigid wedge, he concluded that there existed two independent contributions of work to hull plating penetration: bending which is similar to that done by Minorsky, and plate tearing. The plate tearing work was considered as a surface energy function per unit length of fracture, and it was determined by using Akita and Kitamura's experimental data [6]. By fitting curve with drop-hammer test data from sixty-four experiments, Vaughan [7] was able to formulate an empirical equation for the work done by a rigid wedge, W in $\mathrm{N}\cdot\mathrm{m}$, as follows:

$$W = 5.5\, l t^{1.5} + 0.0044\, l^2 t^2 \tan\theta\ , \tag{1-2}$$

where l is the wedge penetration length in millimeter, t is a plate thickness in millimeter, and θ is a wedge semi-angle in degree. Unfortunately, the above equation also lacks a dimensional consistency.

Woisin [8] conducted nineteen drop-hammer tests with mild steel plate specimens set vertical. It was the first time that a new flap deformation pattern, i.e. braided deformation, was observed and reported; and the importance of frictional force was mentioned. Jones and Jouri [9] conducted a new series of drop-hammer tests with nineteen specimens, which investigated the energy required to cut through thick plates (the thickest specimen is $t = 5.95$ mm in thickness). In their experiments, several different modes of flap deformation were observed and reported. It was said that, due to the coexistence of plastic deformations and fracture, "principles of simple geometrically similar scaling do not work".

Atkins [10] treated the problem of plate cutting as a fracture problem. Based on the idea that the total energy is composed of two components: flap bending energy and near tip fracture energy, a scaling law is derived as follows:

$$\frac{W_p}{\lambda^3 W_m} = \frac{\xi}{\xi+1} + \frac{1}{\xi+1}\cdot\frac{1}{\lambda}\ , \tag{1-3}$$

where W_p and W_m are the energy absorbed by the prototype and the model, respectively; λ is a scaling factor, and ξ is a non-dimensional parameter. He then assumed that ξ would keep constant for both the prototype and the model, which left only one variable, λ, in the above equation. By employing the experimental results from Jones *et al.* [9] [11] and taking a suitable value for the mean plastic strain, he found the material toughness R to be $600\ KJ/\mathrm{m}^2$ which is used in the above equation to determine the fracture energy of a plate. It was concluded, thereafter, that this scaling law helped to explain the results from the tests conducted.

Lu and Calladine [1] performed a large number of plate cutting experiments, but, in their tests, a wedge was driven quasi-statically instead of drop-hammer loading method commonly used at that time. The main advantage of such a new test method is that the whole deformation history of the deformation process can be monitored easily without the presence of any dynamic effects. By applying the dimensional analysis method, Lu and Calladine were able to derive a universal equation correlating the wedge cutting work with the corresponding geometric and material properties. It is worthwhile to mention again that this is the first time in the literature that a dimensionally-consistent empirical equation was reported for the wedge cutting force prediction, which provides a right path to the interpretation of the experimental results in the future. Lu and Calladine's empirical equation shows a general validity over a wide range of transient indentation problems:

$$W = C \cdot \sigma_y \, l^{1.3} t^{1.7} , \tag{1-4}$$

where C is a dimensionless coefficient determined by the controlling parameters, such as wedge semi-angle, plate tilt angle, specimen material, and friction; l is a wedge travelling distance, t is a plate thickness, and σ_y is the material flow stress (even though the yield stress denomination is used). As long as a consistent unit is used for all the parameters, the above equation will be valid regardless of which actual unit system is used. It was experimentally verified that Eq. (1-4) is valid in the range of $5 < l/t < 150$ because, as we shall see below, a large ratio of l/t will cause an alternative failure mode - concertina tearing.

Up until this point of discussion, all the investigators had focused their studies in the experimental determination of the empirical relationships between wedge cutting work and the controlling parameters. In order to obtain a full understanding of the wedge cutting mechanisms and to provide a universally-valid analytical method to solve different wedge cutting problems, Wierzbicki and Thomas [2] pioneered the application of energy postulation into the study of plate transient indentation problem. By assuming a mathematical model with the kinematically admissible velocity and displacement fields, they derived a

closed-form solution for the wedge transient force which has a similar form as Eq. (1-4):

$$F_t = 1.67\sigma_o (\bar{\delta}_t)^{0.2} \; l^{0.4} t^{1.6} g(\theta, \mu) \;, \tag{1-5}$$

where σ_o is the flow stress of a material, l is a wedge indentation length, t is a plate thickness, $g(\theta, \mu)$ is a function of wedge semi-angle and sliding frictional coefficient, and $\bar{\delta}_t$ is a normalized crack opening displacement parameter defined as $\bar{\delta}_t = \delta_t / t$. The above expression is dimensionally consistent and was proved to have a good correlation with the test results over a wide range of wedge semi-angle $10^o \le \theta \le 30^o$ and sliding frictional coefficient $0.1 \le \mu \le 0.4$ [12].

Closed-form solutions for the steady-state wedge cutting through an infinite plate were subsequently formulated by Zheng and Wierzbicki [13] and the supporting experimental data were supplied by Yahiaoui *et al.* [14]. A detailed coverage of this research is to be presented in Chapter 3 which provides all the important information about the theoretical background and the analytical methodology.

Recently, hull grounding study has seen a new trend: complicated specimens are designed to incorporate all the structural details. This is aimed to study the contributions of the secondary members to a grounding failure process. Instead of using the standard practice which smears all the stiffeners and bulkheads into an equivalent uniform thickness plate [15], Kuroiwa *et al.* [16], Bracco [17], and Little [18] tested scaled specimens with the secondary structural elements included. For example, Kuroiwa *et al.* [16] tested two 1:3 scale models representing single and double bottom VLCC (very large crude carriers) which included all the actual ship structure details into the specimens: hull plating, longitudinal stiffeners, transverse frames, and longitudinal bulkheads.

Concertina tearing of metal plates is an alternative grounding failure mode reported first by Kitamura *et al.* on the 1:4 scale wedge indentation tests into single and double hulls [19]. This failure mode was also identified by Wierzbicki [27] on the photograph taken from a

grounding damaged supertanker bottom. Wierzbicki then developed a closed-form solution for the mean concertina indentation force which has been proved to be representative to the experimental results conducted at M.I.T. [12] [27]. Concertina tearing failure mode is induced mainly by pushing a dull wedge through a plate specimen which shows two symmetric cracks running in the plate ahead of the wedge.

Some other new research activities are also under development in M.I.T. on ship grounding study, e.g. double hull stranding and cutting analysis, and non-rupture hull grounding assessment.

The research achievements obtained so far have provided both the academy and the shipbuilding industry an in-depth understanding of the tanker grounding failure mechanisms. Further theoretical, numerical, and experimental studies should be conducted to resolve the remaining issues.

1.5. Categorization of grounding damages

In this section, all the possible types of grounding damages are presented and categorized. In order to cover different aspects of the grounding phenomena, several categories are defined, e.g. the cutting process category is used to describe the different stages of cutting process, the flap deformation category gives different flap deformation patterns, the failure mode category separates the central indentation from the concertina tearing failure mode, and so on.

1.5.1. Stages in a cutting process

Three wedge cutting stages are identified from the available experimental results [14]. The first stage is defined as the transient indentation process characterizing the initiation of hull plating damage. Normally, the ruptured area in this stage increases with the wedge inden-

tation length and an ascending force-displacement curve is usually observed. If a wedge has a limited size and keeps advancing, the second stage of cutting will begin but it is not easy to identify. This stage typically shows a bump in the force-displacement curve and its peak generally gives the maximum resistance of a plate specimen under the specified test conditions [18]. The last stage of a cutting process shows a constant wedge force in the force-displacement diagram. This stage is terminated as the steady-state wedge cutting process.

1.5.2. Flap deformation

Two types of flap deformation are identified from the wedge indentation experiments [1] [14]: braided and curling flap deformations. The former is caused by the unbalanced frictional force in the out-of-plane direction [2] which is less known to the academy; and the latter is much simpler to deal with and is to be studied in this dissertation.

Under the steady-state cutting process, the portion of a flap at the back of a wedge attack surface is terminated as a stable flap. For the stable flap with a single curling deformation, there exist two different deformation patterns: wavy buckled flap shape and smooth cylindrical flap shape. Both of them are observed from experiments [1] [14] and will be analyzed in Chapter 3.

1.5.3. "Clean" cut *vs.* concertina tearing modes

Two completely different failure modes from cutting an individual plate can be identified. One is the "clean" cut failure mode which consists of a plate central separation in front of a wedge tip and flap bending on both sides of a wedge attack surface. Another is the concertina tearing failure mode which characterizes plate folding back and forth in front of a dull wedge with a symmetric edge tearing along the remote boundaries. For the "clean" cut mode, either braided or smoothly curling flap deformation may develop depending on the test conditions encountered, and a cutting process can be either transient or steady-state.

For the concertina tearing mode, two distinct modes of failure were observed from the tests: confined concertina tearing failure with a plate specimen torn along parallel stiffeners [14], and diverging concertina tearing failure with two symmetric cracks radiating from a wedge tip [20]. The former is a steady-state deformation process with a regular pattern of plate folding in front of a wedge tip, and the latter is a transient process with the increasing width of folds until the radiating cracks hit the remote boundaries or an alternative failure mode takes over. When a critical condition is reached, it is possible that both "clean" cut and concertina failure modes can coexistent in the same specimen (Fig. 5-3). Section 3.5.2. provides a set of boundary curves which can be used as a guide line for the failure mode predictions.

1.5.4. Environmental impact

The aim of hull plating indentation study is to design a new generation hull structure which can absorb a large amount of kinetic energy during tanker grounding without losing its oil cargo. Many possible design methods are proposed, such as double hull, double side, and flexible hull plating designs. The ultimate grounding damage evaluation should be performed by considering both ship structure failure and the environmental impact. The latter is more important to the public and needs to be taken into a great care because of its direct relation to the environmental protection. The oil spillage prevention plus environmental protection is an inter-disciplinary subject which should be included in the future research.

1.6. Overview of the theoretical analysis method

Like all the structural analysis problems, it is a very important step to construct a correct mathematical model. Due to the complicated nature of the wedge indentation problem, one way to give a theoretical solution is to apply an upper bound theorem which is, in essence,

an approximate method. It is well known that an upper bound theory will give a very good approximation to the real solution if a constructed kinematic model satisfies all the boundary conditions and has a deflected shape compatible with the deformation pattern observed from the corresponding tests. In the following two chapters, kinematically admissible models for different failure cutting modes are proposed based on the experimental results and simple physical model constructions. Since so many assumptions and simplifications are made in the theoretical analysis, the correctness and accuracy of the theory can only be justified by the experiment. M.I.T. experimental team [14] played an important role in the verification the theoretical solutions derived here, and their contributions are equally important to the success of the current research project. The step-by-step descriptions of the current theory are summarized below, which serves as a backbone of our entire theoretical study performed in Chapters 2 and 3.

The first stage of analysis is to build a kinematically admissible model from the available experimental results and simple physical model constructions. Although the minimum requirement for an upper bound theorem can be fully satisfied, it is difficult for the constructed kinematic model to incorporate the global out-of-plate deflection observed commonly from the damaged specimens. It is difficult to determine theoretically whether the omission of this additional deformation pattern in the current analysis will still give us an upper bound solution or not. As pointed already, the only feasible approach to resolve such doubt is to verify the theory with test results which is the fifth stage of analysis to be discussed later.

The second stage of analysis is to formulate all the deformation energy rates involved in a wedge indentation process by analyzing the kinematic models constructed in Stage I. In order to simplify our analysis, the only deformation energy rates included are those which contribute mostly to the plate cutting resistance. This means that some of the minor deformations might be ignored in the analysis, which will further reduce the total deformation energy rate computed. This reduction has a counteractive effect on the energy overestima-

tion normally seen in an upper bound theory, but this gives an additional uncertainty factor to the accuracy of our theoretical solutions which can be clarified solely by the experimental results.

The third stage is to formulate closed-form solutions of the problem by first equating the total internal energy rate to the external work rate and then minimizing the rate of internal energy dissipation. Note that, at this stage, the frictional force has not been included yet, because it can be treated as an independent term to the cutting force expressions [2].

The fourth stage is to determine the friction contribution to the wedge force expression derived in the previous stage. Two frictional forces are identified in our analysis: sliding and machining frictional forces. The former is seen to be existed between flap and wedge surfaces which is encountered normally. The latter is actually a misnomer used to describe the machining process existed between a wedge tip and the plate material. In reality, a wedge cutting process is characterized by the local shear failure of weaker material (usually plate) occurring in the so-called *rake face* region causing energy loss. The machining friction has a constant value under a given cutting condition, and it may be neglected if a large plastic deformations are involved in the plate cutting process. It is worthwhile to mention here that the machining friction can only exist when the hypothesis of direct cutting at a wedge tip is used.

The fifth stage is to verify the accuracy of the theoretical solutions by the typical experimental results. Comparisons are made between the theoretical predictions and test results. If a small difference is observed from the comparison, the analytical solutions can be confidently stated as a valid theory. Size effect should be considered if only a batch of small scale tests is conducted.

We have listed the main procedures used to derive the closed-form solutions for the wedge indentation problem. However, the above approach is generally valid for finding a solution of all the similar failure problems such as car crashworthy evaluation [21].

1.7. Scope and outline of the dissertation

In this dissertation, research on wedge "clean" cutting through metal plates is performed theoretically. It aims to solve the practical problem of oil tanker grounding damage on a knife-shaped reef. Both transient and steady-state cutting processes are to be studied with the corresponding closed-form solutions derived. Throughout this dissertation, a basic hypothesis is made which assumes that a wedge tip has a direct contact with a plate material at the near-tip plastic zone. Experimental results on plate cutting support such an assumption under certain circumstances discussed early, e.g. Lu and Calladine [1], Maxwell [12], Yahiaoui *et al.* [14], and Trauth [20].

The study of transient indentation process presented in Chapter 2 is a continuation of the theoretical analysis pioneered by Wierzbicki and Thomas [2]. The new hypothesis assuming a direct cutting at a wedge tip is made in the current analysis, whereas Wierzbicki and Thomas's theory assumes a fracture or tearing existed in front of a wedge. A closed-form solution is derived for the new kinematic model following the analytical procedures listed in Section 1.6. with the following steps summarized. That is, first, a kinematic model is constructed and the corresponding energy dissipation rates from all different deformation mechanisms are calculated. Next, a closed-form solution for the indentation force is derived by applying the energy postulation discussed in the previous section. Frictional effects are then added to the force expression. Finally, comparisons of the theoretical solution with the typical experimental results are performed to check the correctness and accuracy of the derived closed-form solution and the corresponding kinematics assumed for the problem. A good correlation is reported from the comparisons made as will be seen in Chapter 2. For a detailed description of the experimental procedures, a reader is referred to the work of Maxwell [12]. In Chapter 2, comparisons are also conducted between Wierzbicki and Thomas's theory [2] and the current one. It is concluded that both theories are correct and their application depends on the specific cutting conditions involved.

The theoretical study of a steady-state cutting process presented in Chapter 3 is a new research. This cutting process should be clearly distinguished from the previous transient (or initial) indentation process studied extensively in the literature, e.g. Lu and Calladine [1], Wierzbicki and Thomas [2], Vaughan [5], and Jones and Jouri [9]. A transient indentation has a relatively simple deformation pattern, i.e. plate tearing or cutting near a wedge tip together with plate bending along two inclined moving hinges. But a steady-state cutting process has a more complex deformation pattern because, in addition to the deformations discussed in the transient cutting process, it has a significant membrane tension/compression deformation in the transition zone located between the transient and stable flaps.

Two kinematically admissible models shown in Fig. 3-4 will be developed in Chapter 3. Both of them are assumed to be under the "clean" cut condition. In the first model, flaps are assumed to be curled smoothly with a uniform rolling radius throughout the flaps, whereas the second model consists of flat flaps bent upright from its original plane of the plate. Both models have their merits. For example, one kinematic model might give a better failure prediction than the other in certain cases as will be seen in Chapter 3.

In Chapter 3, the closed-form solutions for the steady-state indentation force are derived for both kinematic models discussed above. The detailed analytical procedures involve the following steps. First, the kinematics of cutting process are analyzed and the energy dissipation rates corresponding to different deformation mechanisms are calculated. Then, the closed-form solutions of the problem are derived by applying the energy postulation discussed previously. Frictional effects on the steady-state cutting process are added to the derived force expressions next. Finally, comparisons with typical test results are performed to check the validity of the theoretical solutions and their corresponding kinematics of the problem. Again, a good correlation is reported in Chapter 3. For a detailed description of the experimental procedure, the reader is referred to the work of Yahiaoui *et al.* [14].

The writing style of Chapters 2 and 3 is meant to treat them as two complete and independent articles to save time for future journal publications. That is, in each chapter, all the

useful information, such as basic assumptions and derivation steps, are presented in detail regardless of the possible redundancy. The reader is recommended to skip those repeated sentences and paragraphs in the dissertation while reading.

Chapter 2

Study of Transient Wedge Indentation Process

2.1. Introduction

In this chapter, a closed-form solution for the transient wedge cutting through an infinitely wide plate is first derived based on the observations of typical test results and simple physical model constructions. The hypothesis that assumes a direct contact existed between a wedge tip and the plate material is used throughout the current analysis. In Wierzbicki and Thomas's theory [2], an alternative hypothesis was assumed: a fracture or tearing existed in front of a wedge tip. Both mathematical models have their merits as will be seen in sequel. Graphical comparisons between the two models are made in Section 2.7., which shows that they lead to similar results. This is due to the fact that, for both models, the local failure near a wedge tip contributes almost the same amount of energy towards the total indentation force. Comparisons of experimental results with both theoretical solutions are conducted in Section 2.8. in order to verify the correctness of the theory.

The analysis of the transient wedge indentation process through metal plates is actually an idealization of ship hull damage scenario when a ship is aground upon a sharp undersea reef or rock with its hull cut initially. The phenomena were observed by many experimenters, including Lu and Calladine [1], Maxwell [12], and Astrup [26]. Wierzbicki and Thomas [2] were the first to successfully apply the energy theorem in the searching of a closed-form solution for the problem. This chapter is a continuation and extension of such an effort to make the transient indentation analysis complete.

The kinematic model proposed in the present theory is shown in Fig. 2-1. It is based in part on the visual analysis of the experimental results presented in Ref. [1], and in part on

the simple physical model constructions. The hypothesis that there exists a direct contact between a wedge tip and the plate material is incorporated in the model which serves as a basic hypothesis throughout this dissertation.

The analysis involves primarily the following steps: (i) establishment of kinematically admissible model for the transient indentation process; (ii) calculation of energy dissipation rates corresponding to each individual deformation mechanisms; (iii) derivation of a closed-form solution for the transient wedge force by applying the energy postulation; (iv) incorporation of frictional effects into the derived solution; and (v) validation of the analytical solutions and the corresponding kinematics with typical experimental results. A good correlation between the theory and experiments is reported in Section 2.8. For a detailed description of the experimental procedures and results, the reader is referred to the work of Maxwell [12].

2.2. Characteristics of transient wedge cutting process

Under the transient indentation process, a plate is first separated at a wedge tip and then bends up into two flaps on both sides of the wedge attack surfaces. A typical "clean" cut implies that the flaps curl up smoothly only on one side of the plate, i.e. no braided deformation is allowed. During the cutting experiments conducted in M.I.T., a close contact of wedge surfaces with the curled flaps was observed, which provides an important geometric relationship: the flap opening angle is equal to the wedge angle (Fig. 2-1). From the observation of Lu's experimental results [23], it can be concluded that the only deformation existed in the curling flaps is the bending process along the two inclined plastic moving hinges with the remaining part of the flap rotating as a rigid body. Such deformation pattern produces a spiral curvature in the flap's cross-sectional direction because the rolling radius of flaps increases with the wedge indentation length. Wierzbicki and Thomas proved that the only feasible curling flap shape at any given instant is a cylinder since it acquires the

least amount of deformation energy [2].

2.3. Internal energy rate under transient indentation process

Two major energy dissipation forms are identified in a transient indentation process. They are membrane deformation at a wedge tip and bending along two moving plastic hinges. In order to simplify our analysis with an acceptable accuracy, several assumptions and simplifications are made as follows:

(i) Plate material is assumed to be rigid-perfectly plastic with an average flow stress, σ_o. Its value can be either determined from tensile tests or calculated from hardness test results. A precise definition of the flow stress is presented by Wierzbicki [27] which completely clarifies many reader's misunderstanding and confusion about the concept of flow stress.

(ii) It is assumed that both bending and membrane deformation modes have the same flow stress, σ_o. But this assumption can be easily relaxed by allowing different flow stresses in different regions, depending on the level of average strain.

(iii) The plastic interaction between bending moment and membrane force is neglected in the plastic zone near a wedge tip. This hypothesis will overestimate the actual rate of energy dissipation in the membrane action and will partially compensate the energy lost by ignoring the bending energy in a near-tip zone.

(iv) Plastic shear strain is ignored. The validity of this assumption has been discussed in detail by Wierzbicki and Thomas [2].

(v) Plastic work in the near-tip zone is predominantly dissipated by the diffused mode. In other words, no local necking is considered and the plate thickness is

taken to be constant.

(vi) Plate material obeys von Mises yield criterion. Under the plane stress condition, the criterion can be expressed as:

$$\sigma_{xx}^2 - \sigma_{xx}\sigma_{yy} + \sigma_{yy}^2 + 3\sigma_{xy}^2 = \sigma_o^2, \tag{2-1}$$

where σ_{xx}, σ_{xy}, and σ_{yy} are the in-plane components of stress tensor. The corresponding flow rule gives:

$$\begin{cases} \dot{\varepsilon}_{xx} = \dot{\lambda}(2\sigma_{xx} - \sigma_{yy}) , \\ \dot{\varepsilon}_{yy} = \dot{\lambda}(2\sigma_{yy} - \sigma_{xx}) , \\ \dot{\varepsilon}_{xy} = 6\dot{\lambda}\sigma_{xy} . \end{cases} \tag{2-2}$$

2.3.1. Plastic zone near a wedge tip

In all experiments performed at M.I.T. with a sharp wedge of a semi-angle $\theta = 30^o$ or $\theta = 45^o$, it is observed that a wedge tip always has a direct contact with the plate material [12]. This is called plate cutting as opposed to plate fracture and/or tearing where the wedge forces are applied at a remote location causing fracture process in front of a wedge tip. Accordingly, it is assumed in the kinematic model that a wedge tip coincides with the tip of a plate crack, which is confirmed experimentally by many mild metal specimens [1]. The large stress and strain observed in the plate material near a wedge tip generally cause plastic deformation of the material. The shape and size of a near-tip plastic zone was measured experimentally and reported by Lu [23]. His test results showed that a finite area surrounding a wedge tip undergoes a membrane deformation under the in-plane plastic flow.

The near-tip plastic zone length is denoted as l_p (Fig. 2-1). Lu reported that the l_p value

is around seven times of the plate thickness for a wedge semi-angle equal to 20^o with a plate tilt angle 20^o. It is believed that the plastic zone size varies according to the controlling geometric parameters like wedge shape, plate thickness, and inclination angle; although, under a given test condition, l_p will remain constant. Based on the physical model construction, it is assumed that the near-tip plastic zone on a plate is extended from a wedge tip to the intersection of two inclined transient plastic hinges having a depth (Fig. 2-1):

$$l_p = \frac{R}{\sin\theta}, \tag{2-3}$$

where R is an instantaneous rolling radius of the curling flaps to be analyzed below, and θ is a wedge semi-angle. Note that the above equation does not explicitly take plate inclination into account. But it implies that, with the increment of a plate tilt angle, the near-tip plastic zone depth increases accordingly. This is because, in reality, θ should be calculated by a wedge angle projected on the cutting plate (Fig. 2-2) which produces a smaller angle than that of an actual wedge. This, in turn, yields a larger plastic zone size according to Eq. (2-3). Since the plastic zone size is confined to the range only several plate thickness long, it is safe to neglect the bending deformation in that zone induced by the eccentricity of an indentation force. To further simplify our analysis, it is assumed that the plate tilt angle is zero, which can be easily corrected by using the wedge angle projection method discussed previously.

In a near-tip plastic zone, the membrane deformation rate in the direction normal to the cutting velocity was analyzed by Wierzbicki and Thomas [2]. By considering the compatibility of the transverse displacement and velocity fields, they derived a simplified expression for the separation velocity near a wedge tip as follows:

$$v_x \equiv 0,$$

$$v_y = \begin{cases} V \tan\theta \left(\dfrac{x}{l_p}\right)^2, & \text{for } x \le l_p, \\ V \tan\theta, & \text{for } x > l_p, \end{cases} \tag{2-4}$$

where V is the wedge advancing velocity, and x is the coordinate along x-axis with its origin at the intersection of two inclined moving hinges (Fig. 2-1).

For a very blunt wedge, such as a wedge having a semi-circular cross-section, a crack can be initiated and run in front of a wedge tip. This has been clearly demonstrated in one of the tests run by Maxwell [12]. The case with a crack running ahead of a wedge tip was studied theoretically by Wierzbicki and Thomas [2]. It was found that the size of a near-tip plastic zone is controlled by the Crack Tip Opening Displacement (CTOD) parameter δ_t. From their study, it can be concluded that the dependence of the wedge indentation force on the magnitude of δ_t was very weak.

The question whether a wedge indentation leads to a cutting or fracture failure has been subjected to a debate in the literature. Atkins [24] argued for the latter viewpoint while Lu and Calladine [1] and Calladine [25] defended the former. We believe that either situation can develop, depending on the scale of the problem. As already mentioned, in all thin and mild steel plates up to the thickness of $t = 2$ mm, no cracks were emanating from the tip of a wedge. However, for the intermediate scale experiments conducted at the DnV facility in Bergen on plates with $t = 15$ mm, cracks were clearly observed in front of the wedge tip [26].

2.3.2. Membrane energy rate inside near-tip plastic zone

Under the transient indentation process, the rate of membrane energy under the plane stress condition is defined by the following expression:

$$\dot{E}_{\mathrm{m}} = t \int_{S} \sigma_{\alpha\beta}\, \dot{\varepsilon}_{\alpha\beta}\, dS\,, \tag{2-5}$$

where S denotes an area in a membrane displacement zone, t is the plate thickness, and $\sigma_{\alpha\beta}$ and $\dot{\varepsilon}_{\alpha\beta}$ are the components of stress and strain rate tensors, respectively. The strain rate tensor is defined as:

$$\dot{\varepsilon}_{\alpha\beta} = \frac{1}{2}\left(\dot{u}_{\alpha,\,\beta} + \dot{u}_{\beta,\,\alpha}\right)\,, \tag{2-6}$$

where $\dot{u}_{\alpha} = (v_x, v_y)$ are the components of the velocity vector projected in the x- and y-directions. The above equation carries the assumption that the small out-of-plane displacement near a wedge tip is neglected in the strain calculation which will give an underestimation in the calculation of the total internal energy rate.

When a wedge cuts through a plate, the component of strain rate in the direction of wedge motion, $\dot{\varepsilon}_{xx}$, should be zero in a near-tip plastic zone. The validity of such an assumption is obvious from the observation of the test results [1], because the material in the front of a wedge tip would accumulate if $\dot{\varepsilon}_{xx}$ were not zero. According to assumption (iv), $\dot{\varepsilon}_{xy}$ is also taken to be zero.

Based upon the above discussions and an additional assumption that the plane strain condition exists in the near-tip plastic zone, i.e. $\sigma_{xx} = \sigma_{yy}/2$, the in-plane membrane energy rate, Eq. (2-5), can be expressed as:

$$\dot{E}_{\mathrm{m}} = t \int_{S} \frac{2}{\sqrt{3}}\, \sigma_{\mathrm{o}}\, \dot{\varepsilon}_{yy}\; dS\,, \tag{2-7}$$

where S is a membrane deformation area at the near-tip plastic zone. The contributions of this zone towards the membrane energy rate is to be analyzed next.

Fig. 2-1 shows that there exists a zone in front of a wedge tip locally undergoing out-of-plane bending and in-plane membrane deformations, which causes the plate material to

yield in that area. This plastic zone extends in the y-direction to a boundary, $\delta(x)$, beyond which the material behaves elastically. Lu's experimental result [23] reveals that this plastic zone is confined in a small range which is about several times the plate thickness around the wedge tip. The shape of the plastic zone is actually not important in the calculation of the membrane energy rate in that region as will see in sequel. The controlling factors are the plastic zone depth, l_p, which is measured from the wedge tip to $x = 0$ and is equated in Eq. (2-3), and the y-direction separation velocity, $v_y(x)$, in the plastic zone, Eq. (2-4).

Substituting Eqs. (2-3), (2-4), and (2-6) into the above integration, Eq. (2-7), we get the membrane energy rate in the near-tip plastic zone [2]:

$$\begin{aligned}\dot{E}_{\mathrm{m}} &= t\int_S \frac{2}{\sqrt{3}}\sigma_0 \frac{\mathrm{d}v_y}{\mathrm{d}y}\,\mathrm{d}x\mathrm{d}y \\ &= 2t\int_0^{l_p} \frac{2}{\sqrt{3}}\sigma_0\, v_y|_{y=0}\,\mathrm{d}x \\ &= \frac{4}{3\sqrt{3}}\sigma_0 t l_p V\tan\theta \\ &= \frac{4}{3\sqrt{3}}\sigma_0 t\frac{R}{\cos\theta}V.\end{aligned} \tag{2-8}$$

In the above derivation, v_y is taken as zero at the elasto-plastic boundary in the near wedge tip plastic zone.

2.3.3. Bending energy rate

Under the transient wedge cutting process, all bending energies are concentrated in the two inclined plastic moving hinges (Fig. 2-1) and no work is done in the curled portion of a transient flap since it rotates as a rigid body about the plastic hinge line, OP. The length of an inclined plastic hinge is a function of wedge indentation length, l^*, and wedge semi-angle, θ, as formulated below:

$$\overline{OP} = \frac{l^*}{\cos\theta}. \tag{2-9}$$

For a rigid-perfectly plastic material, the out-of-plate plastic bending moment under the plane-strain condition per unit length along the moving hinge is

$$M_o = \left(\frac{2}{\sqrt{3}}\sigma_o\right) \cdot \frac{t^2}{4}. \tag{2-10}$$

The rate of flap rotation, $\dot{\omega}$, along an inclined plastic hinge is related to rolling radius, R, wedge semi-angle, θ, and wedge advancing velocity, V. The condition of kinematic continuity leads to the following relationship:

$$\dot{\omega} = \frac{V_n}{R} = \frac{V\sin\theta}{R}, \tag{2-11}$$

where V_n is the normal component of V to the cylinder center line of a transient flap. For a given rate of rotation, $\dot{\omega}$, the rate of bending energy is defined as

$$\dot{E}_b = 2\, M_o \frac{l^*}{\cos\theta}\, \dot{\omega}. \tag{2-12}$$

Substituting Eqs. (2-9) ~ (2-11) into Eq. (2-12) yields the rate of bending energy expression under the transient indentation process:

$$\begin{aligned} \dot{E}_b &= 2\left(\frac{2}{\sqrt{3}}\sigma_o\right) \cdot \frac{t^2}{4} \cdot \frac{l^*}{\cos\theta} \cdot \frac{V\sin\theta}{R} \\ &= \frac{4}{\sqrt{3}} \cdot \frac{\sigma_o t^2}{4} \cdot \frac{l^*}{R} \cdot V \cdot \tan\theta. \end{aligned} \tag{2-13}$$

2.4. Wedge force under transient indentation process

Under a transient process of wedge cutting through a wide metal plate, an external force, F, is applied on a wedge in order to separate plate material in front of a wedge tip and to bend flaps along inclined moving hinges. Equating the rate of external work, i.e. the product of wedge cutting force, F, and the corresponding moving velocity, V, to the rate of total internal energy dissipation yields:

$$FV = \dot{E}_b + \dot{E}_m , \tag{2-14}$$

where $\dot{E}_b$ and $\dot{E}_m$ are the bending and membrane energy rates, respectively. Note that the work loss due to friction is not a second order term and it will be taken into account in the next section.

The rates of bending energy and membrane energy have already been formulated in Eqs. (2-8) and (2-13), respectively. Substituting them into Eq. (2-14) and canceling the common term V on both sides of the equation, we obtain a closed-form solution for the transient indentation force as follows:

$$F = \frac{4}{\sqrt{3}} \sigma_o t^2 \left\{ \frac{1}{3} \cdot \frac{R}{t \cdot \sin\theta} + \frac{l^*}{4R} \right\} \cdot \tan\theta . \tag{2-15}$$

The above wedge cutting force expression is seen to be a direct function of the flap rolling radius, R, which is an unknown parameter yet to be determined. Postulating the actual resistance force adjusts itself so as to reach a minimum of Eq. (2-15). By minimizing F with respect to R, i.e. $dF/dR = 0$, we obtain the optimized rolling radius expression as:

$$R = \frac{1}{2}\sqrt{3\, t\, l^* \sin\theta} \approx 0.866\, t^{0.5} (l^*)^{0.5} (\sin\theta)^{0.5} . \tag{2-16}$$

Substituting the above equation back into Eq. (2-15), we get the optimized wedge cutting force expression as follows:

$$F = \frac{4}{3}\sigma_o t^{1.5} \left(l^*\right)^{0.5} \cdot \frac{(\sin\theta)^{0.5}}{\cos\theta} \cdot \tag{2-17}$$

2.5. Frictional force study

Friction has significant influences to a plate cutting process. It not only increases the wedge force needed to cut through a plate but also controls the deformed flap shape. For example, owing to the unbalanced frictional force existed in the out-of-plane direction, braided flaps are observed in tests for plate specimens with no title angle towards the cutting force direction [1]. During his wedge cutting tests, Lu [23] tried to use the unloading and re-loading technique to determine the frictional effects on the total wedge cutting force. It was found that the machining friction can seldom be reduced by the lubrication method and suggested that the total frictional force might significantly contribute to the total cutting force.

Careful study of frictional mechanisms reveals that there exist two distinct frictional forces in a wedge cutting process (Fig. 2-3). One is sliding friction existed between wedge surface and transient flaps, which is a normally encountered frictional effect. Wierzbicki and Thomas included the sliding friction in their analysis of transient wedge cutting force and correctly formulated the frictional force component [2]. The second frictional effect is a machining frictional force at a wedge tip, which has a much larger frictional coefficient than that of a simple sliding friction case but is limited to a very narrow region. The sliding frictional force increases with the advance of the wedge, but the machining friction remains a constant value under transient indentation process. Both frictional contributions will be added directly to the closed-form cutting force expression derived, Eq. (2-17). The effect of sliding friction is postulated to be in direct proportion to the corresponding force term in Eq. (2-15) producing flap bending along plastic moving hinges. The machining friction is an independent term which is governed purely by the problem geometry, such as plate

thickness, wedge angle, and plate tilt angle [28].

2.5.1. Sliding friction

The derivation of sliding frictional force, F_{fs}, follows exactly the same procedures proposed by Wierzbicki and Thomas [2]. This frictional force exists between wedge attack surfaces and transient flaps, and it acts in the out-of-plane direction which restrains the transient flap sliding movement. The velocity of this relative sliding movement is found to be equal to the wedge advancing velocity, V, and it is independent of wedge semi-angle, θ. The frictional coefficient, μ_s, is typically within a range 0.1~0.4 for the steel-to-steel dry sliding condition. If a plate tilt angle is greater than or equal to θ, the resultant sliding frictional force will have the same direction as the wedge advancing direction which will prevent any possible braided flap deformation. The sliding frictional force is assumed in direct proportion to the bending force expression, $F_b = \dot{E}_b / V$ defined in Eq. (2-13), because the physical model construction reveals that this friction can be introduced into the cutting mechanism mainly by the bending force acting in the normal direction of the wedge attack surface. (The membrane deformation force at a wedge tip is balanced internally by the near tip plastic zone so that it does not have any effect on the sliding friction.) Based on the assumption made, the sliding friction can be formulated as follows:

$$F_{fs} = \mu_s F_b \cot\theta \, . \tag{2-18}$$

Note that the frictional coefficient, μ_s, in Eq. (2-18) is not necessarily equal to the sliding frictional coefficient found in the literature but it can be liberated to include any additional sliding frictional effects found in tests which has not been covered so far. For instance, the scoring observed on the transient flap surface of Maxwell's specimens [12] will definitely increase the frictional coefficient value. Substituting the bending force expression, Eq. (2-13), into Eq. (2-18) yields the complete sliding frictional force equation:

$$F_{fs} = \mu_s \frac{\sigma_o t^2}{\sqrt{3}} \cdot \frac{l^*}{R}, \tag{2-19}$$

where the rolling radius, R, is an unknown parameter to be optimized later in this section.

2.5.2. Machining friction

During a cutting process, the plate material near a wedge tip is plastically deformed and separated by a wedge cutting edge. Since the cut material flows plastically near a wedge tip, the coefficient of machining friction is much higher than that of sliding friction [29]. Tests on tool machining mechanism [28] reveal that, near a wedge tip, there exists a close contact zone between wedge surface and cut plate material termed *rake face*. The rake face is confined in a limited area close to a wedge tip, and its length along the wedge surface is roughly around one to two times a plate thickness. Under slow cutting speed and by cutting through a ductile material such as mild steel, it is observed that the chipped material welds itself to the wedge tip at the rake face zone. Shear work is required to shear off the weaker of the two contact materials across the rake face, and its value is found to be independent of the normal force applied [28]. The energy needed to push the cut material across the rake face is so large that the energies required to form new surfaces in front of the wedge tip are generally insignificant so that they are neglected in the analysis [28]. The existence of rake face in a wedge cutting process is clearly shown in several wedges used in M.I.T. laboratory which exhibit a shiny, grounding-like, and narrow strip area along the wedge tip surface.

Because of the shearing mechanism involved in plate material movement on a rake face, the use of machining frictional coefficient, μ_m, is only a convenient way to handle all the complex phenomena behind it. At a rake face, the cutting process is very like a plane stress indentation problem with friction being present. Tests show that, for steel-to-steel machining friction, μ_m is within a range of 0.6~0.7 [23]. In the following analysis, it is assumed

that the material at rake face is fully yielded and the length of rake face is equal to $\zeta \cdot t$ where ζ represents the ratio of rake face length and plate thickness. Based upon the above analysis, the machining friction force can be formulated as (Fig. 2-4):

$$F_{fm} = 2\,\zeta\,\mu_m \cdot \left(\frac{2}{\sqrt{3}}\sigma_o\right) \cdot t^2 \cos\theta \ . \tag{2-20}$$

2.6. Transient indentation force including friction

Adding the sliding and machining frictional forces discussed in the previous section into the derived cutting force equation, Eq. (2-17), we get the final expression for the closed-form transient indentation force equation:

$$F_f = \frac{2}{\sqrt{3}}\sigma_o t^2 \, f_f(l^*, t, \theta) \ , \tag{2-21}$$

where the dimensionless coefficient including the frictional effects is formulated as

$$f_f(l^*, t, \theta) = \left[\frac{2}{3} \cdot \frac{R}{t\sin\theta} + \frac{l^*}{2R}(1 + \mu_s \cot\theta)\right] \cdot \tan\theta + 2\zeta\mu_m \cos\theta \ . \tag{2-22}$$

Postulating the actual wedge force required to cut through a plate adjusts itself so as to reach the minimum of Eq. (2-22). By minimizing f_f with respect to R, i.e. $df_f/dR = 0$, we obtain a final expression for the optimized rolling radius including friction as:

$$R = \frac{1}{2}\sqrt{3\,t\,l^*\,(1 + \mu_s \cot\theta)\,\sin\theta} \ . \tag{2-23}$$

Note that the above rolling radius equation is a general expression for Eq. (2-16), and it will be used solely in the following analysis.

Substituting the above equation back into Eq. (2-22), we get the optimized dimensionless

coefficient for the transient wedge cutting force including friction as follows:

$$f_f(l^*,t,\theta) = \left[2\sqrt{\frac{l^*(1+\mu_s\cot\theta)}{3t\sin\theta}} \right] \cdot \tan\theta + 2\zeta\mu_m\cos\theta \,. \tag{2-24}$$

2.7. Comparison with tearing model solution

Wierzbicki and Thomas [2] derived a similar transient indentation force based on the assumption that a fracture or split is existed in front of a wedge tip as follows:

$$F_w = \frac{2}{\sqrt{3}}\sigma_0 t^2 f_w(l^*,t,\theta) \,, \tag{2-25}$$

where the dimensionless coefficient including friction is given by

$$f_w(l^*,t,\theta) = 1.446\,(\bar{\delta}_t)^{0.2} \cdot \left(\frac{l^*}{t}\right)^{0.4} \cdot \frac{\tan\theta+\mu_s}{(\sin\theta)^{0.6}(\cos\theta)^{0.8}} \,, \tag{2-26}$$

In the above equation $\bar{\delta}_t$ is a dimensionless parameter which is defined as the COD (crack opening displacement) parameter normalized by the plate thickness, i.e. $\bar{\delta}_t = \delta_t / t$. It was assumed that this parameter is independent of the wedge indentation depth and it fully characterizes the rigid-plastic plane stress tearing of metal sheets. The estimated value for the parameter $\bar{\delta}_t$ is reported to be in the range of 0.1~1 depending on the material tested and plate thickness involved.

2.7.1. Cutting force *vs.* indentation length

By assuming that the sliding frictional coefficient is $\mu_s = 0.25$, the machining frictional

coefficient is $\mu_m = 0.6$, and the ratio of rake face length and plate thickness equals unity, a series of normalized curves is plotted for several values of wedge semi-angle, θ, correlating the wedge force with the indentation length (Fig. 2-5). From the diagrams, some interesting phenomena can be observed. For example, if a wedge semi-angle, θ, and/or the normalized indentation length, l^*/t, are small, there is a good chance that a direct cutting in front of a wedge tip will occur since the cutting model, Eq. (2-22), falls between a set of tearing model curves, Eq. (2-26), with $\bar{\delta}_t$ varying from 0.1 to 1. But one can never exclude the possibility of having a crack running in front of a wedge tip because of the complicated nature of the parameter $\bar{\delta}_t$, e.g. dural material [1] and thick steel plate [26] generally have lower $\bar{\delta}_t$ values than that of thin mild steel plate so that they tend to have a fracture instead of a pure cut in front of a wedge tip. For a large wedge semi-angle together with a large indentation length, a fracture will probably occur in front of a wedge tip because the cutting model, Eq. (2-22), yields a higher cutting force than that of the tearing one. Astrup [26] reported four thick plate wedge indentation experiments (two of them used 15 mm thick plates and the other two 20 mm from the same material) which showed a crack running in front of a wedge for one specimen and pure cutting for the rest of the specimens. For the specimen reported to have a fracture in front of a wedge tip, the test curve showed a second force drop during the cutting process (Fig. 2-11) which seldom happens under a normal test condition. This is partially due to the transition from the pure cutting process into a fracture failure near a wedge tip and partially due to the global inverse bending of the specimen. A careful study of the corresponding theoretical curves (Fig. 2-5b) shows that either failure modes, i.e. cutting or tearing failure in front of a wedge tip, can occur since there exists very little difference between the two failure curves when $l^*/t < 35$ and $\bar{\delta}_t = 1$.

2.7.2. Plastic zone size comparison

From the wedge cutting hypothesis, the normalized plastic zone depth expression in front of a wedge tip can be derived from Eqs. (2-3) and (2-16) as follows:

$$\frac{l_p}{t} = 0.866 \cdot \left(\frac{l^*}{t}\right)^{0.5} (\sin\theta)^{-0.5}. \tag{2-27}$$

Wierzbicki and Thomas [2] derived a similar plastic zone depth expression for the tearing model as

$$\frac{l_p}{t} = 1.30\,(\bar{\delta}_t)^{0.2} \cdot \left(\frac{l^*}{t}\right)^{0.4} (\cos\theta)^{-0.2} (\sin\theta)^{-0.6}. \tag{2-28}$$

Note that no frictional effect is included in the above equations for the sake of simplicity.

Fig. 2-6 is a series of normalized curves for several wedge semi-angle values correlating plastic zone depth with its corresponding indentation length. From those diagrams, the same phenomena as before can be observed. First, if a wedge semi-angle, θ, and/or the relative indentation length, l^*/t, are small, there will be a good chance that a direct cutting at a wedge tip will occur since Eq. (2-27) falls between a set of Eq. (2-28) curves with $\bar{\delta}_t$ varying from 0.1 to 1. Again one cannot exclude the possibility that a crack runs in front of a wedge tip because of the complicated nature of $\bar{\delta}_t$. Second, if a wedge semi-angle is large accompanied by a large relative indentation length, a tearing failure mode will probably occur in front of a wedge tip because Eq. (2-27) gives a larger plastic zone depth than that of the tearing model. Since the plastic zone near a wedge tip is a local deformation process, it is advisable not to use it as a guide for the actual failure mode interpretation. It is important to point out again that the size effect should never be neglected in the split model solution, Eq. (2-28).

Lu [23] did an experimental investigation of the plastic zone depth, l_p, near a wedge tip for a 20^o semi-angle wedge cutting through a 2 mm thick specimen. It was reported that the l_p/t ratio is around 7 for the wedge indentation depth equal to $l^* = 100$ mm. The corresponding theoretical prediction, Eq. (2-27), under the same conditions gives $l_p/t = 11$, which is in the same magnitude as the test result.

2.8. Experimental validation of the theoretical solutions

In Chapter 1, it has already been emphasized the importance of verifying the theoretical solutions by experiments. This is because all of the assumptions made in the current theory have both pros and cons to the final accuracy of the solution obtained. The only feasible approach to validate the current theory is to compare it with test results. Maxwell [12] made the first experimental investigation on the accuracy of the theoretical solutions towards the transient indentation process. Good correlations were observed from the tests on thin steel specimens with thickness ranging from 0.749 mm to 1.829 mm. The reader is referred to Maxwell's work for a full coverage of his experimental verification of the current theory presented above. Figs. 2-7, 2-8, and 2-9 are the reproduction of Maxwell's test curves accompanied with the theoretical transient force-displacement prediction. In addition to the Maxwell's work, three more experimental validations are provided here. Note that the frictional coefficients for sliding and machining frictions are difficult to determine from wedge indentation experiments. From the author's experience and engineering judgement, those coefficients are assumed to be $\mu_s = 0.25$ and $\mu_m = 0.6$ throughout the experimental validations.

The first experimental result presented here was performed by Lu and Calladine [1]. A "clean" cut of the transient wedge indentation was made through a thin plate by a triangu-

lar shaped wedge with a plate thickness of 0.9 mm and a wedge semi-angle of 20^{o}. The specimen had a tilt angle of 10^{o} angle to the wedge advancing direction so that the alternative folding deformation can be suppressed [2]. Fig. 2-10 shows a comparison of the theoretical solutions with the test result. Since the specimen had no pre-cut in front of a wedge, the first peak load shown in the force-displacement test curve represents a transition from initial plate bending deformation to actual transient indentation. During the first one-third of the cutting process, both theoretical solutions discussed above give reasonable predictions to the wedge force and indentation length relationship. But the remaining two-thirds of the theoretical curves give higher wedge force values than that observed from the test. This softening effect exhibited in the test is probably caused by the global out-of-plane flexibility existed in the thin specimen.

The second and third experimental results were obtained by Astrup [26]. Both tests had the same test set-up and were intended to obtain duplicated results on the transient indentation through thick plates. A "clean" cut was observed in test No. P1-15 by using a triangular shaped wedge with a plate thickness of 15 mm and a wedge semi-angle of 30^{o}. The specimen had a tilt angle of 10^{o} to the wedge advancing direction so that the flaps will be formed on one side of the plate only [2]. However, test No. P2-15 showed an alternative braided flap deformation pattern. This is because that the plate tilt angle is probably not large enough so that the out-of-plane frictional force could not be counteracted in this case. Both specimens were seen to have a large, global out-of-plane deformation pattern which contributes an additional bending energy term to the total energy rate expression. For thick plates, the contribution of this global bending energy is significant compared to all other deformation energies. That is why the test curves exhibit steep slopes than those from the theoretical solutions because the current theory does not take the global bending deformation into account (Fig. 2-11). Although differences are observed in Fig. 2-11, a comparison of those curves shows that the theory captures the main features of the transient indentation

characteristics.

The experimental validations presented so far confirm the correctness of the current theoretical solutions for a wide range of plate thickness and wedge semi-angle. Size effect has been captured by the theory.

2.9. Discussions and conclusions

A theoretical analysis for the transient indentation process is performed in this chapter with a closed-form solution derived. For the complete theory of the transient indentation analysis, two hypotheses are presented in the literature covering all the possible failure modes in front of a wedge tip, i.e. tearing and cutting failure modes. Both assumptions are proved to be valid depending on the controlling parameters of an actual problem. For example, a large wedge semi-angle and certain brittle material might have a tearing failure in front of a wedge tip during a transient indentation. Also, a transformation from cutting to tearing failure may happen for a deep wedge indentation even though a wedge semi-angle is small. But, for the majority of the transient indentation problem, cutting failure is dominant at a wedge tip.

Comparisons between the two kinematic models show that a cutting failure in front of a wedge tip is most probable when a small indentation depth and/or a sharp wedge is used, whereas a tearing failure may happen for a deep indentation and/or a dull wedge.

The current theory deals with the case of wedge indentation through an infinitely wide plate only, which implies that the flaps can curl freely. If stiffeners are presented in a specimen, the bent-up flaps may be caught up by the reinforcements which will definitely introduce a sudden rise of the indentation force because of the additional deformation energy introduced into the system. Little [18] and Paik [34] observed such failure mode from their experiments. Modifications of the current theory are needed to handle this special case.

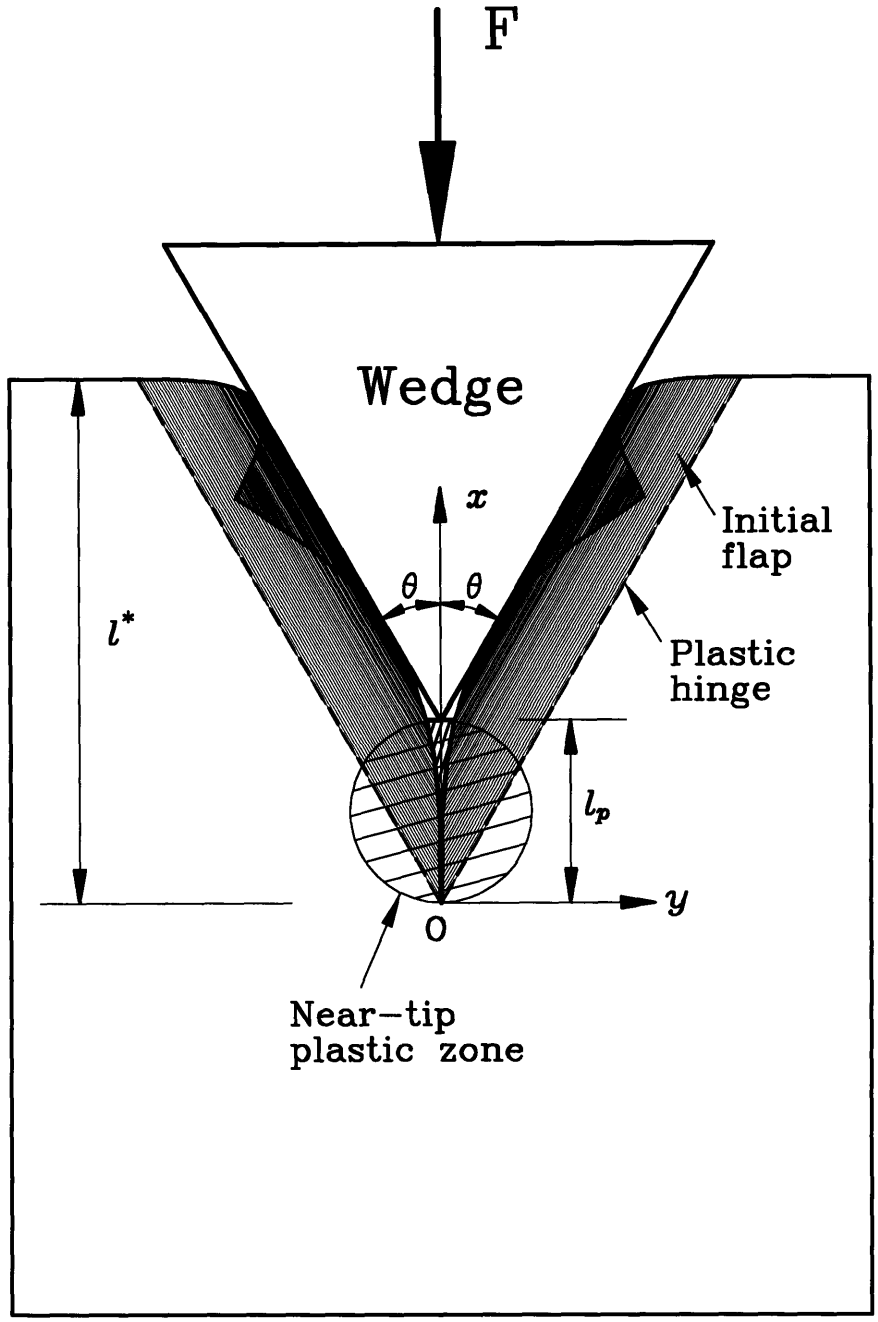

Fig. 2-1 Kinematic model for transient wedge indentation

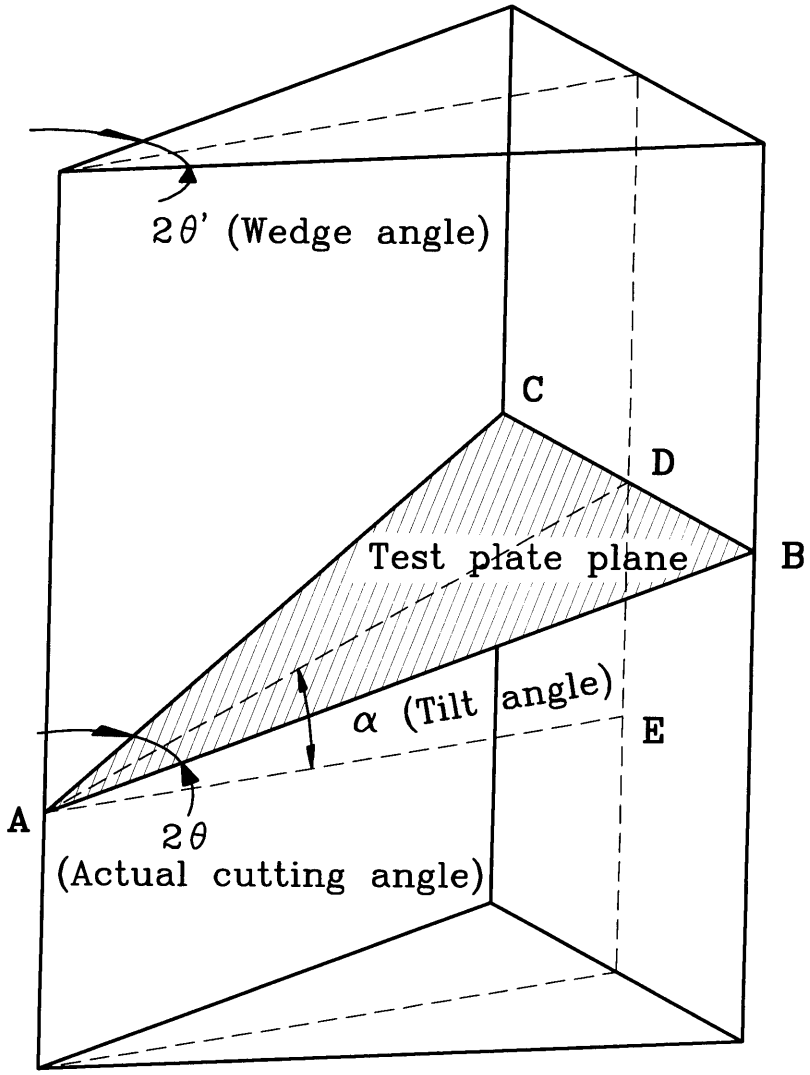

$$AD = AE / \cos\alpha$$
$$BD = AE \cdot \tan\theta'$$
$$\tan\theta = BD / AD$$
$$\tan\theta = \tan\theta' \cdot \cos\alpha$$

Fig. 2-2 Wedge angle projected on tilt plate, θ

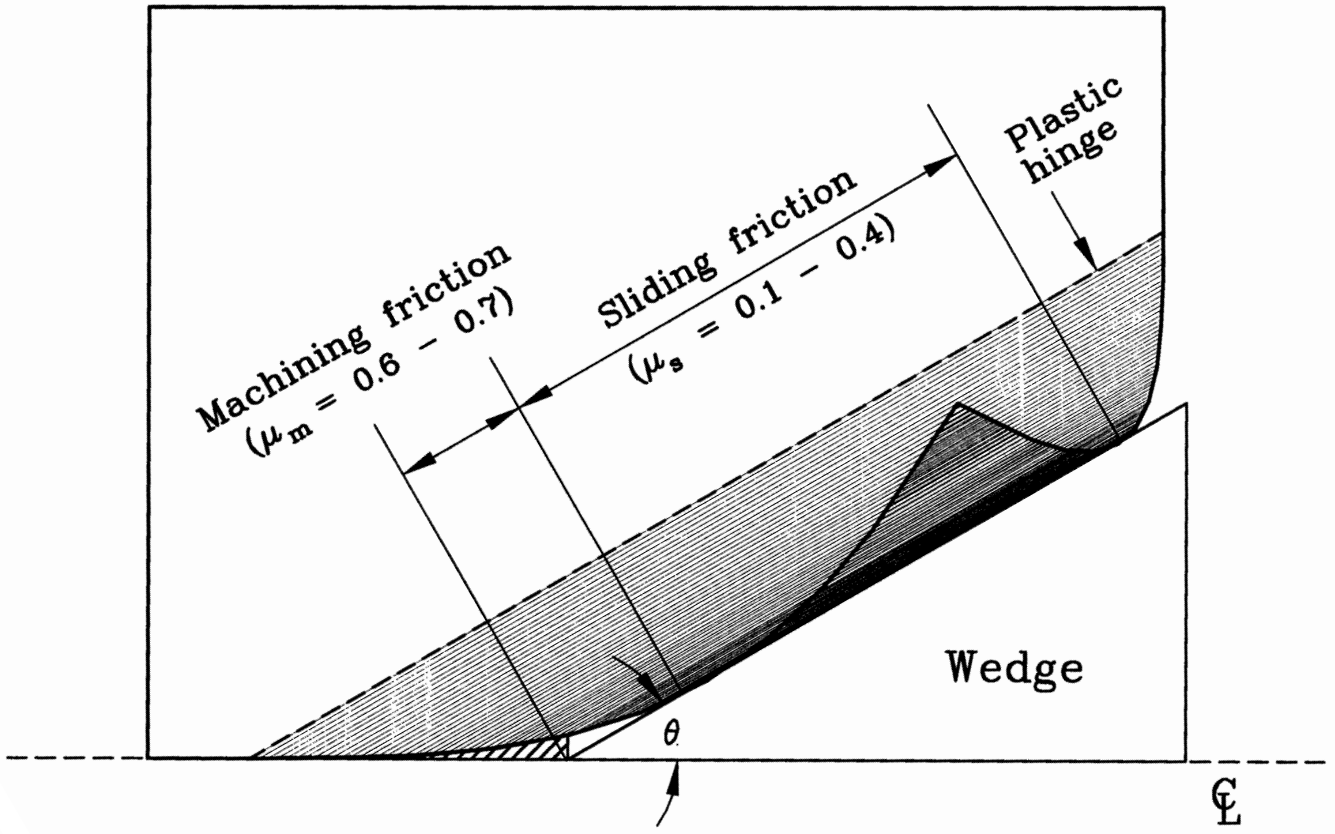

Fig. 2-3 Friction in wedge cutting process

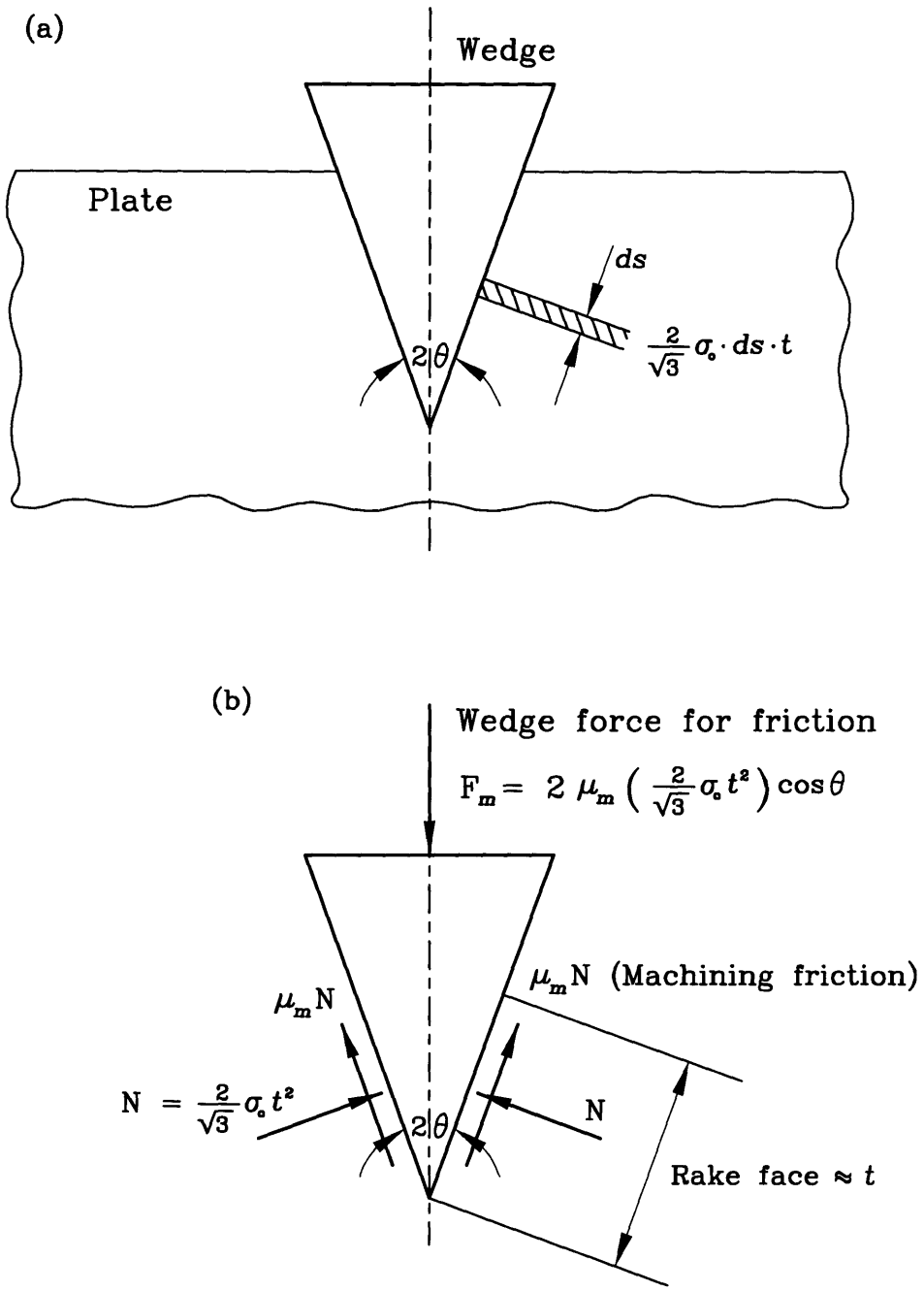

Fig. 2-4 Machining friction near a wedge tip

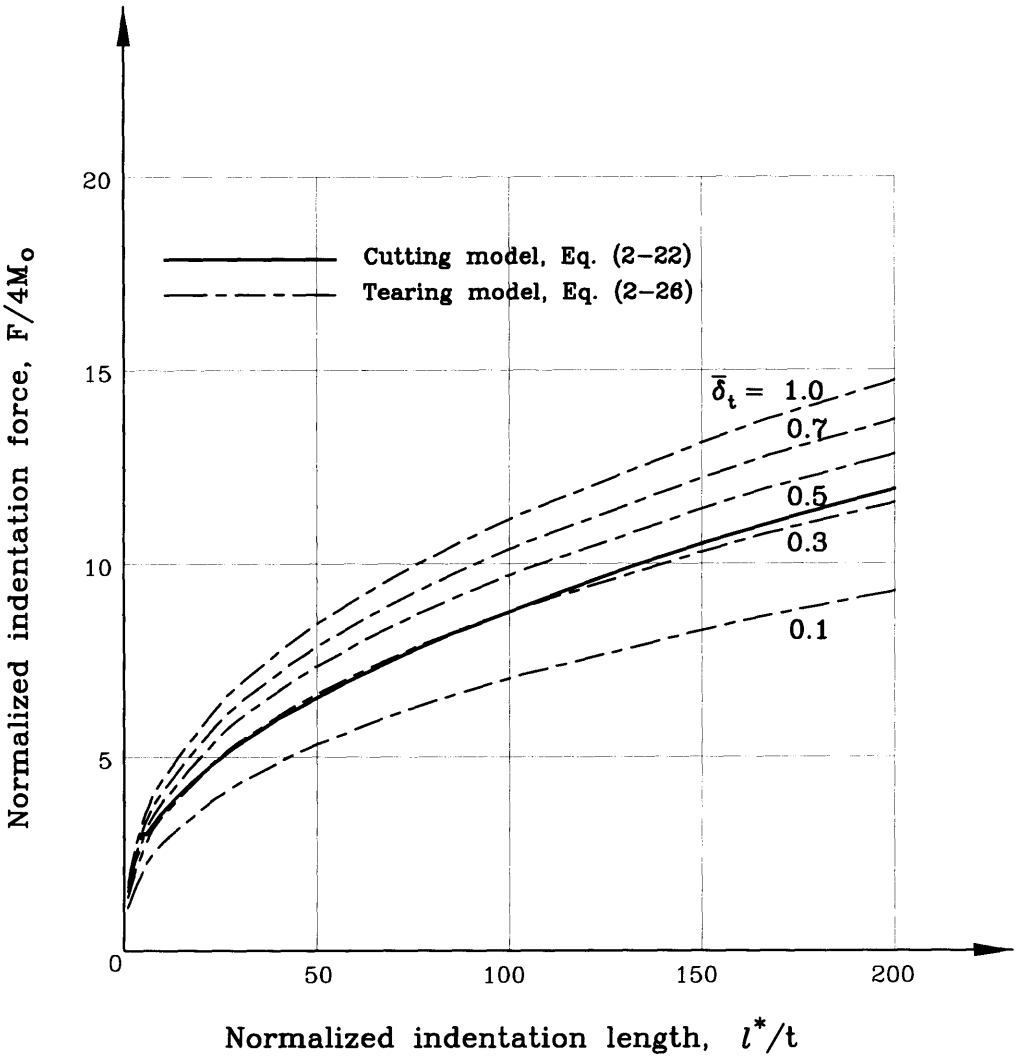

Fig. 2-5 (a) Normalized curve relating cutting force and indentation length for $\theta = 10^o$

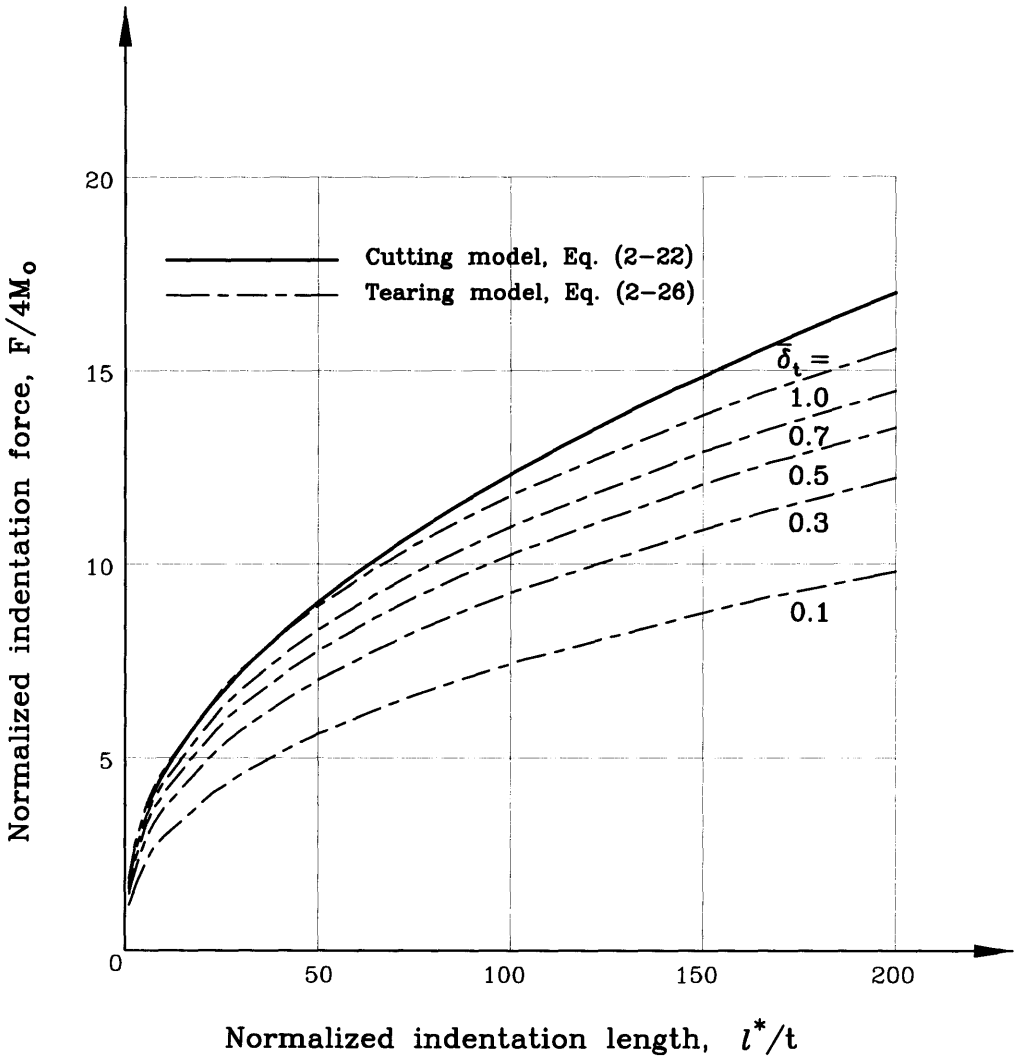

Fig. 2-5 (b) Normalized curve relating cutting force and indentation length for $\theta = 30^o$

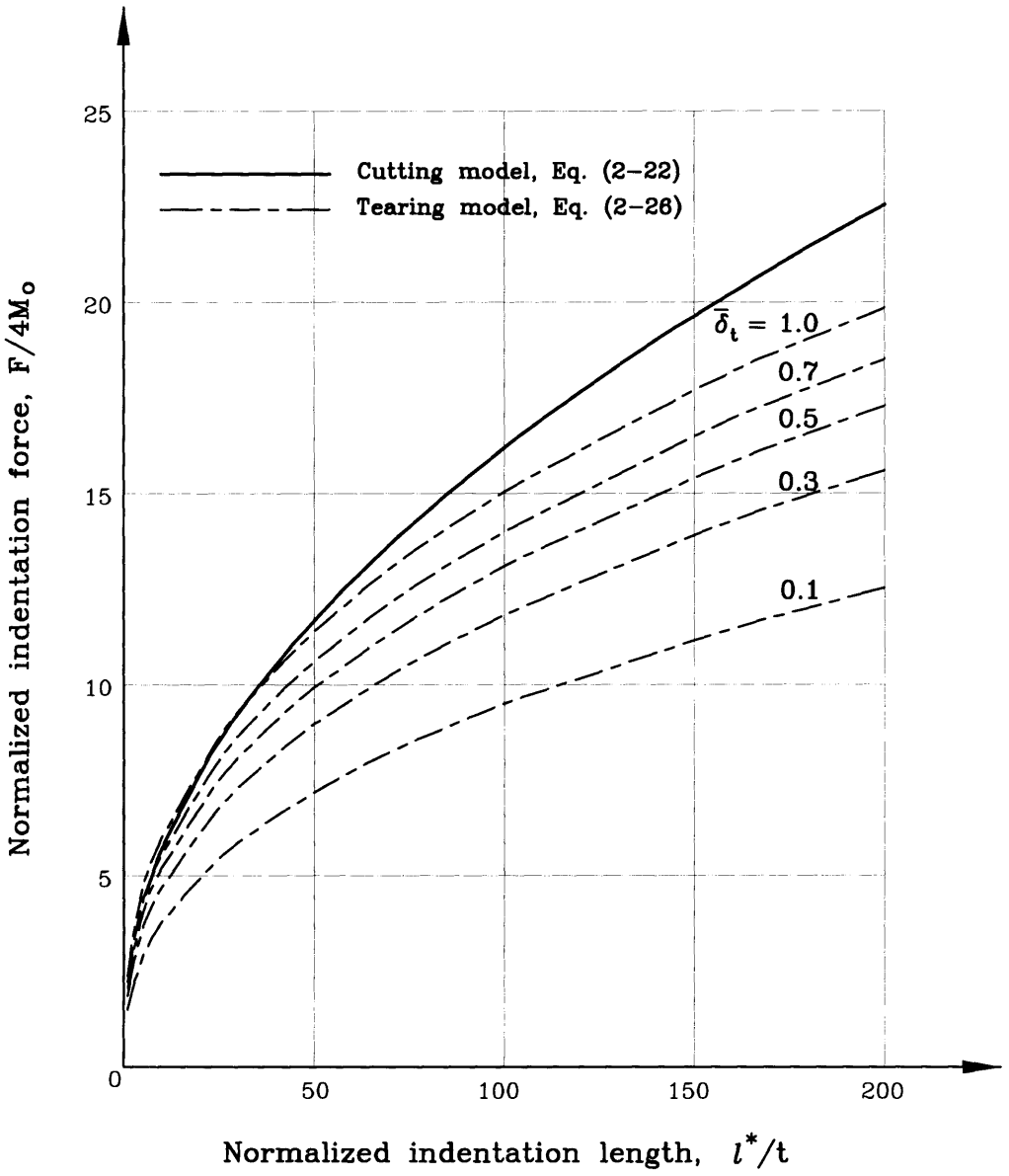

Fig. 2-5 (c) Normalized curve relating cutting force and indentation length for $\theta = 45^o$

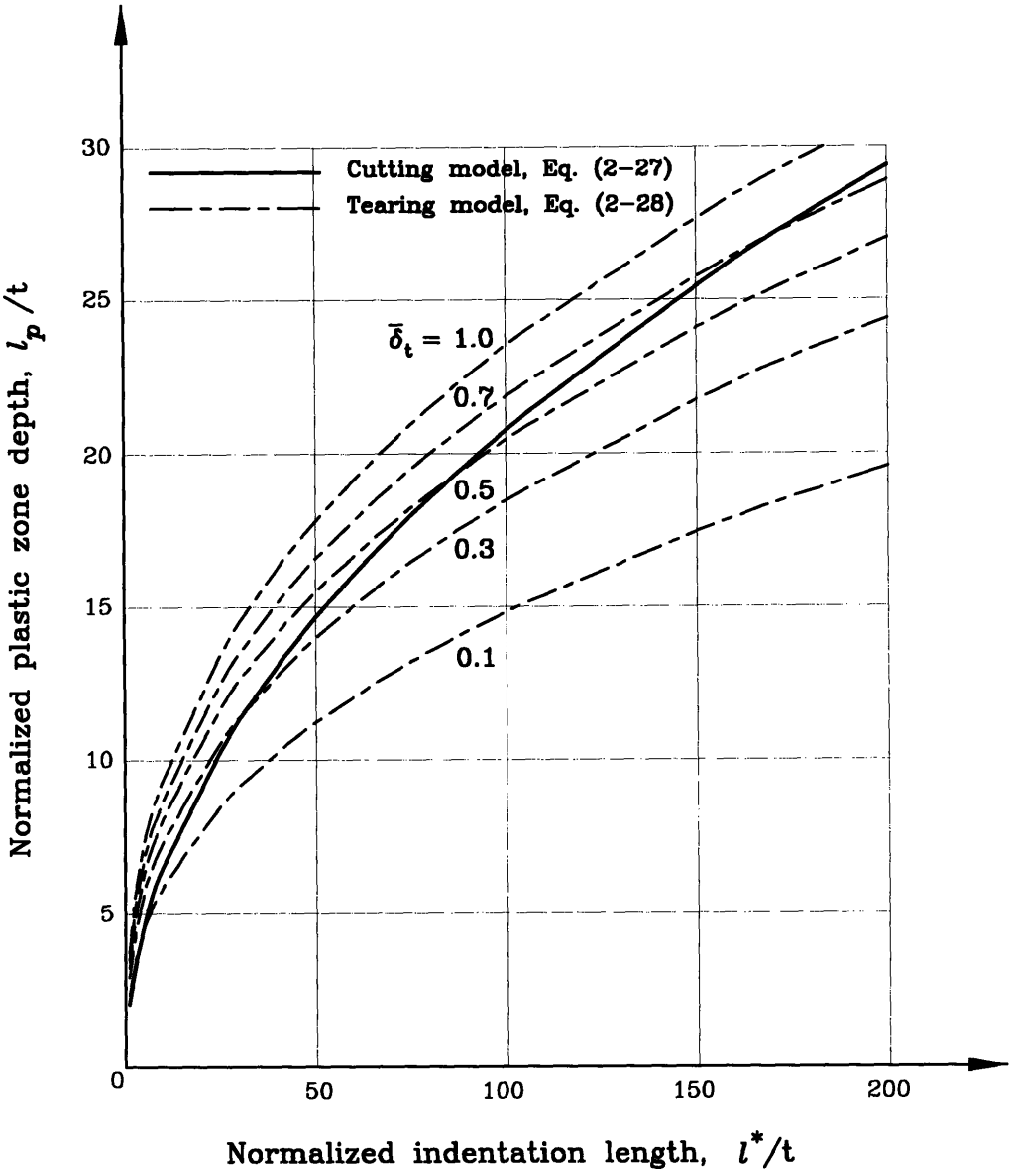

Fig. 2-6 (a) Normalized curve relating plastic zone depth and indentation length for $\theta = 10^o$

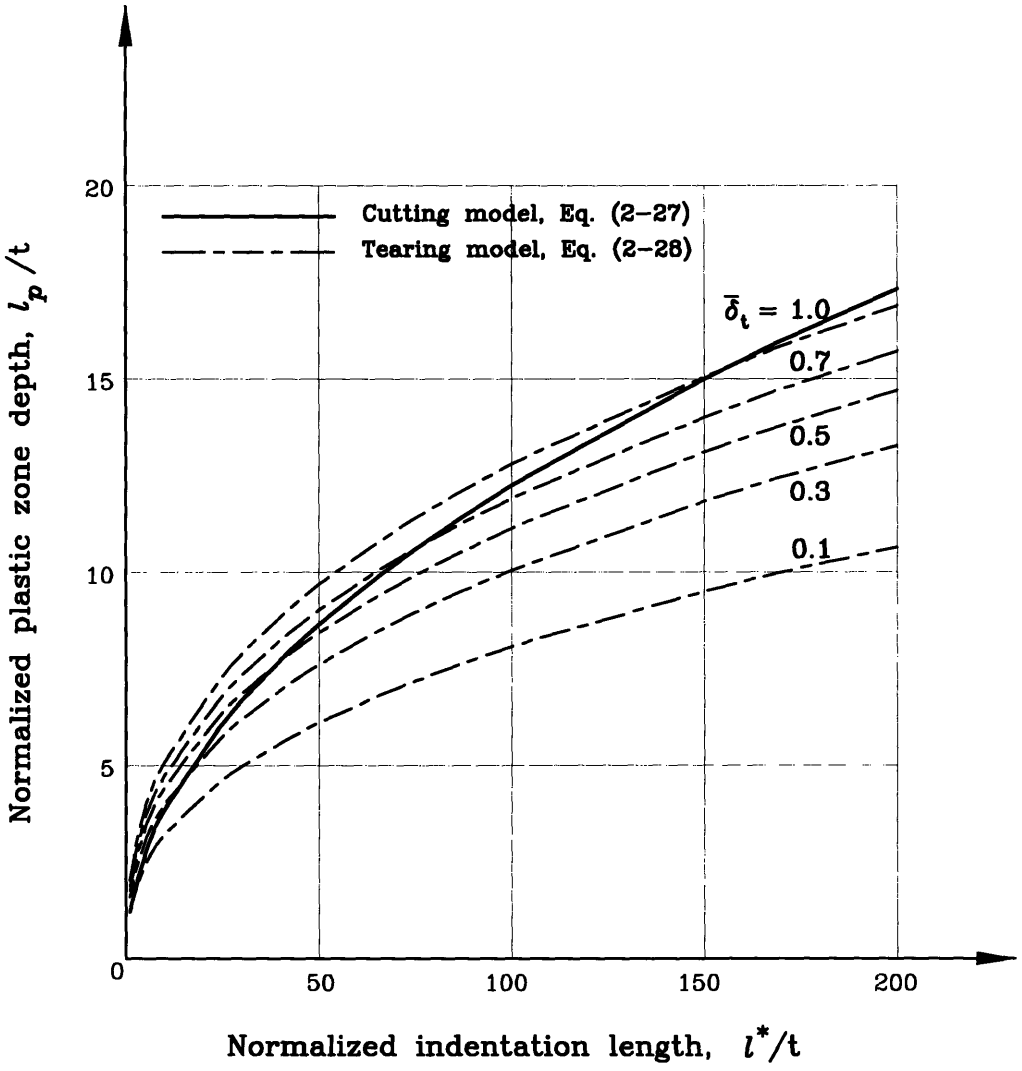

Fig. 2-6 (b) Normalized curve relating plastic zone depth and indentation length for $\theta = 30^o$

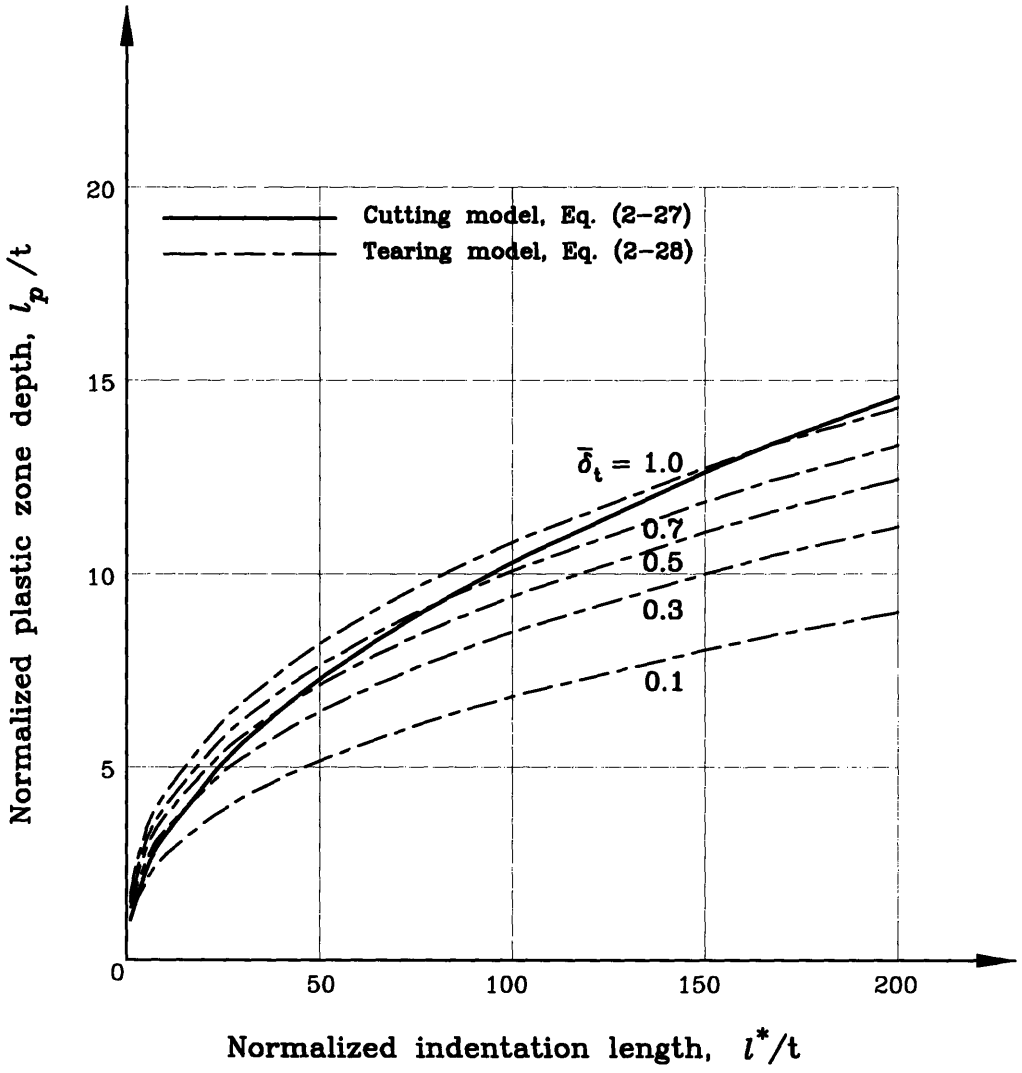

Fig. 2-6 (c) Normalized curve relating plastic zone depth and indentation length for $\theta = 45^o$

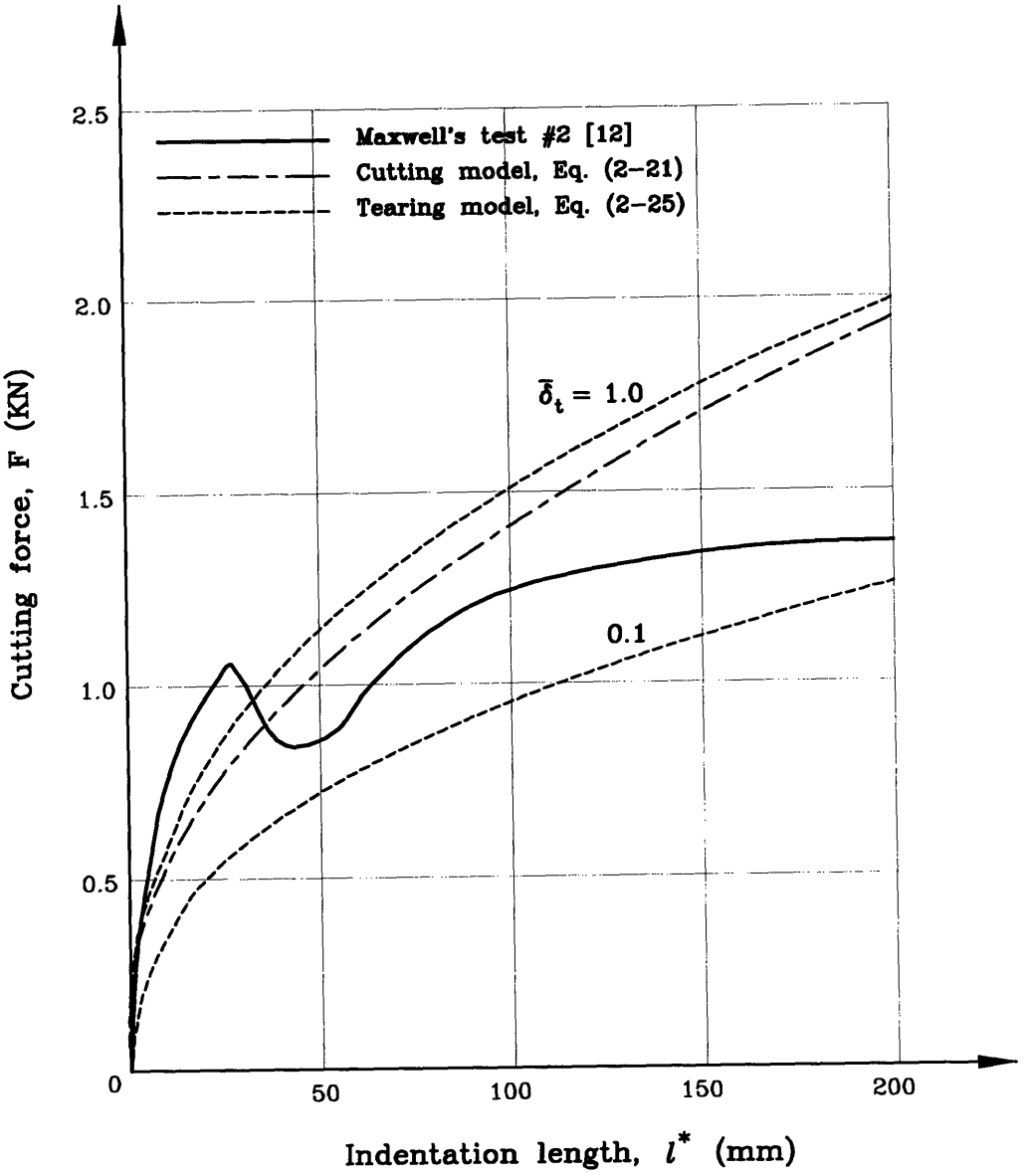

Fig. 2-7 Comparison of experimental *vs.* theoretical transient indentation force results for $\theta = 20^\circ$, $\alpha = 20^\circ$, $t = 0.749$ mm, and $\sigma_o = 187$ MPa

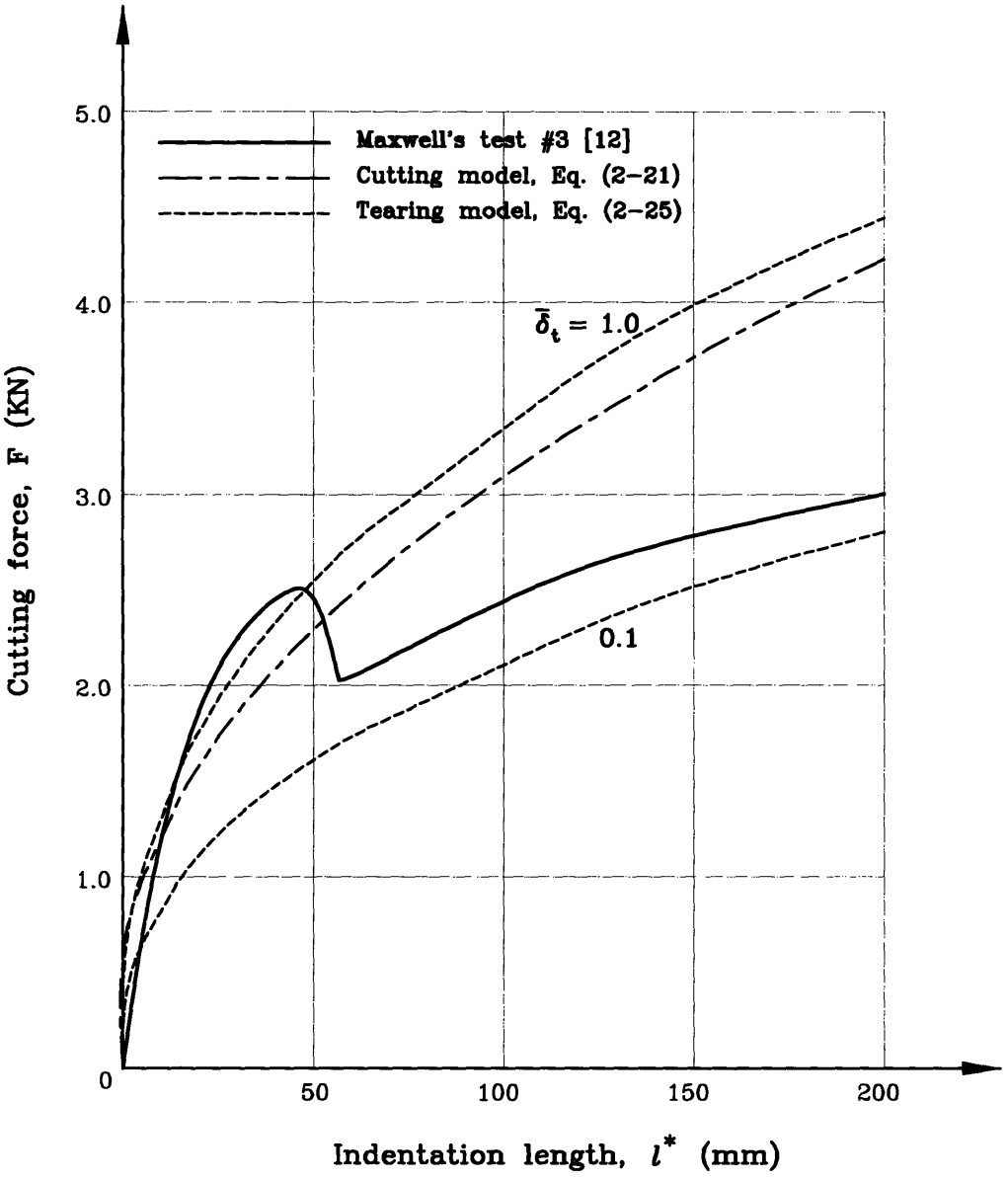

Fig. 2-8 Comparison of experimental *vs.* theoretical transient indentation force results for $\theta = 20^{\circ}$, $\alpha = 20^{\circ}$, $t = 1.143$ mm, and $\sigma_o = 212$ MPa

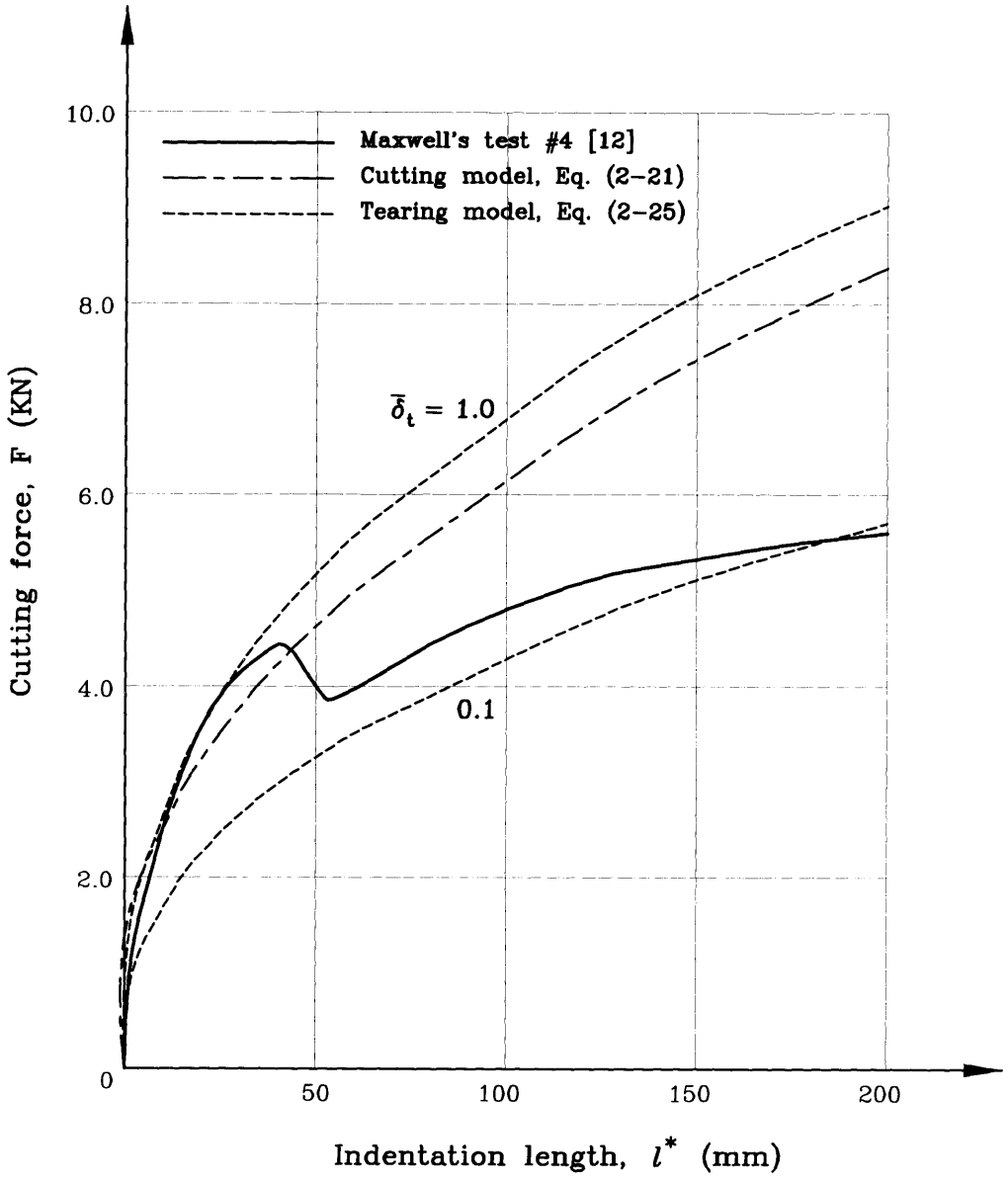

Fig. 2-9 Comparison of experimental *vs.* theoretical transient indentation force results for $\theta = 20^{\circ}$, $\alpha = 20^{\circ}$, $t = 1.829$ mm, and $\sigma_o = 203$ MPa

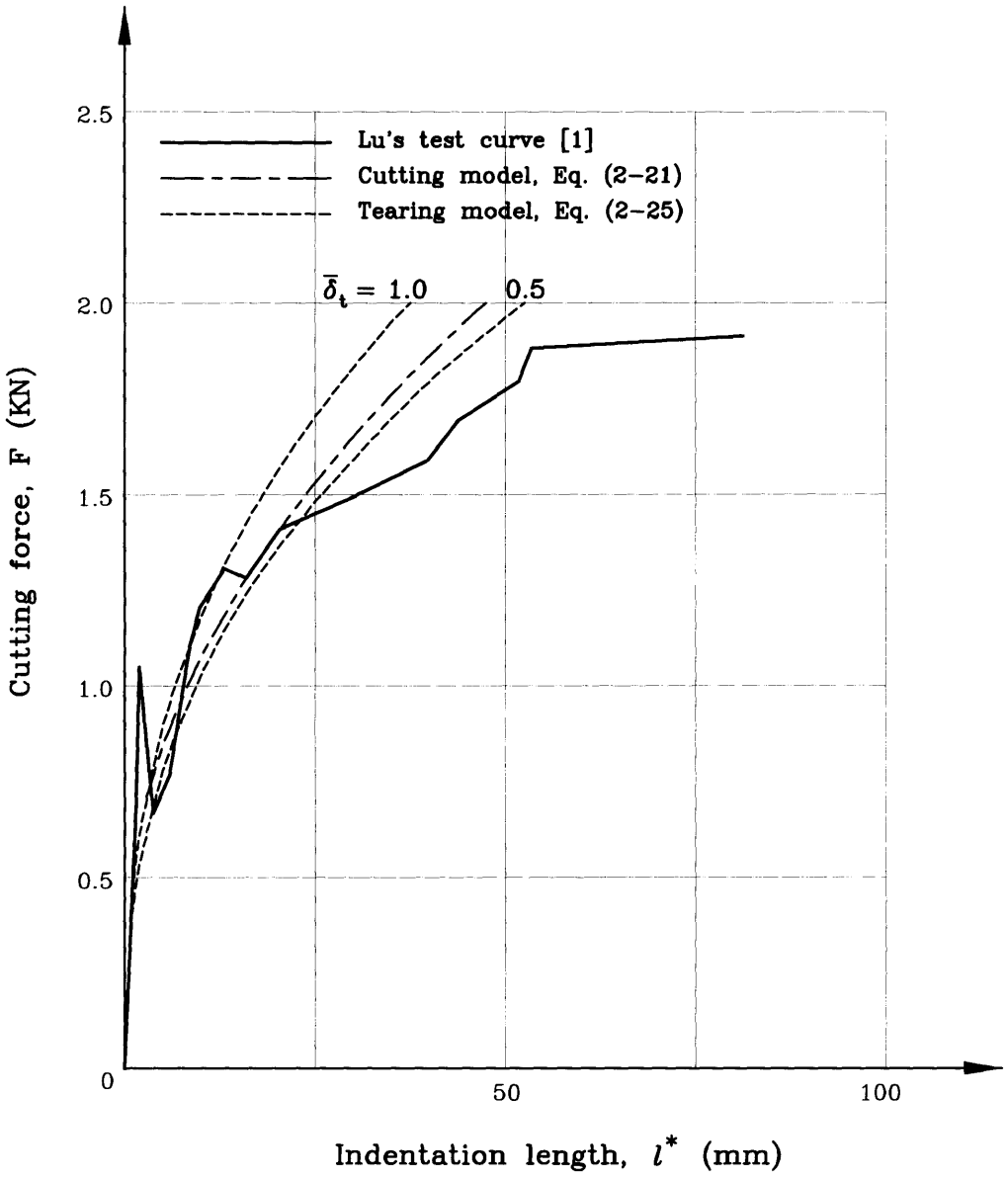

Fig. 2-10 Comparison of experimental *vs.* theoretical transient indentation force results for $\theta = 20^{o}$, $\alpha = 10^{o}$, $t = 0.9$ mm, and $\sigma_o = 272$ MPa

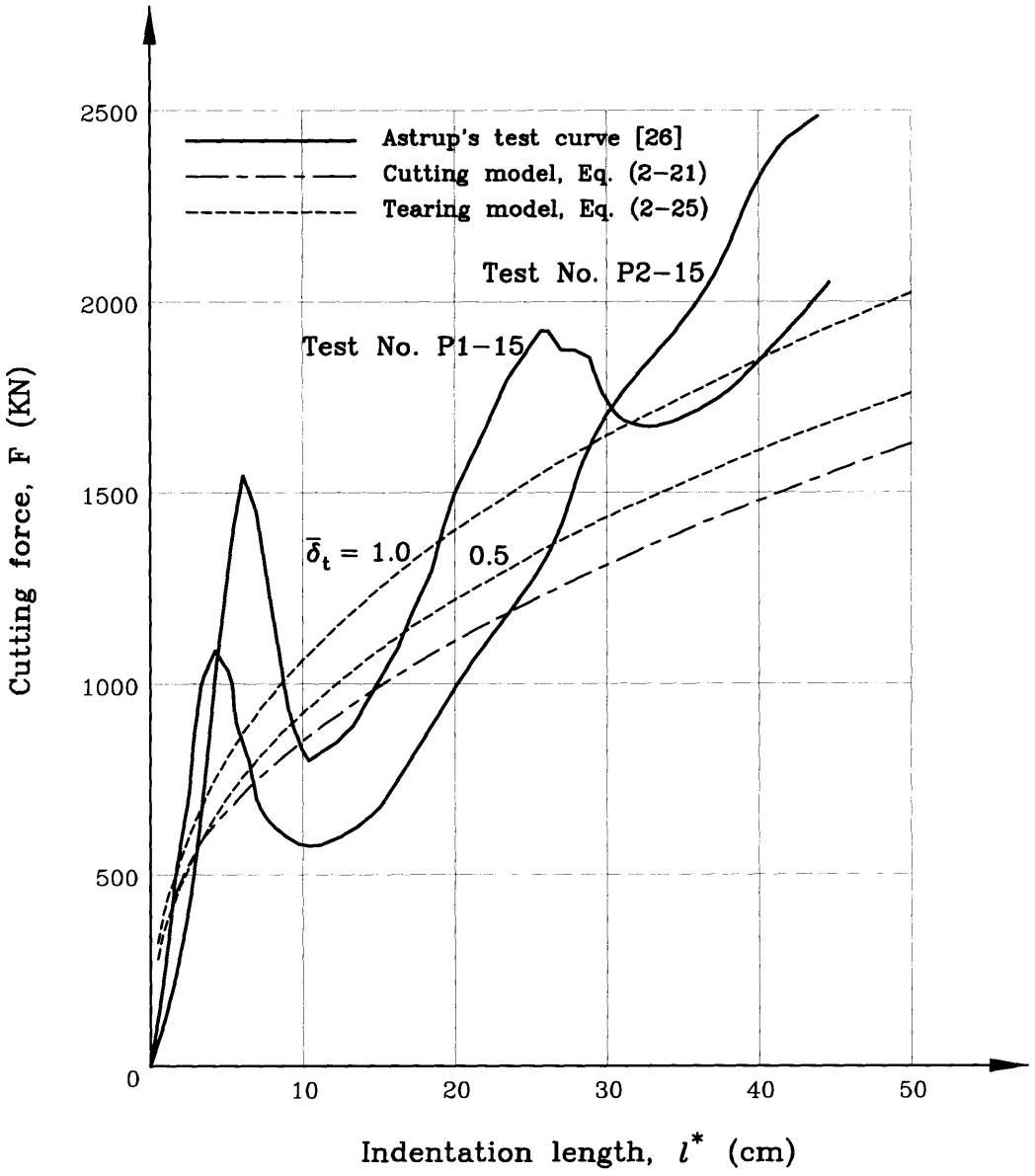

Fig. 2-11 Comparison of experimental *vs.* theoretical transient indentation force results for $\theta = 30^{\circ}$, $\alpha = 10^{\circ}$, $t = 15$ mm, and $\sigma_o = 417$ MPa with two specimens cut simultaneously

Chapter 3

Theoretical Study of steady-state wedge cutting process

3.1. Introduction

In this chapter, theoretical study on a steady-state wedge cutting through a wide plate are performed based on the observations of typical test results and simple physical model constructions. The analysis is aimed to model the actual ship hull grounding damage scenario when a ship is aground upon a sharp undersea rock and its hull is cut through under a relatively constant speed. Closed-form solutions of the problem are derived in this chapter by first equating the total internal energy rate to the external work rate and then minimizing the rate of internal energy dissipation. In Chapter 5, the theoretical results are to be compared with the small and large scale experimental results to validate the accuracy of the theory. The phenomena of a steady-state wedge cutting were observed and reported by many experimenters, including Lu and Calladine [1], Yahiaoui *et al.* [14], and Astrup [26]. The complex nature of the problem clearly transpires from a careful inspection of the experimental results, which mainly involves a central separation of the plate material and the formation of steady-state flaps bent on one side of the plate plane.

The steady-state wedge cutting process should be clearly distinguished from the transient wedge indention process studied extensively in Chapter 2, because the steady-state failure mode is much more complicated than the previous case. In addition to the deformations found from a typical transient indentation process, the steady-state failure is seen to have a unique deformation pattern: membrane tension and compression deformations in the flap transition zones shown in Fig. 3-1.

Two kinematic models for the steady-state cutting process are proposed here in order to

capture the typical failure modes observed from different test results. Our first model, termed curling flap model, assumes that a flap is composed of two cylindrical surfaces connected smoothly by a toroidal transition zone (shaded area in Fig. 3-4a). The second model, called upright flap model, consists of three flat bent-up segments for one flap with a triangular-shaped transition zone (Fig. 3-4b). Both models have their merits, i.e. one kinematic model might give a better failure prediction than the other in certain cases as will be seen in the sequel. For example, the first model gives good results for cases when a wedge angle is acute and the B/t ratio (ratio of wedge half shoulder width to plate thickness) is small, whereas the second model is mainly used for analyzing a blunt wedge cutting process. Comparing the mathematical involvement encountered in both models, the curling flap model requires more computational efforts, while the upright flap model leads to a simple algebra.

In this chapter, the closed-form solutions for a steady-state indentation process are derived for both of the kinematic models presented above. The theoretical analysis involves primarily the following steps: (i) establishment of kinematically admissible models for the steady-state cutting process; (ii) calculation of energy dissipation rates corresponding to each individual deformation mechanisms; (iii) derivation of closed-form cutting force expressions for each kinematic model by applying the energy postulation discussed above; and (iv) adding frictional effects into the closed-form solutions. The validation of the analytical solutions and the corresponding kinematics with typical experimental results are presented in Chapter 5.

3.2. Characteristics of steady-state wedge cutting process

Under a steady-state wedge cutting process, a plate is first separated at a wedge tip and then curls up into two flaps on both sides of the wedge attack surfaces. A typical "clean" cut

implies that the curling flaps bend only on one side of the plate plane, i.e. no braided flap deformations (Fig. 3-3) are allowed. As in the case of a transient cutting process, the transient flaps undergo bending along two inclined plastic moving hinges. In order for a steady-state wedge cutting process to initiate, a wedge must have a limited width, which yields either a triangular-shaped or a shouldered wedge. Under a steady-state indentation process, the transient flaps have been stretched significantly in order to form a transition zone which smoothly connects the transient and stable flaps (Fig. 3-5). By a careful examination of cut specimens and a simple physical model construction, two kinematic models are proposed: curling and upright flap models (Fig. 3-4), which is meant to capture the characteristics of the steady-state cutting process from the different point of view. The kinematic models assume a close contact existed between the stable flaps and the wedge shoulder surfaces, but this restriction can be easily relaxed. In the following analysis, friction is considered to be independent to the steady-state cutting force derivation and it will be included after the primary cutting force expressions have been derived.

3.3. Steady-state cutting analysis using curling flap model

This section analyzes the curling flap model (Fig. 3-4a) theoretically with a closed-form solution of the steady-state wedge force derived.

3.3.1. Plastic zone near a wedge tip

In all the experiments performed at M.I.T. with a sharp wedge of a semi-angle $\theta = 30^{o}$ or $\theta = 45^{o}$, it is observed that a wedge tip is always in direct contact with the plate specimens (Maxwell [12], Yahiaoui *et al.* [14], Trauth [20], and Thomas [22]). Such a situation is referred to as plate cutting as opposed to plate fracture and/or tearing where a wedge force

is applied at a remote location causing fracture process in front of a wedge tip. Accordingly, it is assumed in the current model that a wedge tip coincides with a plate crack, which is confirmed experimentally by many mild metal specimens [1]. The large stress and strain observed near a wedge tip generally cause the plate material to yield around a wedge tip. The shape and size of a near-tip plastic zone was measured experimentally and reported by Lu [23]. His test results showed that a finite area surrounding a wedge tip undergoes a membrane deformation under the in-plane plastic flow. (Note that a part of the plastic zone in Lu's test photograph is due to the machining process to be discussed in Section 3.3.10.)

The plastic zone depth along the wedge advancing direction is denoted as l_p (Fig. 3-5). Lu measured from his specimens that the l_p value is around seven times of the plate thickness for a wedge semi-angle equal to 20^o with a plate tilt angle 20^o. It is believed that the plastic zone size varies according to the controlling geometric parameters like wedge shape, plate thickness, and inclination angle; although, under a given steady-state cutting condition, l_p will remain constant. Based on the physical model construction, it is assumed that the near-tip plastic zone on a plate is extended from a wedge tip to the intersection of two inclined transient plastic hinges having a depth (Fig. 3-6):

$$l_p = \frac{R}{\sin\theta}, \tag{3-1}$$

where R is a constant rolling radius of the curling flaps to be discussed below, and θ is a wedge semi-angle. Note that the above equation does not explicitly take plate inclination into account. But it implies that, with the increment of a plate tilt angle, the near-tip plastic zone depth increases accordingly. This is because, in reality, θ should be calculated by a wedge angle projected on the plate plane (Fig. 3-16) which produces a smaller angle than the actual wedge angle. This, in turn, yields a larger plastic zone size according to Eq. (3-1). Since the plastic zone size is confined to the range only several plate thickness long, it

is safe to neglect the bending deformation induced by the eccentricity of a wedge force in that zone. To further simplify our analysis, it is assumed that the plate tilt angle is zero, which can be easily corrected by using the wedge angle projection method discussed.

In a near-tip plastic zone, the membrane deformation rate in the direction normal to the cutting velocity was analyzed by Wierzbicki and Thomas [2]. By considering the compatibility of the transverse displacement and velocity fields, they derived a simplified expression for the separation velocity near a wedge tip as follows:

$$v_x \equiv 0,$$

$$v_y = \begin{cases} V\tan\theta\left(\dfrac{x}{l_p}\right)^2, & \text{for } x \le l_p, \\ V\tan\theta, & \text{for } x > l_p, \end{cases} \tag{3-2}$$

where V is the wedge advancing velocity, and x is the coordinate along x-axis with its origin at the intersection of two inclined moving hinges as shown in Fig. 3-5.

For a very blunt wedge, such as a wedge having a semi-circular shape, a crack can be initiated and run in front of a wedge tip. This has been clearly demonstrated in one of the tests run by Maxwell [12]. The case with a crack running ahead of a wedge tip was studied theoretically by Wierzbicki and Thomas [2]. It was found that the size of a near-tip plastic zone is controlled by the Crack Tip Opening Displacement (CTOD) parameter δ_t. From their study, it can be concluded that the dependence of the wedge indentation force on the magnitude of δ_t was very weak.

The question whether a wedge indentation leads to a cutting or fracture failure has been subjected to a debate in the literature. Atkins [24] argued for the latter viewpoint while Lu and Calladine [1] and Calladine [25] defended the former. We believe that either situation can develop, depending on the scale of the problem. As already mentioned, in all thin and mild steel plates up to the thickness of t = 2 mm, no cracks were found at a wedge tip.

However, for the intermediate scale experiments conducted at the DnV facility in Bergen on plates with $t = 15$ mm, cracks were clearly seen in front of the wedge tip [26].

3.3.2. Kinematics of transient flaps

When transient flaps bend up on both sides of a wedge, they form instantaneous cylindrical surfaces. It was argued [2] that it is highly unlikely that other geometric shapes, e.g. double curvature flaps or conical flaps, are able to develope because the former would require a considerable membrane deformation in addition to bending which would greatly increase the amount of energy involved, while the latter would cause the wedge to lose contact with flap surfaces which is contrary to experimental observations. The radius of the cylindrical surface is denoted by R. This so-called "rolling radius" R is an increasing function of the wedge indentation length in the transient indentation process [2] but remains a constant under the steady-state cutting process. The center line for a cylindrical transient flap is located at a distance R from the original plate plane, and the angle between the center line and the wedge indentation direction is equal to the wedge semi-angle, θ (Fig. 3-4a). The inclined plastic moving hinge line of a transient flap lies in the original plate plane and is parallel to the center line of the cylindrical transient flap. It was observed from the experiments that the plastic hinge moves at the same speed as that of a wedge advancement, V.

3.3.3. Kinematics of stable flaps

The construction of a curling flap model for a steady-state cutting process is based on the assumption that the stable flaps deform into a cylindrical surface and have the same radius as that of a transient flap. The boundary between the stable cylindrical flaps and the undeformed plate lies in the original plate plane which is a straight line parallel to the wedge advance direction. The radius of the stable flaps, R, is an unknown parameter of the problem to be determined in the course of the solution. As shown in Fig. 3-5, a stable flap is

assumed to have a direct contact with a wedge shoulder surface which is not always true from experimental observations. Fortunately, it is easy to incorporate such a phenomenon into the derived closed-form wedge force solution by using the actual stable flap opening dimension in place of the wedge shoulder width $2B$.

3.3.4. Kinematics of transition zone

In all the reported steady-state cutting experiments, it is seen that there exists a smoothly curved transition zone connecting the cylindrical surfaces of the transient and stable flaps. This transition zone has a double curvature surface (a segment of the toroidal surface) and its small toroidal radius must be equal to the rolling radius R of both transient and stable flaps. According to the physical model construction, it is found that the membrane deformations are induced in the transition zone by first stretching the transient flap in order to form the transition zone surface and then compressing the transition zone material back into zero size to conform the stable flap geometry. Depending on the controlling parameters of a problem, this large in-plane compressive force might cause the plate structure in the stable flap region to buckle. Periodical buckling wave forms along stable flaps are observed in several steady-state cutting specimens (Fig. 3-2). The process of first stretching then compressing the flap material under a steady-state wedge indentation process has not been documented in any literature dealing with the plate cutting problems so far. In the following analysis, the geometry and the membrane deformation energy inside the transition zone will be studied in the following sections.

3.3.5. Simplification of transition zone geometry

The geometry of a toroidal surfaced transition zone will definitely lead to a very complicated mathematical computation without the guarantee of additional accuracy. Therefore, it is a good idea to simplify the transition zone geometry in the first place. By acknowledg-

ing the fact that the principle of virtual work usually gives an upper bound solution, it can reasonably be assumed that the transition zone is simply constructed by a family of straight lines connecting the corresponding points on both sides of the transient and stable flap boundaries (Fig. 3-6). This hypothesis will definitely underestimate the internal deformation energy with a second-order error, but it greatly simplifies the mathematical computations encountered in the analysis. Part of the deformation energy relieved due to the adoption of the approximate transition zone proposed will be compensated by the overestimation of other deformation energies discussed later. But the validity of this geometry simplification can only be checked by experimental results which will be discussed in Chapter 5.

The distance, u, representing the straight line length inside the approximate transition zone and the amount of transient flap stretching, is calculated in Appendix A. Its mathematical expression has the following form:

$$u = R \cdot Q, \tag{3-3}$$

in which the dimensionless coefficient, Q, is formulated as

$$Q = \sqrt{[\cos\phi - \cos(C\phi)]^2 + [\sin\phi - C\sin(C\phi) - S^2\phi]^2 + S^2[C\phi - \sin(C\phi)]^2},$$

where $C = \cos\theta$ and $S = \sin\theta$. Note that this distance expression is in direct proportion to the rolling radius, R. A parametric study also reveals that u is approximately in direct proportion to a wedge semi-angle, θ, but it is a parabolic function of the rolling angle, ϕ. Based on the parametric study results, Eq. (3-3) can be approximated as

$$u = 0.32R\theta\phi^2. \tag{3-4}$$

Eq. (3-4) is compared graphically with its original form in Fig. 3-7 for ϕ in a range from 0 to 180°. When a wedge semi-angle, θ, is small, Eq. (3-4) will overestimate the distance,

u, by roughly 12% for a ϕ near 90^o. However, if ϕ is greater than 90^o, the error becomes small. Also the difference between the actual and the approximate distance equations reduces rapidly with the increment of wedge semi-angle for a fixed rolling angle, ϕ. The analytical result shown in Section 3.5.3. proves that the ϕ value is always greater than 90^o which explains why the error induced by using Eq. (3-4) in the cutting force solution is negligible. The physical model construction (Fig. 3-5) indicates that the maximum rolling angle, ϕ_{max}, is again a function of the rolling radius, R, as follows:

$$\phi_{max} = \frac{B+R}{R}, \tag{3-5}$$

where B is the half width of a wedge shoulder. Note that Eq. (3-5) is valid only for $90^o \leq \phi \leq 180^o$ which is always true for the curling flap model (Refer Section 3.5.3.).

3.3.6. Internal energy rate under steady-state wedge cutting process

Based on the above discussions, we are able to study the mechanisms of plate deformation and separation under a steady-state wedge cutting process thoroughly. In order to simplify the problem even further with an acceptable accuracy in mind, several more assumptions are made:

(i) Plate material is assumed to be rigid-perfectly plastic with an average flow stress, σ_0. Its value can be either determined from tensile tests or calculated from hardness test results. A precise definition of flow stress is presented in Ref. [27] which completely clarifies many reader's misunderstanding and confusion about the concept of flow stress.

(ii) It is assumed that both bending and membrane deformation modes have the same flow stress, σ_0. But this assumption can be easily relaxed by allowing different

flow stresses in different regions, depending on the level of average strain.

(iii) The plastic interaction between bending moment and membrane force is neglected in the plastic zones near a wedge tip and inside a transition zone. This hypothesis will overestimate the actual rate of energy dissipation in the membrane action and will partially compensate the energy lost by ignoring the bending energy in the near-tip and transition zones and the underestimation of membrane energy in transition zones.

(iv) Plastic shear strain is ignored. The validity of this assumption has been discussed in detail by Wierzbicki and Thomas [2].

(v) Plastic work in the near-tip zone is predominantly dissipated by the diffused mode. In other words, no local necking is considered and the plate thickness is taken to be constant. In most of our experiments the torn free edge of the plate is seen to have a considerable thinning due to high tensile strains at the near-tip region. This interaction between the primary (near tip) and secondary (transitional) membrane zones is not taken into account in the current analysis.

(vi) Plate material obeys von Mises yield criterion. Under the plane stress condition, the criterion can be expressed as:

$$\sigma_{xx}^2 - \sigma_{xx}\sigma_{yy} + \sigma_{yy}^2 + 3\sigma_{xy}^2 = \sigma_o^2, \tag{3-6}$$

where σ_{xx}, σ_{xy}, and σ_{yy} are the in-plane components of stress tensor. The corresponding flow rule gives:

$$\begin{cases} \dot{\varepsilon}_{xx} = \dot{\lambda}(2\sigma_{xx} - \sigma_{yy}), \\ \dot{\varepsilon}_{yy} = \dot{\lambda}(2\sigma_{yy} - \sigma_{xx}), \\ \dot{\varepsilon}_{xy} = 6\dot{\lambda}\sigma_{xy}. \end{cases} \tag{3-7}$$

3.3.7. Bending energy rate

Under a steady-state wedge cutting process, all the bending energies involved are concentrated in the two inclined plastic moving hinges (Fig. 3-5) and no work is done in the curled flap itself. The transient flap is observed to rotate as a rigid body about its plastic hinge line, OP. The length of an inclined plastic hinge, l = OP, is a function of half shoulder width, B, rolling radius, R, and wedge semi-angle, θ, as shown below:

$$l = \frac{B+R}{\sin\theta}. \tag{3-8}$$

The above equation is correct only when the rolling angle, ϕ, is greater than 90° which is always true for the curling flap model (Refer Section 3.5.3.). For a rigid-perfectly plastic material, the out-of-plate plastic bending moment under the plane-strain condition per unit length along the moving hinge is

$$M_o = \left(\frac{2}{\sqrt{3}}\sigma_o\right)\cdot\frac{t^2}{4}, \tag{3-9}$$

where t is the plate thickness. The rate of flap rotation, $\dot{\omega}$, along an inclined plastic moving hinge is related to rolling radius, R, wedge semi-angle, θ, and wedge advancing velocity, V. The condition of kinematic continuity leads to the following relationship:

$$\dot{\omega} = \frac{V_n}{R} = \frac{V\sin\theta}{R}, \tag{3-10}$$

where V_n is the normal component of V to the cylindrical center line of a transient flap. For a given rate of rotation, $\dot{\omega}$, the rate of bending energy is defined as

$$\dot{E}_b = 2\, M_o\, l\,\dot{\omega}. \tag{3-11}$$

In the steady-state cutting process, substituting Eqs. (3-8) ~ (3-10) into Eq. (3-11) yields the

rate of bending energy expression:

$$\begin{aligned}\dot{E}_b &= 2\left(\frac{2}{\sqrt{3}}\sigma_o\right)\cdot\frac{t^2}{4}\cdot\frac{B+R}{\sin\theta}\cdot\frac{V\sin\theta}{R} \\ &= \frac{4}{\sqrt{3}}\cdot\frac{\sigma_o t^2}{4}\cdot\frac{B+R}{R}\cdot V .\end{aligned} \tag{3-12}$$

3.3.8. Membrane energy rate

As mentioned earlier, there are two localized membrane deformation zones in a steady-state wedge cutting process: plastic zone near a wedge tip, and transition zone between transient and stable flaps. The rate of membrane energy under the plane stress condition is defined as:

$$\dot{E}_m = t\int_S \sigma_{\alpha\beta}\,\dot{\varepsilon}_{\alpha\beta}\cdot dS\,, \tag{3-13}$$

where S denotes an area in a membrane displacement zone, and $\sigma_{\alpha\beta}$ and $\dot{\varepsilon}_{\alpha\beta}$ are the components of stress and strain rate tensors, respectively. The strain rate tensor is defined as:

$$\dot{\varepsilon}_{\alpha\beta} = \frac{1}{2}\left(\dot{u}_{\alpha,\beta} + \dot{u}_{\beta,\alpha}\right)\,, \tag{3-14}$$

where $\dot{u}_\alpha = (v_x, v_y)$ are the components of the velocity vector projected in x- and y-directions. The above equation carries the assumption that the small out-of-plane displacement near a wedge tip and the bending deformation in the toroidal transition zone are neglected in the strain calculation which will give an underestimation to the total internal energy rate formulated.

When a wedge cuts through a plate, the component of the strain rate in the direction of wedge motion, $\dot{\varepsilon}_{xx}$, should be zero in a near-tip plastic zone. The validity of such an assumption is obvious from the observation of the test results [1], because the material in

the front of a wedge tip would accumulate if $\dot{\varepsilon}_{xx}$ were not zero. According to assumption (iv), $\dot{\varepsilon}_{xy}$ is also taken to be zero.

Based upon the above discussions and an additional assumption that the plane strain condition exists both in the near-tip plastic zone and along a flap edge, i.e. $\sigma_{xx} = \sigma_{yy}/2$, the in-plane membrane energy rate, Eq. (3-13), can be expressed as:

$$\dot{E}_{\mathrm{m}} = t \int_S \frac{2}{\sqrt{3}} \sigma_0 \dot{\varepsilon}_{yy} \cdot dS \,, \tag{3-15}$$

where S is a membrane deformation area which, for a steady-state cutting process, includes two zones discussed above: near-tip plastic zone and transition zone. The contributions of each zone towards the membrane energy rate are to be calculated individually next.

3.3.8.1. Membrane energy rate near wedge tip

Fig. 3-5 shows that a zone in front of a wedge tip locally undergoes out-of-plane bending and in-plane membrane deformations, which causes plate material to yield in that area. This plastic zone extends in the y-direction to a boundary, $\delta(x)$, beyond which the material behaves elastically. Lu's experimental result [23] reveals that this plastic zone is confined in a small region extending about several times the plate thickness around a wedge tip. The actual shape of this plastic zone is not important in the calculation of the membrane energy rate in that zone as will see in sequel. The controlling factors are the plastic zone depth, l_p, which is measured from the wedge tip to $x = 0$ and is equated in Eq. (3-1), and the y-direction separation velocity, $v_y(x)$, in the plastic zone, Eq. (3-2).

Substituting Eqs. (3-1), (3-2), and (3-14) into the above integration, Eq. (3-15), we get the membrane energy rate in the near-tip plastic zone [2]:

$$
\begin{aligned}
\dot{E}_{m1} &= t \int_S \frac{2}{\sqrt{3}} \sigma_o \frac{dv_y}{dy} dx dy \\
&= 2t \int_0^{l_p} \frac{2}{\sqrt{3}} \sigma_o \, v_y|_{y=0} dx \\
&= \frac{4}{3\sqrt{3}} \sigma_o t l_p V \tan\theta \\
&= \frac{4}{3\sqrt{3}} \sigma_o t \frac{R}{\cos\theta} V .
\end{aligned}
\tag{3-16}
$$

In the above derivation, v_y is taken as zero at the elasto-plastic boundary in the near wedge tip plastic zone.

3.3.8.2. Membrane energy rate in transition zone

Section 3.3.5. described the procedure how the toroidal shaped transition zone between the transient and stable flaps is approximated into a simple surface constructed by a family of straight lines. The approximate expression for the material stretching inside a transition zone, u of Eq. (3-4), will be used here to compute the membrane energy rate, $\dot{E}_{m2}$, contributed by the transition zone membrane deformation. As discussed in Section 3.3.4., $\dot{E}_{m2}$ consists of two stage deformations: (i) stretching of the transient flap to form a transition zone surface, and (ii) compressing of the same zone back to conform the stable flap geometry. The energies of these two stages are generally not equal. The ratio of total *vs.* stretching energies is defined as γ. As will be proved in Chapter 4, the value of γ can be taken as unity if a stable flap buckles or two if a stable flap has a smooth surface [1]. A local coordinate system, $\xi-\eta$, is introduced on the simplified transition zone surface: the η-axis is along the direction of material stretching streamline and the ξ-axis follows the stable flap curling direction (Fig. 3-5). Note that $\xi = R\phi$. In the local coordinate system the components of the velocity strains and the rate of separation displacement are as follows:

$$\begin{cases} \dot{\varepsilon}_{\xi\xi} = \dot{\varepsilon}_{\xi\eta} = 0 , \\ \dot{\varepsilon}_{\eta\eta} = \dfrac{\partial \dot{u}_{\eta}}{\partial \eta} , \\ \dot{u}(\xi) = 0.32\theta\tan\theta \cdot V \cdot \dfrac{\xi^2}{R(B+R)} , \end{cases} \tag{3-17}$$

where the expression for $\dot{u}(\xi)$ is derived in Appendix B. Based upon the above analysis, the membrane energy rate due to the transition zone membrane deformation can be formulated as

$$\begin{aligned} \dot{E}_{m2} &= \gamma \left(t \int_S \frac{2}{\sqrt{3}} \sigma_o \dot{\varepsilon}_{\eta} \, dS \right) \\ &= \gamma \left[2t \int_0^{B+R} \left(\int_0^{\eta(\xi)} \frac{2}{\sqrt{3}} \sigma_o \frac{d\dot{u}}{d\eta} \, d\eta \right) d\xi \right] \\ &= \frac{4\gamma}{\sqrt{3}} \sigma_o t \int_0^{B+R} \dot{u}\Big|_0^{\eta(\xi)} d\xi \\ &= \frac{4\gamma}{\sqrt{3}} \sigma_o \, t \int_0^{B+R} \frac{0.32\theta\tan\theta}{R(B+R)} \cdot V \cdot \xi^2 \, d\xi \\ &= \frac{4\gamma}{\sqrt{3}} \sigma_o \, t \cdot V\tan\theta \cdot \frac{d}{3} , \end{aligned} \tag{3-18}$$

where d represents the maximum material stretching in the transition zone, which equals the distance between points A and B in Fig. 3-5. The mathematical expression for d can be derived from Eqs. (3-4) and (3-5) as follows:

$$d = 0.32R\theta\phi_{max}^2 = \frac{0.32\theta(B+R)^2}{R} . \tag{3-19}$$

3.3.8.3. Total membrane energy rate

The total membrane energy rate is the sum of Eqs. (3-16) and (3-18):

$$\dot{E}_m = \dot{E}_{m1} + \dot{E}_{m2} , \tag{3-20}$$

i.e.

$$\dot{E}_m = \frac{4}{3\sqrt{3}} \sigma_o t \left[\frac{R}{\cos\theta} + d \cdot \tan\theta \right] V. \tag{3-21}$$

In order to express $\dot{E}_m$ as a direct function of R, the simplified expression for d, Eq. (3-19), is used in the above equation which produces an approximate equation for $\dot{E}_m$:

$$\dot{E}_m = \frac{4}{3\sqrt{3}} \sigma_o t \left[\frac{R}{\cos\theta} + 0.32\gamma\theta \tan\theta \cdot \frac{(B+R)^2}{R} \right] V. \tag{3-22}$$

3.3.9. Wedge force under steady-state cutting process

Under the process of a steady-state wedge cutting through a wide metal plate, an external force, F, is applied on the wedge in order to separate plate material in front of a wedge tip and to bend flaps along inclined moving hinges. Equating the rate of external work, i.e. the product of wedge cutting force, F, and the corresponding moving velocity, V, to the rate of total internal energy dissipation yields:

$$FV = \dot{E}_b + \dot{E}_m, \tag{3-23}$$

where $\dot{E}_b$ and $\dot{E}_m$ are the bending and membrane energy rates, respectively. Note that the work loss due to friction is not a second order term and it will be taken into account in the next section.

The rates of bending energy and membrane energy have already been formulated in Eqs. (3-12) and (3-21), respectively. Substituting them into Eq. (3-23) and canceling the common term V on both sides of the equation, we obtain a closed-form solution for the steady-state wedge cutting force as follows:

$$F = \frac{4}{\sqrt{3}} \sigma_o t^2 \left\{ \frac{B+R}{4R} + \frac{1}{3t} \cdot \left[\frac{R}{\cos\theta} + \gamma \tan\theta \cdot d \right] \right\}. \tag{3-24}$$

To express F as a function of R, the simplified expression for d, Eq. (3-19), is used to replace the distance d in Eq. (3-24). The resulting equilibrium is

$$F = \frac{4}{\sqrt{3}}\sigma_o t^2 \left\{ \frac{B+R}{4R} + \frac{R}{3t} \cdot \left[\frac{1}{\cos\theta} + 0.32\gamma \left(\frac{B+R}{R} \right)^2 \theta \tan\theta \right] \right\}. \tag{3-25}$$

The above wedge cutting force expression is seen to be a direct function of the rolling radius, R, which is an unknown parameter to be determined. It is postulated that the actual wedge force required to cut through a plate should have the minimum value of Eq. (3-25). By minimizing F with respect to R, i.e. $dF/dR = 0$, we obtain the optimized rolling radius expression as:

$$R = B\sqrt{\frac{0.75\,(t/B)\cos\theta + 0.32\gamma\theta\sin\theta}{1 + 0.32\gamma\,\theta\sin\theta}}. \tag{3-26}$$

Substituting the above equation back into Eq. (3-25), we obtain the optimized wedge cutting force expression as follows:

$$F = \frac{2}{\sqrt{3}}\sigma_o t^2 f(R), \tag{3-27}$$

where the dimensionless function $f(R)$ can be expressed as follows:

$$f(R) = 2\left\{ \frac{B+R}{4R} + \frac{R}{3t} \cdot \left[\frac{1}{\cos\theta} + 0.32\,\gamma \left(\frac{B+R}{R} \right)^2 \cdot \theta\tan\theta \right] \right\} \tag{3-28}$$

and R is the optimized rolling radius expressed in Eq. (3-26).

3.3.10. Frictional force study

Friction has significant influences to a plate cutting process. It not only increases the wedge force needed to cut through a plate but also controls the deformed flap shape. For example, owing to the unbalanced frictional force existed in the out-of-plane direction, braided flaps are observed in tests for plate specimens with no title angle towards the cutting force direction (Fig. 3-3). During his wedge cutting tests, Lu [23] tried to use the unloading and reloading technique to determine the frictional effects on the total wedge cutting force. It was found that the machining friction can seldom be reduced by the lubrication method and suggested that the total frictional force might significantly contribute to the total cutting force.

Careful study of frictional mechanisms reveals that there exist two distinct frictional forces in a wedge cutting process (Fig. 3-8). One is sliding friction existed between wedge surface and transient flaps, which is a normally encountered frictional effect. Wierzbicki and Thomas included the sliding friction in their analysis of transient wedge cutting force and correctly formulated the frictional force component [2]. The second frictional effect is a machining frictional force at a wedge tip, which has a much larger frictional coefficient than that of a simple sliding friction case but is limited to a very narrow region. Both frictional forces have constant values under a steady-state wedge cutting process and their contributions will be added directly to the derived cutting force expression derived, Eq. (3-27), as independent terms. The effect of sliding friction is postulated to be in direct proportion to the corresponding force terms in Eq. (3-27) producing transient extension and bending of the flaps. The machining friction is an independent term which is governed purely by the problem geometry, such as plate thickness, wedge angle, and plate tilt angle [28].

3.3.10.1. Sliding friction

The derivation of sliding frictional force, F_{fs}, follows exactly the same procedures as proposed by Wierzbicki and Thomas [2]. This frictional force exists between wedge attack sur-

faces and transient flaps, and it acts in the out-of-plane direction which is against the transient flap sliding movement. The velocity of this relative sliding movement is found to be equal to the wedge advancing velocity, V, and it is independent of wedge semi-angle, θ. The frictional coefficient, μ_s, is typically within a range 0.1~0.4 for the steel-to-steel dry sliding condition. If a plate tilt angle is greater than or equal to θ, the resultant sliding frictional force will have the same direction as the wedge advancing direction which will prevent any possible braided flap deformation. The sliding frictional force is assumed in direct proportion to the bending force expression, $F_b = \dot{E}_b/V$ defined in Eq. (3-12), and the membrane force expression in the transition zones, $F_{m2} = \dot{E}_{m2}/V$ defined in Eq. (3-18). This membrane force contribution to the sliding frictional force is believed to be initiated by the introduction of an additional normal force between wedge attack surface and transient flap. (The membrane deformation force at a wedge tip is balanced internally by the near tip plastic zone so that it does not have any effect on the sliding friction.) Based on the assumption made above, the sliding friction can be formulated as:

$$F_{fs} = \mu_s (F_b + F_{m2}) \cot\theta \,, \tag{3-29}$$

Note that the frictional coefficient, μ_s, in Eq. (3-29) is not necessarily equal to the sliding frictional coefficient found in the literature but it can be liberated to include any additional sliding frictional effects found in tests which has not been covered so far. For instance, the scoring observed on the transient flap surface of Maxwell's specimens [12] will definitely increase the frictional coefficient value. Substituting the force expressions from Eqs. (3-12) and (3-18) into Eq. (3-29) yields the complete sliding frictional force equation:

$$F_{fs} = \mu_s \frac{(B+R)\,\sigma_o\, t^2}{\sqrt{3}\,R} \cdot \left[\cot\theta + \frac{0.43\gamma}{t} \cdot (B+R) \cdot \theta \right]. \tag{3-30}$$

3.3.10.2. Machining friction

During a plate cutting process, the plate material near a wedge tip is plastically deformed and separated by a wedge cutting edge. Since the cut material flows plastically at a wedge tip, the coefficient of machining friction is much higher than that of sliding friction [29]. Tests on tool machining mechanism [28] reveal that, near a wedge tip, there exists a close contact zone between wedge surface and cut plate material termed *rake face*. The rake face is confined in a limited area close to a wedge tip, and its length along the wedge surface is roughly around one to two times a plate thickness. Under slow cutting speed and by cutting through a ductile material such as mild steel, it is observed that the chipped material welds itself to the wedge tip at the rake face. Shear work is required to shear off the weaker of the two contact materials across the rake face, and its value is found to be independent of the normal force applied [28]. The energy needed to push the cut material across the rake face is so large that the energies required to form new surfaces in front of the wedge tip are generally insignificant so that they are neglected in our analysis [28]. The existence of rake face in a wedge cutting process is clearly shown in several wedges used in M.I.T. laboratory which exhibit a shiny, grounding-like, and narrow strip area along the wedge tip surface.

Because of the shearing mechanism involved in plate material movement on a rake face, the use of machining frictional coefficient, μ_m, is only a convenient way to handle all the complex phenomena behind it. At a rake face, the cutting process is very like a plane stress indentation problem with friction being present. Tests show that, for steel-to-steel machining friction, μ_m is within a range of 0.6~0.7 [23]. In the following analysis, it is assumed that the material at rake face is fully yielded and the length of rake face is equal to $\zeta \cdot t$ where ζ represents the ratio of rake face length and plate thickness. Based upon the above analysis, the machining friction force can be formulated as (Fig. 3-9):

$$F_{fm} = 2\,\zeta\,\mu_m \cdot \left(\frac{2}{\sqrt{3}}\sigma_o\right) \cdot t^2 \cos\theta \,. \tag{3-31}$$

3.3.11. Steady-state wedge cutting force including friction

Adding the sliding and machining frictional forces obtained in the previous section into the derived cutting force expression, Eq. (3-27), we get the final expression for the closed-form steady-state cutting force equation:

$$F_f = \frac{2}{\sqrt{3}} \sigma_0 t^2 f_f(R) , \tag{3-32}$$

where the dimensionless coefficient including the frictional effects is formulated as

$$f_f(R) = 2\left\{ \frac{B+R}{4R} \cdot (1+\mu_s \cot\theta) + \frac{R}{3t} \cdot \left[\frac{1}{\cos\theta} + \right.\right.$$
$$\left.\left. + 0.32\gamma \cdot (1+\mu_s \cot\theta) \left(\frac{B+R}{R}\right)^2 \theta \tan\theta \right] + \zeta \mu_m \cos\theta \right\} . \tag{3-33}$$

Postulating the actual wedge force equation derived above adjusts itself to the minimum of Eq. (3-33). The optimized rolling radius R can then be formulated by minimizing the above function with respect to R, i.e. $\partial f_f / \partial R = 0$, which yields:

$$R_f = B \sqrt{\frac{0.75\,(t/B)\cos\theta + 0.32\gamma\theta\sin\theta}{\frac{1}{1+\mu_s \cot\theta} + 0.32\gamma\theta\sin\theta}} . \tag{3-34}$$

3.3.12. Simplification of the cutting force expression

A parametric study on Eq. (3-33) (Section 3.3.13.) reveals that the bending energy has little contribution towards the total wedge cutting force, so that it is safe to neglect its corresponding terms from the total wedge cutting force expression for the purposes of simplicity and energy reduction. (Remember that the energy theorem is an upper bound approximation of the problem.) Removing the bending energy term from Eq. (3-33), we obtain a sim-

plified closed-form solution for the steady-state wedge cutting force:

$$F_s = \frac{2}{\sqrt{3}} \frac{\sigma_0 t^2}{4} f_s(R) = M_0 f_s(R) , \tag{3-35}$$

where the dimensionless coefficient is

$$f_s(R) = 8\left\{\frac{R}{3t} \cdot \left[\frac{1}{\cos\theta} + 0.32\gamma(1+\mu_s\cot\theta)\left(\frac{B+R}{R}\right)^2 \theta \tan\theta\right] + \zeta\mu_m \cos\theta\right\} . \tag{3-36}$$

The optimized rolling radius R in Eq. (3-36) can be determined by minimizing the above resisting force with respect to R, i.e. $\partial f_s / \partial R = 0$, which yields:

$$R_s = B\sqrt{\frac{0.32\gamma\theta\sin\theta}{\frac{1}{1+\mu_s\cot\theta} + 0.32\gamma\theta\sin\theta}} . \tag{3-37}$$

Substitute the above optimized rolling radius expression into Eq. (3-36), one can conclude that the simplified steady-state wedge cutting force expression is in direct proportion to the B/t ratio which is clearly demonstrated in Fig. 3-10.

3.3.13. Parametric study of complete and simplified solutions

In the previous two sections, both complete and simplified wedge force expressions have been derived. In this section, a comparison is performed between the complete wedge force expression, Eq. (3-32), and the simplified one, Eq. (3-35). For the practical purposes, some of the controlling parameters are limited to the ranges of interests for our current research and application:

- Plate thickness, t, varies between 0.5 mm and 1.5 mm;
- Half wedge shoulder width, B, varies between 5 mm and 50 mm;

- Wedge semi-angle, θ, varies between 30^{o} and 45^{o};
- Sliding frictional coefficient, μ_s, varies between 0 and 0.5;
- Machining frictional coefficient, μ_m, varies between 0 and 1.

Other parameters are given as fixed numbers:

- Ratio of total *vs.* stretching energies in transition zone is $\gamma = 1$ by assuming that stable flaps are not compressed back but buckled instead;
- Ratio of rake face length and plate thickness for machining friction is $\zeta = 1.5$.

3.3.13.1. Effect of half wedge shoulder width *B* variation

Fig. 3-10 shows the wedge indentation force versus half wedge shoulder width, B, for several values of wedge semi-angle, θ, and plate thickness, t. The relative difference between the complete and simplified wedge force solutions is seen to be small when the B/t ratio is large. For instance, when the B/t ratio is greater than 20, the error is within 10% which is a good estimation for such a complicated problem. Also from Fig. 3-10, it is observed that the variation of wedge semi-angle, θ, has little effect on the difference between the complete and simplified results. Fig. 3-10 confirms the assumption that the wedge force, F, is a linear function of half wedge shoulder width, B, when $B/t \geq 5$.

3.3.13.2. Effect of plate thickness t variation

A dependence of the cutting force on plate thickness, t, for several values of wedge semi-angle, θ, and half wedge shoulder width, B, is demonstrated in Fig. 3-11. From the set of figures, it is quite evident that the difference between the complete and simplified wedge force solutions is small when the B/t ratio is large. Also from Fig. 3-11, it is observed that an error between the complete and simplified results is independent of wedge semi-angle

θ. Fig. 3-11 (a) shows a nonlinear relationship between wedge force, F, and plate thickness, t, when the B/t ratio is small indicating that both bending and membrane resistances contribute to the solution. For a large B/t ratio, the membrane energy predominates and the wedge cutting force becomes a linear function of t.

3.3.13.3. Effect of wedge semi-angle θ variation

Fig. 3-12 shows the effect of a varying wedge semi-angle, θ, for several values of plate thickness, t, and two chosen values of half wedge shoulder width: $B = 5$ mm in Fig. 3-12 (a) and $B = 50$ mm in Fig. 3-12 (b). From the set of figures, it is evident that the difference between the complete and simplified results is small when the B/t ratio is large. Fig. 3-12 also shows a nonlinear relationship between wedge force, F, and wedge semi-angle, θ. It should be noted that F tends to infinity when $\theta \rightarrow 90^{o}$ indicating that some other failure mechanisms such as concertina tearing must take over to render the indentation force finite.

3.3.13.4. Effect of sliding frictional coefficient μ_s variation

The effect of varying the sliding frictional coefficient, μ_s, plate thickness, t, and half wedge shoulder width, B, is shown in Fig. 3-13. From the set of figures, it is evident that the difference between the complete and simplified results is small when the B/t ratio is large. Fig. 3-13 also shows a linear relationship between wedge force, F, and sliding friction coefficient, μ_s. Because the sliding friction contributes very little to the solution, the slope of F *vs.* μ_s curve is very small.

3.3.13.5. Effect of machining frictional coefficient μ_m variation

Fig. 3-14 shows that the effect of the machining friction coefficient, μ_m, for the complete and simplified solutions is very weak for the given ranges of plate thickness, t, and half

wedge shoulder width, B. From the set of figures, it is evident that the difference between the complete and simplified results is small when the B/t ratio is large. Fig. 3-14 also demonstrates a linear relationship between wedge force, F, and machining friction coefficient, μ_m.

3.3.14. Energy partition in the simplified total wedge force, F

Fig. 3-15 shows a distribution of three contributing deformation mechanisms to the total wedge force as a function of half wedge shoulder width, B, for several values of plate thickness, $t = 0.5 \sim 1.5$ mm. It is shown that the membrane energy in a transition zone contributes most to the total wedge cutting force value. The second major contributing mechanism is the membrane energy near a wedge tip. At the same time, the energy loss due to the machining friction has such a small influence to the total work done that it can safely be neglected. As discussed in the previous section, the bending contribution has already been removed from the simplified cutting force expression, Eq. (3-35). This partition of different energy contributions towards the total cutting force value is representative to almost all the cases considered in this dissertation. Based on the results presented in Fig. 3-10, the above conclusions will also apply to the complete solution, Eq. (3-32).

3.4. Steady-state cutting analysis using upright flap model

The kinematic model presented in Fig. 3-4b provides a basis for making a less rigorous but quick estimate on the steady-state wedge indentation force. In this model, all the flaps are assumed to be flat and bent up perpendicular to the original plate plane. As before, the plate material resists the wedge motion by developing bending deformation in the transient flaps and membrane action in the near-tip zone and transition zones. The following analysis

adopt the same procedures presented in the curling model study (Section 3.3): first, each of the energy dissipation rate is evaluated; then, the energy postulate method is applied to derive a closed-form solution for the wedge cutting force of the model.

3.4.1. Near-tip membrane energy

Due to the absence of the cylindrical flaps with a rolling radius R in the curling flap model analyzed in the previous section, the present model cannot employ the concept of a near-tip plastic zone length, l_p, as before from Eq. (3-1). A simplified method is used here based on the concept of specific work to fracture, R^*, in order to calculate the rate of membrane energy which is defined by

$$\dot{E}_{m1} = R^* t \, V . \tag{3-38}$$

In general, R^* is not a material constant but depends on plate thickness. Therefore, the parameter R^* must be determined from suitably devised tests on plates with the same thickness. According to Atkins [24], the value of R^* is in the range $R^* = 300 \sim 1000$ N/mm.

3.4.2. Membrane energy in transition zone

The general formulation for the membrane energy rate in a transition zone presented in Eq. (3-18) is still applicable to the current model:

$$\dot{E}_{m2} = \frac{4}{\sqrt{3}} \sigma_0 t \cdot \int_0^B \dot{u}(\xi) \, d\xi , \tag{3-39}$$

except that the separation velocity derived in Appendix B, Eq. (B-3), is no longer valid and must be replaced by a new equation. From the kinematics of the problem (Fig. 3-4b), the separation displacement and velocity must be a linear function of the coordinate ξ as follows:

$$\dot{u} = \dot{u}_o \cdot \frac{\xi}{B}, \tag{3-40}$$

where $\dot{u}_o$ is the maximum stretching velocity at the edge fiber on top of the flaps and it can be formulated as:

$$\dot{u}_o = \frac{\Delta u}{\Delta t} = \frac{B\sin\theta}{\left(\frac{B}{V\tan\theta}\right)} = V\sin\theta\cos\theta. \tag{3-41}$$

Substituting Eqs. (3-40) and (3-41) into Eq. (3-39) and integrating once, one gets an equation for the membrane energy rate in a transition zone as

$$\dot{E}_{m2} = \frac{2}{\sqrt{3}}\sigma_o t B V \sin\theta \tan\theta . \tag{3-42}$$

3.4.3. Bending energy in transient flaps

The rate of bending energy in a steady-state process is defined approximately by

$$\dot{E}_b = 2M_o V\phi, \tag{3-43}$$

where $\phi = \pi/2$ is the total rotation angle and two in the above equation stands for the two identical hinge lines existed.

3.4.4. Indentation force

The steady-state wedge cutting force for the upright flap model can now be derived from Eqs. (3-38), (3-42), and (3-43) by applying the energy postulation, Eq. (3-23). After cancelling the common term V from both sides of the equation, a general wedge cutting force expression is derived:

$$F = \frac{2}{\sqrt{3}}\gamma\sigma_0 tB\sin\theta\tan\theta + \pi M_0 + R^* t\,. \tag{3-44}$$

Normalizing the right side of the equation with respect to the fully plastic bending moment, M_0, gives

$$F = M_0\left(\frac{4B}{t}\gamma\sin\theta\tan\theta + \pi + \frac{4\sqrt{3}R^*}{2\sigma_0 t}\right). \tag{3-45}$$

A relative contribution of the various energy dissipation terms depend on three controlling parameters: width to thickness ratio B/t, wedge semi-angle θ, and the specific work to fracture parameter R^*. Part of the last term in Eq. (3-45) can be expressed, using an approximate formula $R^* = \sqrt{3}\sigma_0\delta_t$, into an alternative form

$$\frac{4R^*}{\sigma_0 t} = 4\sqrt{3}\,\frac{\delta_t}{t}\,. \tag{3-46}$$

Since the dimensionless crack opening displacement parameter δ_t/t is always less than unity, it can be concluded that the last term in Eq. (3-45) is of the order of 2π or less. Thus for a very narrow wedges with a small B/t ratio and/or a sharp wedge with a small wedge semi-angle θ, Eq. (3-45) for the indentation force simplifies to

$$F \approx 3\pi M_0\,. \tag{3-47}$$

In a grounding scenario, the B/t ratio is generally large and θ is taken to be $30 \sim 45^0$. In this case the contribution of bending and fracture is small and the plate resistance is given approximately by

$$F = 4\gamma M_0\frac{B}{t}\sin\theta\tan\theta = \frac{2}{\sqrt{3}}\gamma\sigma_0 Bt\sin\theta\tan\theta\,. \tag{3-48}$$

It is of interest to compare the last equation, Eq. (3-48), with its counterpart in the rigorous,

full solution given by Eqs. (3-27) and (3-28). The leading term in that solution comes from the membrane stretching in the transition zone:

$$F_{m2} = \frac{2 \times 0.64}{3\sqrt{3}} \cdot \gamma \sigma_o R t \cdot \left(\frac{B+R}{R}\right)^2 \cdot \theta \tan\theta \ . \tag{3-49}$$

The wedge cutting force attains minimum when $B = R$. Incidentally, the minimization condition gives a unique value of the wrap angle $\phi_{max} = 1 + (B/R) = 2$, which then stays always within the validity range of the exact solution $\pi/2 \le \phi_{max} \le \pi$. The corresponding minimum force is obtained from Eq. (3-49) as

$$(F_{m2})_{min} = 0.985 \cdot \gamma \sigma_o B t \cdot \theta \tan\theta \ . \tag{3-50}$$

Both solutions, i.e. Eqs. (3-48) and (3-50), are almost identical by considering the fact that γ is always greater than unity. For example, taking $\theta = 45^o$ the respective numerical coefficients in the above equations are 0.816 in the upright flap model solution versus 0.774 in the curling flap one. The above comparative study proves the merit of using the upright flap computational model shown in Fig. 3-4b.

According to the parametric study performed in the preceding section, the contribution of the machining friction is small, so that this component will be neglected in the present theory. However, the contribution of the sliding friction is significant. The frictional effect is included into the steady-state wedge force expression derived above by multiplying the indentation force by a factor of $(1 + \mu \cot\theta)$. The final plate resistance expression to the steady-state wedge indentation for the upright flap model is

$$F = M_o \left(4 \cdot \gamma \frac{B}{t} \sin\theta \tan\theta + 3\pi\right) \cdot (1 + \mu \cot\theta) \ . \tag{3-51}$$

3.5. Discussions and Conclusions

In this section, many interesting topics not discussed so far are to be presented giving an in-depth review of the theoretical analysis for the steady-state wedge cutting process. Analytical results presented below such as plate failure mode prediction and rolling angle magnitude have direct engineering application potentials. Investigation on flap deformation details, e.g. flap tensile strain and thickness variation measurement, are of academic interest and need to be studied further.

3.5.1. General

The closed-form solutions for a steady-state cutting process of the wedge indentation through a metal plate were derived by using two kinematically acceptable deformation models conforming the actual cutting damage format (Fig. 3-4). The curling and upright flap analytical models proposed in this chapter contain three loading resistance mechanisms: plastic deformations, tearing fracture, and friction. From the analytical results, it is known that the magnitude of an indentation force is mainly controlled by the following parameters: wedge shoulder width $2B$, wedge semi-angle θ, plate thickness t, flow stress of the material σ_0, and sliding friction μ_s. Other parameters such as the specific work of fracture R^*, and a machining friction μ_m were shown to have a weaker effect on the solutions.

A number of experimentally observed phenomena, such as lifting of plate at a wedge tip, a pre-tension at a near-tip plastic zone, have not been incorporated into the present theoretical solutions. This concern will be clarified in Chapter 5 after experimental validations have been made.

The two kinematic models proposed in this chapter assume that a plate can freely deform without being restrained by any obstacle. In reality, the bottom hull of a ship is constructed

by both longitudinal stiffeners and transverse bulkheads, which may limit the movement of the cut flaps. Paik [34] observed a large increase of wedge force due to the contacts established between the flap and longitudinal stiffener. A new kinematic model should to be developed for such failure modes. This can be done by modifying the existing curling flap model with the flap rotation restraint condition added.

3.5.2. Failure mode prediction

When a plate is cut by a wedge, one of the two major failure modes, i.e. concertina and clean cut, may occur depending on the B/t ratio and a wedge semi-angle involved. The following analysis provides an example of predicting a possible failure mode which has the largest probability to occur by taking the above two geometric parameters as input. Since there exist two models in the clean cut failure mode, i.e. curling and upright flap models, both of them are to be compared with the concertina failure mode in order to obtain the corresponding boundary curves. With the help of those two boundary curves, three wedge cutting failure zones can be identified which characterize different failure modes. Due to the complexity of the problem, we can only provide a simple example here.

3.5.2.1. Boundary curve for concertina and upright flap failures

The dependence of the theoretical solutions on a wedge semi-angle will be considered first. Let us focus our attention on the leading term of the upright flap model solution, Eq. (3-48). The plate resistance is seen to grow infinitely with $\theta \to \pi/2$. However, as a wedge semi-angle flattens, the angle between the inclined wedge surface and the wedge shoulder, i.e. $\pi - \theta$, becomes smaller so that there is a very good chance that a central separation gives way to the formation of two symmetric crack on both sides of a wedge tip. Such a failure mode has been identified as concertina tearing (Fig. 3-17). An approximate expression for the corresponding wedge pushing force is derived by Wierzbicki [27] as

$$F_{conc} = 14.2 M_0 \cdot \left(\frac{B}{t}\right)^{1/3} . \tag{3-52}$$

It is plausible to assume that a transition between these two distinct failure modes occurs when the corresponding wedge forces are the same. By equating Eqs. (3-48) and (3-52) the following equation is obtained relating critical transition parameters

$$\frac{B}{t} = \frac{6.7}{(\sin\theta\tan\theta)^{3/2}} . \tag{3-53}$$

A plot of the boundary curve between the regime of a central separation and a concertina tearing is shown in Fig. 3-18. The small scale tests conducted at M.I.T. were in the range of $3 < B/t < 13$ and the corresponding critical angle is found to be $45^0 < \theta_a < 60^0$ from the boundary curve. Indeed, in one experiment with a round wedge, which can be approximated by $\theta \approx 45^0$, the above two failure modes were co-existing (Fig. 5-3). The force level corresponding to these modes was also similar.

3.5.2.2. Boundary curve for concertina and curling flap failures

Similar arguments as in the derivation of boundary curve between the concertina and upright flap failure modes are to be used here. A boundary curve separating the curling flap and concertina tearing failure modes can also be derived by equating the cutting force equation for the curling flap model, Eq. (3-35), and the concertina tearing force equation, Eq. (3-52). The follow analysis is aimed to find a lower bound solution for the boundary curve, so that it is assumed that, during a steady-state cutting process, no friction is existed and stable flaps will buckle, i.e. $\mu_s = \mu_m = 0$ and $\gamma = 1$. The boundary curve can be derived as

$$\frac{B}{t} = 12.3 \cdot \left\{ \frac{\cos\theta \cdot \sqrt{1 + 0.32\theta\sin\theta}}{\sqrt{0.32\theta\sin\theta}\left[1 + \left(\sqrt{0.32\theta\sin\theta} + \sqrt{1 + 0.32\theta\sin\theta}\right)^2\right]} \right\}^{3/2} . \tag{3-54}$$

Fig. 3-18 shows that the above boundary curve is lower than the boundary curve from Eq. (3-53). This implies that a plate may conform to an upright flap failure mode instead of a concertina tearing failure mode if a point defined by the geometric coordinates, B/t and θ which represent the controlling parameters in a steady-state cutting process, falls into the area between curves of Eqs. (3-53) and (3-54) on the diagram of Fig. 3-18.

3.5.2.3. Application of boundary diagram to failure mode prediction

With the help of the derived boundary curves (Fig. 3-18), plate cutting failure mode can be predicted in advance for the first time. In other words, if test information is available beforehand, i.e. B/t and θ are predefined, a failure mode can be predicted easily by allocating the point representing the controlling parameter pair on the boundary diagram. It is worthwhile to point out that the failure boundary diagram can only provide a possible plate failure mode. If a point located on the boundary diagram is close to a boundary curve, difficulty will arise to give a correct prediction of a failure mode. A good experimental example is shown in Fig. 5-3, which consists of both clean and concertina failure modes in one specimen. Despite a non-uniqueness in the failure modes, the plate resisting force is uniquely calculated which allows to make a reliable prediction in the ship hull grounding damage.

Fig. 3-18 shows that there exists a high probability for a plate to fail conforming the curling flap model when a small wedge angle and a small B/t ratio are used. With the increment of either parameter, other failure modes may take over if less energy is required for its substitution. It is important to note that the boundary diagram presented here (Fig. 3-18) needs to be justified when it is used in the real world plate failure prediction. This is because that, based on user's experiences, some empirical parameters might be introduced into the theory in order to incorporate the complicated nature of the problem.

3.5.3. Rolling angle calculation

From the formulation of wedge cutting force for the curling flap model, an important assumption is made throughout the analysis without giving any proof: a stable flap rolling angle, ϕ, is always greater than 90^{o}. Experimental results give a sound evidence of such an assumption. Here, we will provide a theoretical proof of such an assumption as long as the curling flap failure mode prevails.

The maximum rolling angle is defined in Eq. (3-5) as a function of flap rolling radius, R, and wedge half shoulder width, B. Substituting the rolling radius expression, Eq. (3-37), into Eq. (3-5) yields

$$\phi_{max} = 1 + \frac{B}{R_s} = 1 + \sqrt{1 + \frac{1}{0.32\,\gamma \times (1 + \mu_s \cot\theta) \cdot \theta \sin\theta}} > \frac{\pi}{2} . \qquad (3\text{-}55)$$

This proves that a stable flap rolling angle, ϕ, is always greater than 90^{o}.

3.5.4. Comparison of two kinematic models presented

Fig. 3-4 presents two kinematically admissible failure modes under a steady-state wedge cutting process: curling and upright flap models. The former has a cylindrically bent-up flap with a rolling radius, R, to be optimized; whereas the latter has a flat flap which is much simpler to analyze. The curling flap model assumes a parabolic distribution of the transition zone stretching length, Eq. (3-4), along the stable flap curling direction, while the upright flap model adopts a linear distribution of the corresponding stretching length, Fig. 3-4(b). It is proved that d in the curling flap model will equal to u_0 numerically if the rolling angle, ϕ, is assigned as 90^{o}. Since the deformation energy inside a transition zone has a large contribution towards the cutting force, it is clear that a curling flap failure mode will give way to an upright flap failure mode if a large rolling angle, ϕ, is found from the curling flap

model solution. Of course, the rolling angle, ϕ, is not the only controlling parameter for the final cutting failure mode, especially in a thick plate cutting process discussed in Tests #6 and #7 of Chapter 5.

3.5.5. Flap deformation study

A special characteristics of a steady-state cutting process is the existence of a flap transition zone. This zone consumes a large amount of deformation energy (Fig. 3-15) so that a large tensile strain is involved in the cutting process. The following study provides some details about the flap local deformations. Interesting observations are to be presented here.

3.5.5.1. Flap tensile strain

By using the upright flap kinematic model presented in Fig. 3-4(b), a lower bound solution for the flap tensile strain, ε, can be derived. As can be conclude from the kinematic model, the total deformed flap length along the top free edge of the transient and transition zones is a summation of the transient flap length and the stretching deformation inside the flap transition zone. The length on top of the transient flap can be formulated by using the geometric relationship which gives $l_1 = B\cot\theta$ and the stretching deformation on top of the transition zone is calculated as $u_0 = B\sqrt{2(1-\cos\theta)}$. Based upon the above calculations and the strain definition for a large deformation:

$$\varepsilon = \frac{1}{2}\left[1 - \left(\frac{l}{L}\right)^2\right], \tag{3-56}$$

the tensile strain along the deformed flap can be derived as follows:

$$\varepsilon = \frac{1}{2}\cdot\left[1 - \left(\frac{\cot\theta}{\cot\theta + \sqrt{2(1-\cos\theta)}}\right)^2\right], \tag{3-57}$$

which is a direct function of a wedge semi-angle. Fig. 3-19 shows that the flap tensile strain increases with the increment of a wedge semi-angle. Large strain will be reached if a wedge angle becomes large. For example, when $\theta = 45^{o}$, the flap tensile strain becomes 34%. This strain is so large that a standard tensile coupon will usually neck and fracture. For the thin plate specimens tested at M.I.T. (Tests #4 and #5 of Chapter 5), no necking and/or fracture are observed on the failure specimens. This is because that the tensile coupon test of the same batch of material has an average fracture strain equal to 38% [36] which is a little bit over the calculated flap tensile strain. Another reason for no flap fracture observed in a thin plate cutting is probably due to the fact that the strain is partially relieved by the global out-of-plane deformation of the specimens, which gives a little bit different deformation pattern than the upright flap model presented here.

3.5.5.2. Thickness variation along flap curling direction

Measurements of flap thickness are performed in order to investigate the thickness variation along the flap curling direction. Slicing of the flaps from a wedge cut specimen starts from an area close to the near tip plastic zone (Fig. 3-20a) and moves all the way back to the stable flap region (Fig. 3-20f). At the very tip of almost every flap cross-section, it can be seen that a sudden change of thickness takes place locally in the free edge region which extends a distance around one plate thickness inward. This abrupt change is caused by the wedge cutting process and will not be further considered here. Plate thickness varies smoothly for the major part of the flap cross-section. A large change of plate thickness happens at the area near the flap free edge indicating the existence of a non-uniform tensile strain distribution along the flap curling direction. Maximum through thickness strain is measured as 20% which conforms the material incompressibility law of material plastic deformation.

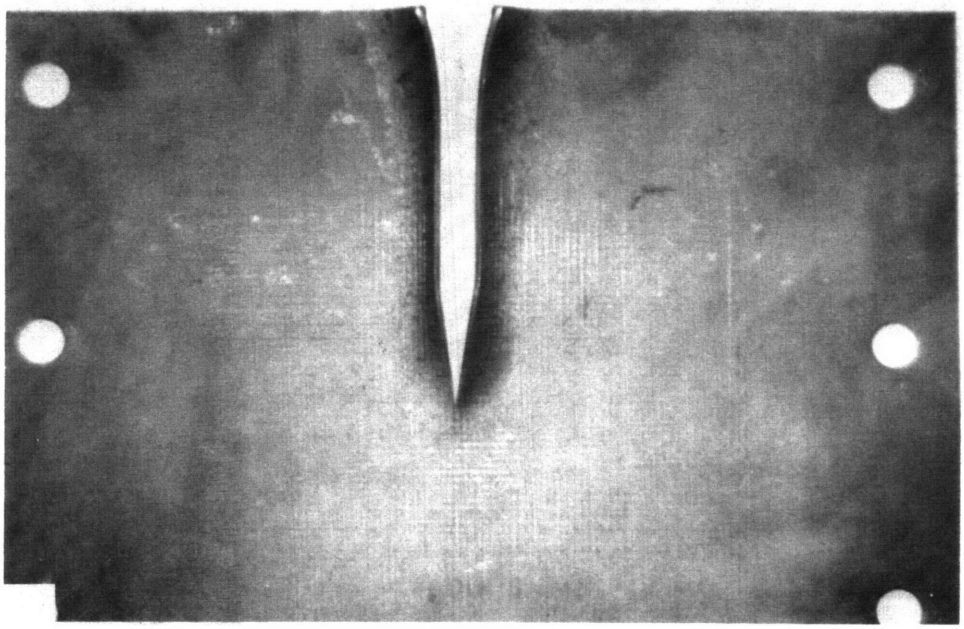

Fig. 3-1 Center clean cut of a plate by a sharp wedge with smooth stable flap

(Test #1)

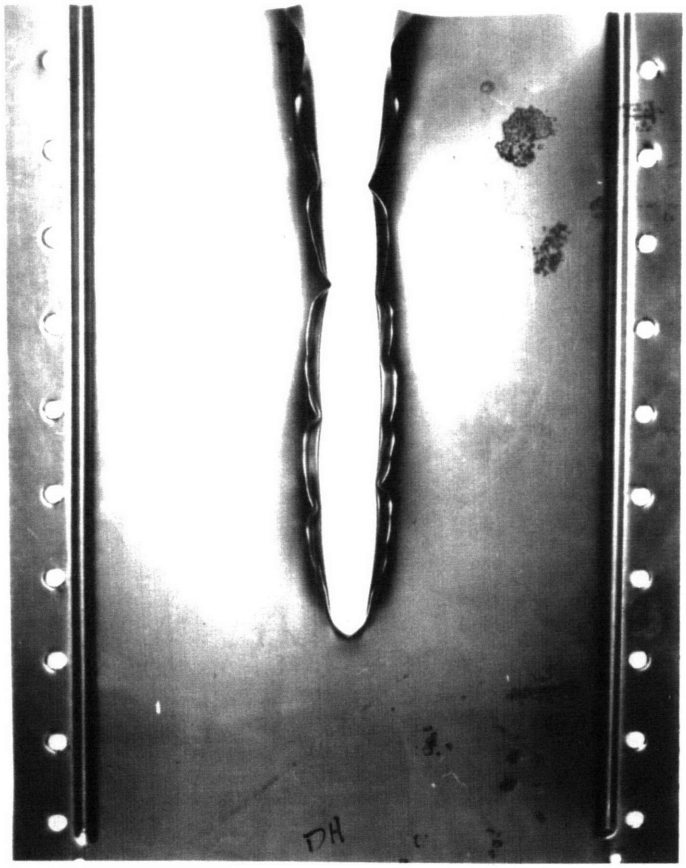

Fig. 3-2 Center clean cut of a plate by a sharp wedge with stable flap buckled

(Test #5)

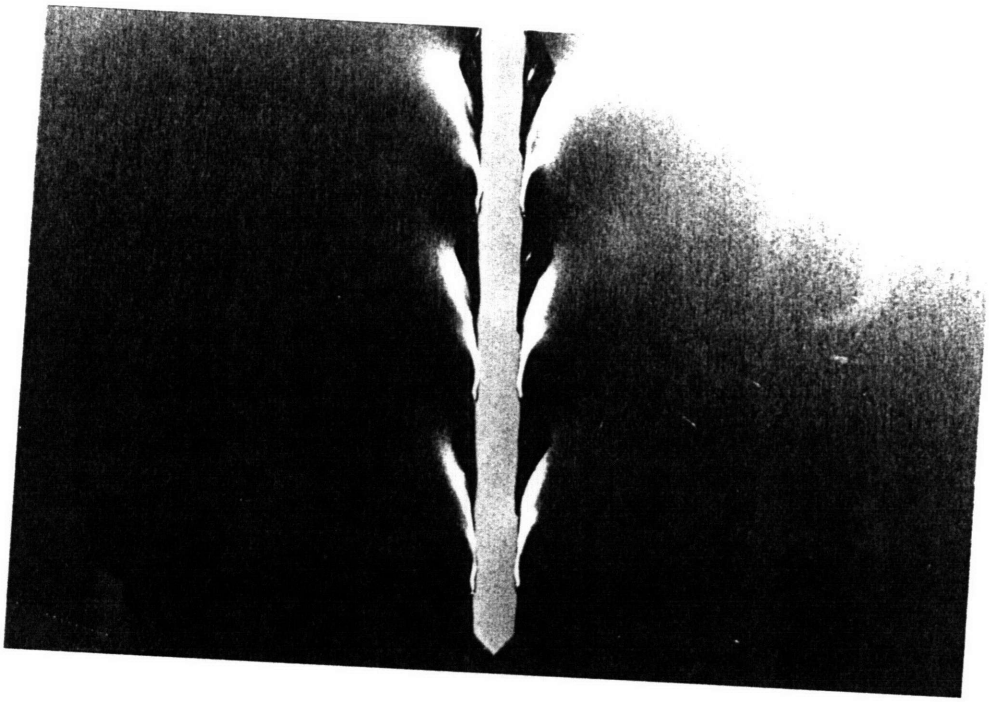

Fig. 3-3 Braided tearing of a plate by a narrow wedge

(Test #2)

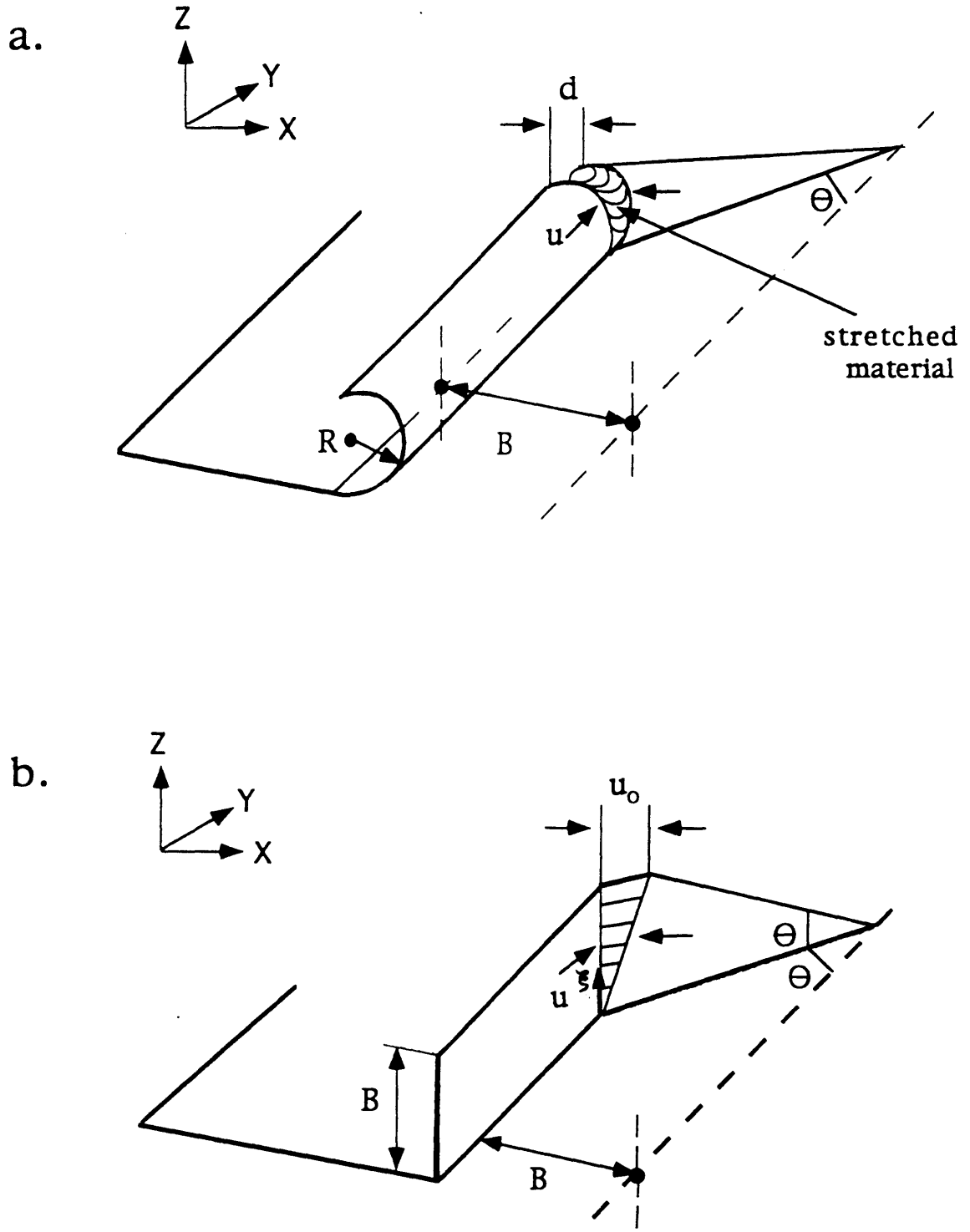

Fig. 3-4 Two kinematic models of the steady-state wedge penetration

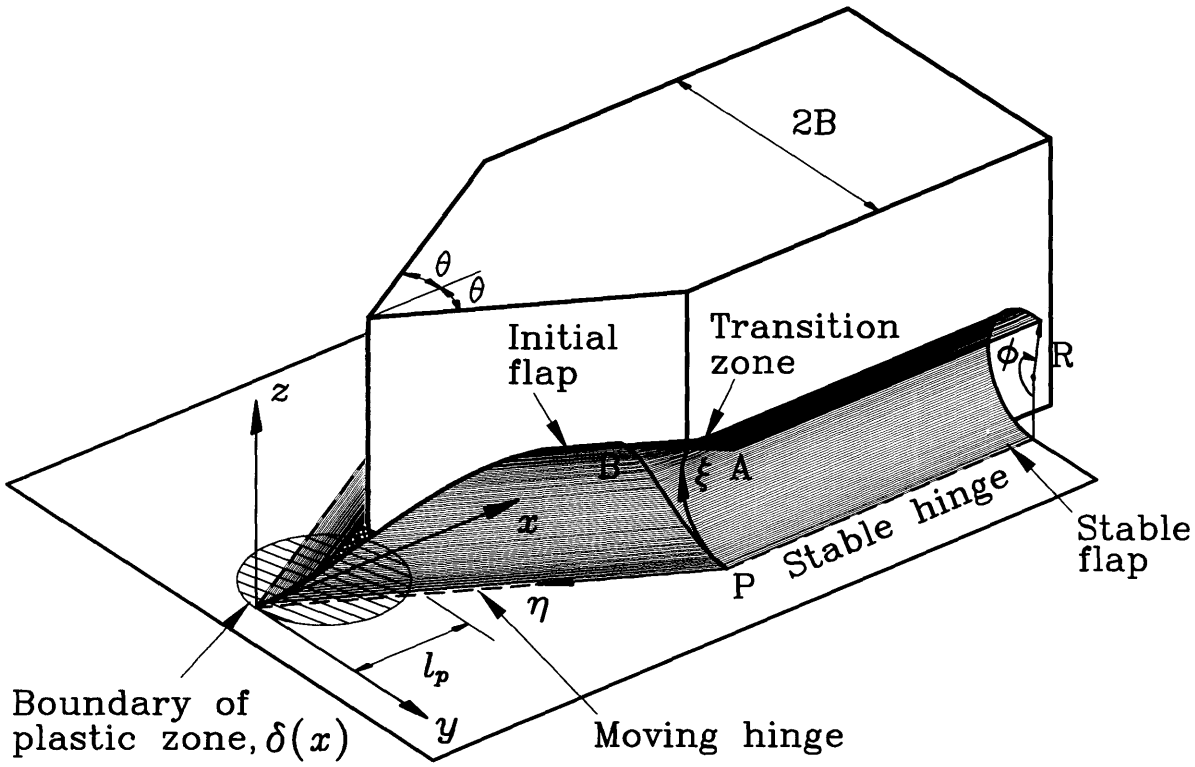

Fig. 3-5 Curling flap model for steady-state wedge cutting

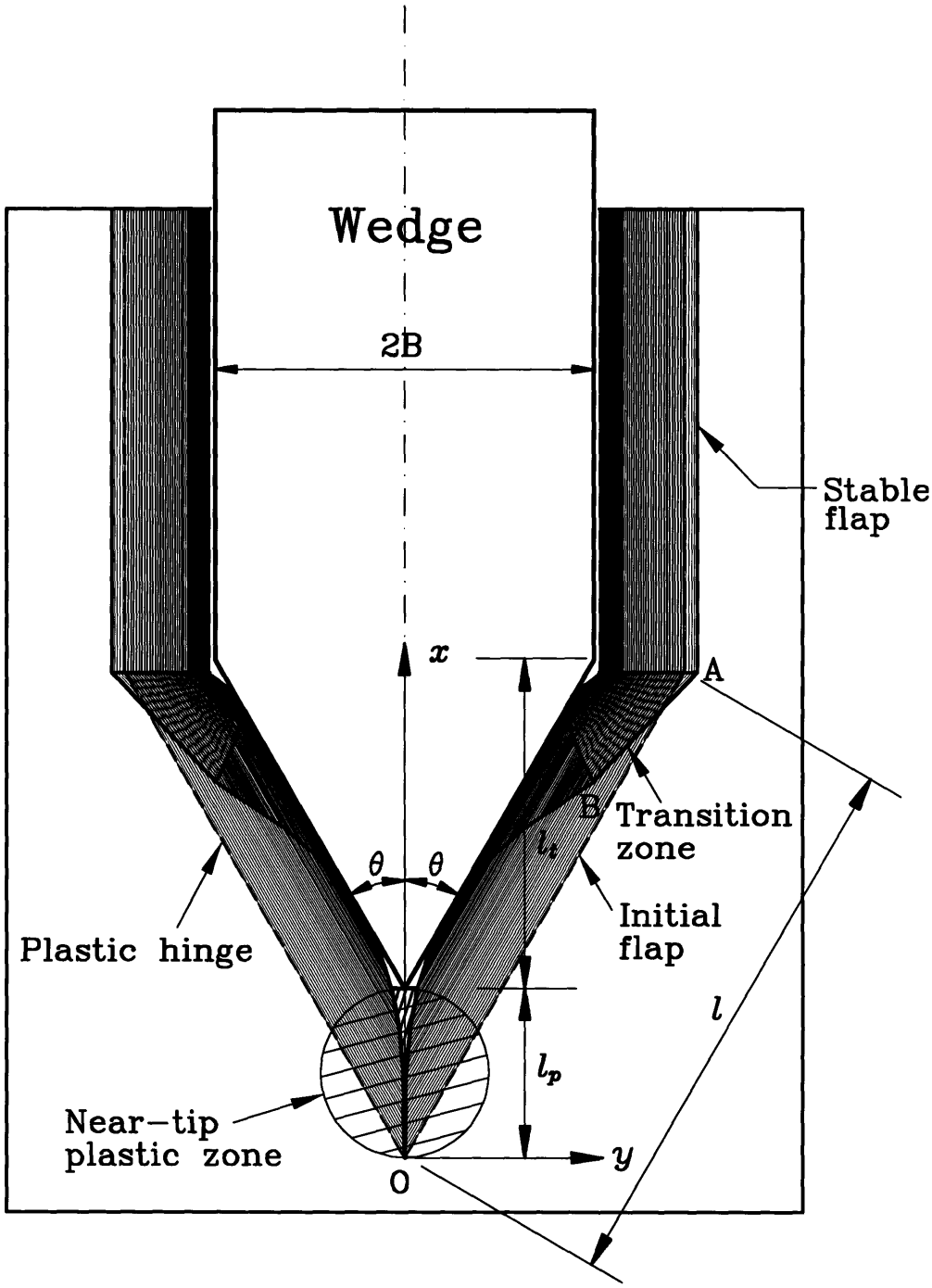

Fig. 3-6 Aerial view of curling flap model

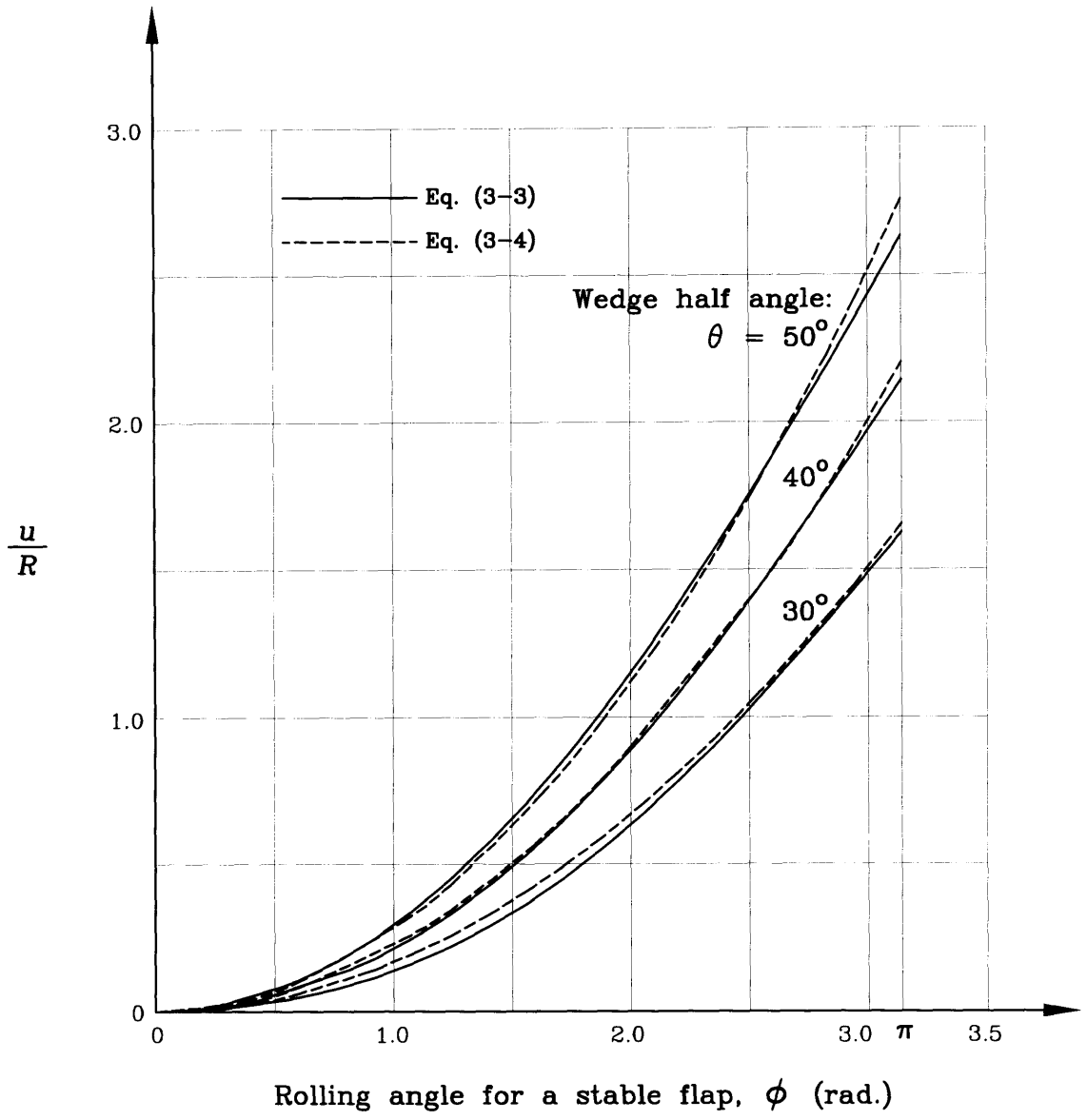

Fig. 3-7 Comparison of Eqs. (3-3) and (3-4)

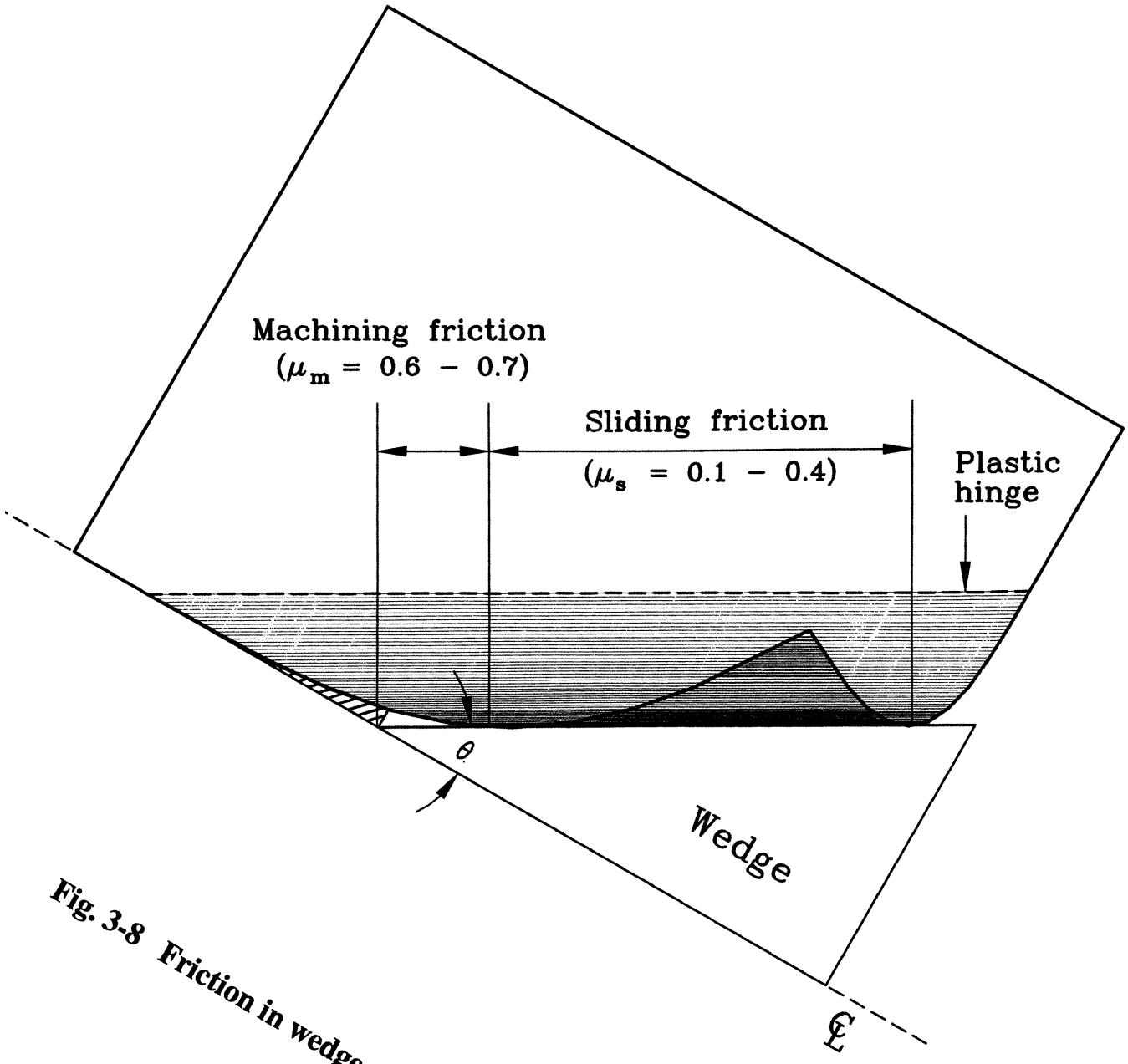

Fig. 3-8 Friction in wedge cutting process

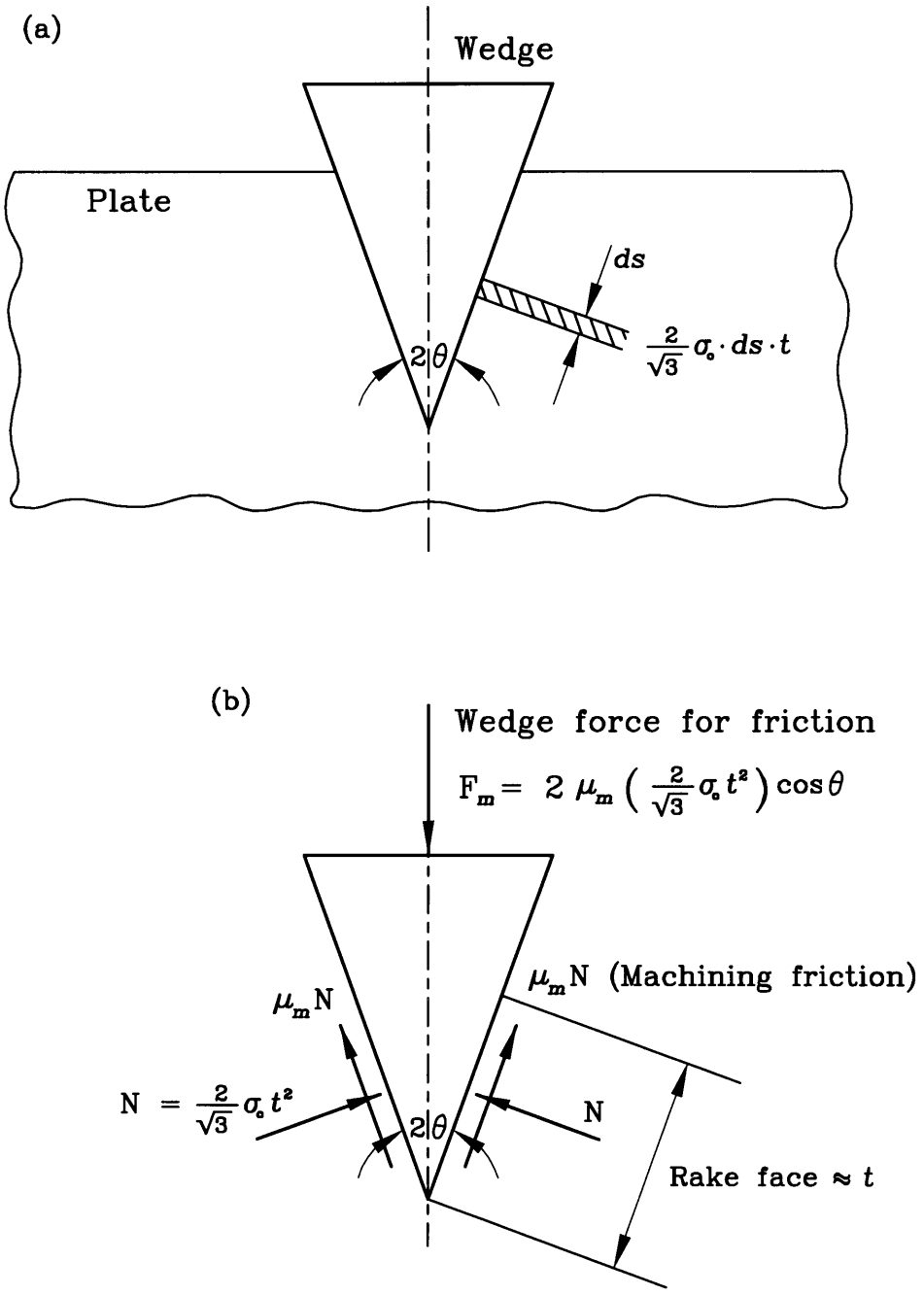

Fig. 3-9 Maching friction near a wedge tip

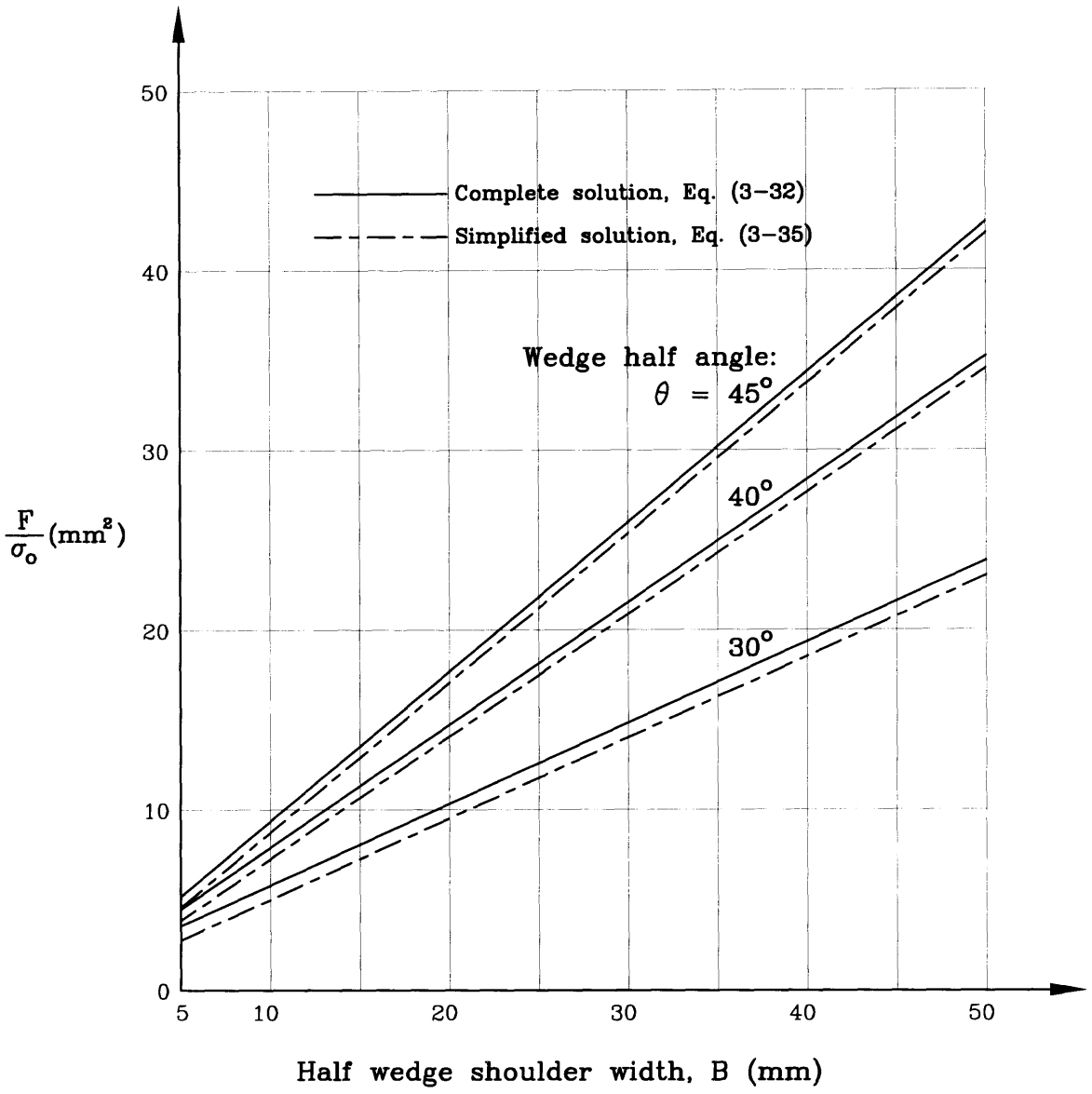

Fig. 3-10 (a) Comparison of complete *vs.* simplified wedge cutting force equations

(t = 0.5 mm, γ = 1, μ_s = 0.3, ζ = 1.5, μ_m = 0.7)

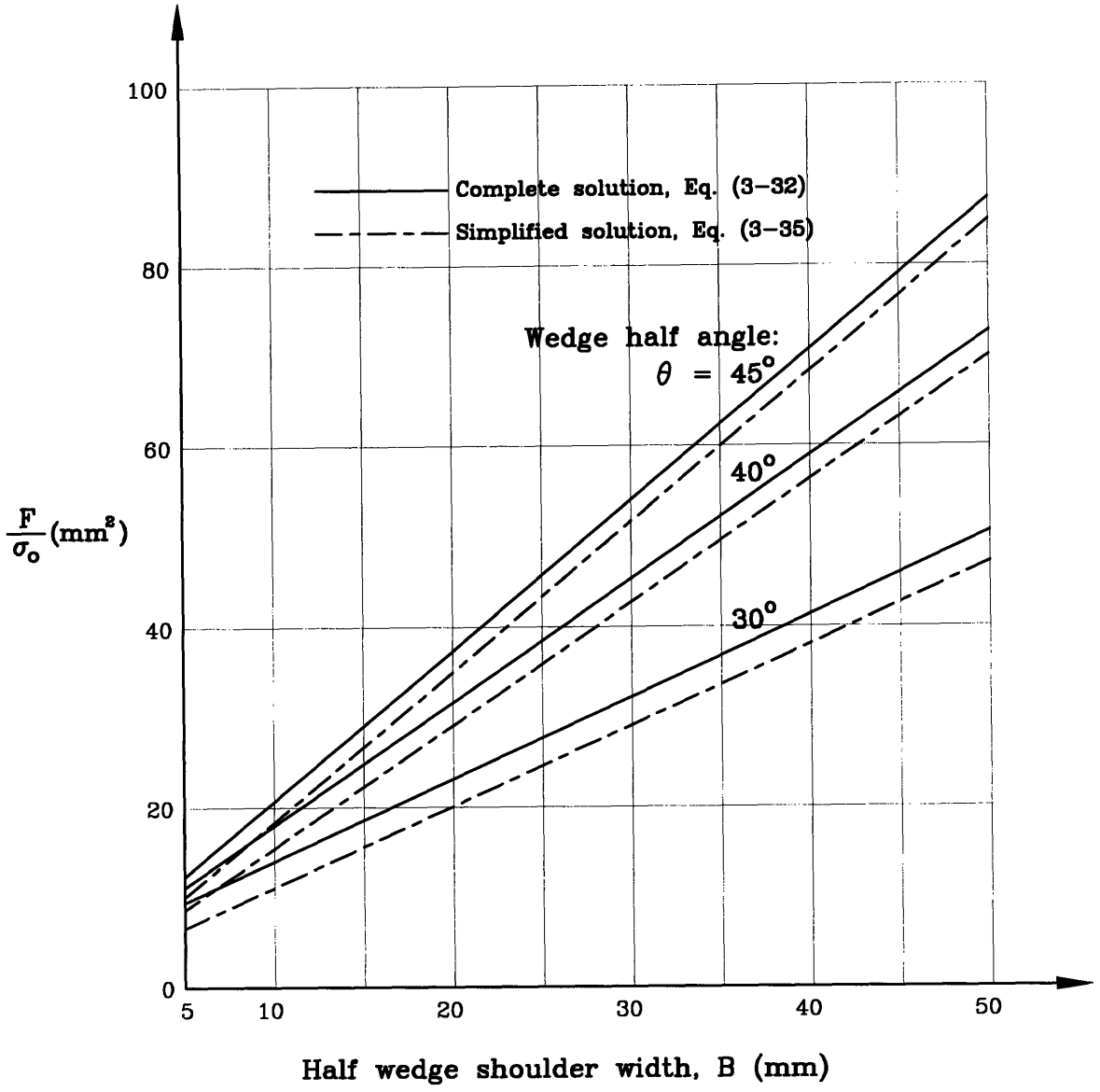

Fig. 3-10 (b) Comparison of complete *vs.* simplified wedge cutting force equations

(t = 1.0 mm, γ = 1, μ_s = 0.3, ζ = 1.5, μ_m = 0.7)

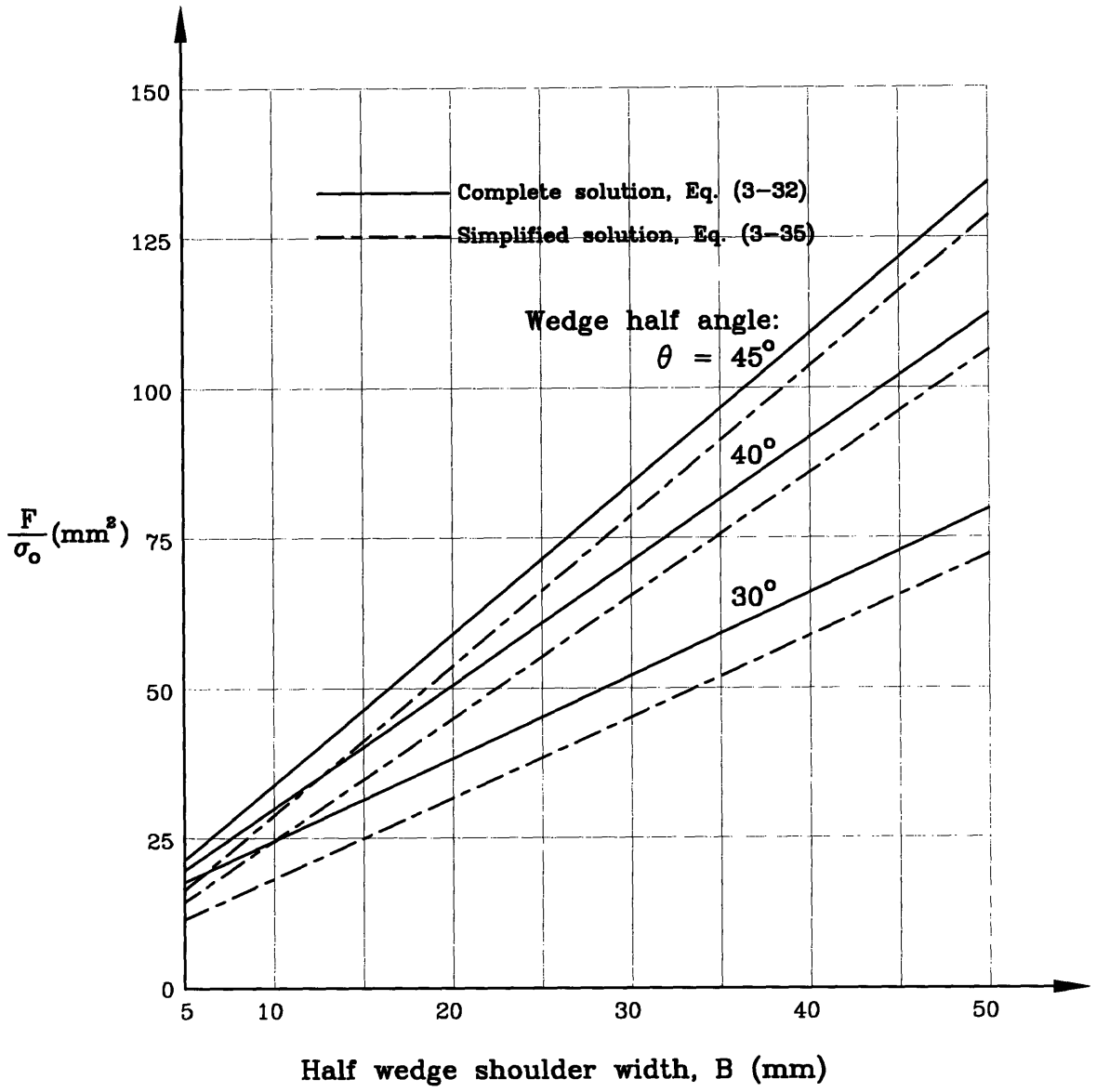

Fig. 3-10 (c) Comparison of complete *vs.* simplified wedge cutting force equations

(t = 1.5 mm, γ = 1, μ_s = 0.3, ζ = 1.5, μ_m = 0.7)

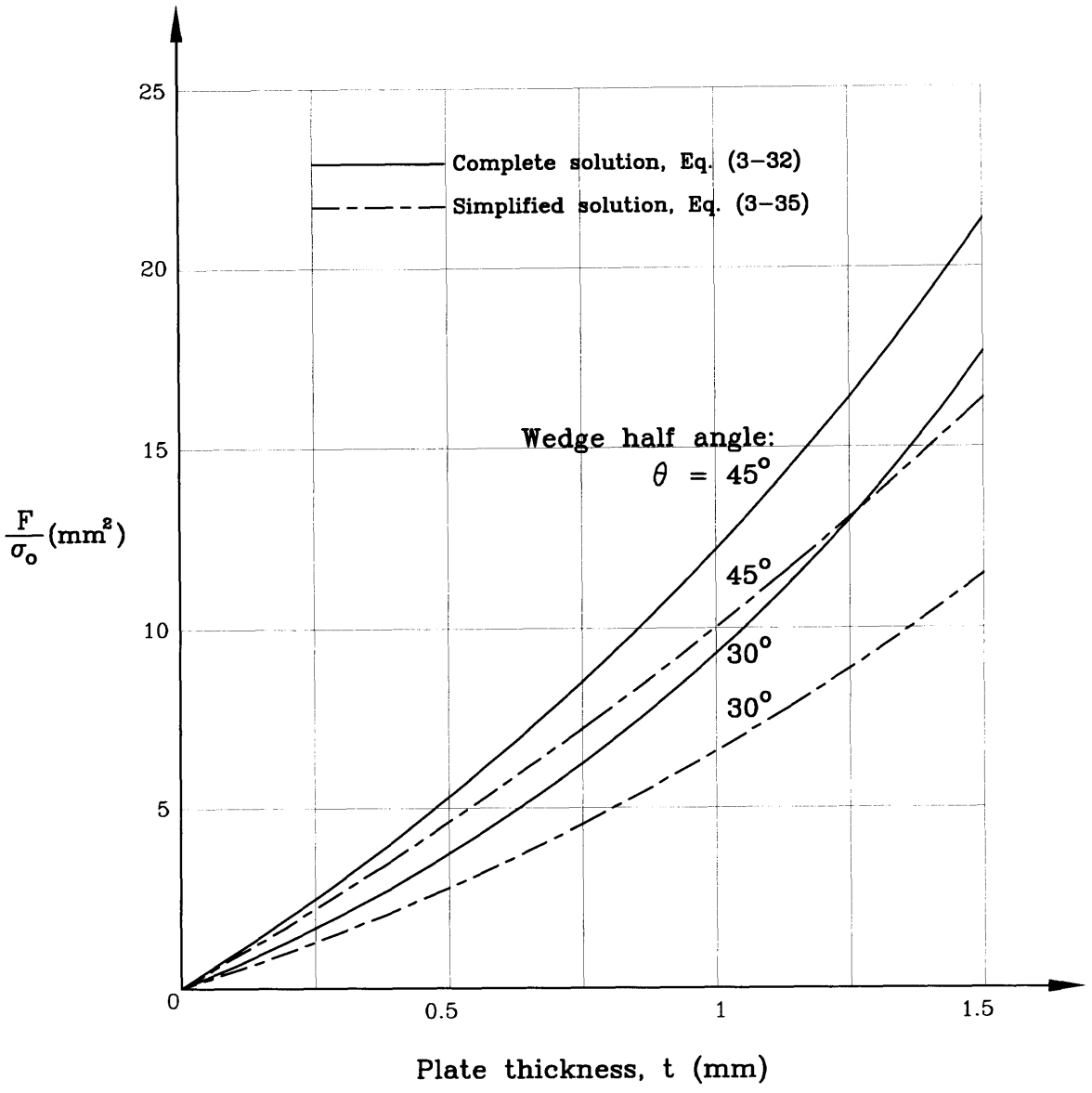

Fig. 3-11 (a) Comparison of complete *vs.* simplified wedge cutting force equations

(B = 5 mm, γ = 1, μ_s = 0.3, ζ = 1.5, μ_m = 0.7)

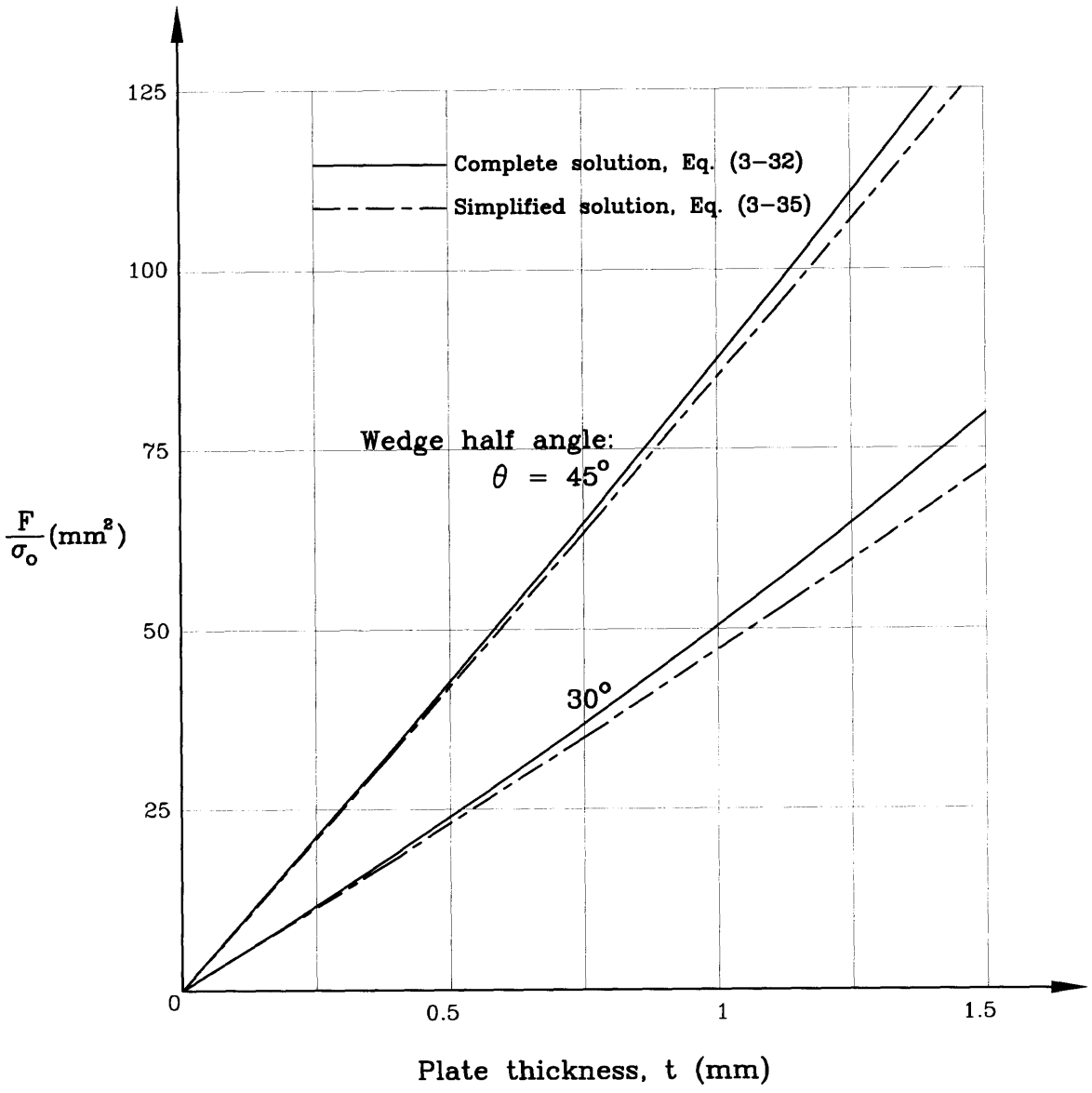

Fig. 3-11 (b) Comparison of complete *vs.* simplified wedge cutting force equations

(B = 50 mm, γ = 1, μ_s = 0.3, ζ = 1.5, μ_m = 0.7)

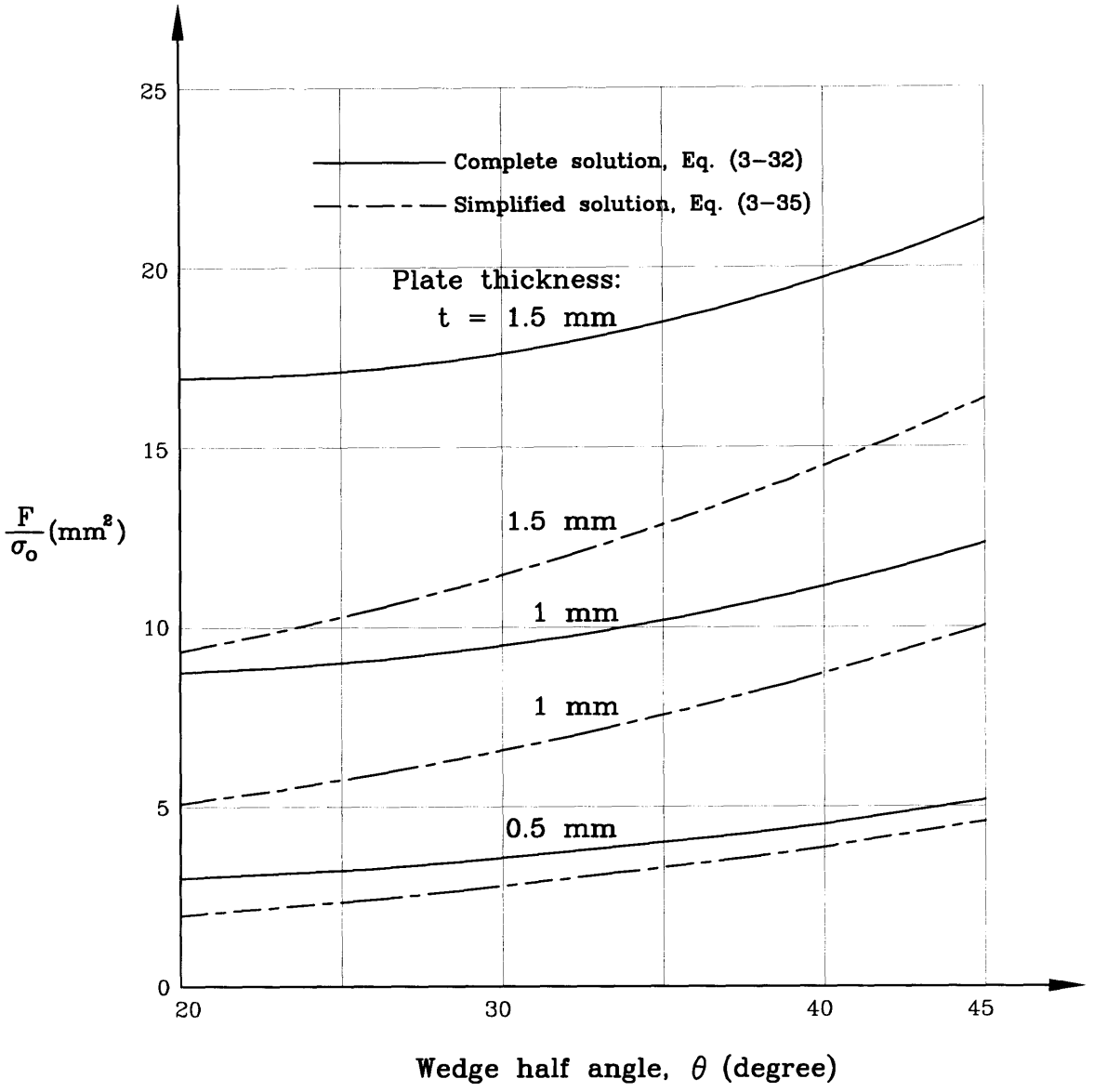

Fig. 3-12 (a) Comparison of complete *vs.* simplified wedge cutting force equations

(B = 5 mm, γ = 1, μ_s = 0.3, ζ = 1.5, μ_m = 0.7)

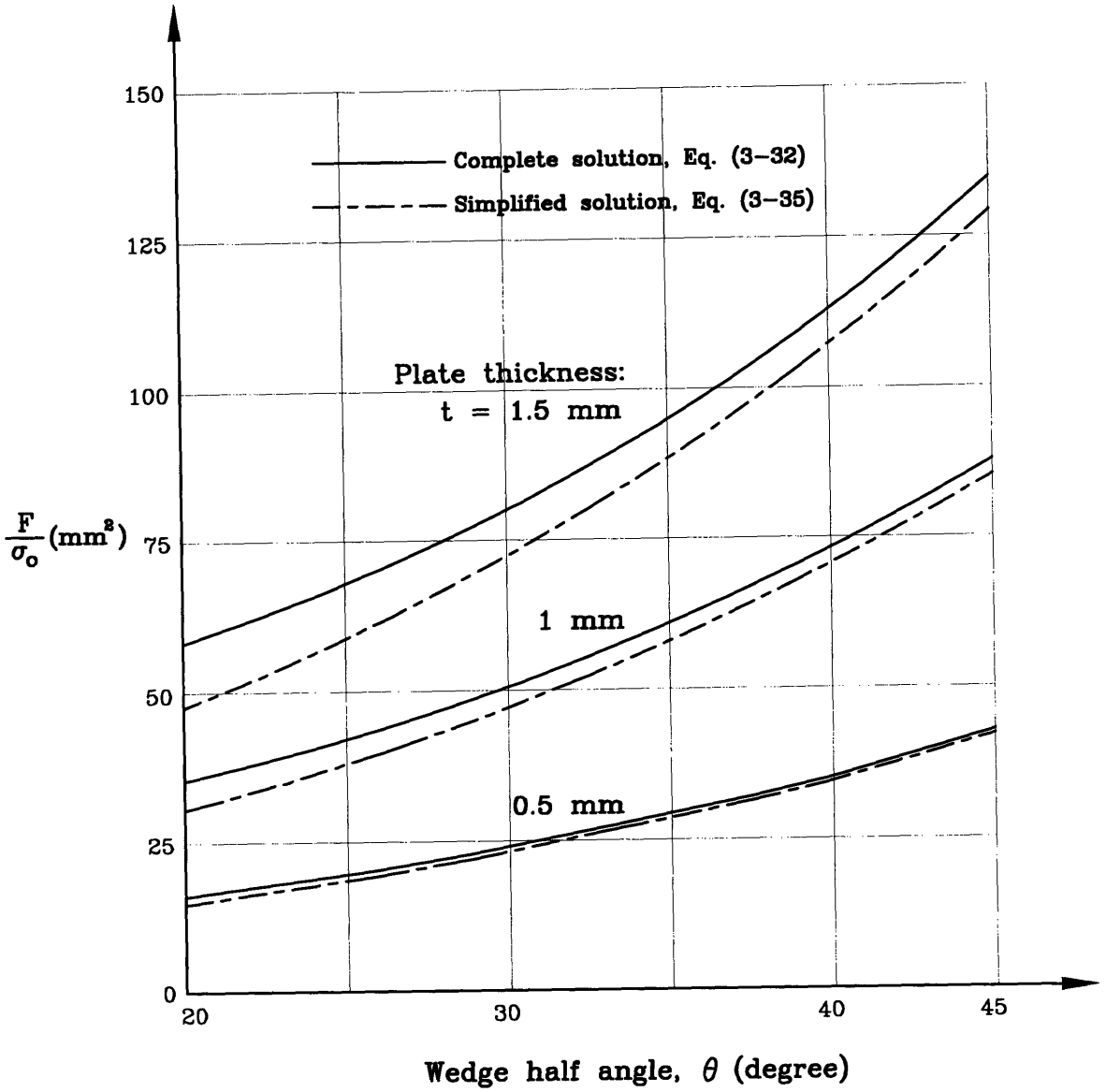

Fig. 3-12 (b) Comparison of complete *vs.* simplified wedge cutting force equations

(B = 50 mm, γ = 1, μ_s = 0.3, ζ = 1.5, μ_m = 0.7)

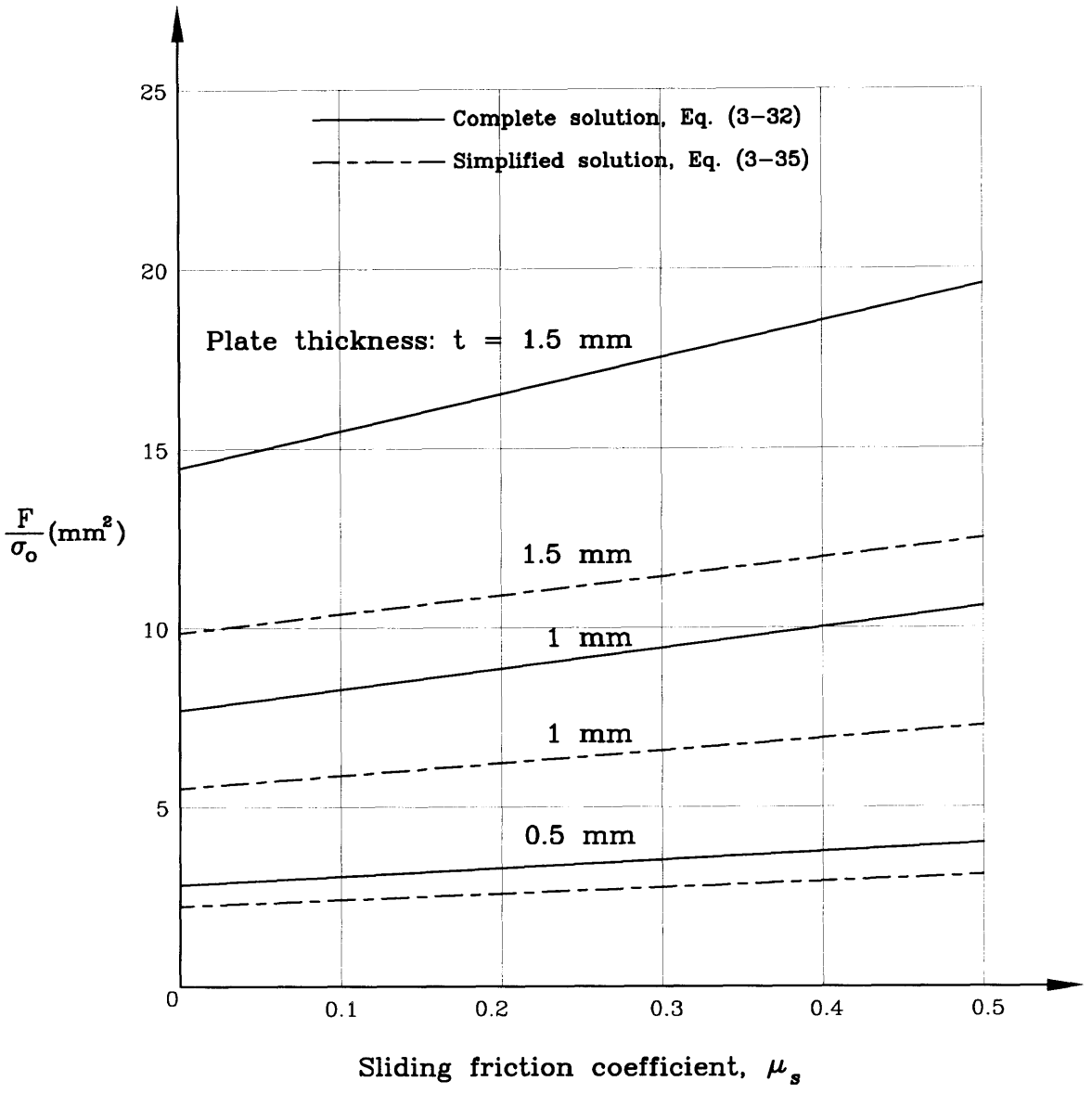

Fig. 3-13 (a) Comparison of complete *vs.* simplified wedge cutting force equations

(B = 5 mm, $\theta = 30^{o}$, $\gamma = 1$, $\zeta = 1.5$, $\mu_m = 0.7$)

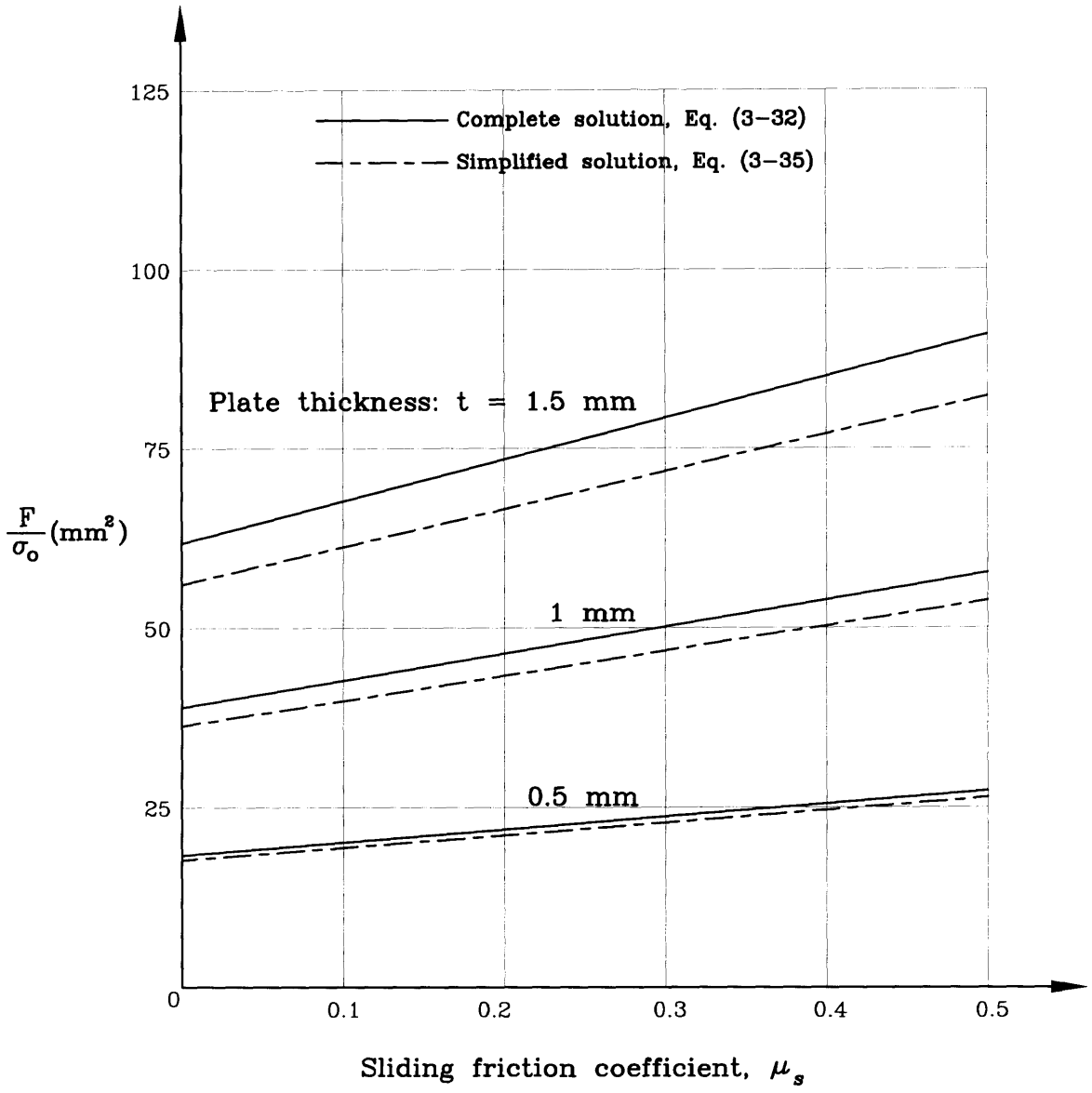

Fig. 3-13 (b) Comparison of complete *vs.* simplified wedge cutting force equations

(B = 50 mm, $\theta = 30^{o}$, $\gamma = 1$, $\zeta = 1.5$, $\mu_m = 0.7$)

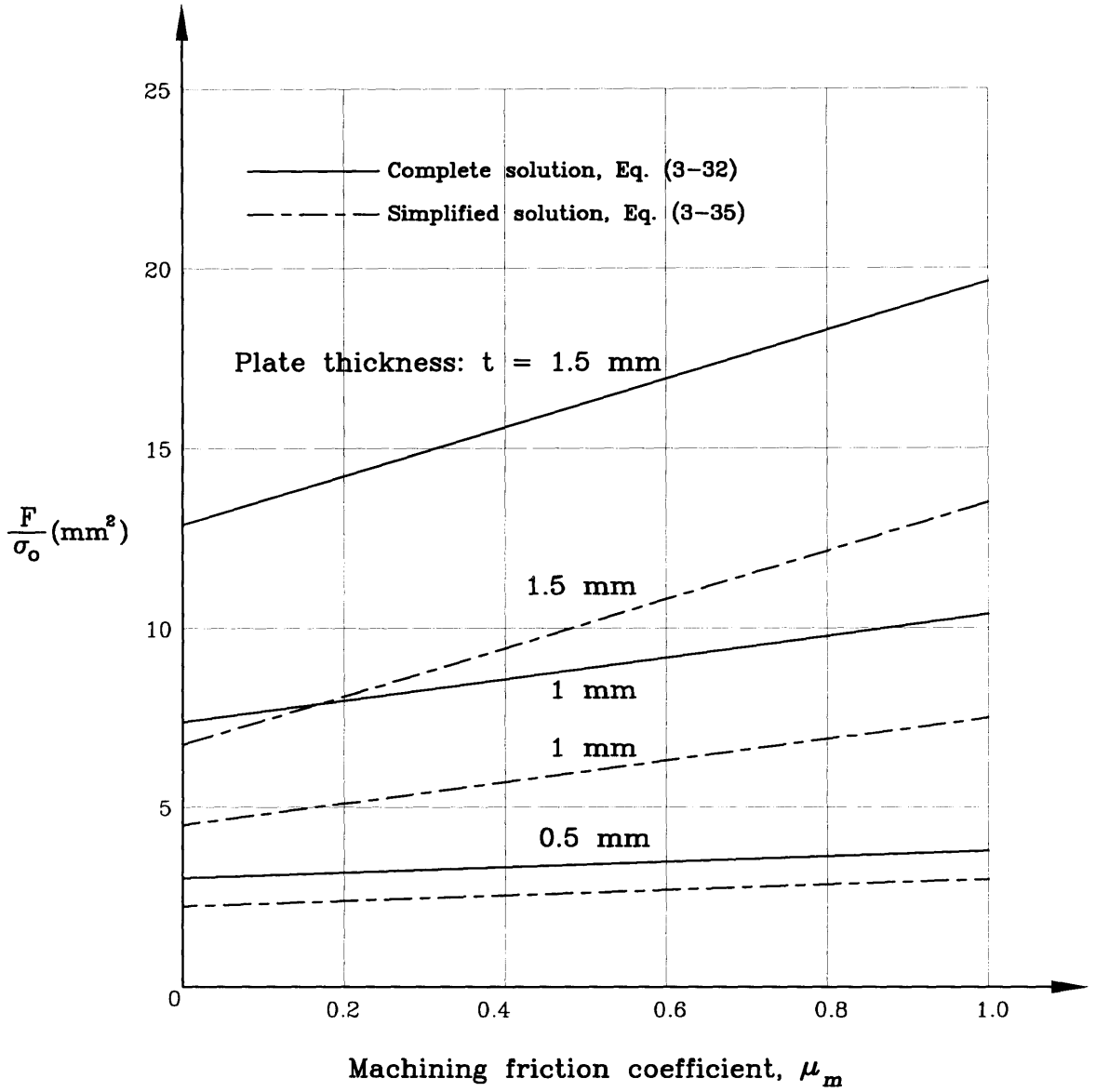

Fig. 3-14 (a) Comparison of complete *vs.* simplified wedge cutting force equations

(B = 5 mm, $\theta = 30^{\circ}$, $\gamma = 1$, $\zeta = 1.5$, $\mu_s = 0.3$)

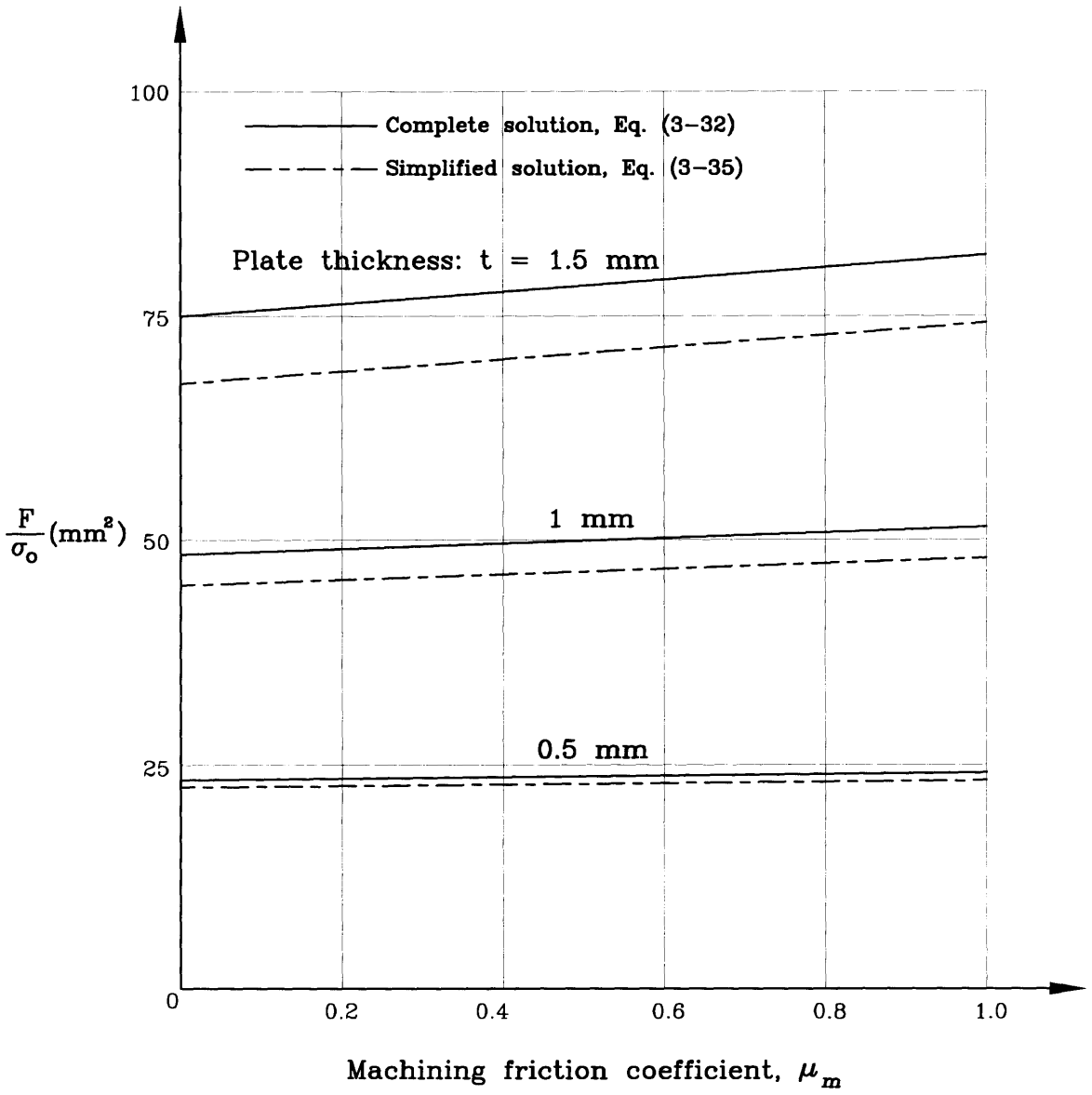

Fig. 3-14 (b) Comparison of complete *vs.* simplified wedge cutting force equations

(B = 50 mm, $\theta = 30^{o}$, $\gamma = 1$, $\zeta = 1.5$, $\mu_m = 0.7$)

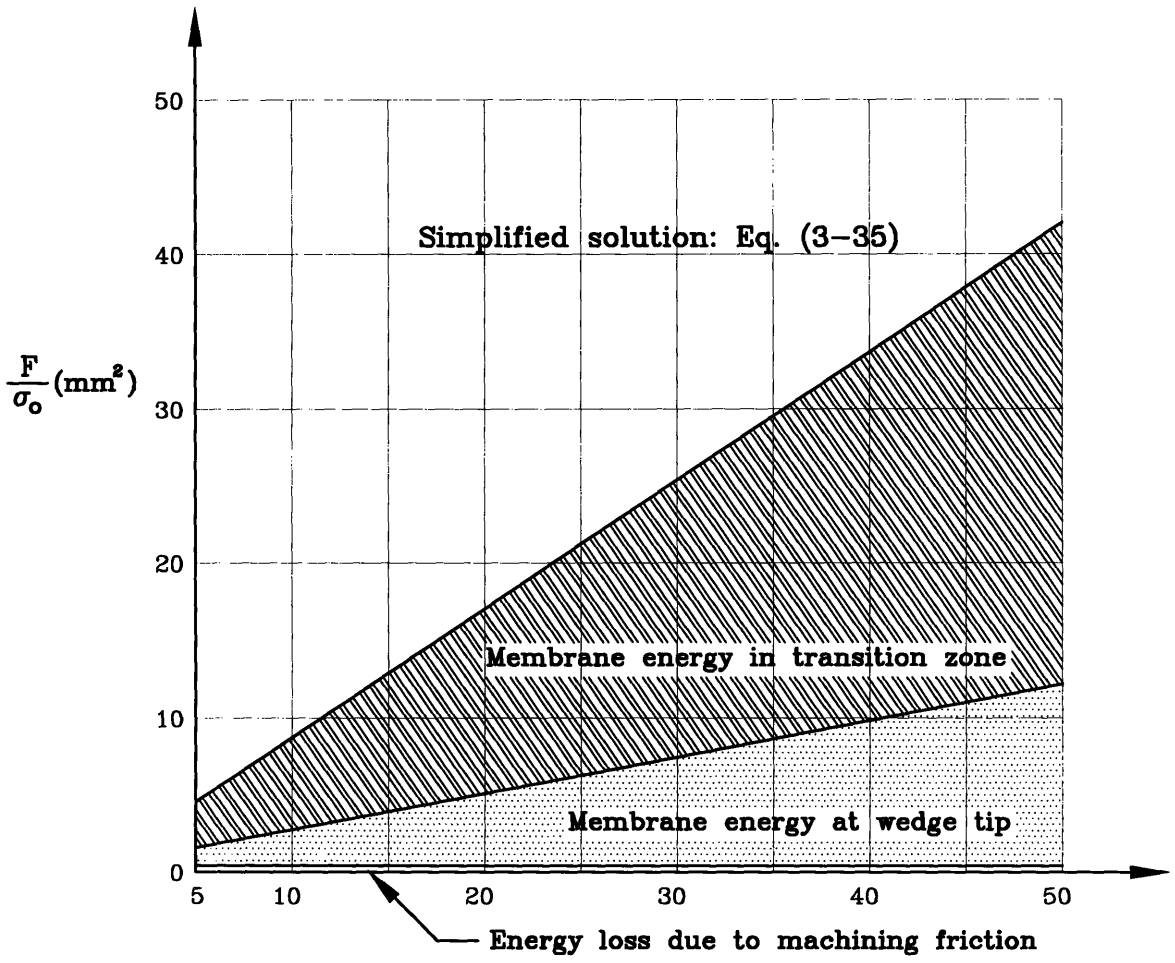

Fig. 3-15 (a) Energy partition in a steady-state wedge cutting process

(t = 0.5 mm, $\theta = 45^o$, $\gamma = 1$, $\zeta = 1.5$, $\mu_s = 0.3$, $\mu_m = 0.7$)

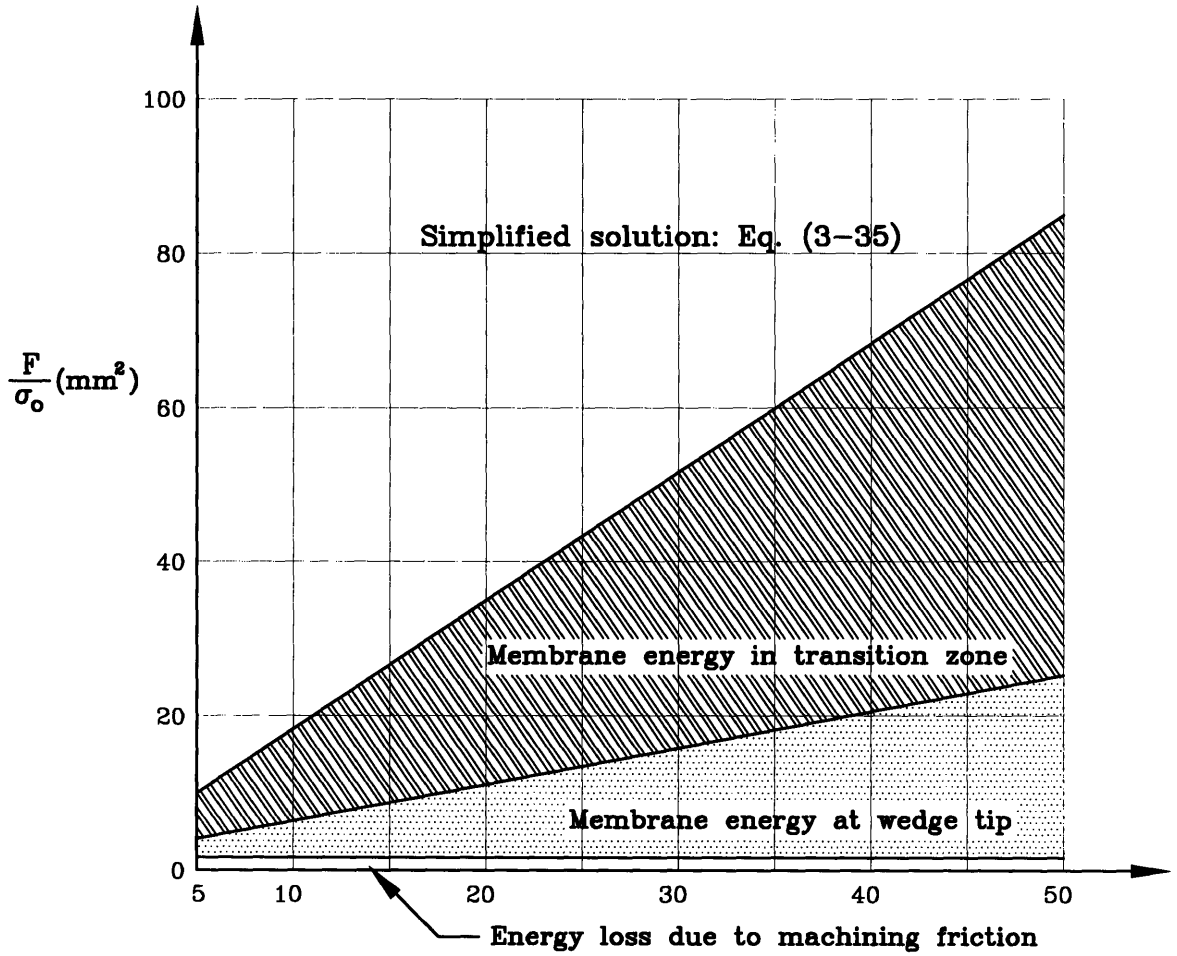

Fig. 3-15 (b) Energy partition in a steady-state wedge cutting process

(t = 1.0 mm, $\theta = 45^{o}$, $\gamma = 1$, $\zeta = 1.5$, $\mu_s = 0.3$, $\mu_m = 0.7$)

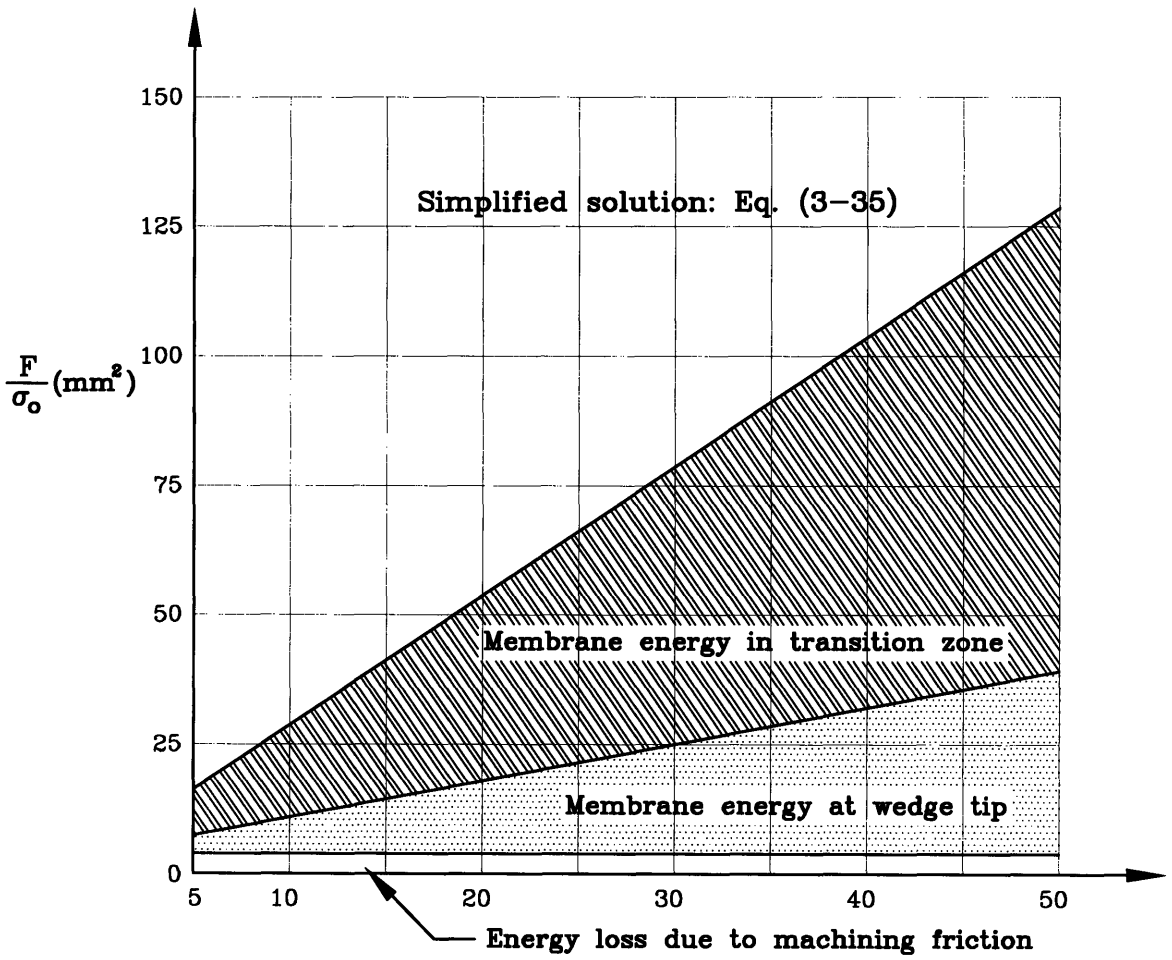

Fig. 3-15 (c) Energy partition in a steady-state wedge cutting process

(t = 1.5 mm, $\theta = 45^o$, $\gamma = 1$, $\zeta = 1.5$, $\mu_s = 0.3$, $\mu_m = 0.7$)

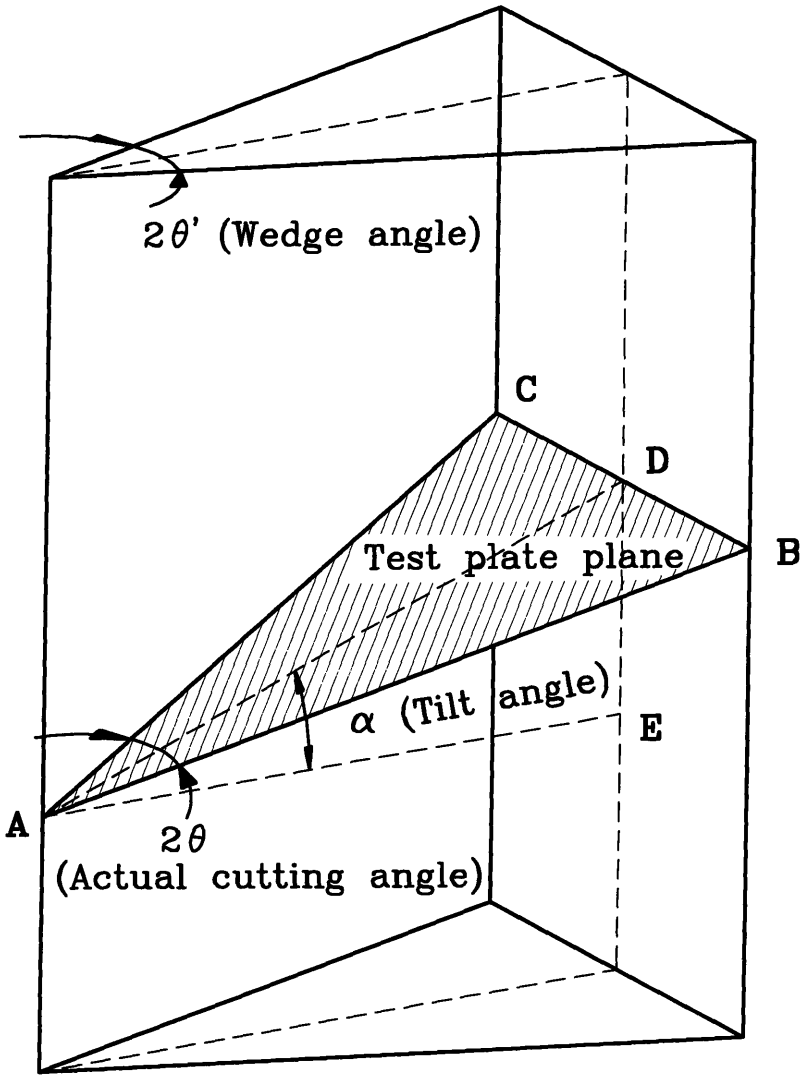

$$AD = AE / \cos\alpha$$
$$BD = AE \cdot \tan\theta'$$
$$\tan\theta = BD / AD$$
$$\tan\theta = \tan\theta' \cdot \cos\alpha$$

Fig. 3-16 Wedge angle projected on tilt plate, θ

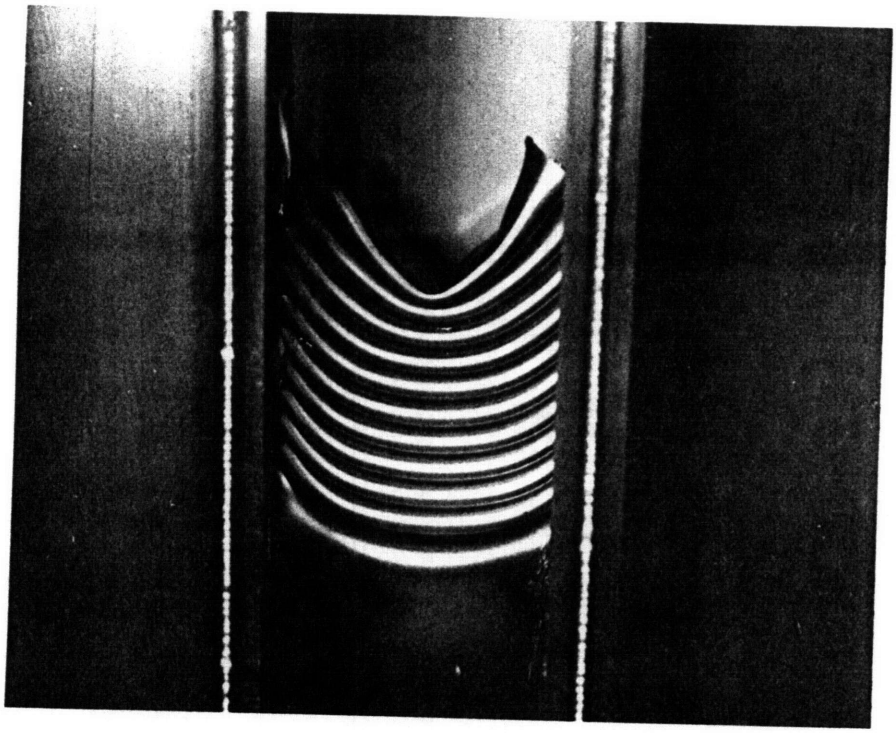

Fig. 3-17 Concertina tearing failure by wedge pushing

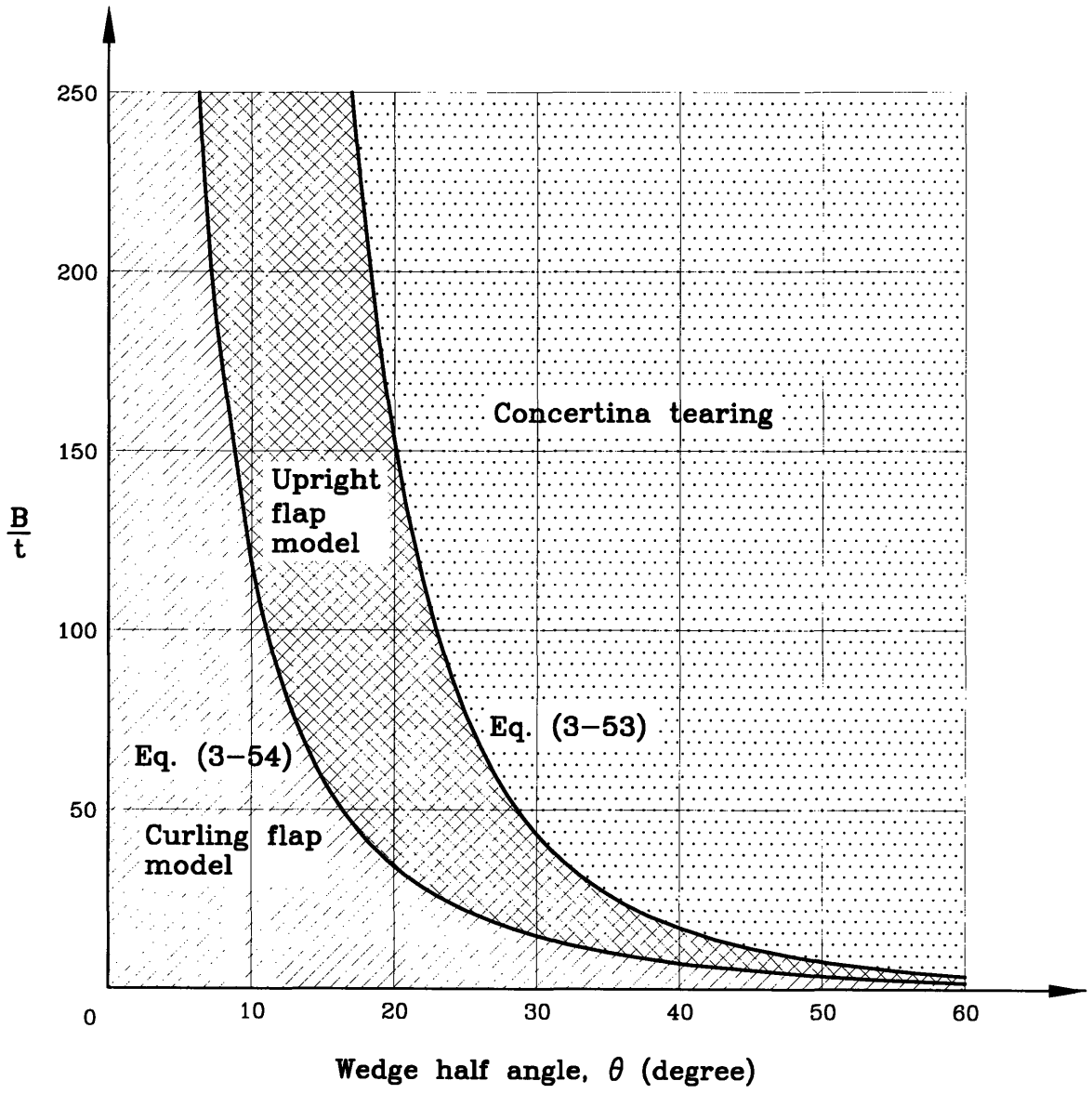

Fig. 3-18 Boundary curve separating the "clean cut" and "concertina tearing" failure modes

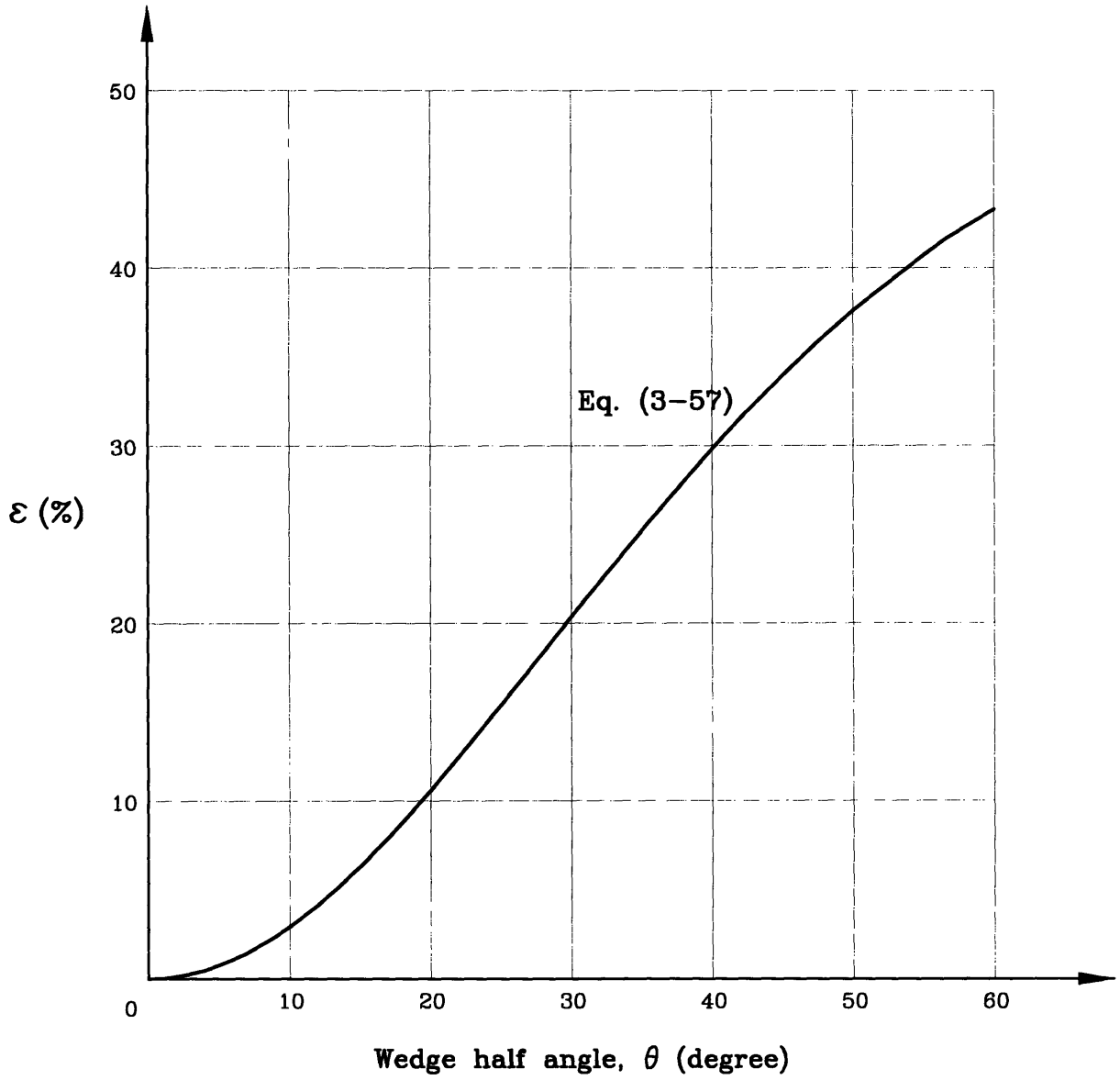

Fig. 3-19 Flap tensile strain *vs.* wedge semi-angle curve

a)

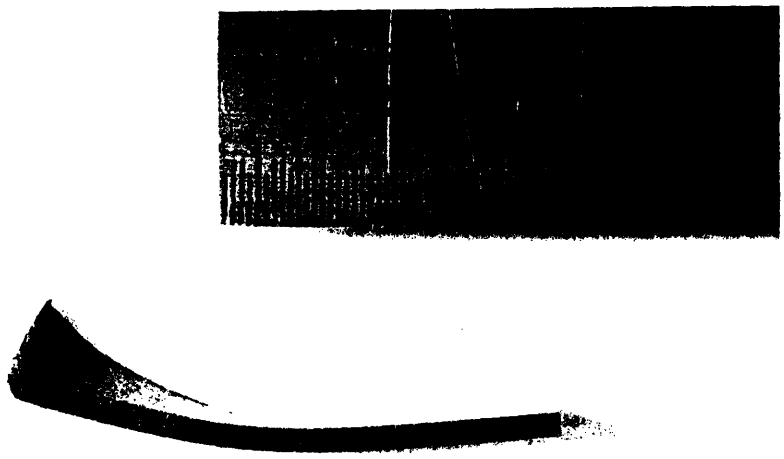

b)

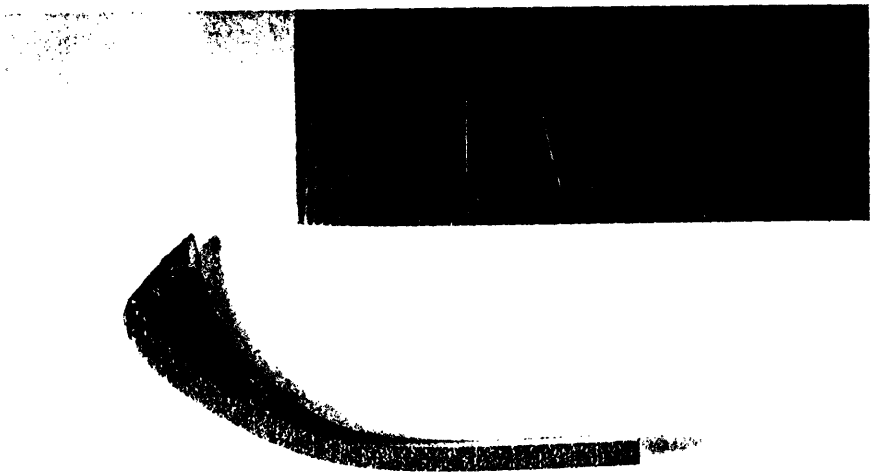

Fig. 3-20 Cross-section of flap sliced along cutting direction

(To be continued)

c)

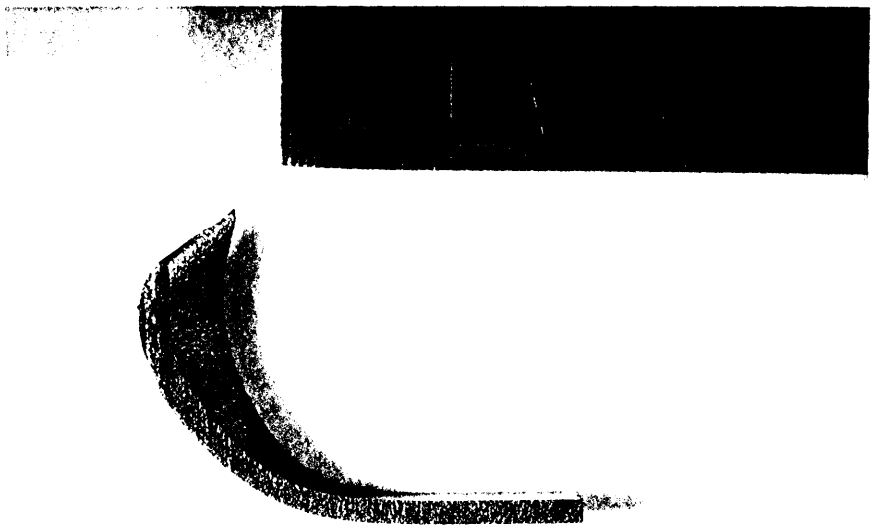

d)

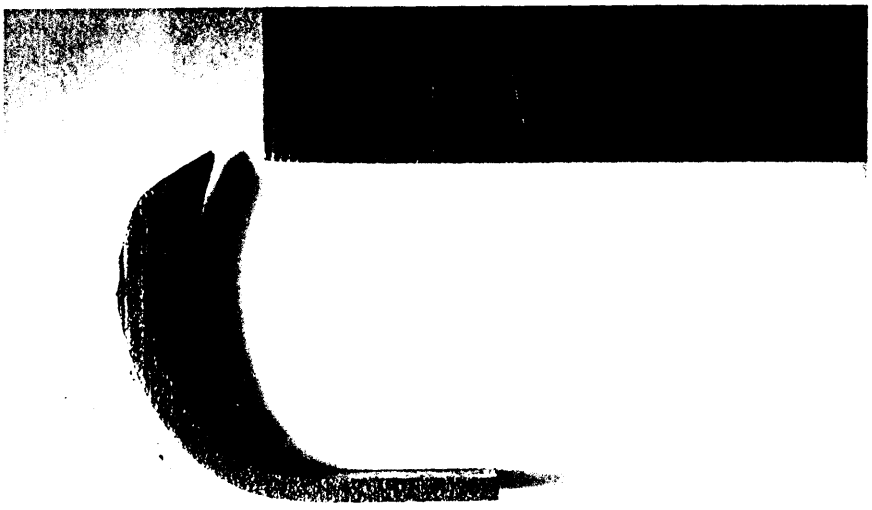

Fig. 3-20 Cross-section of flap sliced along cutting direction

(Continued from the last page and to be continued)

e)

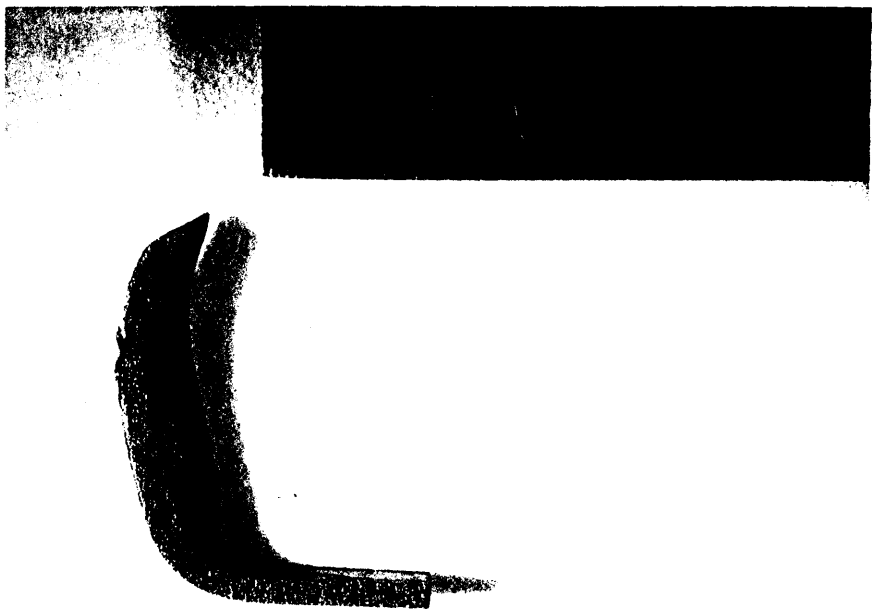

f)

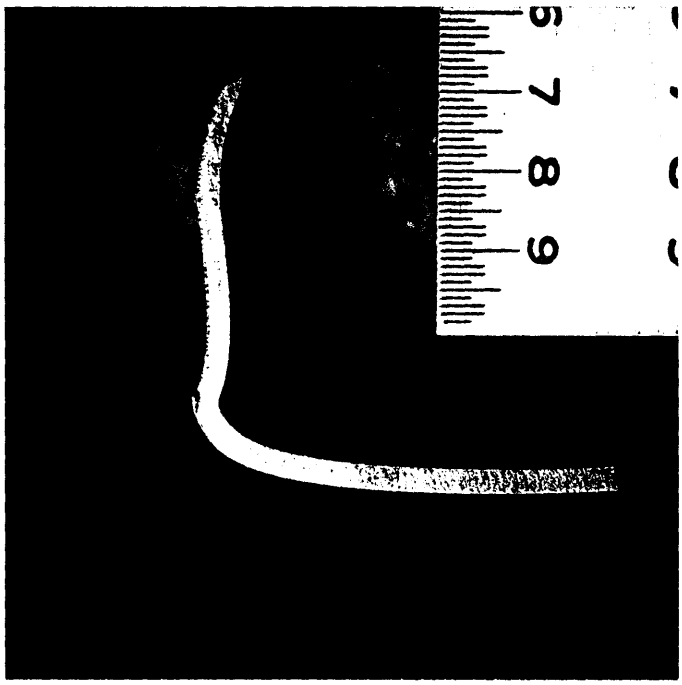

Fig. 3-20 Cross-section of flap sliced along cutting direction

(End of continuation from last page)

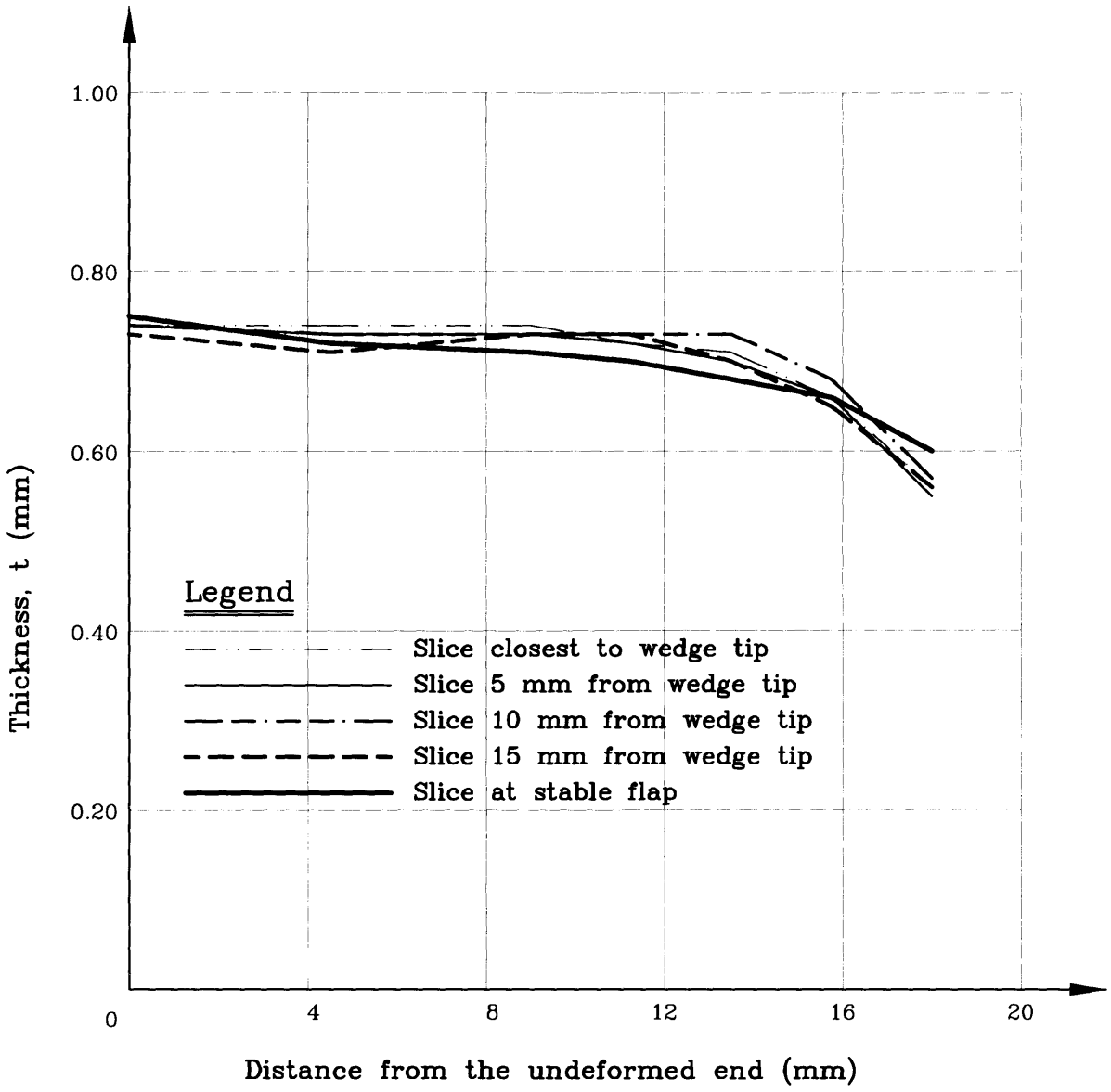

Fig. 3-21 Thickness variation along flap curling direction

Chapter 4

Analysis of Stable Flap Buckling

4.1. Introduction

Under a steady-state wedge cutting process, stable flaps may buckle due to the extremely large compressive strain present in the transition zone when the B/t ratio is large (Fig. 3-2). In this chapter, theoretical buckling analysis for a non-uniform thickness plate with three edges fixed and one edge free is first performed to derive a compressive buckling coefficient which establishes a buckling criterion for the stable flaps. Energy conservation law is then applied to determine the force required to buckle the stable flaps if a stable flap buckling does occur. It can be concluded from the subsequent analysis that the contribution of stable flap buckling towards the total wedge cutting force is negligible. This chapter is, in essence, to provide a sound proof for such an important conclusion.

4.2. Buckling of a rectangular plate with non-uniform thickness

This section aims to solve the buckling problem for a non-uniform thickness rectangular plate subjected to uni-axial compressive stress. Three edges of a plate are assumed to be fixed, and the fourth one is set free (Fig. 4-1). Garlerkin's method and MAPLE computer software are employed here to derive a closed-form solution for this classical elastic buckling problem. Comparison with Hill's result [30] for the uniform thickness plate buckling analysis having the same boundary conditions shows that a good agreement is obtained, but the current theory extends the theory into the non-uniform thickness plate buckling region.

A closed-form expression for the critical strain is derived subsequently so that the buckling solution based on elastic theory can be used in the plastic plate buckling prediction as seen in sequel.

4.2.1. Introduction

The phenomenon of buckling of non-uniform thickness rectangular plate was observed during the steady-state wedge cutting tests conducted in M.I.T. [14]. Thin plate in the stable flap region is subjected to a large in-plane compressive stress which causes the stable flap to buckle in a regular pattern (Fig. 3-2). The introduction of flap thickness non-uniformity was chiefly owing to the fact that the steady-state wedge cutting process introduces a large tensile deformation in the transition zone which causes the stable flap thickness variation.

Hill [30] pioneered a systematic study on the rectangular plate buckling problems, in which many different boundary conditions were included. In his analysis, plates are assumed to have a uniform thickness and subjected to a uni-axial compressive stress. Garlerkin's method was used to solve the classical buckling problem and a chart of compressive buckling coefficient *vs.* plate aspect ratio was presented. Hill's approach of solving the buckling problem is so effective that this method is also adopted in our analysis. Lang [31] introduced thickness non-uniformity into the plate buckling study. He derived a general solution for the buckling problem of a simply-supported rectangular plate with a non-uniform thickness, although the mathematical manipulation involved was seen to be tedious and complicated.

This section is providing a solution of the buckling problem of a rectangular plate with a linearly-varying thickness and subjected to a uni-axial compressive stress (Fig. 4-1). The loaded edges are assumed to be fixed. One of the unloaded edges is fixed whereas the other is free. A state-of-art computer software (MAPLE) is employed here to solve the mathematical problem symbolically. The application of MAPLE into our analysis presents a good

example of how to solve such a complicated problem accurately and efficiently.

4.2.2. Boundary conditions

For the analytical model shown in Fig. 4-1 with the established coordinate system, one can formulate the boundary conditions as follows:

$$\begin{cases} w|_{x=0,a} = 0, \\ \left.\dfrac{\partial w}{\partial x}\right|_{x=0,a} = 0. \end{cases} \tag{4-1}$$

$$\begin{cases} w|_{y=0} = 0, \\ \left.\dfrac{\partial w}{\partial x}\right|_{y=0} = 0. \end{cases} \tag{4-2}$$

$$\begin{cases} \left.\dfrac{\partial^2 w}{\partial y^2} + \nu \dfrac{\partial^2 w}{\partial x^2}\right|_{y=b} = 0, \\ \left.\left[\dfrac{\partial^3 w}{\partial y^3} + (2-\nu) \cdot \dfrac{\partial^3 w}{\partial x^2 \partial y}\right]\right|_{y=b} = 0. \end{cases} \tag{4-3}$$

where ν is Poisson's ratio. Eqs. (4-1) and (4-2) represent the geometric boundary conditions, and Eq. (4-3) is a force boundary condition representing the zero moment and shear force conditions along the free edge.

4.2.3. Derivation of buckled shape expression

Since it is very difficult to find an exact solution for the plate buckling problem shown in Fig. 4-1, Garlerkin's method is to be used to derive an upper bound approximation solution. It is well known that the accuracy of the method is highly dependent upon how close is the assumed buckled shape to reality. It is proved that an exact solution will be obtained if the buckled shape assumed is exactly the same as an actual deformed one; otherwise, only an

upper bound solution is available. In the following analysis, the assumed buckling shape is proved to conform both geometric and force boundary conditions, which is believed to yield a very good estimation to the problem.

Let's first assume that a general buckled shape has the following expression:

$$w = f(x)\, g(y)\,. \tag{4-4}$$

Substituting Eq. (4-4) into the two force boundary conditions in Eq. (4-3) yields:

$$f(x)\, g''(b) + \mu \cdot f''(x)\, g(b) = 0\ , \tag{4-5}$$

and

$$f(x)\, g^{(3)}(b) + (2-\mu) \cdot f''(x)\, g'(b) = 0\ . \tag{4-6}$$

The primes and parenthesized number in the superscripts of the above functions represent the order of derivatives about the variable y. Eliminating $f(x)$ from the above two equations gives the following relationship for the function $g(y)$ at $y = b$:

$$\mu\, g(b)\, g^{(3)}(b) = (2-\mu)\, g'(b)\, g''(b)\,. \tag{4-7}$$

The above relationship makes sure that the assumed shape would unconditionally satisfy the force boundary condition, Eq. (4-3).

Next, let us assume that the plate buckling shape conforms the following expression

$$w = A \sin\left(\frac{\pi x}{a}\right) \sin\left(\frac{m\pi x}{a}\right) \cdot \left(1 - \cos\frac{ny}{b}\right), \tag{4-8}$$

where m is an integer determining the number of waves along x-axis, and the parameters A and n are variables to be determined. It is clear that the above buckling shape, Eq. (4-8), satisfies all the geometric boundary conditions, Eqs. (4-1) and (4-2). In order to satisfy the force boundary condition, Eq. (4-7), the unknown parameter n in Eq. (4-8) must satisfy the following relationship:

$$n = \text{acos}\left[\frac{\mu}{2(-1+\mu)}\right]. \tag{4-9}$$

Now, the proposed plate buckling shape, Eq. (4-8), can satisfy both the geometric and force boundary conditions if n is defined as Eq. (4-9).

4.2.4. Step-by-step solution for the plate buckling problem

Appendices C, D, and E list the step-by-step derivations of the non-uniform thickness plate buckling problem by using MAPLE [32]. Each Appendix gives one buckling mode, e.g. Appendix C corresponds to the buckling mode $m = 1$, etc. The symbols and their corresponding equations are explained in detail next.

The differential equation for the rectangular plate buckling problem is derived by Timoshenko [33]. In order to apply Garlerkin's method, first the differential equation representing plate deformation is evaluated as:

$$DE = \left(\frac{\partial^2 w}{\partial x^2} + \frac{\partial^2 w}{\partial y^2}\right)^2 - 2(1-\nu)\left[\frac{\partial^2 w}{\partial x^2}\cdot\frac{\partial^2 w}{\partial y^2} - \left(\frac{\partial^2 w}{\partial x \partial y}\right)^2\right]. \tag{4-10}$$

Integrating the above equation once with respect to x gives a complicated expression:

$$Z1 = \int_0^a (DE)\cdot dx. \tag{4-11}$$

Integrating $Z1$ once more with respect to y yields an expression representing the total internal virtual energy of the plate, and it has the following form:

$$Z2 = \int_0^b \left(1 - \beta\cdot\frac{y}{b}\right)^3 \cdot Z1 \cdot dy, \tag{4-12}$$

where the cubic term in the above expression represents the plate thickness non-uniformity.

The external virtual work has the following expression:

$$Z3 = \int_0^b \int_0^a \left(1 - \beta \cdot \frac{y}{b}\right) \cdot \left(\frac{\partial w}{\partial x}\right)^2 \cdot dxdy, \tag{4-13}$$

where the linear term in the above equation represents the uniform compressive stress applied along the plate loaded edges.

The variational function of the total virtual work can now be defined as:

$$U = Z2 - X \cdot Z3\ , \tag{4-14}$$

where the coefficient X has the following form:

$$X = \frac{\sigma \cdot t_o}{D_o}, \tag{4-15}$$

and σ is the uni-axial compressive stress and D_o is the plate bending stiffness.

The principle of virtual work is applied here to minimize the total virtual work U, i.e.

$$Z4 = \frac{\partial U}{\partial A} = c_1\ A = 0, \tag{4-16}$$

where c_1 is a constant containing a linear term of the coefficient X. Finding a non-zero solution of A from the above algebraic equation yields:

$$c_1 = 0, \tag{4-17}$$

which is a linear equation of X. After solving and simplifying the above equation by MAPLE, we get a simplified expression for X:

$$X2 = \text{Roof of Eq. (4-17)}\ . \tag{4-18}$$

The compressive buckling coefficient is a dimensionless equation which is defined as:

$$K = \frac{X2 \cdot b^2}{\pi^2} = \frac{12\,(1-\mu^2)}{E\,\pi^2} \cdot \left(\frac{b}{t_0}\right)^2 \cdot \sigma. \tag{4-19}$$

In the above expression, the coefficient K is seen as a direct function of the following parameters: number of waves in a deformed plate m, coefficient representing plate thickness non-uniformity β, plate aspect ratio λ, and Poisson's ratio μ.

4.2.5. Comparison with Hill's solution

Since exactly the same buckling shape is assumed in both Hill's solution [30] and ours, it is expected that both results should be identical when the β value is assigned to be zero in the current solution. This corresponds to the special case in which the plate thickness is uniform. For the first buckling mode, i.e. $m = 1$, Hill's compressive buckling coefficient is

$$K = \frac{4}{\lambda^2} + 0.0993\lambda^2 + 0.624, \tag{4-20}$$

whereas ours is very close to the above equation:

$$K = \frac{4.0000}{\lambda^2} + 0.09932\lambda^2 + 0.62570. \tag{4-21}$$

This is a good check of the MAPLE formulation correctness.

Fig. 4-2 shows a set of compressive buckling coefficient curves for the different mode flat plate buckling derived from MAPLE. It is not clear in Hill's paper [30] how he obtained his envelop curve for the compressive buckling coefficient, but the comparison of his curve with ours shows that both envelop curve converges towards $K = 1.4$. This provides a second check of our MAPLE formulation correctness.

4.2.6. Non-uniform thickness plate buckling curve

Yahiaoui *et al.* [14] conducted several thin plate cutting tests with a relatively sharp and wide wedge. The specimen studied here (see Section 3.5.5.) has an original thickness of 0.75 mm and its true flow stress is $\sigma_0 = 270$ MPa. The wedge half angle used is $\theta = 45^o$, and its shoulder width is $2B = 19$ mm. Stable flaps are seen to be buckled during the steady-state wedge cutting process (Fig. 3-2). Sectioning of the stable flap has been done in order to measure the plate thickness variation. In Section 3.5.5., it is reported that the measured non-uniformity of plate thickness in stable flaps is very small (the total slope angle is only about one degree) except at the very tip of a flap free-end where a sudden change of thickness is observed locally due to the wedge initial cutting process (Figs. 3-20 and 3-21). This abrupt thickness change is not considered in our analysis because it will not affect the global flap buckling behavior.

Fig. 4-3 shows a set of buckling curve for a given plate non-uniformity coefficient $\beta = \dfrac{(0.75 - 0.60)\text{ mm}}{0.75\text{ mm}} = 0.2$ which represents a relative flap thickness variation at both ends. From the envelop curve drawn in Fig. 4-3, one can perceive that the minimum K value occurs at $K = 1.2$. This is close to the minimum K value observed from the plate buckling curve with a uniform thickness. Due to the initial flap imperfection, no higher order buckling wave forms were observed from the cut specimens.

4.2.7. Compressive buckling strain calculation

The plate buckling strength, Eq. (4-19), derived above is based on the elastic buckling theory. It is of interest to extend the above theoretical solution into the plastic plate buckling analysis, experiences show that the critical plastic buckling stress can be calculated empirically by first obtaining the buckling strain from the elastic buckling theory and then mapping the calculated strain into the uni-axial stress-strain curve from a standard coupon test

to obtain the corresponding plastic buckling stress [35]. In the following analysis, the buckling strain equation is derived which is seen not to contain elastic modulus E.

Since one of the unloaded plate edge in the mathematical model is free (Fig. 4-1), the plate can be considered under the uni-axial compression condition, i.e.

$$\begin{cases} \sigma_{xx} \neq 0, \\ \sigma_{yy} = 0. \end{cases} \tag{4-22}$$

The corresponding compressive buckling strain can be obtained based on the constitutive equation as

$$\varepsilon_{xx} = \frac{\sigma_{xx}}{E} = \frac{K \cdot \pi^2}{12\,(1-\mu^2)} \cdot \left(\frac{t_0}{b}\right)^2, \tag{4-23}$$

where K is the compressive buckling coefficient derived in Eq. (4-19) which has only a geometric parameter. Note that the Poisson's ratio used in the above equation should be equal to 0.5 if a plastic buckling problem is encountered. This buckling strain can now be used to find the empirical plastic buckling stress discussed above.

4.2.8. Discussions and conclusions

A set of closed-form solutions for the buckling problem of a non-uniform thickness rectangular plate is derived. The plate has three edges fixed and one unloading edge free. Uniform in-plane compressive stress is applied at the opposite fixed edges. Compressive buckling coefficient charts are plotted which can be used as either determining a critical buckling stress level or finding a buckling wave length for a given problem for both uniform and non-uniform thickness rectangular plates. Comparison with Hill's solution for the flat plate buckling problem shows a good agreement, and both solutions having the envelop buckling curve converge to $K = 1.4$. Compressive buckling strain has been derived too, and it can be used to find an empirical solution for the plastic buckling stress. Plate initial imperfec-

tions are not included in the current model, which should be considered in the future study and the post-buckling analysis is recommended to find the actual plate resistance.

4.3. Calculation of plastic buckling force inside stable flaps

Under a steady-state cutting process, stable flaps with a large B/t ratio may buckle due to a large compressive strain coming from the transition zone deformation. Periodical buckling waves are observed from the cut specimen shown in Fig. 3-2. By observing the deformation process during the wedge cutting experiments, it is found that a stable flap buckles non-uniformly with a very significant out-of-plane deformation observed at the beginning of the buckling wave. The reason is that, in order to satisfy the deformation compatibility condition, the stretched material inside the transition zone must be pushed back immediately when it enters the stable flap region. Since the compressive strain is so big at the very beginning of the buckling process, a large out-of-plane flap deformation happens there with a very little additional buckling deformation afterwards. Careful measurement shows that one buckled wave length along the stable flap top is exactly equal to the summation of the transition zone stretching and its projected length (l in Fig. 4-4).

In this section, the contribution of stable flap buckling towards the total wedge cutting force will be estimated. To simplify our analysis, it is assumed that the buckled flap has a sinusoidal wave form along the material flow direction (i.e. x-axis in Fig. 4-4) as follows:

$$w = w_0 \cdot \frac{y}{H} \cdot \sin\frac{\pi x}{l}, \tag{4-24}$$

where H is flap height, l is the original flap length, w_0 is the maximum deflection on top of the stable flap. It is verified that this approximation gives a small error to the final result.

A general form of the total deformation energy required to buckle a stable flap (Fig. 4-4) can be written as

$$W_p = \int_S M_0 \kappa \, dS + \int_l M_0 \theta \, dl \ , \tag{4-25}$$

where the first integration equation calculates the plate bending energy and the second one calculates the bending energy along plastic hinges. M_0 in the above equation represents the fully plastic bending moment defined in Eq. (3-9). Substituting Eq. (4-24) into the above equation and noting that there exist two plastic hinges in the problem yield the total work done by the buckling force F' travelling at a distance l as:

$$\begin{aligned} W_p = F'l = M_0 \left(\int_0^l \int_0^H \left| \frac{\partial^2 w}{\partial x^2} \right| dxdy + 2 \int_0^H \left. \frac{\partial w}{\partial x} \right|_{x=0} dy \right) \\ = \frac{2\pi w_0 H M_o}{l} = \frac{\pi \sigma_0 t^2}{\sqrt{3}} \cdot \frac{w_0}{l} \ . \end{aligned} \tag{4-26}$$

The ratio w_0/l in the above equation can be expressed in turn by the maximum strain ε along the top of a buckled wave (Appendix F):

$$\frac{w_0}{l} = \frac{\sqrt{\varepsilon}}{2.2} \ , \tag{4-27}$$

where the strain expression due to a large out-of-plane displacement is defined as

$$\varepsilon = \frac{1}{2} \cdot \left[1 - \left(\frac{l}{L} \right)^2 \right] . \tag{4-28}$$

The above expression calculates the average value of the actual strain distribution along the free edge of stable flap with a magnitude of 3~5% measured from the specimen shown in Fig. 3-2.

Substituting Eq. (4-27) into Eq. (4-26) and including two buckled flaps on both sides of the wedge give the total force required to buckle the stable flap:

$$F'_t = \frac{\pi \sigma_0 t^2 H \sqrt{\varepsilon}}{1.1 \times \sqrt{3} \cdot l}, \tag{4-29}$$

where $H = R\phi_{max}$ for the curling flap model and $H = B$ for the upright flap model.

First, let's compare the derived buckling force F'_t with the transition zone stretching force F_m for the curling flap model. From Eqs. (3-18), (3-19), and (4-29), we can formulate the force ratio as follows:

$$\frac{F'_t}{F_m} = \frac{\pi \sigma_0 t^2 H \sqrt{\varepsilon}}{1.1 \times \sqrt{3} \cdot l} \cdot \frac{3\sqrt{3}}{4\sigma_0 t \cdot d\tan\theta} = \frac{3\pi t R \sqrt{\varepsilon}}{1.41 l (B+R) \cdot \theta \tan\theta}. \tag{4-30}$$

Eq. (3-37) gives the relation $B \approx R$ if frictional effect is neglected. For the specimen shown in Fig. 3-2, the plate thickness is measured to be $t = 0.75$ mm, the buckling wave length is $l = 75 \sim 80$ mm, the average strain value for one buckled wave length along the stable flap free edge is $\varepsilon \approx 3.5\%$, and the wedge semi-angle is $\theta = 45^o$. Based on the data given, the ratio of buckling force *vs.* transition zone stretching force can be found as:

$$\frac{F'_t}{F_m} = 0.7 \sim 0.8\%. \tag{4-31}$$

This ratio is so small that the contribution of buckling force F'_t can be safely neglected in the total wedge cutting force formulas.

For the upright flap model, the corresponding force ratio can be computed by dividing Eq. (4-29) by Eq. (3-42):

$$\frac{F'_t}{F_{m2}} = \frac{\pi \sigma_0 t^2 H \sqrt{\varepsilon}}{1.1 \times \sqrt{3} \cdot l} \cdot \frac{\sqrt{3}}{2\sigma_0 t \cdot B \sin\theta \tan\theta} = \frac{\pi t \sqrt{\varepsilon}}{2.2\ l\ \sin\theta \tan\theta}. \tag{4-32}$$

Note that the relation $B = R$ is used in the derivation of the above equation. Applying the same test data to the above equation gives:

$$\frac{F'_t}{F_{m2}} = 0.4\% \,. \tag{4-33}$$

Again, the above ratio is very small.

The conclusion from the above analysis is that the stable flap buckling deformation need not to be taken into account in the steady-state wedge cutting force study, which confirms that γ is equal to unity if the stable flap buckling does occur.

4.4. Conclusions

In this chapter, theoretical analysis is conducted for stable flap buckling under a steady-state wedge cutting process. The compressive buckling coefficient, K, is derived for a non-uniform thickness rectangular plate having one edge free and the other three fixed, which can be used to set a criterion for stable flap stability. Plastic buckling analysis is also performed. Comparison of stable flap buckling force with the deformation force needed in transition zone shows that, as soon as a stable flap buckles, the buckling force has negligible contribution towards the total wedge force expressions.

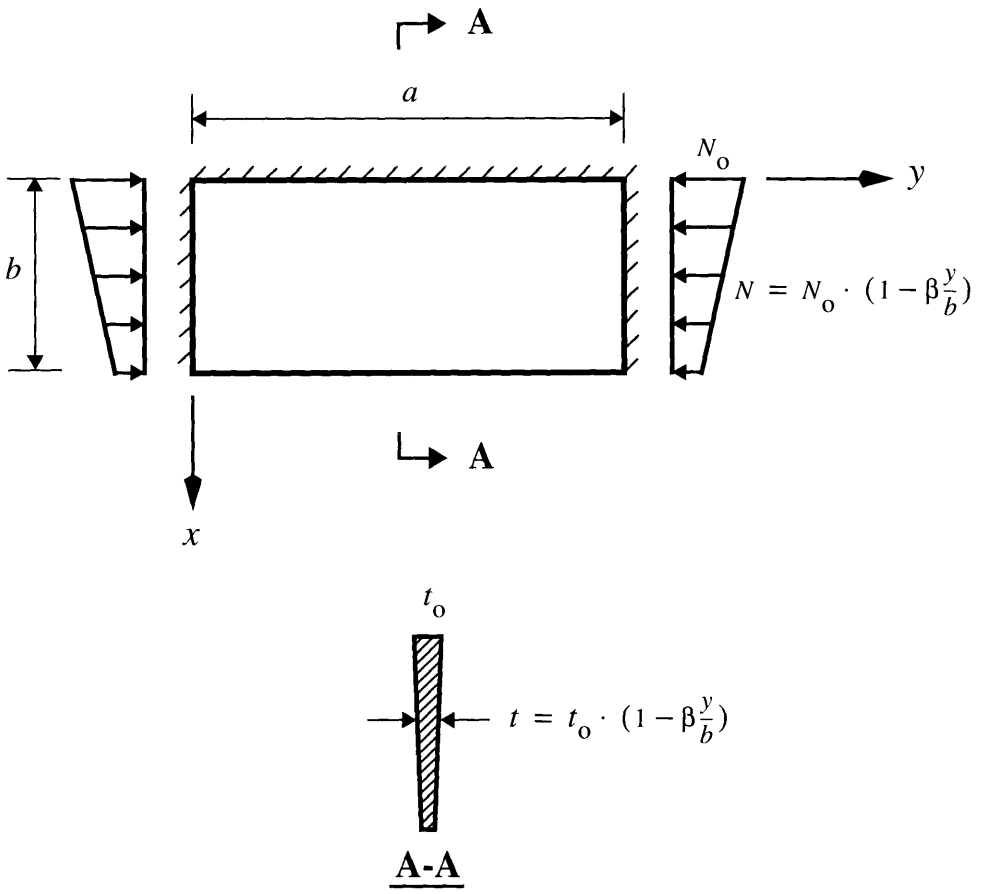

Fig. 4-1 Mathematical model for the plate buckling analysis

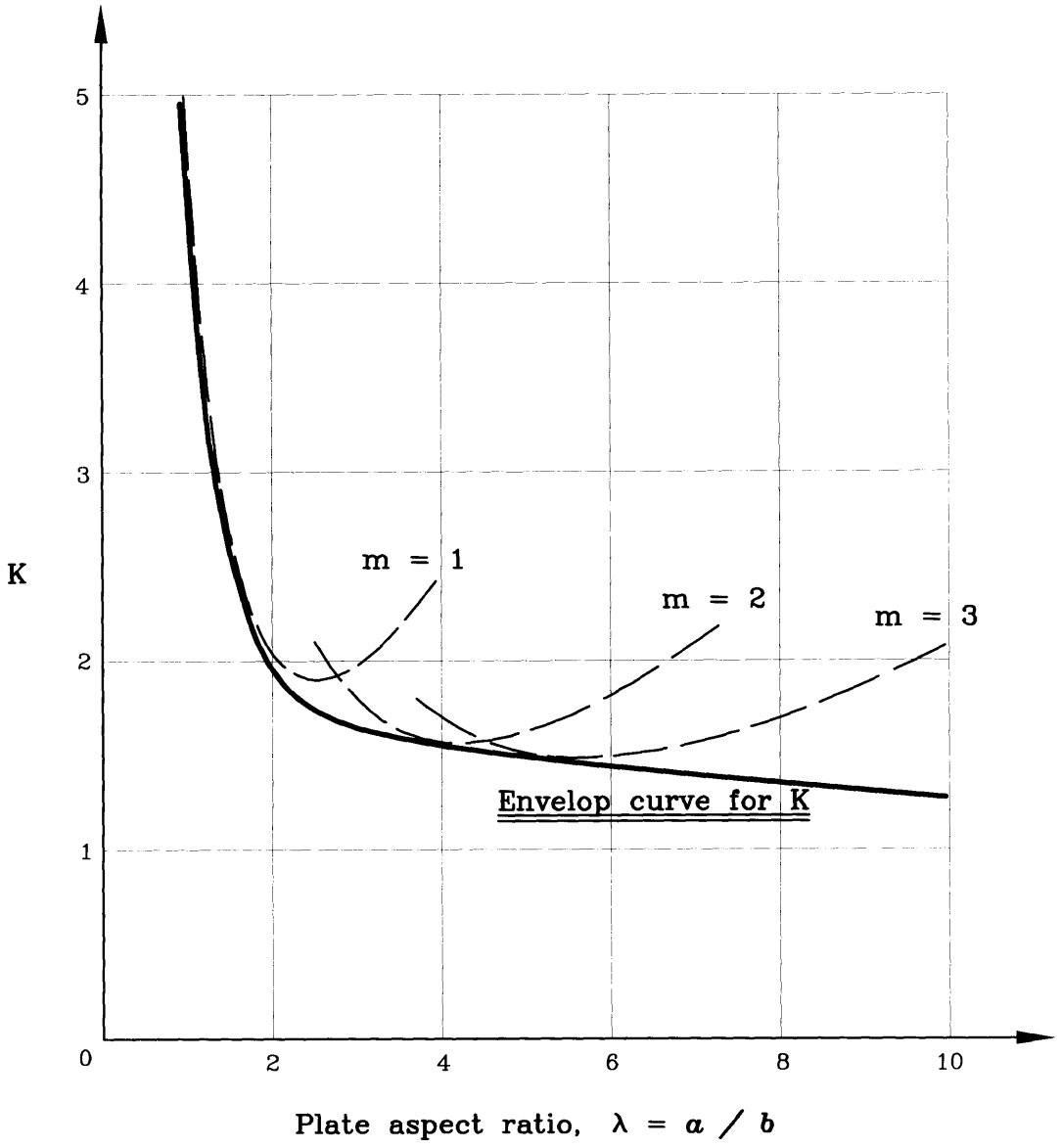

Fig. 4-2 Compressive buckling coefficient chart, K

($\beta = 0$)

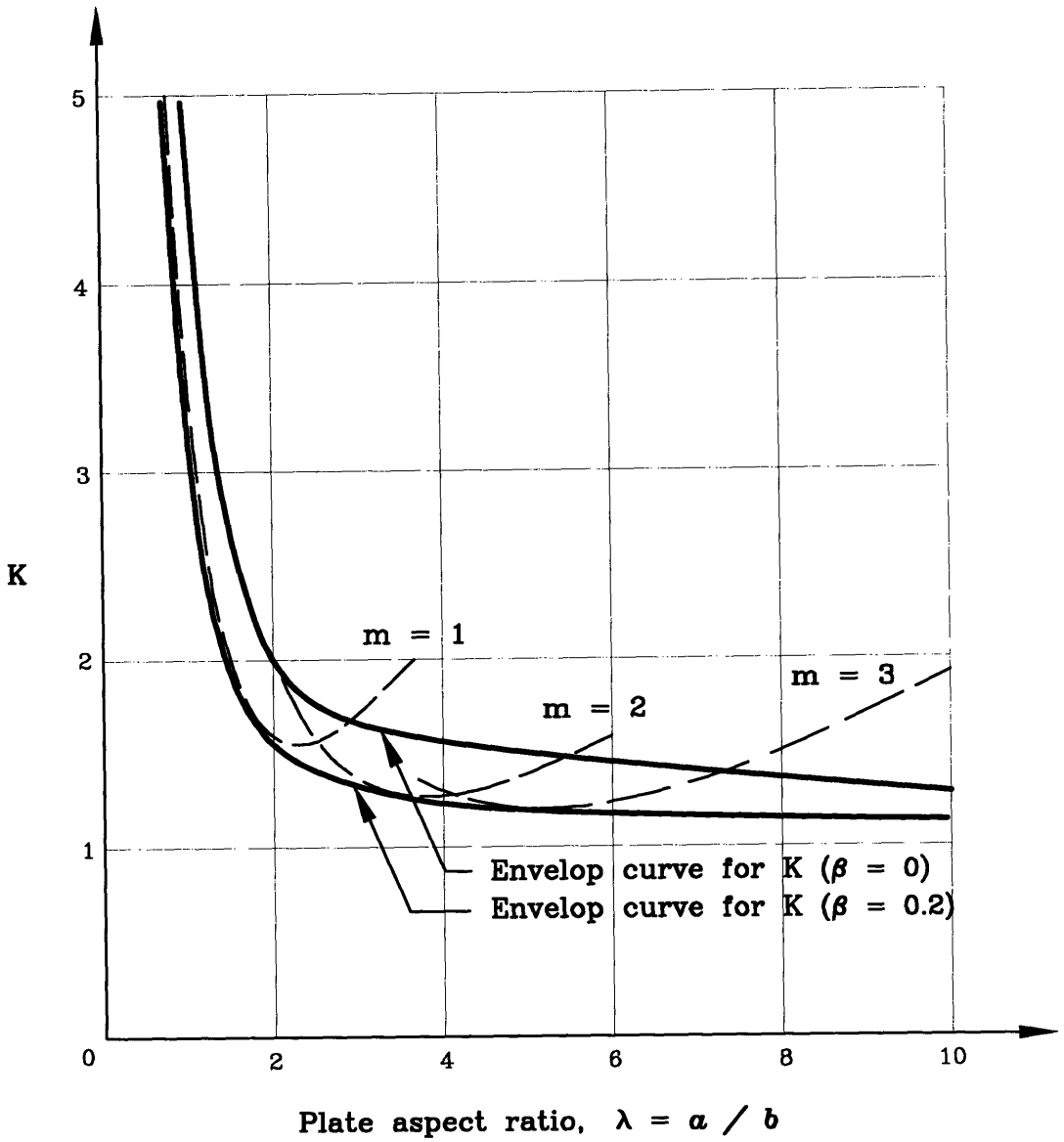

Fig. 4-3 Compressive buckling coefficient chart, K

($\beta = 0.2$)

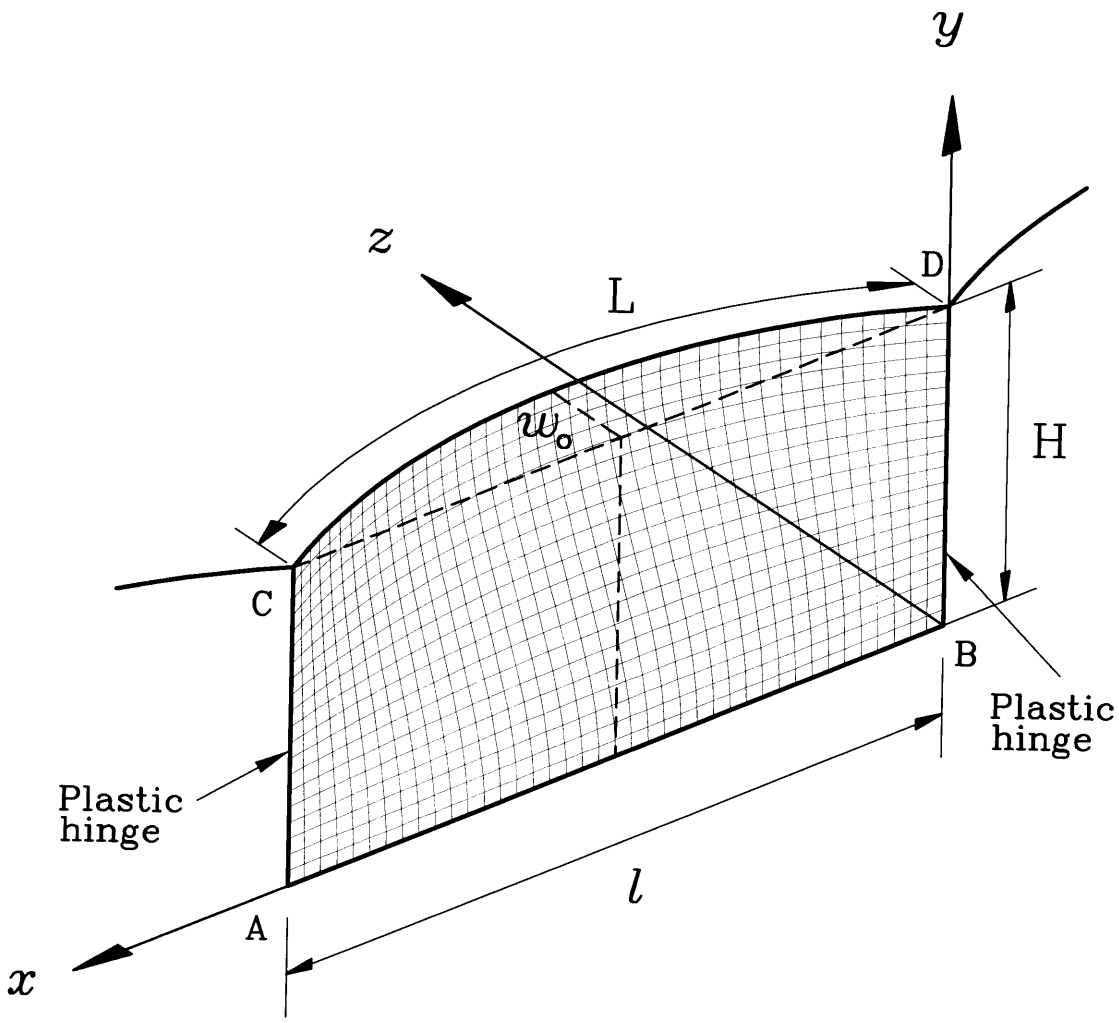

Fig. 4-4 Kinematic model for stable flap buckling analysis

Chapter 5

Experimental Validation of Steady-state Wedge Force Solutions

5.1. Introduction

Almost all the experiments reported previously in the literature deals with wedge transient indentation problems. Recently, new experiments were performed by Lu and Calladine [1], Maxwell [12], and Astrup [26] focusing on the failure conditions close to a steady-state wedge cutting process. The damaged specimens in those tests showed all the features of a steady-state indentation process; but the corresponding force-displacement curves not always gave evidence of a distinct force plateaux representing a constant force typically present in a steady-state cutting process. In order to present a sound experimental proof of the important hypothesis that a steady-state cutting force should be constant, new tests were designed and conducted at M.I.T. A reader is referred to the work by Yahiaoui *et al.* [14] for the details of the experimental procedures used. Even though wedge cutting tests are relatively simple and easy to interpret, some difficulties arise in quantifying the effect of plate tilt angle, frictional coefficient, and buckled stable flaps on the steady-state wedge force. Despite these difficulties the correlation between the theoretical solutions and tests was found to be very good. The following comparisons are made by including all the representative cases available up to date. A summary of the comparisons is provided in Table 1.

5.2. Comparison with narrow wedge experimental results

Three test results are presented here to compare with the theoretical solutions. All the tests

used a narrow wedge relative to the plate thickness used: $B/t \leq 6$. Lu's test (Test #1) has a B/t ratio of 3 which gives a failure mode close to our curling flap model. The other two tests end up with a braided flap deformation pattern which is difficult to analyze and has not been studied so far. But comparisons are still made for those cases to give a rough check of the difference between the predicted and test results.

5.2.1. Test #1

One test result from Lu's series of experiments on wedge cutting through thin plates gave a typical steady-state cutting failure mode [23]. The plate thickness was 1.6 mm and its flow stress $\sigma_0 = 272$ MPa. The specimen has a tilt angle $\alpha = 10^o$ to the wedge advancing direction. Wedge semi-angle is $\theta' = 10^o$, and its shoulder width is $2B = 10$ mm. The wedge semi-angle projected on the plate plane can be calculated as (Fig. 3-16):

$$\theta = \text{atan}\,[\cos\alpha \cdot \tan\theta'] = 9.85^o\,, \tag{5-34}$$

which gives a slightly sharper angle than its original shape. The plate failure mode shows that the flaps on both sides of the wedge are smooth, which indicates that the transition zone was first fully stretched to its toroidal shape and then compressed back completely to a zero length to conform the stable flap geometry. This gives the ratio of compressing *vs.* stretching energies in the transition zone to be unity, which yields $\gamma = 2$. The ratio of rake face length to plate thickness for machining friction is assumed to be $\zeta = 1.7$, because it is believed that the rake face length should be more than the actual plate thickness near a wedge tip but not greater than two times of t. Based on the engineering judgment and available information about friction, sliding friction coefficient is chosen as $\mu_s = 0.3$ for steel-to-steel friction, and machining friction coefficient is given as $\mu_m = 0.65$.

The rolling radius is calculated from Eq. (3-34) to be $R = 4.1$ mm. The rolling angle is

$\phi = 128^{o}$ which sounds reasonable by comparing with the test result. The cutting force predicted from Eq. (3-32) is $F = 5.9$ KN in which 15.1% comes from bending energy, 29.9% from sliding friction, 23.3% from membrane deformation near wedge tip, 2.2% from membrane deformation inside transition zone, and 29.5% from machining friction as expected by Lu [23]. A comparison of the present solution with the test result is shown in Fig. 5-1. The plotted experimental cutting force increases with the wedge advancement and, for $u > 75$ mm, it converges to a constant value $F_{exp} = 5.9$ KN which is the same as the curling flap model prediction. A slightly lower value $F = 5.57$ KN is obtained from the upright flap model with friction, Eq. (3-51).

It is of interest to investigate the stable flap buckling criterion for this specimen. With the given information: $B = 5$ mm, $t_0 = 1.6$ mm, $\sigma = \sigma_0 = 272$ MPa, $E = 2000$ MPa, and $\mu = 0.3$, the compressive buckling coefficient can be found as $K = 1.47$ which corresponds to $\lambda = (a/b) \rightarrow \infty$ from Fig. 4-3. This proves that the stable flap will not buckle even though the compressive stress goes to the level of flow stress. In reality, yielding stress is smaller than σ_0 and the corresponding K value will be less than what we get above. It can be seen from this experimental result that a small B/t ratio gives a smooth stable flap without buckling problem presented.

5.2.2. Test #2

Trauth [20] conducted a series of steady-state wedge cutting test in M.I.T.'s Remergence Lab using three different wedge shapes. Because the specimens were cut at a right angle to the wedge indentation direction, braided flap deformations were observed [2]. The specimen thickness was measured as 0.41 mm and the flow stress is $\sigma_0 = 270$ MPa. The wedge semi-angle was $\theta = 45^{o}$, and the wedge shoulder width is measured as $2B = 5$ mm. Since the braided flap failure mode (Fig. 3-3) has not been studied in the literature, a com-

parison with the existing kinematic models should be considered tentative. Shiny scoring on the braided flap surface was observed giving the evidence of large frictional force existed during wedge cutting process. This additional friction force is not included in our analytical results since it is acting in the perpendicular direction to the wedge advancement. The ratio of total *vs.* stretching energies in transition zone is assumed to be $\gamma = 1$, by taking only the transition zone stretching deformation into account. For the machining friction, the ratio of rake face length and plate thickness is assumed to be $\zeta = 1.7$ because the actual rake face length should be greater than one plate thickness but less than twice of t. The sliding frictional coefficient is chosen as $\mu_s = 0.3$, and the machining frictional coefficient is $\mu_m = 0.7$.

The rolling radius is found from Eq. (3-34) to be $R = 1.3$ mm which is a fictitious number because no smoothly bent-up flaps were observed. The cutting force computed from the curling flap model solution, Eq. (3-32), is $F = 0.7$ KN in which 11.5% comes from bending energy, 14.4% from sliding friction, 24.4% from membrane deformation near wedge tip, 36.4% from membrane deformation inside transition zone, and 13.3% from machining friction. This theoretical value is lower than the average cutting force recorded from the Trauth's experiment which is approximately 0.9 KN (Fig. 5-2). This is probably because the energy loss due to the scoring of transient flaps and the folding of stable flaps are not included in the current theory. The upright flap model, Eq. (3-51), predicted the wedge force of $F = 0.45$ KN which is half of the average cutting force value.

5.2.3. Test #3

Yahiaoui *et al.* [14] performed a very interesting wedge cutting experiment in M.I.T. using a round wedge and zero tilt angle. The coexistence of two failure modes (Fig. 5-3), i.e. a concertina tearing together with a braided flap deformation pattern, gives us a good example of failure mode complexity when the B/t ratio is near a boundary curve separating two

different failure modes (Fig. 3-18). It was observed that the concertina tearing failure mode was initiated first and sustained for more than half way through the total wedge cut. Then, a clean cut took over the position since the width of the diverging concertina tearing became so big that a clean cut provided an alternative failure mode requiring less energy input. At the very end of the test, concertina tearing was seen to initiate again owing to the fact that this plate was expected to fail under the concertina tearing mode because of the semi-circular shaped wedge used. The specimen thickness was measured as 0.41 mm and its flow stress is $\sigma_0 = 270$ MPa. The wedge semi-angle was approximated by $\theta = 45^o$ for the semi-circular shaped wedge, and the shoulder width is $2B = 5$ mm. The ratio of total *vs.* stretching energies in transition zone is assumed again to be $\gamma = 1$, because the stable flaps buckled. The sliding frictional coefficient is chosen as $\mu_s = 0.2$. Machining friction need not be considered here because a crack ran in front of the round wedge tip so that no real wedge cut is existed.

The rolling radius is calculated from Eq. (3-34) to be $R = 1.3$ mm. The wedge force calculated from the curling flap model solution, Eq. (3-32), is found to be $F = 0.7$ KN. The theoretical value of $F = 0.7$ KN is low compared to the recorded mean cutting force from Yahiaoui's experiment which is roughly 1.0 KN (Fig. 5-4) because the energy loss due to scoring friction at the flaps are not considered here. The upright flap model solution, Eq. (3-51), gives the wedge force of $F = 0.8$.

5.3. Comparison with wide wedge cutting experimental results

The two experiments performed in M.I.T. by using the narrow wedges (reported above) did not give the expected failure modes studied in our analysis. This is because, in the above tests, no tilt angle between plate specimen and the wedge advance direction was introduced

which led to the braided deformation pattern of flaps. The following two tests [14] were conducted to achieve an actual clean cut failure mode studied in this chapter with a plate tilt angle $\alpha = 10^{o}$. The wedge shoulder width is $2B = 19$ mm and the plate thickness $t = 0.749$ mm. This gives a much larger ratio of $B/t = 12.7$ than that of the previous tests but the probability of developing the concertina tearing is smaller due to the introduced plate tilt angle. A sharp wedge with a semi-angle $\theta = 45^{o}$ was used. The flow stress was measured as $\sigma_0 = 270$ MPa. The difference between tests #4 and #5 exists mainly in the way how the cutting process was initiated.

5.3.1. Test #4

In test #4, the free edge on the top of the plate specimen had a pre-cut length of 50 mm in front of a wedge tip which is aligned in the wedge cutting path. This was intended to provide a guide to the initiation of the steady-state cutting process immediately. The force–displacement curve is reproduced in Fig. 5-5 and the damaged specimen picture is shown in Fig. 3-2. The force level during the initial 50 mm wedge travel (length of the pre-cut) is low since only plate bending deformation is involved. A steady-state wedge force level of $F = 2.5$ KN is reached after the 230 mm wedge advancement. The delay of the steady-state process initiation is due to the flexibility caused by the free edge deformation.

5.3.2. Test #5

In test #5, the specimen had opened a small window near its free edge. This is intended to use the linkage provided at the free edge to give enough constraint for the free edge deformation. The wedge was inserted into the opening and started cutting from there. A similar pre-cut discussed in Test #4 was also made there. The steady-state cutting process started much earlier than Test #4, and the initial travelling distance was only 30 mm long (Fig. 5-

6). The wedge force reached and maintained the level of $F_{exp} = 2.45$ KN for the rest of the test, showing a very good reproducibility of the results.

Both tests presented above showed a steady-state wedge cutting process accompanied with stable flap buckling. Those are the first set of successful tests reported so far to reproduce the theoretical clean cut model proposed here. In the following calculation of the theoretical results, in addition to the data given above, other parameters needed in the analysis are assumed to be $\gamma = 1$, $\mu_s = 0.3$, and $\mu_m = 0.7$. The theoretical cutting force, resulting from the curling flap model solution, is $F = 3.7$ KN. The overestimation of the cutting force by using the curling flap model is due to the fact that the actual failure mode is close to the upright flap model because it requires less energy. As expected the upright flap model solution, Eq. (3-51), predicts the wedge force to be $F = 2.6$ KN, which is much closer to the experimental values.

It is of interesting to check the buckling criterion for the stable flap of the above two wide wedge cutting tests by using Fig. 4-3. It is measured that the stable flap non-uniformity coefficient is $\beta = 0.2$ (Ref. Section 3.5.5.). Substituting $\sigma_0 = 270$ MPa into Eq. (4-19) and giving $b = 10.7$ mm and $t_0 = t = 0.75$ mm, we get

$$K = \frac{270 \text{ MPa}}{\left(\frac{0.75}{10.7}\right)^2 \cdot \frac{2 \times 10^3 \text{ MPa} \cdot \pi^2}{12\,(1 - 0.3^2)}} = 30\,, \tag{3-35}$$

which gives $\lambda = (a/b) \approx 0.4$ from Fig. 4-3 curve for $\beta = 0.2$, indicating an immediate buckling process as soon as a wedge passes the vertical plastic hinge (Fig. 4-4). In reality, the compressive stress, σ, is closer to the material yielding stress, σ_y, which is less than the flow stress, σ_0, by definition [27]. This will give a lower K value and, in return, some delay of the buckling process predicted above. The measured initial buckling length is around 5~8 mm which is in the right order from the theoretical prediction: $\lambda b = 4$ mm.

5.4. Comparison with thick plate cutting experimental results

The validation of our analytical solutions due to the size effect was performed in this section by using the DnV experimental results for a wedge cutting through thick plates with $t = 20$ mm [26]. In general, it is important to check the size effect in every study of fracture mechanics because a fracture might be inhibited in a thin plate due to the much thorough work done through the plate thickness and a less probability of material defects. With the DnV experiments with standard ship plating, it is very encouraging to note that our theoretical solutions for the steady-state cutting process are still valid to predict the actual ship hull grounding scenario. This is because that the major damages involved in a steady-state cutting process is not related to the material fracture but to the plate membrane deformation which is believed to have no size effect at all. The hypothesis that a wedge tip has a direct contact with the plate crack tip is still correct in the thick plate cutting experiments (Fig. 5-7). Also, the steady-state cutting process can be achieved for the thick plate specimen by viewing the top picture in Fig. 5-7 where the stable flaps were clearly represented.

Tests #6 and #7

Two thick plate cutting tests were performed in DnV. Each test was composed of two plate specimens in order to preserve a symmetric loading condition and to prevent possible load cell uplifting damage. The two sets of experiment were identical and the wedge cutting were conducted in a 25,000 KN testing machine. The wedge semi-angle used is $\theta = 30^{\circ}$, a plate tilt angle of $\alpha = 10^{\circ}$ is imposed by a specially designed wedge, the total wedge shoulder width is measured as $2B = 125$ mm, and the flow stress is reported as $\sigma_0 = 526$ MPa. In addition to the information presented, it is assumed in our analysis that the frictional coefficients are $\mu_s = 0.3$ and $\mu_m = 0.7$. Since the transverse fractures are observed in the stable flaps (Fig. 5-8), the ratio of total *vs.* stretching energies in transition zone is chosen to be $\gamma = 1$ because the stable flaps can never be compressed back in those tests.

Note that the existence of the stable flap fracture observed in the thick plate cutting tests gives us a sound proof of size effect in certain fracture mechanics applications. By comparing the damaged specimens for both thin and thick plates, it is found that the large tensile strain in the transition zone which can be easily incorporated in thin specimen seems intolerable for the thick plate specimens which demonstrated a fracture failure in the stable flaps. The steady-state cutting force from the curling flap model is calculated from Eq. (3-32) as F = 4205 KN and the corresponding upright flap model, Eq. (3-51), gives F = 3177 KN. Those theoretical results have already taken into account of two identical plate specimens cut at the same time, which is the actual DnV test set-up discussed above. Figs. 5-9 and 5-10 show that the curling flap model predicts a value closer to the average wedge force than that from the upright one. This is because, for a thick plate, it is difficult to conform the prescribed deformation pattern assumed in the upright flap model since the large plastic hinge bending moment prohibits such deformation pattern. Both test curves (Figs. 5-9 and 5-10) show that the steady-state cutting process have not been achieved because of the existence of flap fracture mechanism which greatly distorts the loading path. However, the attempt to conduct the steady-state cutting test through the standard ship plates is highly appraised.

5.5. Conclusions

In this section, the closed-form solutions derived in Chapter 3 for a steady-state cutting process of the wedge indentation through a metal plate were validated by the large and small scale experimental results. A comparison with seven typical tests on the different thickness plates and wedge geometries gives a remarkably high degree of correlation. In all the cases, the difference encountered between the test results and the theoretical solutions was less than 7%, which is excellent considering the complexity of the physical problem encoun-

tered and the approximate nature of the present theory. Generally, the upright flap model, Eq. (3-51), gives as good accuracy as the so called "exact" solution, Eqs. (3-32) ~ (3-34). As we can seen from Table 1 that both kinematic models have their merits and their accuracy really depends upon the controlling parameters involved. For example, a small B/t ratio and a small wedge semi-angle give a failure mode close to the curling flap model; but the increment of either parameter listed above may end up with a upright flap failure mode and/or a concertina failure mode (see Section 3.5.2. for detail).

The validation of the theoretical solutions has been checked for both thin and thick plate specimens covering a range of plate thickness from t_{min} = 0.41 mm to t_{max} = 20.0 mm. Because the steady-state wedge indentation force is mainly developed from the plastic deformations and to a much lesser extent to material fracture, the present analytical solutions are proved to have little sensitivity to the plate thickness variation. Both the curling and upright flap model solutions predict a linear dependence of the wedge force on the wedge shoulder width, $2B$. This condition is correct for the intermediate values of B/t, which are of most interest to the oil-tanker grounding problem. For a very narrow (knife) or very wide wedge, different failure modes, not covered by the present theory, must be considered.

In summary, it can be stated with confidence that a reliable analytical tool has been developed to predict the wedge cutting force required in a steady-state penetration mode for a wide range of plate thickness and rock geometries. The principle failure patterns are the central separation with curled or upright flaps or a concertina tearing.

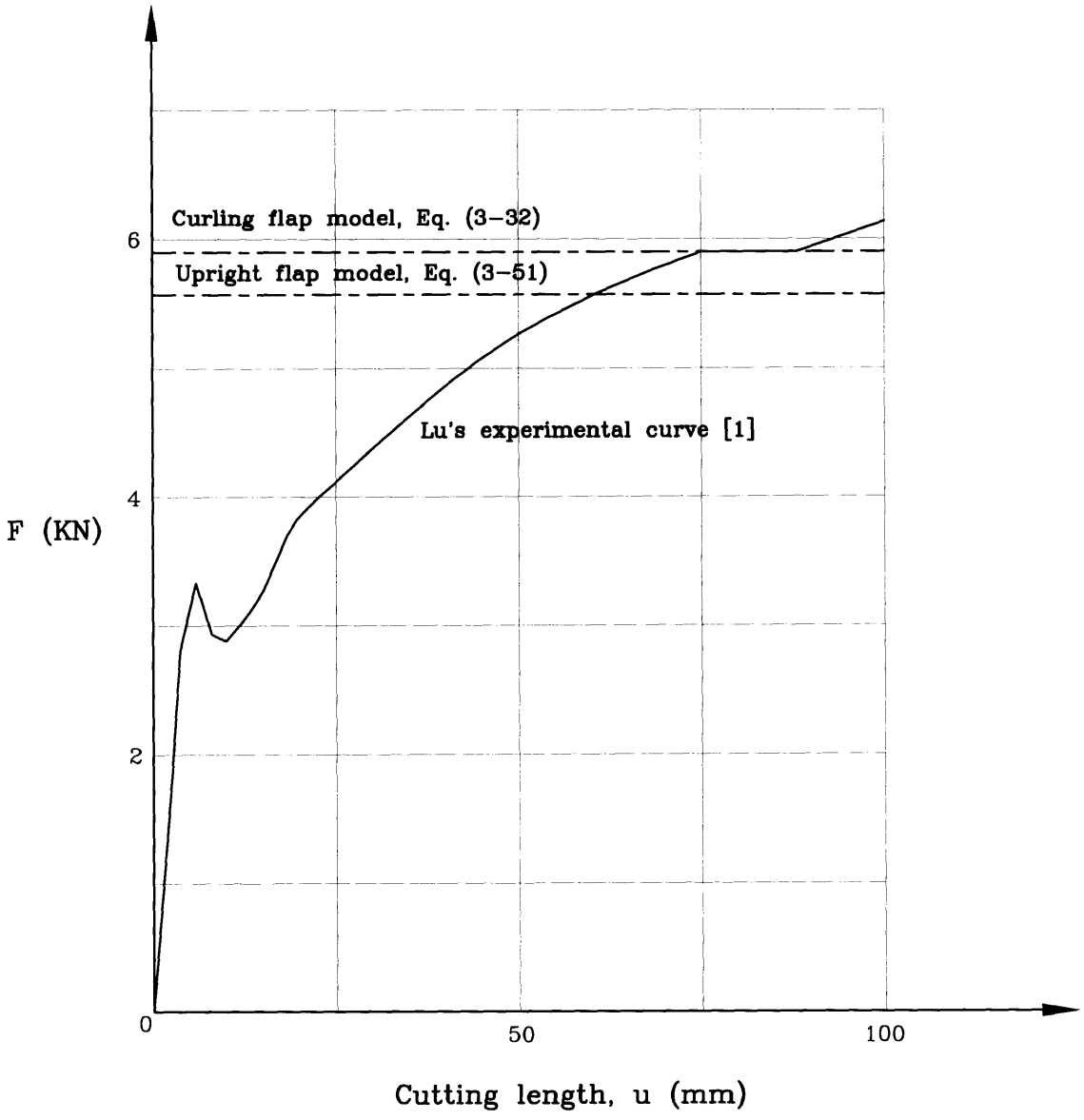

Fig. 5-1 Comparison of experimental *vs.* theoretical cutting force results in Test #1

(B = 5 mm, t = 1.6 mm, σ_o = 272 MPa, $\theta = 10^o$, $\alpha = 10^o$)

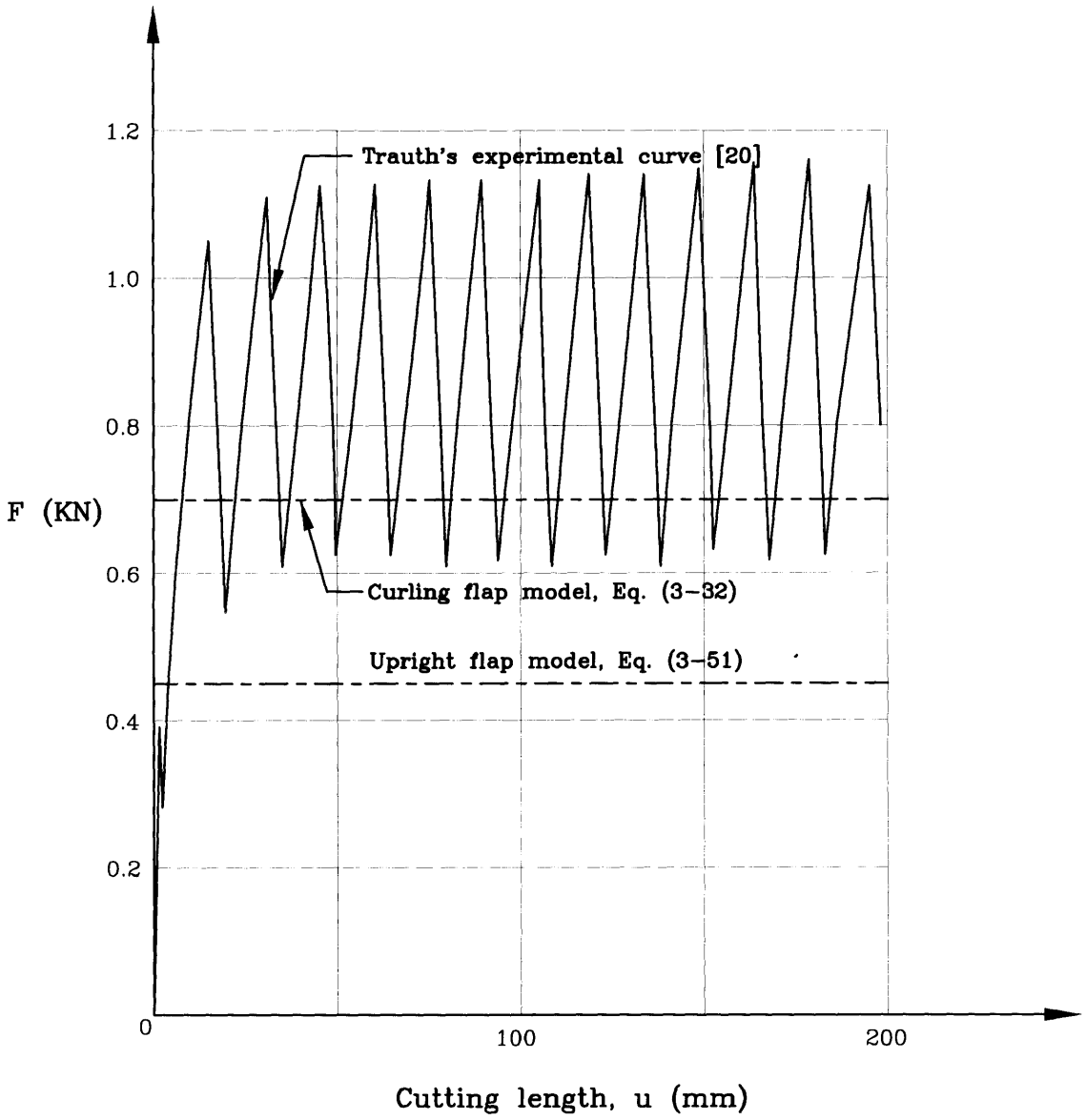

Fig. 5-2 Comparison of experimental *vs.* theoretical cutting force results in Test #2

(B = 2.5 mm, t = 0.41 mm, σ_o = 270 MPa, $\theta = 45^o$, $\alpha = 0^o$)

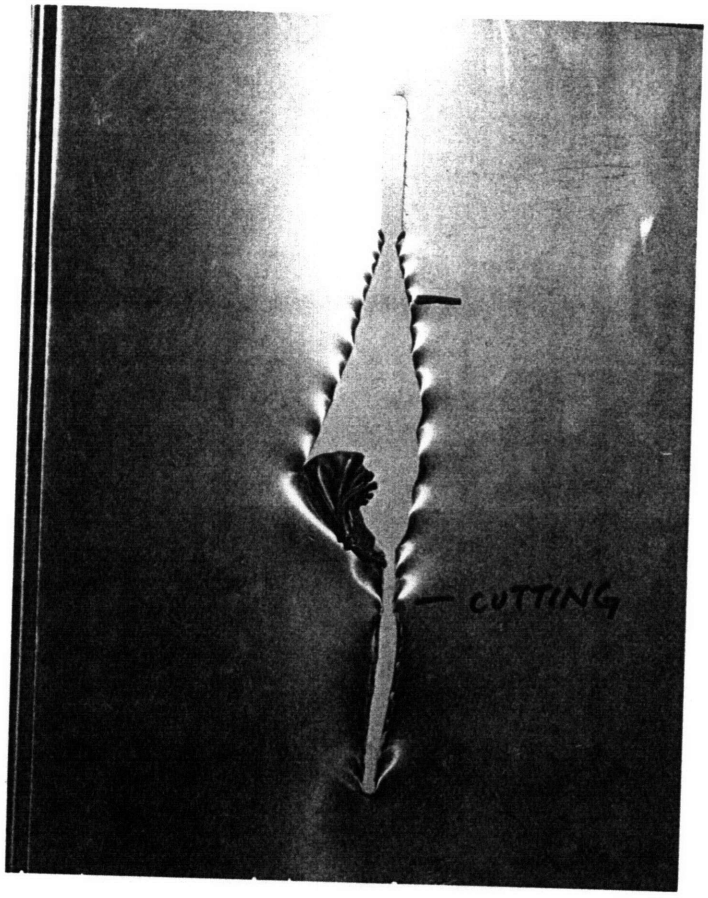

Fig. 5-3 Photograph of Test #3 result showing the co-existance of two different failure modes

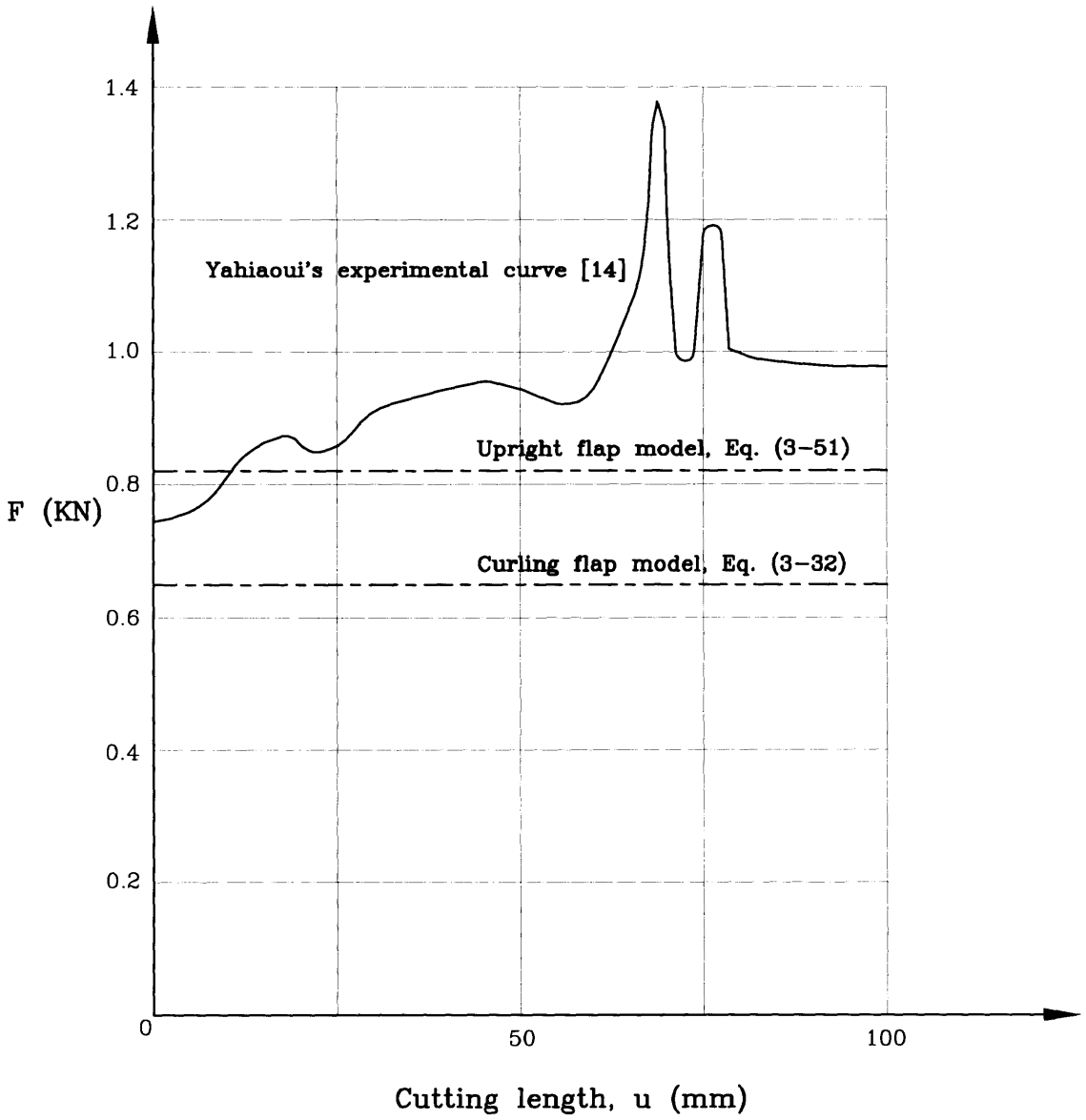

Fig. 5-4 Comparison of experimental *vs.* theoretical wedge cutting force results in Test #3

(B = 2.5 mm, t = 0.41 mm, σ_o = 270 MPa, $\theta = 45^o$, $\alpha = 0^o$)

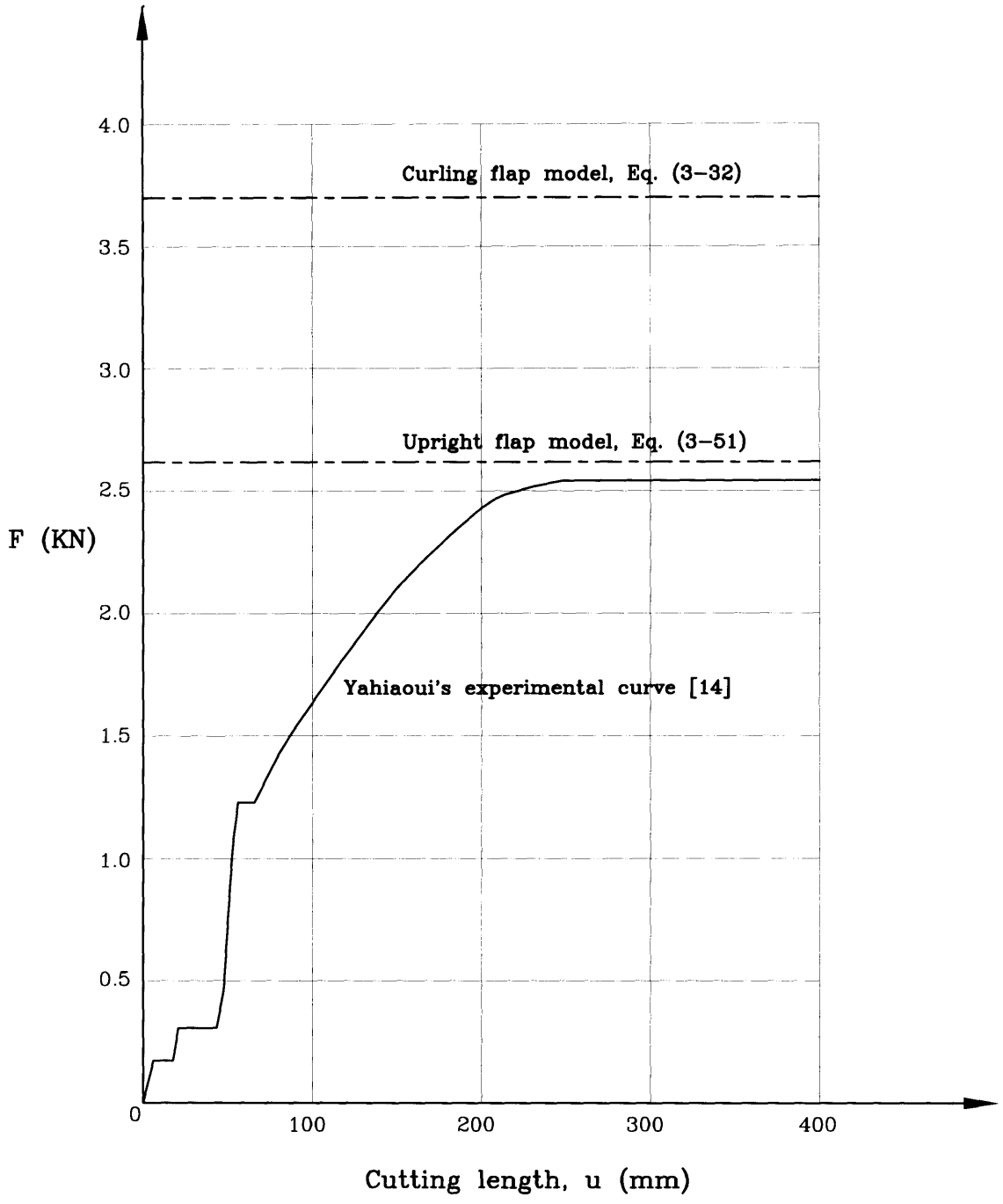

Fig. 5-5 Force-displacement diagram of a steady-state clean cut failure initiated from the free edge in Test #4

(B = 9.5 mm, t = 0.75 mm, σ_o = 270 MPa, $\theta = 45^o$, $\alpha = 10^o$)

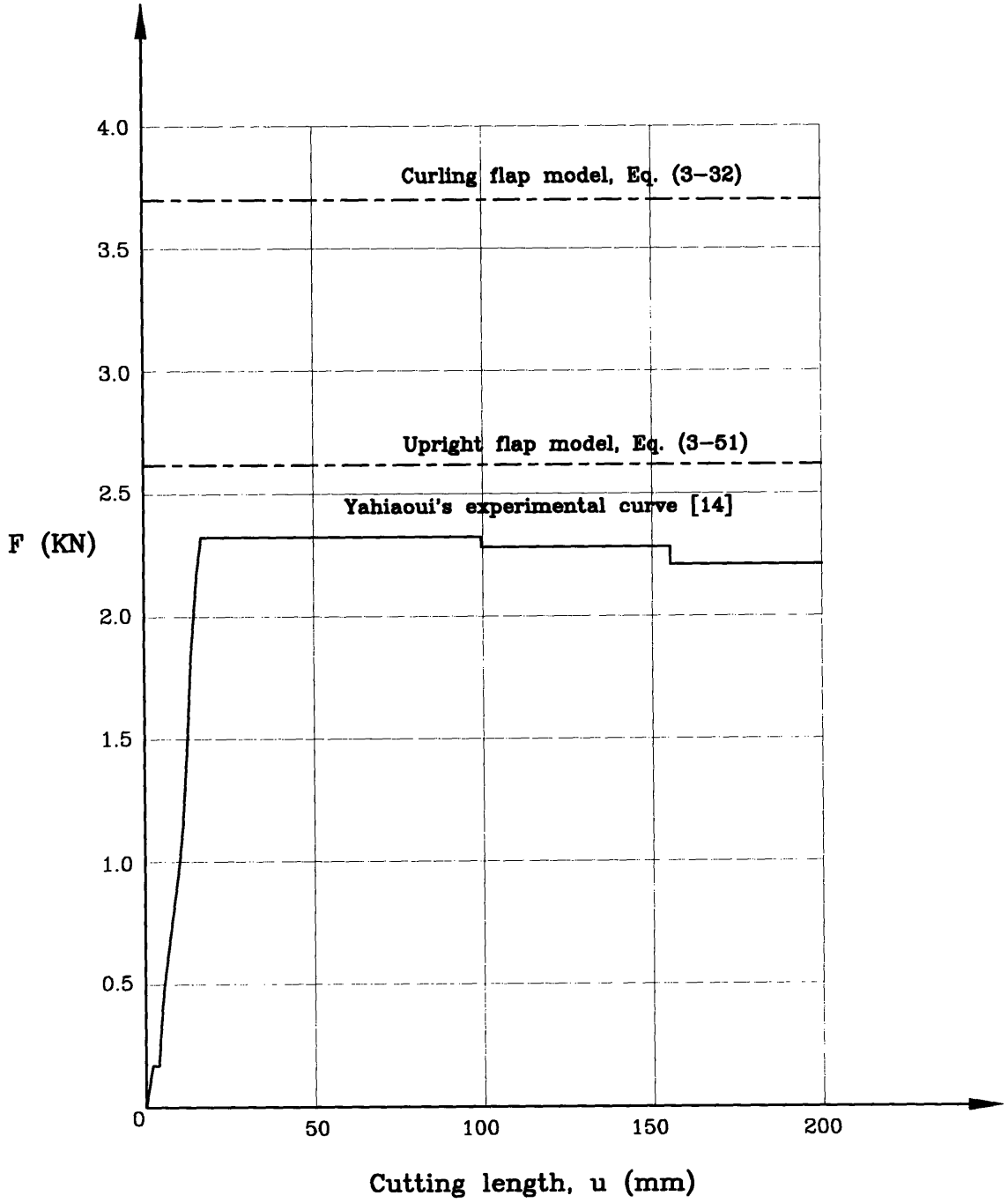

Fig. 5-6 Force-displacement diagram of a steady-state clean cut failure initiated from a central cut in Test #5

(B = 9.5 mm, t = 0.75 mm, σ_o = 270 MPa, $\theta = 45^o$, $\alpha = 10^o$)

a)

b)

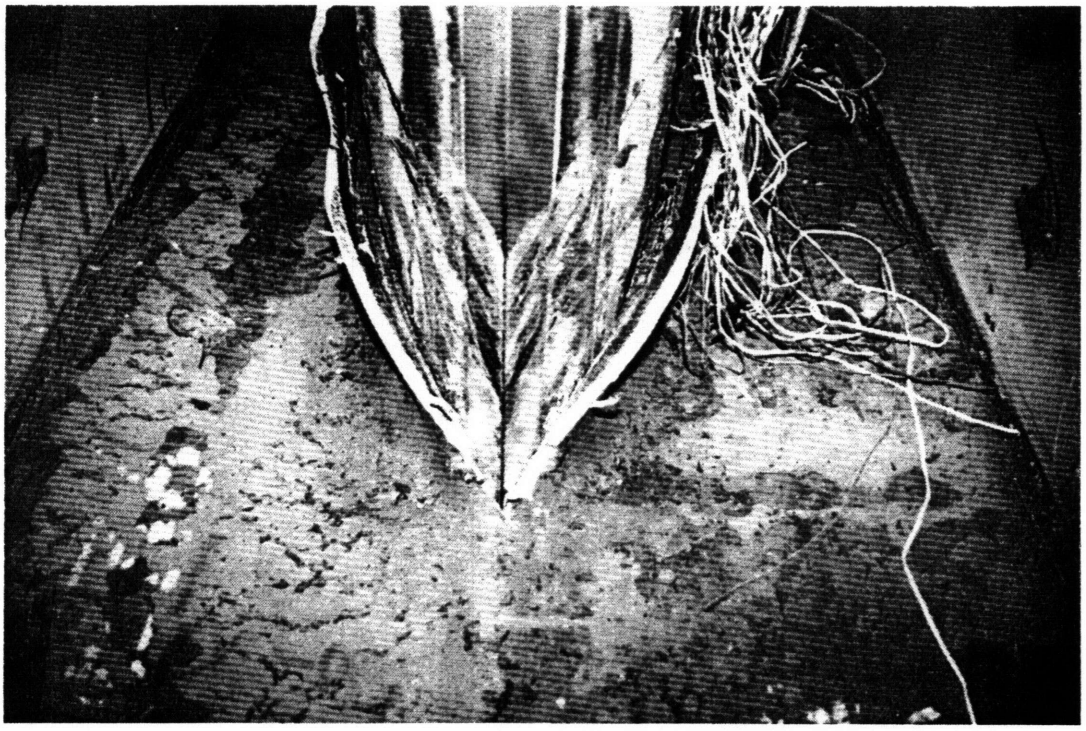

Fig. 5-7 Steady-state cutting failure of 20 mm thick specimen (S1-20)

(Courtesy of DnV)

Fig. 5-8 The complete cut length of specimen S2-20

(Courtesy of DnV)

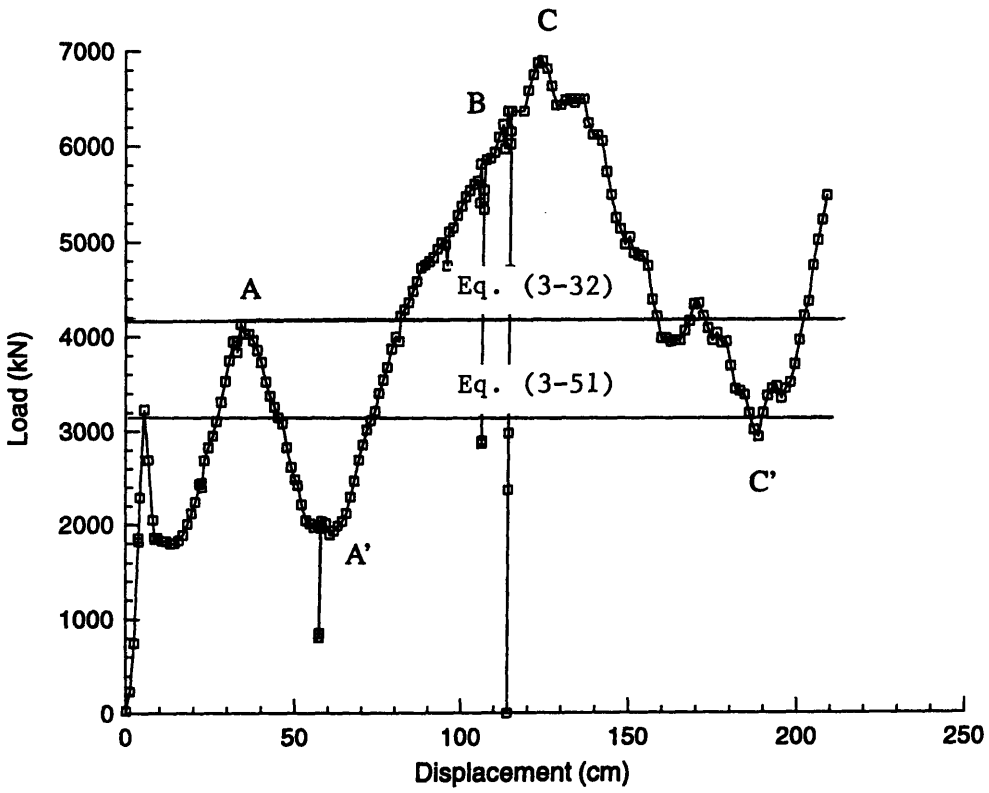

Fig. 5-9 Force-displacement diagram of a steady-state clean cut failure in thick plate experiments (Test #6)

(B = 125 mm, t = 20 mm, σ_o = 526 MPa, θ = 30°, α = 10°)

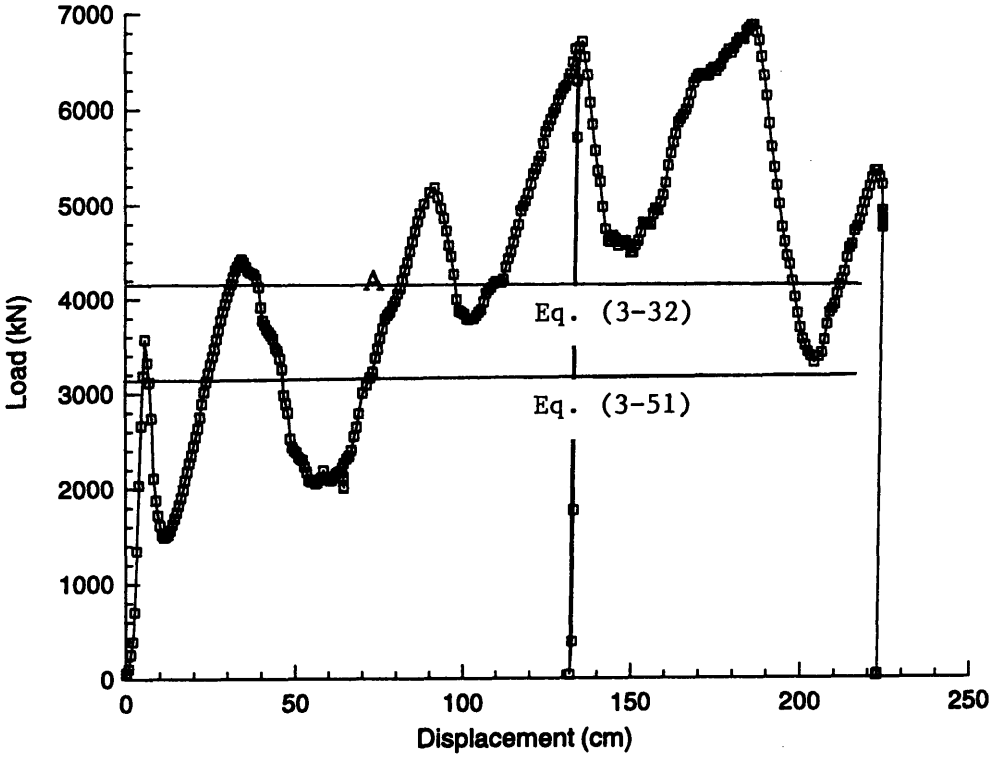

Fig. 5-10 Force-displacement diagram of a steady-state clean cut failure in thick plate experiments (Test #7)

(B = 125 mm, t = 20 mm, σ_o = 526 MPa, θ = 30°, α = 10°)

TABLE 1. Summary of experimental and theoretical results

Test No.	α (degree)	t (mm)	B (mm)	θ (degree)	σ_o (N/mm^2)	$F_{exp.}$ (KN)	$F_{theo.}$, Eq. (3-32) (KN)	$F_{app.}$, Eq. (3-51) (KN)
#1 [1]	10	1.60	5.0	10	272	5.9	5.9	5.6
#2 [20]	0	0.41	2.5	45	270	0.9	0.7	0.5
#3 [14]	0	0.41	2.5	45	270	0.9	0.7	0.8
#4 [14]	10	0.75	9.5	45	320	2.5	3.7	2.6
#5 [14]	10	0.75	9.5	45	320	2.4	3.7	2.6
#6 & #7 [26]	10	20.0	125	30	526	4500	4205	3177

Chapter 6

Summary and Recommendations

6.1. Summary

Closed-form solutions were derived for both transient indentation and steady-state cutting processes. The hypothesis of material cutting instead of fracturing at a wedge tip is adopted throughout the dissertation. Suitable scaling laws are developed valid in the wide range of geometrical parameters.

For a transient indentation process, a new analytical solution was derived and compared with the earlier splitting model proposed by Wierzbicki and Thomas [2] which assumes that a fracture or tearing is occurring in front of a wedge. Both kinematic models are closely related. Either failure mode might happen depending on the application geometry. Experimental validation was also performed and good correlation was reported between the theoretical solutions and experimental results.

For a steady-state wedge cutting process, two kinematic models were proposed with curled and upright flaps. Either model may give closer predictions depending on the actual problem geometry. Comparison of the theoretical solutions with typical experimental results shows a good correlation. Stable flap buckling due to compressive stress in the transition zone was analyzed and the diagram of the theoretical buckling coefficient was plotted for a non-uniform thickness plate under uni-axial compression.

Comparison with the concertina tearing failure mode was also performed and bounding curves were defined separating varies regions in the deformation map diagram.

6.2. Recommendations

Experimental verification is very important to the success of the current theory. More experimental work is suggested to simulate the actual ship grounding scenario, especially for thicker plates, such as the tests reported by Astrup [26]. Design of future specimens should limit the global flexibility in the out-of-plane direction by using effective stiffening methods. With the advance of computer technology, it is possible to analyze such a complicated problem accurately and economically by using general purpose nonlinear finite element codes. Computational results on double hull stranding failure and steady-state wedge cutting process were reported by using Dyna-3D finite element software but these methods are not in common use because of time consuming modelling efforts. For the structural failure analysis of any type, the upper bound theorem of plasticity was used in this dissertation in conjunction with the force minimum postulate. It should be pointed out that this methodology may not always give a useful answer. For example, the problem of undersea pipe buckling propagation was difficult to solve using the current theory.

References

[1] G. Lu and C.R. Calladine: *On the Cutting of a Plate by a Wedge*, Int. J. Mech. Sci., **32**, 293-313 (1990).

[2] T. Wierzbicki and P. Thomas: *Closed-form Solution for Wedge Cutting Force Through Thin Metal Sheets*, Int. J. Mech. Sci., **35**, 209-229 (1993).

[3] T. Wierzbicki, E. Rady, D. Peer, and J.G. Shin: Damage Estimates in High Energy Grounding of Ships, Joint MIT–Industry Program on Tanker Safety, Report No. 1, Department of Ocean Engineering, M.I.T. (1990).

[4] V.U. Minorsky: *An Analysis of Ship Collisions with Reference to Protection of Nuclear Power Plants*, J. Ship Research, **3**, 1-4 (1959).

[5] H. Vaughan: *Bending and Tearing of Plate with Application to Ship-bottom Damage*, The Naval Architect, 97-99, (May 1978).

[6] Y. Akita, and K. Kitamura: *A Study on Collision by an Elastic Stem to a Side Structure of Ships* (in Japanese), J. Society of Naval Architects of Japan, **131**, 307-317 (1972).

[7] H. Vaughan: *The Tearing of Mild Steel Plate*, J. Ship Res., **24**, 96-100 (1980).

[8] G. Woisin: *Comments on Vaughan: The Tearing Strength of Mild Steel Plate*, J. Ship Res., **26**, 50-52 (1982).

[9] N. Jones and W. S. Jouri: *A Study of Plate Tearing for Ship Collision and Grounding Damage*, J. Ship Res., **31**, 253-268 (1987).

[10] A.G. Atkins: *Scaling in Combined Plastic Flow and Fracture*, Int. J. Mech. Sci., **30**, 173-191 (1988).

[11] N. Jones, W.S. Jouri, and R.S. Birch: *On the Scaling of Ship Collision Damage*, in

Proceedings of 3rd Int. Congress on Marine Tech. in Athens, Int. Maritime Assoc. E. Mediterranean, Phivos Pub. Co., Greece, 287-294 (1984).

[12] L.M. Maxwell: *Effect of Rock Geometry on the Failure Mode of Plates and the Forces in Grounding Experiments*, M.Sc. Thesis, Department of Ocean Engineering, M.I.T. (1993).

[13] Z.M. Zheng, and T. Wierzbicki: *A Theoretical Analysis of a Steady-state Wedge Cutting Through Metal Plates*, Joint MIT–Industry Program on Tanker Safety, Report No. 19, Department of Ocean Engineering, M.I.T. (Jan. 1994).

[14] M. Yahiaoui, M. Bracco, P. Little, and K. Trauth: *Experimental Studies on Scale Models for Grounding*, Joint MIT–Industry Program on Tanker Safety, Report No. 18, Department of Ocean Engineering, M.I.T. (Jan. 1994).

[15] H. Vaughan: *Damage to Ships due to Collision and Grounding*, Det norske Veritas, Report No. DnV 77-345.

[16] T. Kuroiwa, Y. Kawamoto, and T. Yuhara: *Study on Damage of Ship Bottom Structures due to Grounding*, Conference on Marine Safety and Environment/Ship Production, Delft, Netherlands (Jun. 1992).

[17] M. Bracco: *Grounding Resistance of Longitudinally Stiffened Single and Double Hulls*, Joint MIT–Industry Program on Tanker Safety, Report No. 30, Department of Ocean Engineering, M.I.T. (Jun. 1994).

[18] P. Little: *Failure of Transverse Frames and Bulkheads in Grounding*, Joint MIT–Industry Program on Tanker Safety, Report No. 31, Department of Ocean Engineering, M.I.T. (Jun. 1994).

[19] K. Kitamura, Y. Okumoto, and T. Shibue: *On the Model Tests of Double Bottom*

Strength for Stranding (in Japanese), J. Society of Naval Architects of Japan, **143**, 346-356 (1978).

[20] K. Trauth: *Report on Testing Results of Plate Cutting and Tearing Failures*, 3rd Steering Committee Meeting of the Joint MIT–Industry Program on Tanker Safety, M.I.T. (1993).

[21] T. Wierzbicki, and W. Abramowicz: *On the Crushing Mechanics of Thin-walled Structures*, J. Appl. Mech., **5**, 727-734 (1983).

[22] P. Thomas: *Application of Plate Cutting Mechanics to Damage Prediction in Ship Groundings*, Joint Industry Program on Tanker Safety, Report No. 8, Department of Ocean Engineering, M.I.T. (1992).

[23] G. Lu: *Cutting of a Plate by a Wedge*, Ph.D. Dissertation, University of Cambridge (1989).

[24] A.G. Atkins: *Letter to the Editor*, Int. J. Mech. Sci., **33**, 69-71 (1991).

[25] G. Lu and C.R. Calladine: *Author's Reply*, Int. J. Mech. Sci., **33**, 73-74 (1991).

[26] O. Astrup: *Cutting of Thick Plates by a Wedge - an Experimental Study*, Joint MIT–Industry Program on Tanker Safety, Report No. 27, Department of Ocean Engineering, M.I.T. (Jan. 1994).

[27] T. Wierzbicki: *Concertina Tearing of Metal Plates - Improved Solution and Comparison with Experiments*, Joint MIT–Industry Program on Tanker Safety, Report No. 22, Department of Ocean Engineering, M.I.T. (Jan. 1994).

[28] E.M. Trent: *Metal Cutting*, 3rd ed., Butterworth Heinemann (1991).

[29] F. Jaklitsch: *Metal Cutting Technology*, Valeron Co., Berkley, Michigan (1983).

[30] H.N. Hill: *Chart for Critical Compressive Stress of Flat Rectangular Plates*, NACA TN #773 (1940).

[31] A.L. Lang: *The Buckling of a Non-uniform Plate*, Structures Memo #4, Supersonic Laboratory, M.I.T. (1950).

[32] B.W. Char, K.O. Geddes, *at al*: *First Leaves: A Tutorial Introduction to Maple V*, Springer-Verlag, New York (1992).

[33] S.P. Timoshenko and J.M. Gere: *Theory of Elastic Stability*, 2nd ed., McGraw-Hill, New York (1961).

[34] J. K. Paik: *Cutting of a Longitudinally Stiffened Steel Plate by a Rigid Wedge*, submitted to J. Ship Res. (1993).

[35] J. Rhodes: *Ultimate Strength of Thin-walled Components*, in The Manual of Crash-worthiness Engineering, Vol. **IV**, Center for Transportation Studies, M.I.T. (1989).

[36] P. Little: *Failure of Transverse Frames and Bulkheads in Grounding,* Joint MIT–Industry Program on Tanker Safety, Report No. 31, Department of Ocean Engineering, M.I.T. (Jun. 1994).

Appendix A

Transition zone geometry

In order to calculate the total deformation energy in a transition zone, it is important to find the coordinates for the corresponding end nodes connecting a family of straight lines which is used to approximate the transition zone toroid surface (Section 3.3.). Two local coordinate systems are built up: XYZ and $x'y'z'$ shown in Fig. A-1. Both coordinate systems share a common origin and a common x-axis, and the angle between Y- and y'-axes is θ (wedge half-angle).

Stable flap is located in XYZ cylindrical coordinate system. Point A is an intersection of the stable flap ridge line and the transition zone ridge line. It can be shown that the coordinate for point A is

$$\begin{cases} X = R\cos\phi , \\ Y = R\sin\phi , \\ Z = 0 . \end{cases} \tag{A-1}$$

The total arc length of the curling flap, AP, is:

$$l_1 = R\phi , \tag{A-2}$$

where ϕ is the rolling angle along the stable flap curling direction.

The transient flap is located in the local $x'y'z'$ cylindrical coordinate system shown in Fig. A-1(b). Point B is an intersection of the transient flap ridge line and the transition zone ridge line. It can be calculated that the coordinates for point B is

$$\begin{cases} x' = R\cos\phi' , \\ y' = R\sin\phi' , \\ z' = \overline{BB'} = \overline{PB'}\tan\theta = R\phi'\tan\theta . \end{cases} \tag{A-3}$$

The total arc length, BP, is:

$$l_2 = \frac{\overline{PB'}}{\cos\theta} = \frac{R\phi'}{\cos\theta} . \tag{A-4}$$

From the physical model construction, it is found that both arc lengths l_1 and l_2 come from an identical line before cutting. Since there is no axial force along those arcs, they must be equal after cutting. This provides an important relationship between the two coordinate systems:

$$l_1 = l_2 , \tag{A-5}$$

or

$$\phi = \frac{\phi'}{\cos\theta} . \tag{A-6}$$

Transforming $x'y'z'$ into XYZ, we get the following relationship between the two coordinate systems:

$$\begin{Bmatrix} X \\ Y \\ Z \end{Bmatrix} = \begin{bmatrix} 1 & 0 & 0 \\ 0 & \cos\theta & \sin\theta \\ 0 & -\sin\theta & \cos\theta \end{bmatrix} \begin{Bmatrix} x' \\ y' \\ z' \end{Bmatrix} . \tag{A-7}$$

Substituting Eqs. (A-4) and (A-6) into Eq. (A-7), the coordinates for point B can be expressed in XYZ coordinate system as follows:

$$\begin{cases} X = R\cos(\phi\cos\theta) , \\ Y = R\cos\theta\sin(\phi\cos\theta) + R\phi\sin^2\theta , \\ Z = -R\sin\theta\sin(\phi\cos\theta) + R\phi\sin\theta\cos\theta . \end{cases} \tag{A-8}$$

Now, the distance between points A and B can be derived from Eqs. (A-1) and (A-8):

$$u = R \cdot Q , \tag{A-9}$$

and the demensionless coefficient can be expressed as:

$$Q = \sqrt{[\cos\phi - \cos(C\phi)]^2 + [\sin\phi - C\sin(C\phi) - S^2\phi]^2 + S^2[C\phi - \sin(C\phi)]^2}.$$

where $C = \cos\theta$ and $S = \sin\theta$. The above expression gives the transition zone stretching which can be used in the deformation energy calculation conducted in Section 3.3.

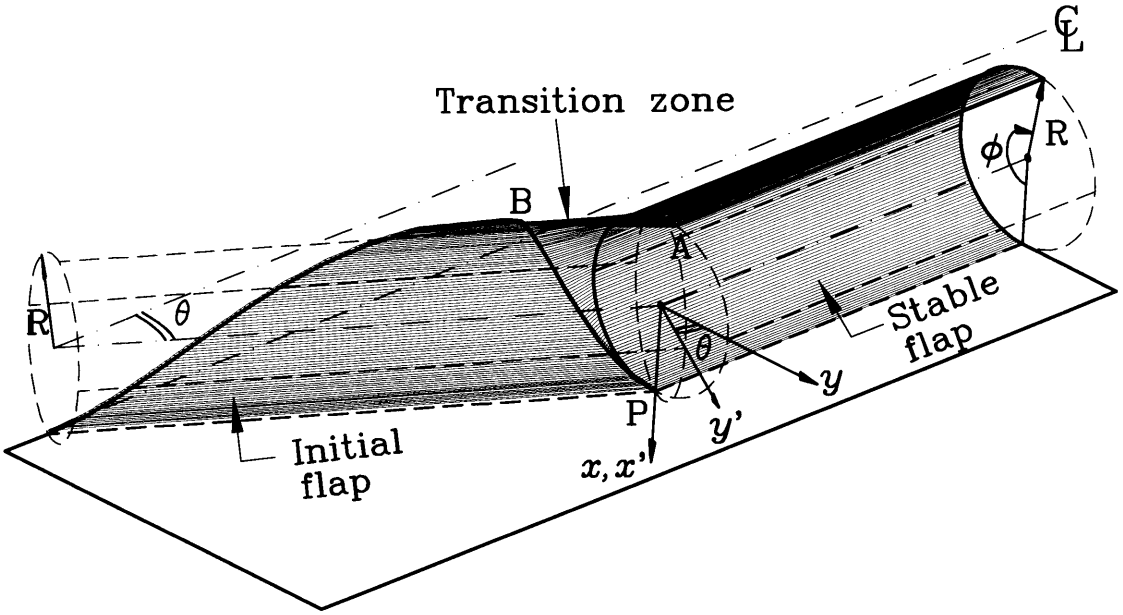

(a) xyz and $x'y'z'$ coordinate system

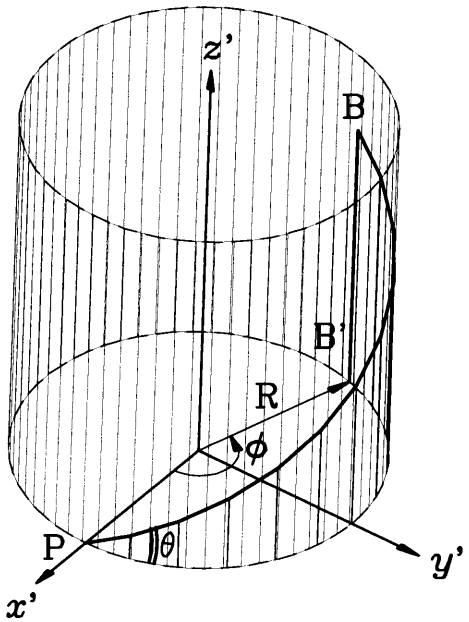

(b) Initial flap geometry

Fig. A-1 Geometric study in the transition zone

Appendix B

Opening rate in transition zone

The opening rate in the transition zone, $\dot{u}(\xi)$, is defined here as the material flow rate along a stream line parallel to the plastic moving hinge. The arc length between the stream line and the plastic hinge is defined as ξ (Fig. 3-4). Assume that, at time t, the near-tip plastic zone arrives at points A and/or B which has zero separation; and, at time $t + \Delta t$, the distance AB reaches its maximum value d (Ref. Section 3.3.8.). During this period of time, the wedge travelled a distance equal to the length $l_p + l_t$ (Fig. 3-6), so that the wedge advancing speed can be formulated as follows:

$$V = \frac{l_p + l_t}{\Delta t} . \tag{B-1}$$

For a given coordinate ξ, the expression of maximum transition zone opening is derived in Section 3.3 and can be re-written as:

$$\Delta u = \frac{0.32\theta}{R} \xi^2 . \tag{B-2}$$

Note that, in the above derivation, the geometric relation $\xi = R\phi$ is incorporated (Ref. Fig. 3-4).

Based upon the above discussions and the geometric relation $(l_p + l_t) = (B + R) / \tan\theta$ (Fig. 3-6), the opening rate in the transition zone can be derived as:

$$\dot{u}(\xi) = \frac{\Delta u}{\Delta t} = \frac{\Delta u}{l_p + l_t} \cdot V = \frac{0.32\theta \tan\theta}{R(B+R)} \cdot V \cdot \xi^2 . \tag{B-3}$$

Appendix C

Derivation of rectangular plate buckling

(m=1)

> a:=lambda*b; n:=arccos(mu/2/(-1+mu)); m:=1;

$$a := \lambda b$$

$$n := \arccos\left(\frac{1}{2}\,\frac{\mu}{-1+\mu}\right)$$

$$m := 1$$

> w:=sin(Pi*x/a)*A*sin(m*Pi*x/a)*(1-cos(n*y/b));

$$w := \sin\left(\frac{\pi x}{\lambda b}\right)^2 A\left(1 - \cos\left(\frac{\arccos\left(\frac{1}{2}\,\frac{\mu}{-1+\mu}\right) y}{b}\right)\right)$$

> DE:=(diff(w,x,x)+diff(w,y,y))^2-2*(1-mu)*(diff(w,x,x)*diff(w,y,y)-(diff(w,x,y))^2);

$$DE := \left(2\,\frac{\cos\left(\frac{\pi x}{\lambda b}\right)^2 \pi^2 A\left(1 - \cos\left(\frac{\%1\, y}{b}\right)\right)}{\lambda^2 b^2} - 2\,\frac{\sin\left(\frac{\pi x}{\lambda b}\right)^2 A\left(1 - \cos\left(\frac{\%1\, y}{b}\right)\right)\pi^2}{\lambda^2 b^2}\right.$$

$$\left. + \frac{\sin\left(\frac{\pi x}{\lambda b}\right)^2 A \cos\left(\frac{\%1\, y}{b}\right)\%1^2}{b^2}\right)^2 - 2\,(1-\mu)\left(\right.$$

$$\left(2\,\frac{\cos\left(\frac{\pi x}{\lambda b}\right)^2 \pi^2 A\left(1 - \cos\left(\frac{\%1\, y}{b}\right)\right)}{\lambda^2 b^2} - 2\,\frac{\sin\left(\frac{\pi x}{\lambda b}\right)^2 A\left(1 - \cos\left(\frac{\%1\, y}{b}\right)\right)\pi^2}{\lambda^2 b^2}\right)\sin\left(\frac{\pi x}{\lambda b}\right)^2$$

$$\left. A\cos\left(\frac{\%1\, y}{b}\right)\%1^2 / b^2 - 4\,\frac{\sin\left(\frac{\pi x}{\lambda b}\right)^2 A^2 \sin\left(\frac{\%1\, y}{b}\right)^2 \%1^2 \cos\left(\frac{\pi x}{\lambda b}\right)^2 \pi^2}{b^4 \lambda^2}\right)$$

$$\%1 := \arccos\left(\frac{1}{2}\,\frac{\mu}{-1+\mu}\right)$$

> Z1:=int(DE, x=0..a);

$$Z1 := \frac{1}{8} A^2 \left(-32\,\pi^4 \cos\left(\frac{\%1\, y}{b}\right) + 3\cos\left(\frac{\%1\, y}{b}\right)^2 \%1^4 \lambda^4 - 8\,\pi^2 \lambda^2 \%1^2 \cos\left(\frac{\%1\, y}{b}\right)\mu + 16\,\pi^4\right.$$

$$+ 8\,\pi^2 \lambda^2 \%1^2 \sin\left(\frac{\%1\, y}{b}\right)^2 - 8\,\pi^2 \lambda^2 \%1^2 \sin\left(\frac{\%1\, y}{b}\right)^2 \mu + 16\,\pi^4 \cos\left(\frac{\%1\, y}{b}\right)^2$$

$$\left. + 8\,\pi^2 \lambda^2 \%1^2 \cos\left(\frac{\%1\, y}{b}\right)^2 \mu\right) / \left(\lambda^3 b^3\right)$$

$$\%1 := \arccos\left(\frac{1}{2}\,\frac{\mu}{-1+\mu}\right)$$

> Z2:=int(Z1*(1-beta*y/b)^3, y=0..b);

$$Z2 := -\frac{1}{64}A^2\left(6\,\beta^3\tan\left(\frac{1}{2}\%1\right)^2\%1^8\,\lambda^4 + 16\,\beta^3\tan\left(\frac{1}{2}\%1\right)^2\%1^6\,\lambda^2\,\pi^2\right.$$

$$+ 96\,\beta^3\tan\left(\frac{1}{2}\%1\right)^2\%1^4\,\pi^4 + 48\,\beta^3\tan\left(\frac{1}{2}\%1\right)^4\%1^4\,\pi^4 + 18\,\beta\,\%1^8\,\lambda^4$$

$$- 36\tan\left(\frac{1}{2}\%1\right)^3\%1^5\,\lambda^4\,\beta^2 + 816\,\beta^3\tan\left(\frac{1}{2}\%1\right)^4\%1^2\,\pi^4 - 24\,\beta^3\tan\left(\frac{1}{2}\%1\right)^4\%1^4\,\pi^2\,\lambda^2$$

$$+ 240\,\beta^3\tan\left(\frac{1}{2}\%1\right)^4\%1^4\,\pi^2\,\lambda^2\,\mu - 192\,\beta^2\tan\left(\frac{1}{2}\%1\right)^3\%1^5\,\lambda^2\,\pi^2$$

$$+ 1920\,\beta^2\tan\left(\frac{1}{2}\%1\right)^3\%1^3\,\pi^4 + 48\,\beta\tan\left(\frac{1}{2}\%1\right)^4\%1^6\,\lambda^2\,\pi^2 - 384\,\beta^3\tan\left(\frac{1}{2}\%1\right)\%1^3\,\pi^4$$

$$- 12\,\beta^2\tan\left(\frac{1}{2}\%1\right)^4\%1^8\,\lambda^4 + 288\,\beta\tan\left(\frac{1}{2}\%1\right)^4\%1^4\,\pi^4 - 192\,\beta^2\tan\left(\frac{1}{2}\%1\right)^4\%1^4\,\pi^4$$

$$- 288\,\beta^3\tan\left(\frac{1}{2}\%1\right)^2\%1^4\,\lambda^2\,\pi^2\,\mu + 576\,\beta\tan\left(\frac{1}{2}\%1\right)^2\%1^4\,\pi^4 - 54\,\beta^3\tan\left(\frac{1}{2}\%1\right)^2\%1^6\,\lambda^4$$

$$+ 96\tan\left(\frac{1}{2}\%1\right)^3\%1^3\,\pi^2\,\lambda^2\,\beta^2 + 144\,\beta^3\tan\left(\frac{1}{2}\%1\right)^2\%1^4\,\lambda^2\,\pi^2$$

$$- 576\tan\left(\frac{1}{2}\%1\right)\%1^3\,\pi^2\,\lambda^2\,\mu\,\beta^2 - 2880\tan\left(\frac{1}{2}\%1\right)\%1\,\pi^4\,\beta^2$$

$$+ 96\,\beta\tan\left(\frac{1}{2}\%1\right)^2\%1^6\,\lambda^2\,\pi^2 + 24\,\beta^3\tan\left(\frac{1}{2}\%1\right)\%1^7\,\lambda^4 - 64\,\beta^3\tan\left(\frac{1}{2}\%1\right)\%1^5\,\lambda^2\,\pi^2$$

$$+ 48\tan\left(\frac{1}{2}\%1\right)^4\%1^4\,\lambda^2\,\pi^2\,\beta^2 - 768\,\beta\tan\left(\frac{1}{2}\%1\right)^2\lambda^2\,\pi^2\,\%1^4\,\mu - 12\tan\left(\frac{1}{2}\%1\right)^4\%1^8\,\lambda^4$$

$$+ 3\,\beta^3\,\%1^8\,\lambda^4 + 48\,\beta^3\,\%1^4\,\pi^4 + 9\,\beta^3\,\%1^6\,\lambda^4 - 720\,\beta^3\,\%1^2\,\pi^4 - 192\tan\left(\frac{1}{2}\%1\right)^4\%1^4\,\pi^4$$

$$- 96\,\beta^3\tan\left(\frac{1}{2}\%1\right)^3\%1^3\,\pi^2\,\lambda^2 + 960\,\beta^3\tan\left(\frac{1}{2}\%1\right)^3\%1^3\,\pi^2\,\lambda^2\,\mu$$

$$\left.+ 36\,\beta^3\tan\left(\frac{1}{2}\%1\right)^3\%1^5\,\lambda^4 + 768\,\beta^2\tan\left(\frac{1}{2}\%1\right)^3\%1^5\,\lambda^2\,\pi^2\,\mu\right.$$

$$+ 72\,\beta^2 \tan\left(\frac{1}{2}\%1\right)^3 \%1^7\,\lambda^4 - 960 \tan\left(\frac{1}{2}\%1\right)^3 \%1^3\,\pi^2\,\lambda^2\,\mu\,\beta^2 - 64 \tan\left(\frac{1}{2}\%1\right)^3 \%1^5\,\lambda^2\,\pi^2$$

$$+ 36\,\beta^3 \tan\left(\frac{1}{2}\%1\right)^2 \lambda^4\,\%1^4 - 24\,\beta^2 \tan\left(\frac{1}{2}\%1\right)^2 \%1^8\,\lambda^4 - 32\,\beta^2 \tan\left(\frac{1}{2}\%1\right)^4 \%1^6\,\lambda^2\,\pi^2$$

$$+ 192\,\beta \tan\left(\frac{1}{2}\%1\right)^2 \lambda^2\,\pi^2\,\%1^4 + 36\,\beta \tan\left(\frac{1}{2}\%1\right)^2 \%1^8\,\lambda^4 + 1152\,\beta^2 \tan\left(\frac{1}{2}\%1\right) \%1^3\,\pi^4$$

$$- 24\,\beta^3 \tan\left(\frac{1}{2}\%1\right)^3 \%1^7\,\lambda^4 + 192\,\beta^2 \tan\left(\frac{1}{2}\%1\right) \%1^5\,\lambda^2\,\pi^2 - 640\,\beta^3 \tan\left(\frac{1}{2}\%1\right)^3 \%1^3\,\pi^4$$

$$+ 64\,\beta^3 \tan\left(\frac{1}{2}\%1\right)^3 \%1^5\,\lambda^2\,\pi^2 - 256\,\beta^3 \tan\left(\frac{1}{2}\%1\right)^3 \%1^5\,\lambda^2\,\pi^2\,\mu - 24 \tan\left(\frac{1}{2}\%1\right)^2 \%1^8\,\lambda^4$$

$$+ 768\,\pi^2\,\beta^3\,\lambda^2\,\%1^2\,\mu - 1536\,\pi^4\,\beta\,\%1^2 - 32\,\beta^2\,\%1^6\,\lambda^2\,\pi^2 - 1920\,\beta \tan\left(\frac{1}{2}\%1\right)^2 \pi^4\,\%1^2$$

$$- 480 \tan\left(\frac{1}{2}\%1\right)^4 \%1^4\,\lambda^2\,\pi^2\,\mu\,\beta^2 - 96\,\beta^3 \tan\left(\frac{1}{2}\%1\right)^2 \pi^2\,\lambda^2\,\%1^2$$

$$+ 960\,\beta^3 \tan\left(\frac{1}{2}\%1\right)^2 \pi^2\,\lambda^2\,\%1^2\,\mu - 32 \tan\left(\frac{1}{2}\%1\right)^4 \%1^6\,\lambda^2\,\pi^2$$

$$+ 256 \tan\left(\frac{1}{2}\%1\right)^3 \%1^5\,\lambda^2\,\pi^2\,\mu + 9\,\beta^3 \tan\left(\frac{1}{2}\%1\right)^4 \%1^6\,\lambda^4 - 3264 \tan\left(\frac{1}{2}\%1\right)^3 \%1\,\pi^4\,\beta^2$$

$$+ 288\,\%1^4\,\pi^2\,\lambda^2\,\mu\,\beta^2 - 32\,\%1^6\,\lambda^2\,\pi^2 - 18\,\%1^6\,\lambda^4\,\beta^2 + 24 \tan\left(\frac{1}{2}\%1\right)^3 \%1^7\,\lambda^4$$

$$- 384 \tan\left(\frac{1}{2}\%1\right)^2 \%1^4\,\pi^4 + 3264\,\beta^3 \tan\left(\frac{1}{2}\%1\right)^2 \pi^4 - 24 \tan\left(\frac{1}{2}\%1\right) \%1^7\,\lambda^4$$

$$+ 640 \tan\left(\frac{1}{2}\%1\right)^3 \%1^3\,\pi^4 + 384 \tan\left(\frac{1}{2}\%1\right) \%1^3\,\pi^4 + 48\,\%1^4\,\lambda^2\,\pi^2\,\beta^2$$

$$+ 72\,\beta \tan\left(\frac{1}{2}\%1\right) \%1^7\,\lambda^4 + 96\,\beta^3 \tan\left(\frac{1}{2}\%1\right) \%1^3\,\pi^2\,\lambda^2 + 2880\,\beta^3 \tan\left(\frac{1}{2}\%1\right) \%1\,\pi^4$$

$$- 288 \tan\left(\frac{1}{2}\%1\right)^2 \%1^4\,\lambda^2\,\pi^2\,\beta^2 - 96 \tan\left(\frac{1}{2}\%1\right) \%1^3\,\pi^2\,\lambda^2\,\beta^2 + 36 \tan\left(\frac{1}{2}\%1\right) \%1^5\,\lambda^4\,\beta^2$$

$$+ 64 \tan\left(\frac{1}{2}\%1\right) \%1^5\,\lambda^2\,\pi^2 + 192\,\beta \tan\left(\frac{1}{2}\%1\right)^3 \%1^5\,\lambda^2\,\pi^2 - 72\,\beta \tan\left(\frac{1}{2}\%1\right)^3 \%1^7\,\lambda^4$$

$$- 768\,\beta \tan\left(\frac{1}{2}\%1\right)^3 \%1^5\,\lambda^2\,\pi^2\,\mu + 3264\,\beta^3 \tan\left(\frac{1}{2}\%1\right)^3 \%1\,\pi^4$$

$$- 1920\,\beta \tan\left(\frac{1}{2}\,\%1\right)^3 \%1^3\,\pi^4 - 384\,\pi^2\,\beta\,\lambda^2\,\%1^4\,\mu - 12\,\beta^2\,\%1^8\,\lambda^4 - 192\,\beta^2\,\%1^4\,\pi^4$$

$$+ 1440\,\%1^2\,\pi^4\,\beta^2 + 576 \tan\left(\frac{1}{2}\,\%1\right)^2 \%1^4\,\lambda^2\,\pi^2\,\mu\,\beta^2 + 576 \tan\left(\frac{1}{2}\,\%1\right)^2 \%1^2\,\pi^4\,\beta^2$$

$$- 64 \tan\left(\frac{1}{2}\,\%1\right)^2 \%1^6\,\lambda^2\,\pi^2 + 108 \tan\left(\frac{1}{2}\,\%1\right)^2 \%1^6\,\lambda^4\,\beta^2$$

$$+ 576\,\beta^3 \tan\left(\frac{1}{2}\,\%1\right) \%1^3\,\pi^2\,\lambda^2\,\mu - 1152\,\beta \tan\left(\frac{1}{2}\,\%1\right) \%1^3\,\pi^4$$

$$- 192\,\beta \tan\left(\frac{1}{2}\,\%1\right) \%1^5\,\lambda^2\,\pi^2 - 36\,\beta^3 \tan\left(\frac{1}{2}\,\%1\right) \%1^5\,\lambda^4 + 288\,\beta\,\%1^4\,\pi^4$$

$$- 18 \tan\left(\frac{1}{2}\,\%1\right)^4 \%1^6\,\lambda^4\,\beta^2 - 72\,\beta \tan\left(\frac{1}{2}\,\%1\right)^2 \lambda^4\,\%1^6 - 1632 \tan\left(\frac{1}{2}\,\%1\right)^4 \%1^2\,\pi^4\,\beta^2$$

$$+ 18\,\beta \tan\left(\frac{1}{2}\,\%1\right)^4 \%1^8\,\lambda^4 - 72\,\beta^2 \tan\left(\frac{1}{2}\,\%1\right) \%1^7\,\lambda^4 - 288\,\beta^3 \tan\left(\frac{1}{2}\,\%1\right)^2 \%1^2\,\pi^4$$

$$+ 8\,\beta^3\,\%1^6\,\lambda^2\,\pi^2 - 384\,\beta^2 \tan\left(\frac{1}{2}\,\%1\right)^2 \%1^4\,\pi^4 - 64\,\beta^2 \tan\left(\frac{1}{2}\,\%1\right)^2 \%1^6\,\lambda^2\,\pi^2$$

$$+ 48\,\beta\,\%1^6\,\lambda^2\,\pi^2 - 144\,\beta^3\,\%1^4\,\pi^2\,\lambda^2\,\mu - 24\,\beta^3\,\%1^4\,\lambda^2\,\pi^2 + 8\,\beta^3 \tan\left(\frac{1}{2}\,\%1\right)^4 \%1^6\,\lambda^2\,\pi^2$$

$$+ 3\,\beta^3 \tan\left(\frac{1}{2}\,\%1\right)^4 \%1^8\,\lambda^4 + 3072\,\pi^4\,\beta^3 - 192\,\%1^4\,\pi^4 - 12\,\%1^8\,\lambda^4 \Bigg) \Bigg/ \Bigg(b^2\,\lambda^3\,\%1^4$$

$$\left(1 + \tan\left(\frac{1}{2}\,\%1\right)^2\right)^2 \Bigg) + 6\,\frac{A^2\,\pi^2\,\beta\left(2\,\lambda^2\,\%1^2\,\mu\,\beta^2 - 4\,\%1^2\,\pi^2 - \lambda^2\,\%1^4\,\mu + 8\,\pi^2\,\beta^2\right)}{b^2\,\%1^4\,\lambda^3}$$

$$\%1 := \arccos\left(\frac{1}{2}\,\frac{\mu}{-1+\mu}\right)$$

```
> int(diff(w,x)^2,x=0..a);
```

$$\frac{1}{2}\,\frac{\pi^2\,A^2\left(-1 + \cos\left(\dfrac{\arccos\left(\dfrac{1}{2}\,\dfrac{\mu}{-1+\mu}\right) y}{b}\right)\right)^2}{\lambda\,b}$$

```
> Z3:=int((1-beta*y/b)*",y=0..b);
```

$$Z3 := -\frac{1}{8}\pi^2 A^2 \left(-6\beta - 12\tan\left(\frac{1}{2}\%1\right)^2 \%1^2 - 6\,\%1^2 - 6\tan\left(\frac{1}{2}\%1\right)^4 \%1^2 - 12\beta\tan\left(\frac{1}{2}\%1\right)\%1 \right.$$
$$+ 3\beta\,\%1^2 + 10\beta\tan\left(\frac{1}{2}\%1\right)^4 + 3\beta\tan\left(\frac{1}{2}\%1\right)^4 \%1^2 + 12\tan\left(\frac{1}{2}\%1\right)\%1$$
$$+ 20\tan\left(\frac{1}{2}\%1\right)^3 \%1 - 20\beta\tan\left(\frac{1}{2}\%1\right)^3 \%1 + 6\beta\tan\left(\frac{1}{2}\%1\right)^2 \%1^2 \Bigg) \Bigg/ \left(\lambda\,\%1^2 \right.$$
$$\left. \left(1 + \tan\left(\frac{1}{2}\%1\right)^2 \right)^2 \right) - \frac{3}{4}\frac{\pi^2 A^2 \beta}{\lambda\,\%1^2}$$

$$\%1 := \arccos\left(\frac{1}{2}\frac{\mu}{-1+\mu}\right)$$

> U:=simplify((Z2-X*Z3)/A^2);

$$U := -\frac{1}{64}\left(72\beta^2 \%1^7 \lambda^4 \cos\left(\frac{1}{2}\%1\right)\sin\left(\frac{1}{2}\%1\right) - 384\,\%1^4 \lambda^2 \pi^2 \beta^2 \cos\left(\frac{1}{2}\%1\right)^2 \right.$$
$$- 1920\beta\,\%1^3 \pi^4 \cos\left(\frac{1}{2}\%1\right)\sin\left(\frac{1}{2}\%1\right) + 160\,X\pi^2 b^2 \lambda^2 \%1^3 \beta\cos\left(\frac{1}{2}\%1\right)\sin\left(\frac{1}{2}\%1\right)$$
$$- 768\beta^3 \%1^4 \lambda^2 \pi^2 \mu\cos\left(\frac{1}{2}\%1\right)^2 - 1920\beta^3 \%1^2 \pi^4 \cos\left(\frac{1}{2}\%1\right)^2$$
$$+ 144\,\%1^6 \lambda^4 \beta^2 \cos\left(\frac{1}{2}\%1\right)^2 + 3840\,\%1^2 \pi^4 \beta^2 \cos\left(\frac{1}{2}\%1\right)^2 - 72\beta^3 \%1^6 \lambda^4 \cos\left(\frac{1}{2}\%1\right)^2$$
$$+ 384\beta^3 \%1^2 \pi^4 \cos\left(\frac{1}{2}\%1\right)^4 - 768\,\%1^2 \pi^4 \beta^2 \cos\left(\frac{1}{2}\%1\right)^4 + 72\beta^3 \%1^6 \lambda^4 \cos\left(\frac{1}{2}\%1\right)^4$$
$$+ 384\,\%1^4 \lambda^2 \pi^2 \beta^2 \cos\left(\frac{1}{2}\%1\right)^4 - 144\,\%1^6 \lambda^4 \beta^2 \cos\left(\frac{1}{2}\%1\right)^4$$
$$- 48\sin\left(\frac{1}{2}\%1\right)\%1^7 \lambda^4 \cos\left(\frac{1}{2}\%1\right)^3 + 384\sin\left(\frac{1}{2}\%1\right)\%1^3 \pi^2 \lambda^2 \mu\beta^2 \cos\left(\frac{1}{2}\%1\right)^3$$
$$+ 384\beta^3 \%1^4 \pi^2 \lambda^2 \mu\cos\left(\frac{1}{2}\%1\right)^4 - 192\beta^3 \%1^4 \lambda^2 \pi^2 \cos\left(\frac{1}{2}\%1\right)^4$$
$$+ 768\beta^2 \%1^5 \lambda^2 \pi^2 \mu\cos\left(\frac{1}{2}\%1\right)\sin\left(\frac{1}{2}\%1\right)$$
$$\left. - 768\beta^2 \%1^5 \lambda^2 \pi^2 \mu\cos\left(\frac{1}{2}\%1\right)^3 \sin\left(\frac{1}{2}\%1\right) + 48\beta^3 \sin\left(\frac{1}{2}\%1\right)\%1^7 \lambda^4 \cos\left(\frac{1}{2}\%1\right)^3 \right)$$

$$
\begin{aligned}
&- 128\,\beta^3 \sin\left(\frac{1}{2}\%1\right)\%1^5\,\lambda^2\,\pi^2 \cos\left(\frac{1}{2}\%1\right)^3 - 256 \sin\left(\frac{1}{2}\%1\right)\%1^3\,\pi^4 \cos\left(\frac{1}{2}\%1\right)^3 \\
&+ 256\,\beta^3 \sin\left(\frac{1}{2}\%1\right)\%1^3\,\pi^4 \cos\left(\frac{1}{2}\%1\right)^3 + 384 \sin\left(\frac{1}{2}\%1\right)\%1\,\pi^4\,\beta^2 \cos\left(\frac{1}{2}\%1\right)^3 \\
&- 768\,\%1^4\,\pi^2\,\lambda^2\,\mu\,\beta^2 \cos\left(\frac{1}{2}\%1\right)^4 - 72\,\beta^3 \sin\left(\frac{1}{2}\%1\right)\%1^5\,\lambda^4 \cos\left(\frac{1}{2}\%1\right)^3 \\
&+ 768\,\beta \sin\left(\frac{1}{2}\%1\right)\%1^3\,\pi^4 \cos\left(\frac{1}{2}\%1\right)^3 - 384\,\beta \sin\left(\frac{1}{2}\%1\right)\%1^5\,\lambda^2\,\pi^2 \cos\left(\frac{1}{2}\%1\right)^3 \\
&- 384\,\beta^3 \sin\left(\frac{1}{2}\%1\right)\%1^3\,\pi^2\,\lambda^2\,\mu \cos\left(\frac{1}{2}\%1\right)^3 - 144\,\beta^2 \sin\left(\frac{1}{2}\%1\right)\%1^7\,\lambda^4 \cos\left(\frac{1}{2}\%1\right)^3 \\
&+ 72 \sin\left(\frac{1}{2}\%1\right)\%1^5\,\lambda^4\,\beta^2 \cos\left(\frac{1}{2}\%1\right)^3 - 192 \sin\left(\frac{1}{2}\%1\right)\%1^3\,\pi^2\,\lambda^2\,\beta^2 \cos\left(\frac{1}{2}\%1\right)^3 \\
&- 960\,\%1^3\,\pi^2\,\lambda^2\,\mu\,\beta^2 \cos\left(\frac{1}{2}\%1\right)\sin\left(\frac{1}{2}\%1\right) - 64\,\%1^5\,\lambda^2\,\pi^2 \cos\left(\frac{1}{2}\%1\right)\sin\left(\frac{1}{2}\%1\right) \\
&+ 192\,\beta^3\,\%1^4\,\lambda^2\,\pi^2 \cos\left(\frac{1}{2}\%1\right)^2 + 1536\,\%1^4\,\lambda^2\,\pi^2\,\mu\,\beta^2 \cos\left(\frac{1}{2}\%1\right)^2 \\
&- 192\,\beta^2\,\%1^5\,\lambda^2\,\pi^2 \cos\left(\frac{1}{2}\%1\right)\sin\left(\frac{1}{2}\%1\right) + 96\,\%1^3\,\pi^2\,\lambda^2\,\beta^2 \cos\left(\frac{1}{2}\%1\right)\sin\left(\frac{1}{2}\%1\right) \\
&+ 3264\,\beta^3\,\pi^4 \cos\left(\frac{1}{2}\%1\right)^2 - 192\,\pi^4\,\beta^3 \cos\left(\frac{1}{2}\%1\right)^4 \\
&- 768\,\beta\,\%1^5\,\lambda^2\,\pi^2\,\mu \cos\left(\frac{1}{2}\%1\right)\sin\left(\frac{1}{2}\%1\right) + 768\,\beta\,\%1^5\,\lambda^2\,\pi^2\,\mu \cos\left(\frac{1}{2}\%1\right)^3 \sin\left(\frac{1}{2}\%1\right) \\
&- 36\,\%1^5\,\lambda^4\,\beta^2 \cos\left(\frac{1}{2}\%1\right)\sin\left(\frac{1}{2}\%1\right) - 64\,X\,\pi^2\,b^2\,\lambda^2\,\%1^3\,\beta \sin\left(\frac{1}{2}\%1\right)\cos\left(\frac{1}{2}\%1\right)^3 \\
&+ 144\,\beta \sin\left(\frac{1}{2}\%1\right)\%1^7\,\lambda^4 \cos\left(\frac{1}{2}\%1\right)^3 + 36\,\beta^3\,\lambda^4\,\%1^4 \cos\left(\frac{1}{2}\%1\right)^2 \\
&- 36 \cos\left(\frac{1}{2}\%1\right)^4 \beta^3\,\lambda^4\,\%1^4 - 384\,\beta^3 \sin\left(\frac{1}{2}\%1\right)\%1\,\pi^4 \cos\left(\frac{1}{2}\%1\right)^3 \\
&+ 64\,X\,\pi^2\,b^2\,\lambda^2\,\%1^3 \sin\left(\frac{1}{2}\%1\right)\cos\left(\frac{1}{2}\%1\right)^3 + 192\,\beta^3 \sin\left(\frac{1}{2}\%1\right)\%1^3\,\pi^2\,\lambda^2 \cos\left(\frac{1}{2}\%1\right)^3 \\
&+ 128 \sin\left(\frac{1}{2}\%1\right)\%1^5\,\lambda^2\,\pi^2 \cos\left(\frac{1}{2}\%1\right)^3 - 768\,\beta^2 \sin\left(\frac{1}{2}\%1\right)\%1^3\,\pi^4 \cos\left(\frac{1}{2}\%1\right)^3
\end{aligned}
$$

$$+ 384\,\beta^2 \sin\left(\frac{1}{2}\%1\right)\%1^5\,\lambda^2\,\pi^2 \cos\left(\frac{1}{2}\%1\right)^3 + 960\,\beta^3\,\%1^3\,\pi^2\,\lambda^2\,\mu \cos\left(\frac{1}{2}\%1\right)\sin\left(\frac{1}{2}\%1\right)$$

$$- 96\,\beta^3\,\%1^3\,\pi^2\,\lambda^2 \cos\left(\frac{1}{2}\%1\right)\sin\left(\frac{1}{2}\%1\right) + 3264\,\beta^3\,\%1\,\pi^4 \cos\left(\frac{1}{2}\%1\right)\sin\left(\frac{1}{2}\%1\right)$$

$$+ 18\,\beta\,\%1^8\,\lambda^4 - 72\,\beta\,\lambda^4\,\%1^6 \cos\left(\frac{1}{2}\%1\right)^2 + 72 \cos\left(\frac{1}{2}\%1\right)^4 \beta\,\lambda^4\,\%1^6 + 3\,\beta^3\,\%1^8\,\lambda^4$$

$$+ 48\,\beta^3\,\%1^4\,\pi^4 + 9\,\beta^3\,\%1^6\,\lambda^4 + 816\,\beta^3\,\%1^2\,\pi^4 - 24\,\beta^3\,\%1^7\,\lambda^4 \cos\left(\frac{1}{2}\%1\right)\sin\left(\frac{1}{2}\%1\right)$$

$$- 768\,\pi^2\,\beta^3\,\lambda^2\,\%1^2\,\mu + 1536\,\pi^4\,\beta\,\%1^2 - 32\,\beta^2\,\%1^6\,\lambda^2\,\pi^2 - 480\,\%1^4\,\pi^2\,\lambda^2\,\mu\,\beta^2$$

$$- 32\,\%1^6\,\lambda^2\,\pi^2 - 18\,\%1^6\,\lambda^4\,\beta^2 + 48\,\%1^4\,\lambda^2\,\pi^2\,\beta^2 + 384\,\pi^2\,\beta\,\lambda^2\,\%1^4\,\mu - 12\,\beta^2\,\%1^8\,\lambda^4$$

$$- 192\,\beta^2\,\%1^4\,\pi^4 - 1632\,\%1^2\,\pi^4\,\beta^2 + 24\,\%1^7\,\lambda^4 \cos\left(\frac{1}{2}\%1\right)\sin\left(\frac{1}{2}\%1\right) + 288\,\beta\,\%1^4\,\pi^4$$

$$- 1920\,\beta\,\pi^4\,\%1^2 \cos\left(\frac{1}{2}\%1\right)^2 + 8\,\beta^3\,\%1^6\,\lambda^2\,\pi^2 + 48\,\beta\,\%1^6\,\lambda^2\,\pi^2 + 240\,\beta^3\,\%1^4\,\pi^2\,\lambda^2\,\mu$$

$$- 24\,\beta^3\,\%1^4\,\lambda^2\,\pi^2 - 24\,X\,\pi^2\,b^2\,\lambda^2\,\%1^4\,\beta + 64\,\beta^3\,\%1^5\,\lambda^2\,\pi^2 \cos\left(\frac{1}{2}\%1\right)\sin\left(\frac{1}{2}\%1\right)$$

$$- 128\,X\,\pi^2\,b^2\,\lambda^2\,\%1^2\,\beta + 160\,X\,\pi^2\,b^2\,\lambda^2\,\%1^2\,\beta \cos\left(\frac{1}{2}\%1\right)^2$$

$$- 32 \cos\left(\frac{1}{2}\%1\right)^4 X\,\pi^2\,b^2\,\lambda^2\,\%1^2\,\beta + 960\,\beta^3\,\pi^2\,\lambda^2\,\%1^2\,\mu \cos\left(\frac{1}{2}\%1\right)^2$$

$$- 192\,\pi^2\,\beta^3\,\lambda^2\,\%1^2\,\mu \cos\left(\frac{1}{2}\%1\right)^4 - 768 \cos\left(\frac{1}{2}\%1\right)^2 \pi^2\,\beta\,\lambda^2\,\%1^4\,\mu$$

$$+ 384\,\pi^2\,\beta\,\lambda^2\,\%1^4\,\mu \cos\left(\frac{1}{2}\%1\right)^4 - 256\,\beta^3\,\%1^5\,\lambda^2\,\pi^2\,\mu \cos\left(\frac{1}{2}\%1\right)\sin\left(\frac{1}{2}\%1\right)$$

$$+ 256\,\beta^3\,\%1^5\,\lambda^2\,\pi^2\,\mu \cos\left(\frac{1}{2}\%1\right)^3 \sin\left(\frac{1}{2}\%1\right) - 192 \cos\left(\frac{1}{2}\%1\right)^4 \beta\,\lambda^2\,\pi^2\,\%1^4$$

$$- 96\,\beta^3\,\pi^2\,\lambda^2\,\%1^2 \cos\left(\frac{1}{2}\%1\right)^2 + 96 \cos\left(\frac{1}{2}\%1\right)^4 \beta^3\,\pi^2\,\lambda^2\,\%1^2$$

$$+ 192\,\beta\,\lambda^2\,\pi^2\,\%1^4 \cos\left(\frac{1}{2}\%1\right)^2 - 72\,\beta\,\%1^7\,\lambda^4 \cos\left(\frac{1}{2}\%1\right)\sin\left(\frac{1}{2}\%1\right) + 48\,X\,\pi^2\,b^2\,\lambda^2\,\%1^4$$

$$- 3264\,\%1\,\pi^4\,\beta^2 \cos\left(\frac{1}{2}\%1\right)\sin\left(\frac{1}{2}\%1\right) - 160\,X\,\pi^2\,b^2\,\lambda^2\,\%1^3 \cos\left(\frac{1}{2}\%1\right)\sin\left(\frac{1}{2}\%1\right)$$

$$+ 640\,\%1^3\,\pi^4\cos\left(\frac{1}{2}\%1\right)\sin\left(\frac{1}{2}\%1\right) + 384\,\pi^4\,\beta\,\%1^2\cos\left(\frac{1}{2}\%1\right)^4$$

$$- 256\,\%1^5\,\lambda^2\,\pi^2\,\mu\cos\left(\frac{1}{2}\%1\right)^3\sin\left(\frac{1}{2}\%1\right) + 256\,\%1^5\,\lambda^2\,\pi^2\,\mu\cos\left(\frac{1}{2}\%1\right)\sin\left(\frac{1}{2}\%1\right)$$

$$- 640\,\beta^3\,\%1^3\,\pi^4\cos\left(\frac{1}{2}\%1\right)\sin\left(\frac{1}{2}\%1\right) + 192\,\beta\,\%1^5\,\lambda^2\,\pi^2\cos\left(\frac{1}{2}\%1\right)\sin\left(\frac{1}{2}\%1\right)$$

$$+ 1920\,\beta^2\,\%1^3\,\pi^4\cos\left(\frac{1}{2}\%1\right)\sin\left(\frac{1}{2}\%1\right) - 3072\,\pi^4\,\beta^3 - 192\,\%1^4\,\pi^4 - 12\,\%1^8\,\lambda^4$$

$$+ 36\,\beta^3\,\%1^5\,\lambda^4\cos\left(\frac{1}{2}\%1\right)\sin\left(\frac{1}{2}\%1\right)\Big)\Big/\left(b^2\,\%1^4\,\lambda^3\right)$$

$$\%1 := \arccos\left(\frac{1}{2}\frac{\mu}{-1+\mu}\right)$$

> Z4:=solve(U, X);

$$Z4 := -\Big(72\,\beta^2\,\%1^7\,\lambda^4\cos\left(\frac{1}{2}\%1\right)\sin\left(\frac{1}{2}\%1\right) - 384\,\%1^4\,\lambda^2\,\pi^2\,\beta^2\cos\left(\frac{1}{2}\%1\right)^2$$

$$- 1920\,\beta\,\%1^3\,\pi^4\cos\left(\frac{1}{2}\%1\right)\sin\left(\frac{1}{2}\%1\right) - 768\,\beta^3\,\%1^4\,\lambda^2\,\pi^2\,\mu\cos\left(\frac{1}{2}\%1\right)^2$$

$$- 1920\,\beta^3\,\%1^2\,\pi^4\cos\left(\frac{1}{2}\%1\right)^2 + 144\,\%1^6\,\lambda^4\,\beta^2\cos\left(\frac{1}{2}\%1\right)^2$$

$$+ 3840\,\%1^2\,\pi^4\,\beta^2\cos\left(\frac{1}{2}\%1\right)^2 - 72\,\beta^3\,\%1^6\,\lambda^4\cos\left(\frac{1}{2}\%1\right)^2 + 384\,\beta^3\,\%1^2\,\pi^4\cos\left(\frac{1}{2}\%1\right)^4$$

$$- 768\,\%1^2\,\pi^4\,\beta^2\cos\left(\frac{1}{2}\%1\right)^4 + 72\,\beta^3\,\%1^6\,\lambda^4\cos\left(\frac{1}{2}\%1\right)^4$$

$$+ 384\,\%1^4\,\lambda^2\,\pi^2\,\beta^2\cos\left(\frac{1}{2}\%1\right)^4 - 144\,\%1^6\,\lambda^4\,\beta^2\cos\left(\frac{1}{2}\%1\right)^4$$

$$- 48\sin\left(\frac{1}{2}\%1\right)\%1^7\,\lambda^4\cos\left(\frac{1}{2}\%1\right)^3 + 384\sin\left(\frac{1}{2}\%1\right)\%1^3\,\pi^2\,\lambda^2\,\mu\,\beta^2\cos\left(\frac{1}{2}\%1\right)^3$$

$$+ 384\,\beta^3\,\%1^4\,\pi^2\,\lambda^2\,\mu\cos\left(\frac{1}{2}\%1\right)^4 - 192\,\beta^3\,\%1^4\,\lambda^2\,\pi^2\cos\left(\frac{1}{2}\%1\right)^4$$

$$+ 768\,\beta^2\,\%1^5\,\lambda^2\,\pi^2\,\mu\cos\left(\frac{1}{2}\%1\right)\sin\left(\frac{1}{2}\%1\right)$$

$$
\begin{aligned}
&- 768\,\beta^2\,\%1^5\,\lambda^2\,\pi^2\,\mu\cos\left(\frac{1}{2}\%1\right)^3\sin\left(\frac{1}{2}\%1\right) + 48\,\beta^3\sin\left(\frac{1}{2}\%1\right)\%1^7\,\lambda^4\cos\left(\frac{1}{2}\%1\right)^3 \\
&- 128\,\beta^3\sin\left(\frac{1}{2}\%1\right)\%1^5\,\lambda^2\,\pi^2\cos\left(\frac{1}{2}\%1\right)^3 - 256\sin\left(\frac{1}{2}\%1\right)\%1^3\,\pi^4\cos\left(\frac{1}{2}\%1\right)^3 \\
&+ 256\,\beta^3\sin\left(\frac{1}{2}\%1\right)\%1^3\,\pi^4\cos\left(\frac{1}{2}\%1\right)^3 + 384\sin\left(\frac{1}{2}\%1\right)\%1\,\pi^4\,\beta^2\cos\left(\frac{1}{2}\%1\right)^3 \\
&- 768\,\%1^4\,\pi^2\,\lambda^2\,\mu\,\beta^2\cos\left(\frac{1}{2}\%1\right)^4 - 72\,\beta^3\sin\left(\frac{1}{2}\%1\right)\%1^5\,\lambda^4\cos\left(\frac{1}{2}\%1\right)^3 \\
&+ 768\,\beta\sin\left(\frac{1}{2}\%1\right)\%1^3\,\pi^4\cos\left(\frac{1}{2}\%1\right)^3 - 384\,\beta\sin\left(\frac{1}{2}\%1\right)\%1^5\,\lambda^2\,\pi^2\cos\left(\frac{1}{2}\%1\right)^3 \\
&- 384\,\beta^3\sin\left(\frac{1}{2}\%1\right)\%1^3\,\pi^2\,\lambda^2\,\mu\cos\left(\frac{1}{2}\%1\right)^3 - 144\,\beta^2\sin\left(\frac{1}{2}\%1\right)\%1^7\,\lambda^4\cos\left(\frac{1}{2}\%1\right)^3 \\
&+ 72\sin\left(\frac{1}{2}\%1\right)\%1^5\,\lambda^4\,\beta^2\cos\left(\frac{1}{2}\%1\right)^3 - 192\sin\left(\frac{1}{2}\%1\right)\%1^3\,\pi^2\,\lambda^2\,\beta^2\cos\left(\frac{1}{2}\%1\right)^3 \\
&- 960\,\%1^3\,\pi^2\,\lambda^2\,\mu\,\beta^2\cos\left(\frac{1}{2}\%1\right)\sin\left(\frac{1}{2}\%1\right) - 64\,\%1^5\,\lambda^2\,\pi^2\cos\left(\frac{1}{2}\%1\right)\sin\left(\frac{1}{2}\%1\right) \\
&+ 192\,\beta^3\,\%1^4\,\lambda^2\,\pi^2\cos\left(\frac{1}{2}\%1\right)^2 + 1536\,\%1^4\,\lambda^2\,\pi^2\,\mu\,\beta^2\cos\left(\frac{1}{2}\%1\right)^2 \\
&- 192\,\beta^2\,\%1^5\,\lambda^2\,\pi^2\cos\left(\frac{1}{2}\%1\right)\sin\left(\frac{1}{2}\%1\right) + 96\,\%1^3\,\pi^2\,\lambda^2\,\beta^2\cos\left(\frac{1}{2}\%1\right)\sin\left(\frac{1}{2}\%1\right) \\
&+ 3264\,\beta^3\,\pi^4\cos\left(\frac{1}{2}\%1\right)^2 - 192\,\pi^4\,\beta^3\cos\left(\frac{1}{2}\%1\right)^4 \\
&- 768\,\beta\,\%1^5\,\lambda^2\,\pi^2\,\mu\cos\left(\frac{1}{2}\%1\right)\sin\left(\frac{1}{2}\%1\right) + 768\,\beta\,\%1^5\,\lambda^2\,\pi^2\,\mu\cos\left(\frac{1}{2}\%1\right)^3\sin\left(\frac{1}{2}\%1\right) \\
&- 36\,\%1^5\,\lambda^4\,\beta^2\cos\left(\frac{1}{2}\%1\right)\sin\left(\frac{1}{2}\%1\right) + 144\,\beta\sin\left(\frac{1}{2}\%1\right)\%1^7\,\lambda^4\cos\left(\frac{1}{2}\%1\right)^3 \\
&+ 36\,\beta^3\,\lambda^4\,\%1^4\cos\left(\frac{1}{2}\%1\right)^2 - 36\cos\left(\frac{1}{2}\%1\right)^4\beta^3\,\lambda^4\,\%1^4 \\
&- 384\,\beta^3\sin\left(\frac{1}{2}\%1\right)\%1\,\pi^4\cos\left(\frac{1}{2}\%1\right)^3 + 192\,\beta^3\sin\left(\frac{1}{2}\%1\right)\%1^3\,\pi^2\,\lambda^2\cos\left(\frac{1}{2}\%1\right)^3 \\
&+ 128\sin\left(\frac{1}{2}\%1\right)\%1^5\,\lambda^2\,\pi^2\cos\left(\frac{1}{2}\%1\right)^3 - 768\,\beta^2\sin\left(\frac{1}{2}\%1\right)\%1^3\,\pi^4\cos\left(\frac{1}{2}\%1\right)^3
\end{aligned}
$$

$$+ 384\,\beta^2 \sin\left(\frac{1}{2}\%1\right)\%1^5\,\lambda^2\,\pi^2 \cos\left(\frac{1}{2}\%1\right)^3 + 960\,\beta^3\,\%1^3\,\pi^2\,\lambda^2\,\mu \cos\left(\frac{1}{2}\%1\right)\sin\left(\frac{1}{2}\%1\right)$$

$$- 96\,\beta^3\,\%1^3\,\pi^2\,\lambda^2 \cos\left(\frac{1}{2}\%1\right)\sin\left(\frac{1}{2}\%1\right) + 3264\,\beta^3\,\%1\,\pi^4 \cos\left(\frac{1}{2}\%1\right)\sin\left(\frac{1}{2}\%1\right)$$

$$+ 18\,\beta\,\%1^8\,\lambda^4 - 72\,\beta\,\lambda^4\,\%1^6 \cos\left(\frac{1}{2}\%1\right)^2 + 72 \cos\left(\frac{1}{2}\%1\right)^4 \beta\,\lambda^4\,\%1^6 + 3\,\beta^3\,\%1^8\,\lambda^4$$

$$+ 48\,\beta^3\,\%1^4\,\pi^4 + 9\,\beta^3\,\%1^6\,\lambda^4 + 816\,\beta^3\,\%1^2\,\pi^4 - 24\,\beta^3\,\%1^7\,\lambda^4 \cos\left(\frac{1}{2}\%1\right)\sin\left(\frac{1}{2}\%1\right)$$

$$- 768\,\pi^2\,\beta^3\,\lambda^2\,\%1^2\,\mu + 1536\,\pi^4\,\beta\,\%1^2 - 32\,\beta^2\,\%1^6\,\lambda^2\,\pi^2 - 480\,\%1^4\,\pi^2\,\lambda^2\,\mu\,\beta^2$$

$$- 32\,\%1^6\,\lambda^2\,\pi^2 - 18\,\%1^6\,\lambda^4\,\beta^2 + 48\,\%1^4\,\lambda^2\,\pi^2\,\beta^2 + 384\,\pi^2\,\beta\,\lambda^2\,\%1^4\,\mu - 12\,\beta^2\,\%1^8\,\lambda^4$$

$$- 192\,\beta^2\,\%1^4\,\pi^4 - 1632\,\%1^2\,\pi^4\,\beta^2 + 24\,\%1^7\,\lambda^4 \cos\left(\frac{1}{2}\%1\right)\sin\left(\frac{1}{2}\%1\right) + 288\,\beta\,\%1^4\,\pi^4$$

$$- 1920\,\beta\,\pi^4\,\%1^2 \cos\left(\frac{1}{2}\%1\right)^2 + 8\,\beta^3\,\%1^6\,\lambda^2\,\pi^2 + 48\,\beta\,\%1^6\,\lambda^2\,\pi^2 + 240\,\beta^3\,\%1^4\,\pi^2\,\lambda^2\,\mu$$

$$- 24\,\beta^3\,\%1^4\,\lambda^2\,\pi^2 + 64\,\beta^3\,\%1^5\,\lambda^2\,\pi^2 \cos\left(\frac{1}{2}\%1\right)\sin\left(\frac{1}{2}\%1\right)$$

$$+ 960\,\beta^3\,\pi^2\,\lambda^2\,\%1^2\,\mu \cos\left(\frac{1}{2}\%1\right)^2 - 192\,\pi^2\,\beta^3\,\lambda^2\,\%1^2\,\mu \cos\left(\frac{1}{2}\%1\right)^4$$

$$- 768 \cos\left(\frac{1}{2}\%1\right)^2 \pi^2\,\beta\,\lambda^2\,\%1^4\,\mu + 384\,\pi^2\,\beta\,\lambda^2\,\%1^4\,\mu \cos\left(\frac{1}{2}\%1\right)^4$$

$$- 256\,\beta^3\,\%1^5\,\lambda^2\,\pi^2\,\mu \cos\left(\frac{1}{2}\%1\right)\sin\left(\frac{1}{2}\%1\right)$$

$$+ 256\,\beta^3\,\%1^5\,\lambda^2\,\pi^2\,\mu \cos\left(\frac{1}{2}\%1\right)^3 \sin\left(\frac{1}{2}\%1\right) - 192 \cos\left(\frac{1}{2}\%1\right)^4 \beta\,\lambda^2\,\pi^2\,\%1^4$$

$$- 96\,\beta^3\,\pi^2\,\lambda^2\,\%1^2 \cos\left(\frac{1}{2}\%1\right)^2 + 96 \cos\left(\frac{1}{2}\%1\right)^4 \beta^3\,\pi^2\,\lambda^2\,\%1^2$$

$$+ 192\,\beta\,\lambda^2\,\pi^2\,\%1^4 \cos\left(\frac{1}{2}\%1\right)^2 - 72\,\beta\,\%1^7\,\lambda^4 \cos\left(\frac{1}{2}\%1\right)\sin\left(\frac{1}{2}\%1\right)$$

$$- 3264\,\%1\,\pi^4\,\beta^2 \cos\left(\frac{1}{2}\%1\right)\sin\left(\frac{1}{2}\%1\right) + 640\,\%1^3\,\pi^4 \cos\left(\frac{1}{2}\%1\right)\sin\left(\frac{1}{2}\%1\right)$$

$$+ 384\,\pi^4\,\beta\,\%1^2 \cos\left(\frac{1}{2}\%1\right)^4 - 256\,\%1^5\,\lambda^2\,\pi^2\,\mu \cos\left(\frac{1}{2}\%1\right)^3 \sin\left(\frac{1}{2}\%1\right)$$

$$+ 256\,\%1^5\,\lambda^2\,\pi^2\,\mu\cos\left(\frac{1}{2}\%1\right)\sin\left(\frac{1}{2}\%1\right) - 640\,\beta^3\,\%1^3\,\pi^4\cos\left(\frac{1}{2}\%1\right)\sin\left(\frac{1}{2}\%1\right)$$

$$+ 192\,\beta\,\%1^5\,\lambda^2\,\pi^2\cos\left(\frac{1}{2}\%1\right)\sin\left(\frac{1}{2}\%1\right) + 1920\,\beta^2\,\%1^3\,\pi^4\cos\left(\frac{1}{2}\%1\right)\sin\left(\frac{1}{2}\%1\right)$$

$$- 3072\,\pi^4\,\beta^3 - 192\,\%1^4\,\pi^4 - 12\,\%1^8\,\lambda^4 + 36\,\beta^3\,\%1^5\,\lambda^4\cos\left(\frac{1}{2}\%1\right)\sin\left(\frac{1}{2}\%1\right)\Bigg)\Bigg/\Bigg($$

$$160\,\pi^2\,b^2\,\lambda^2\,\%1^3\,\beta\cos\left(\frac{1}{2}\%1\right)\sin\left(\frac{1}{2}\%1\right) - 64\,\pi^2\,b^2\,\lambda^2\,\%1^3\,\beta\sin\left(\frac{1}{2}\%1\right)\cos\left(\frac{1}{2}\%1\right)^3$$

$$+ 64\,\pi^2\,b^2\,\lambda^2\,\%1^3\sin\left(\frac{1}{2}\%1\right)\cos\left(\frac{1}{2}\%1\right)^3 - 24\,\pi^2\,b^2\,\lambda^2\,\%1^4\,\beta - 128\,\pi^2\,b^2\,\lambda^2\,\%1^2\,\beta$$

$$+ 160\,\pi^2\,b^2\,\lambda^2\,\%1^2\,\beta\cos\left(\frac{1}{2}\%1\right)^2 - 32\cos\left(\frac{1}{2}\%1\right)^4\pi^2\,b^2\,\lambda^2\,\%1^2\,\beta + 48\,\pi^2\,b^2\,\lambda^2\,\%1^4$$

$$- 160\,\pi^2\,b^2\,\lambda^2\,\%1^3\cos\left(\frac{1}{2}\%1\right)\sin\left(\frac{1}{2}\%1\right)\Bigg)$$

$$\%1 := \arccos\left(\frac{1}{2}\,\frac{\mu}{-1+\mu}\right)$$

> X1:=simplify(Z4);

$$X1 := \frac{1}{8}\Bigg(72\,\beta^2\,\%1^7\,\lambda^4\cos\left(\frac{1}{2}\%1\right)\sin\left(\frac{1}{2}\%1\right) - 384\,\%1^4\,\lambda^2\,\pi^2\,\beta^2\cos\left(\frac{1}{2}\%1\right)^2$$

$$- 1920\,\beta\,\%1^3\,\pi^4\cos\left(\frac{1}{2}\%1\right)\sin\left(\frac{1}{2}\%1\right) - 768\,\beta^3\,\%1^4\,\lambda^2\,\pi^2\,\mu\cos\left(\frac{1}{2}\%1\right)^2$$

$$- 1920\,\beta^3\,\%1^2\,\pi^4\cos\left(\frac{1}{2}\%1\right)^2 + 144\,\%1^6\,\lambda^4\,\beta^2\cos\left(\frac{1}{2}\%1\right)^2$$

$$+ 3840\,\%1^2\,\pi^4\,\beta^2\cos\left(\frac{1}{2}\%1\right)^2 - 72\,\beta^3\,\%1^6\,\lambda^4\cos\left(\frac{1}{2}\%1\right)^2 + 384\,\beta^3\,\%1^2\,\pi^4\cos\left(\frac{1}{2}\%1\right)^4$$

$$- 768\,\%1^2\,\pi^4\,\beta^2\cos\left(\frac{1}{2}\%1\right)^4 + 72\,\beta^3\,\%1^6\,\lambda^4\cos\left(\frac{1}{2}\%1\right)^4$$

$$+ 384\,\%1^4\,\lambda^2\,\pi^2\,\beta^2\cos\left(\frac{1}{2}\%1\right)^4 - 144\,\%1^6\,\lambda^4\,\beta^2\cos\left(\frac{1}{2}\%1\right)^4$$

$$- 48\sin\left(\frac{1}{2}\%1\right)\%1^7\,\lambda^4\cos\left(\frac{1}{2}\%1\right)^3 + 384\sin\left(\frac{1}{2}\%1\right)\%1^3\,\pi^2\,\lambda^2\,\mu\,\beta^2\cos\left(\frac{1}{2}\%1\right)^3$$

$$+ 384\,\beta^3\,\%1^4\,\pi^2\,\lambda^2\,\mu\cos\left(\frac{1}{2}\%1\right)^4 - 192\,\beta^3\,\%1^4\,\lambda^2\,\pi^2\cos\left(\frac{1}{2}\%1\right)^4$$

$$+ 768\,\beta^2\,\%1^5\,\lambda^2\,\pi^2\,\mu\cos\left(\frac{1}{2}\%1\right)\sin\left(\frac{1}{2}\%1\right)$$

$$- 768\,\beta^2\,\%1^5\,\lambda^2\,\pi^2\,\mu\cos\left(\frac{1}{2}\%1\right)^3\sin\left(\frac{1}{2}\%1\right) + 48\,\beta^3\sin\left(\frac{1}{2}\%1\right)\%1^7\,\lambda^4\cos\left(\frac{1}{2}\%1\right)^3$$

$$- 128\,\beta^3\sin\left(\frac{1}{2}\%1\right)\%1^5\,\lambda^2\,\pi^2\cos\left(\frac{1}{2}\%1\right)^3 - 256\sin\left(\frac{1}{2}\%1\right)\%1^3\,\pi^4\cos\left(\frac{1}{2}\%1\right)^3$$

$$+ 256\,\beta^3\sin\left(\frac{1}{2}\%1\right)\%1^3\,\pi^4\cos\left(\frac{1}{2}\%1\right)^3 + 384\sin\left(\frac{1}{2}\%1\right)\%1\,\pi^4\,\beta^2\cos\left(\frac{1}{2}\%1\right)^3$$

$$- 768\,\%1^4\,\pi^2\,\lambda^2\,\mu\,\beta^2\cos\left(\frac{1}{2}\%1\right)^4 - 72\,\beta^3\sin\left(\frac{1}{2}\%1\right)\%1^5\,\lambda^4\cos\left(\frac{1}{2}\%1\right)^3$$

$$+ 768\,\beta\sin\left(\frac{1}{2}\%1\right)\%1^3\,\pi^4\cos\left(\frac{1}{2}\%1\right)^3 - 384\,\beta\sin\left(\frac{1}{2}\%1\right)\%1^5\,\lambda^2\,\pi^2\cos\left(\frac{1}{2}\%1\right)^3$$

$$- 384\,\beta^3\sin\left(\frac{1}{2}\%1\right)\%1^3\,\pi^2\,\lambda^2\,\mu\cos\left(\frac{1}{2}\%1\right)^3 - 144\,\beta^2\sin\left(\frac{1}{2}\%1\right)\%1^7\,\lambda^4\cos\left(\frac{1}{2}\%1\right)^3$$

$$+ 72\sin\left(\frac{1}{2}\%1\right)\%1^5\,\lambda^4\,\beta^2\cos\left(\frac{1}{2}\%1\right)^3 - 192\sin\left(\frac{1}{2}\%1\right)\%1^3\,\pi^2\,\lambda^2\,\beta^2\cos\left(\frac{1}{2}\%1\right)^3$$

$$- 960\,\%1^3\,\pi^2\,\lambda^2\,\mu\,\beta^2\cos\left(\frac{1}{2}\%1\right)\sin\left(\frac{1}{2}\%1\right) - 64\,\%1^5\,\lambda^2\,\pi^2\cos\left(\frac{1}{2}\%1\right)\sin\left(\frac{1}{2}\%1\right)$$

$$+ 192\,\beta^3\,\%1^4\,\lambda^2\,\pi^2\cos\left(\frac{1}{2}\%1\right)^2 + 1536\,\%1^4\,\lambda^2\,\pi^2\,\mu\,\beta^2\cos\left(\frac{1}{2}\%1\right)^2$$

$$- 192\,\beta^2\,\%1^5\,\lambda^2\,\pi^2\cos\left(\frac{1}{2}\%1\right)\sin\left(\frac{1}{2}\%1\right) + 96\,\%1^3\,\pi^2\,\lambda^2\,\beta^2\cos\left(\frac{1}{2}\%1\right)\sin\left(\frac{1}{2}\%1\right)$$

$$+ 3264\,\beta^3\,\pi^4\cos\left(\frac{1}{2}\%1\right)^2 - 192\,\pi^4\,\beta^3\cos\left(\frac{1}{2}\%1\right)^4$$

$$- 768\,\beta\,\%1^5\,\lambda^2\,\pi^2\,\mu\cos\left(\frac{1}{2}\%1\right)\sin\left(\frac{1}{2}\%1\right) + 768\,\beta\,\%1^5\,\lambda^2\,\pi^2\,\mu\cos\left(\frac{1}{2}\%1\right)^3\sin\left(\frac{1}{2}\%1\right)$$

$$- 36\,\%1^5\,\lambda^4\,\beta^2\cos\left(\frac{1}{2}\%1\right)\sin\left(\frac{1}{2}\%1\right) + 144\,\beta\sin\left(\frac{1}{2}\%1\right)\%1^7\,\lambda^4\cos\left(\frac{1}{2}\%1\right)^3$$

$$+ 36\,\beta^3\,\lambda^4\,\%1^4\cos\left(\frac{1}{2}\%1\right)^2 - 36\cos\left(\frac{1}{2}\%1\right)^4\beta^3\,\lambda^4\,\%1^4$$

$$
\begin{aligned}
&- 384\,\beta^3 \sin\left(\frac{1}{2}\%1\right)\%1\,\pi^4 \cos\left(\frac{1}{2}\%1\right)^3 + 192\,\beta^3 \sin\left(\frac{1}{2}\%1\right)\%1^3\,\pi^2\,\lambda^2 \cos\left(\frac{1}{2}\%1\right)^3 \\
&+ 128 \sin\left(\frac{1}{2}\%1\right)\%1^5\,\lambda^2\,\pi^2 \cos\left(\frac{1}{2}\%1\right)^3 - 768\,\beta^2 \sin\left(\frac{1}{2}\%1\right)\%1^3\,\pi^4 \cos\left(\frac{1}{2}\%1\right)^3 \\
&+ 384\,\beta^2 \sin\left(\frac{1}{2}\%1\right)\%1^5\,\lambda^2\,\pi^2 \cos\left(\frac{1}{2}\%1\right)^3 + 960\,\beta^3\,\%1^3\,\pi^2\,\lambda^2\,\mu \cos\left(\frac{1}{2}\%1\right)\sin\left(\frac{1}{2}\%1\right) \\
&- 96\,\beta^3\,\%1^3\,\pi^2\,\lambda^2 \cos\left(\frac{1}{2}\%1\right)\sin\left(\frac{1}{2}\%1\right) + 3264\,\beta^3\,\%1\,\pi^4 \cos\left(\frac{1}{2}\%1\right)\sin\left(\frac{1}{2}\%1\right) \\
&+ 18\,\beta\,\%1^8\,\lambda^4 - 72\,\beta\,\lambda^4\,\%1^6 \cos\left(\frac{1}{2}\%1\right)^2 + 72 \cos\left(\frac{1}{2}\%1\right)^4 \beta\,\lambda^4\,\%1^6 + 3\,\beta^3\,\%1^8\,\lambda^4 \\
&+ 48\,\beta^3\,\%1^4\,\pi^4 + 9\,\beta^3\,\%1^6\,\lambda^4 + 816\,\beta^3\,\%1^2\,\pi^4 - 24\,\beta^3\,\%1^7\,\lambda^4 \cos\left(\frac{1}{2}\%1\right)\sin\left(\frac{1}{2}\%1\right) \\
&- 768\,\pi^2\,\beta^3\,\lambda^2\,\%1^2\,\mu + 1536\,\pi^4\,\beta\,\%1^2 - 32\,\beta^2\,\%1^6\,\lambda^2\,\pi^2 - 480\,\%1^4\,\pi^2\,\lambda^2\,\mu\,\beta^2 \\
&- 32\,\%1^6\,\lambda^2\,\pi^2 - 18\,\%1^6\,\lambda^4\,\beta^2 + 48\,\%1^4\,\lambda^2\,\pi^2\,\beta^2 + 384\,\pi^2\,\beta\,\lambda^2\,\%1^4\,\mu - 12\,\beta^2\,\%1^8\,\lambda^4 \\
&- 192\,\beta^2\,\%1^4\,\pi^4 - 1632\,\%1^2\,\pi^4\,\beta^2 + 24\,\%1^7\,\lambda^4 \cos\left(\frac{1}{2}\%1\right)\sin\left(\frac{1}{2}\%1\right) + 288\,\beta\,\%1^4\,\pi^4 \\
&- 1920\,\beta\,\pi^4\,\%1^2 \cos\left(\frac{1}{2}\%1\right)^2 + 8\,\beta^3\,\%1^6\,\lambda^2\,\pi^2 + 48\,\beta\,\%1^6\,\lambda^2\,\pi^2 + 240\,\beta^3\,\%1^4\,\pi^2\,\lambda^2\,\mu \\
&- 24\,\beta^3\,\%1^4\,\lambda^2\,\pi^2 + 64\,\beta^3\,\%1^5\,\lambda^2\,\pi^2 \cos\left(\frac{1}{2}\%1\right)\sin\left(\frac{1}{2}\%1\right) \\
&+ 960\,\beta^3\,\pi^2\,\lambda^2\,\%1^2\,\mu \cos\left(\frac{1}{2}\%1\right)^2 - 192\,\pi^2\,\beta^3\,\lambda^2\,\%1^2\,\mu \cos\left(\frac{1}{2}\%1\right)^4 \\
&- 768 \cos\left(\frac{1}{2}\%1\right)^2 \pi^2\,\beta\,\lambda^2\,\%1^4\,\mu + 384\,\pi^2\,\beta\,\lambda^2\,\%1^4\,\mu \cos\left(\frac{1}{2}\%1\right)^4 \\
&- 256\,\beta^3\,\%1^5\,\lambda^2\,\pi^2\,\mu \cos\left(\frac{1}{2}\%1\right)\sin\left(\frac{1}{2}\%1\right) \\
&+ 256\,\beta^3\,\%1^5\,\lambda^2\,\pi^2\,\mu \cos\left(\frac{1}{2}\%1\right)^3 \sin\left(\frac{1}{2}\%1\right) - 192 \cos\left(\frac{1}{2}\%1\right)^4 \beta\,\lambda^2\,\pi^2\,\%1^4 \\
&- 96\,\beta^3\,\pi^2\,\lambda^2\,\%1^2 \cos\left(\frac{1}{2}\%1\right)^2 + 96 \cos\left(\frac{1}{2}\%1\right)^4 \beta^3\,\pi^2\,\lambda^2\,\%1^2 \\
&+ 192\,\beta\,\lambda^2\,\pi^2\,\%1^4 \cos\left(\frac{1}{2}\%1\right)^2 - 72\,\beta\,\%1^7\,\lambda^4 \cos\left(\frac{1}{2}\%1\right)\sin\left(\frac{1}{2}\%1\right)
\end{aligned}
$$

$$- 3264\,\%1\,\pi^4\,\beta^2\cos\left(\frac{1}{2}\%1\right)\sin\left(\frac{1}{2}\%1\right) + 640\,\%1^3\,\pi^4\cos\left(\frac{1}{2}\%1\right)\sin\left(\frac{1}{2}\%1\right)$$

$$+ 384\,\pi^4\,\beta\,\%1^2\cos\left(\frac{1}{2}\%1\right)^4 - 256\,\%1^5\,\lambda^2\,\pi^2\,\mu\cos\left(\frac{1}{2}\%1\right)^3\sin\left(\frac{1}{2}\%1\right)$$

$$+ 256\,\%1^5\,\lambda^2\,\pi^2\,\mu\cos\left(\frac{1}{2}\%1\right)\sin\left(\frac{1}{2}\%1\right) - 640\,\beta^3\,\%1^3\,\pi^4\cos\left(\frac{1}{2}\%1\right)\sin\left(\frac{1}{2}\%1\right)$$

$$+ 192\,\beta\,\%1^5\,\lambda^2\,\pi^2\cos\left(\frac{1}{2}\%1\right)\sin\left(\frac{1}{2}\%1\right) + 1920\,\beta^2\,\%1^3\,\pi^4\cos\left(\frac{1}{2}\%1\right)\sin\left(\frac{1}{2}\%1\right)$$

$$- 3072\,\pi^4\,\beta^3 - 192\,\%1^4\,\pi^4 - 12\,\%1^8\,\lambda^4 + 36\,\beta^3\,\%1^5\,\lambda^4\cos\left(\frac{1}{2}\%1\right)\sin\left(\frac{1}{2}\%1\right)\Bigg)\Bigg/\Bigg(\pi^2\,b^2$$

$$\lambda^2\,\%1^2\Bigg(-20\,\%1\,\beta\cos\left(\frac{1}{2}\%1\right)\sin\left(\frac{1}{2}\%1\right) + 8\,\%1\,\beta\sin\left(\frac{1}{2}\%1\right)\cos\left(\frac{1}{2}\%1\right)^3$$

$$- 8\,\%1\sin\left(\frac{1}{2}\%1\right)\cos\left(\frac{1}{2}\%1\right)^3 + 3\,\beta\,\%1^2 + 16\,\beta - 20\,\beta\cos\left(\frac{1}{2}\%1\right)^2 + 4\cos\left(\frac{1}{2}\%1\right)^4\beta$$

$$- 6\,\%1^2 + 20\,\%1\cos\left(\frac{1}{2}\%1\right)\sin\left(\frac{1}{2}\%1\right)\Bigg)\Bigg)$$

$$\%1 := \arccos\left(\frac{1}{2}\,\frac{\mu}{-1+\mu}\right)$$

> X2:=collect(X1, [sin(n/2), cos(n/2)], distributed, factor);

$$X2 := \frac{1}{8}\Bigg(12\left(2\,\%1^2 - 4\,\beta\,\%1^2 - \beta^2 + 2\,\beta^2\,\%1^2\right)\beta$$

$$\left(3\,\%1^4\,\lambda^4 + 16\,\lambda^2\,\pi^2\,\%1^2\,\mu - 8\,\lambda^2\,\pi^2\,\%1^2 + 16\,\pi^4\right)\cos\left(\frac{1}{2}\%1\right)^4 - 12\,\beta\left(6\,\%1^6\,\lambda^4\,\beta^2\right.$$

$$- 272\,\pi^4\,\beta^2 - 3\,\lambda^4\,\%1^4\,\beta^2 + 160\,\%1^2\,\pi^4\,\beta^2 + 64\,\%1^4\,\pi^2\,\lambda^2\,\mu\,\beta^2 - 16\,\%1^4\,\lambda^2\,\pi^2\,\beta^2$$

$$- 80\,\pi^2\,\lambda^2\,\%1^2\,\mu\,\beta^2 + 8\,\lambda^2\,\pi^2\,\%1^2\,\beta^2 + 32\,\beta\,\lambda^2\,\pi^2\,\%1^4 - 320\,\pi^4\,\beta\,\%1^2$$

$$- 128\,\pi^2\,\beta\,\lambda^2\,\%1^4\,\mu - 12\,\beta\,\lambda^4\,\%1^6 + 64\,\lambda^2\,\pi^2\,\%1^4\,\mu - 16\,\lambda^2\,\pi^2\,\%1^4 + 160\,\pi^4\,\%1^2$$

$$\left.+ 6\,\lambda^4\,\%1^6\right)\cos\left(\frac{1}{2}\%1\right)^2 - 4\,(-1+\beta)\,\%1\left(6\,\%1^6\,\lambda^4\,\beta^2 - 16\,\%1^4\,\lambda^2\,\pi^2\,\beta^2\right.$$

$$+ 64\,\%1^4\,\pi^2\,\lambda^2\,\mu\,\beta^2 - 9\,\lambda^4\,\%1^4\,\beta^2 + 160\,\%1^2\,\pi^4\,\beta^2 - 240\,\pi^2\,\lambda^2\,\%1^2\,\mu\,\beta^2$$

$$+ 24\,\lambda^2\,\pi^2\,\%1^2\,\beta^2 - 816\,\pi^4\,\beta^2 + 32\,\beta\,\lambda^2\,\pi^2\,\%1^4 - 320\,\pi^4\,\beta\,\%1^2 - 128\,\pi^2\,\beta\,\lambda^2\,\%1^4\,\mu$$

$$- 12\,\beta\,\lambda^4\,\%1^6 + 64\,\lambda^2\,\pi^2\,\%1^4\,\mu - 16\,\lambda^2\,\pi^2\,\%1^4 + 160\,\pi^4\,\%1^2 + 6\,\lambda^4\,\%1^6\Big)\sin\left(\frac{1}{2}\,\%1\right)$$

$$\cos\left(\frac{1}{2}\,\%1\right) + 8\,(-1+\beta)\,\%1\left(-3\,\beta^2 + 2\,\beta^2\,\%1^2 - 4\,\beta\,\%1^2 + 2\,\%1^2\right)$$

$$\left(3\,\%1^4\,\lambda^4 + 16\,\lambda^2\,\pi^2\,\%1^2\,\mu - 8\,\lambda^2\,\pi^2\,\%1^2 + 16\,\pi^4\right)\sin\left(\frac{1}{2}\,\%1\right)\cos\left(\frac{1}{2}\,\%1\right)^3$$

$$+ 18\,\beta\,\%1^8\,\lambda^4 + 3\,\beta^3\,\%1^8\,\lambda^4 + 48\,\beta^3\,\%1^4\,\pi^4 + 9\,\beta^3\,\%1^6\,\lambda^4 + 816\,\beta^3\,\%1^2\,\pi^4$$

$$- 768\,\pi^2\,\beta^3\,\lambda^2\,\%1^2\,\mu + 1536\,\pi^4\,\beta\,\%1^2 - 32\,\beta^2\,\%1^6\,\lambda^2\,\pi^2 - 480\,\%1^4\,\pi^2\,\lambda^2\,\mu\,\beta^2$$

$$- 32\,\%1^6\,\lambda^2\,\pi^2 - 18\,\%1^6\,\lambda^4\,\beta^2 + 48\,\%1^4\,\lambda^2\,\pi^2\,\beta^2 + 384\,\pi^2\,\beta\,\lambda^2\,\%1^4\,\mu - 12\,\beta^2\,\%1^8\,\lambda^4$$

$$- 192\,\beta^2\,\%1^4\,\pi^4 - 1632\,\%1^2\,\pi^4\,\beta^2 + 288\,\beta\,\%1^4\,\pi^4 + 8\,\beta^3\,\%1^6\,\lambda^2\,\pi^2 + 48\,\beta\,\%1^6\,\lambda^2\,\pi^2$$

$$+ 240\,\beta^3\,\%1^4\,\pi^2\,\lambda^2\,\mu - 24\,\beta^3\,\%1^4\,\lambda^2\,\pi^2 - 3072\,\pi^4\,\beta^3 - 192\,\%1^4\,\pi^4 - 12\,\%1^8\,\lambda^4\Big) \Big/ \Big(\pi^2$$

$$b^2\,\lambda^2\,\%1^2\left(16\,\beta + 3\,\beta\,\%1^2 - 6\,\%1^2 + 4\cos\left(\frac{1}{2}\,\%1\right)^4\beta - 20\,\beta\cos\left(\frac{1}{2}\,\%1\right)^2\right.$$

$$\left.- 20\,(-1+\beta)\,\%1\sin\left(\frac{1}{2}\,\%1\right)\cos\left(\frac{1}{2}\,\%1\right) + 8\,(-1+\beta)\,\%1\sin\left(\frac{1}{2}\,\%1\right)\cos\left(\frac{1}{2}\,\%1\right)^3\right)\Big)\Big)\ .$$

$$\%1 := \arccos\left(\frac{1}{2}\,\frac{\mu}{-1+\mu}\right)$$

> K1:=simplify(X2*b^2/Pi^2);

$$K1 := \frac{1}{8}\Big(72\,\beta^2\,\%1^7\,\lambda^4\cos\left(\frac{1}{2}\,\%1\right)\sin\left(\frac{1}{2}\,\%1\right) - 384\,\%1^4\,\lambda^2\,\pi^2\,\beta^2\cos\left(\frac{1}{2}\,\%1\right)^2$$

$$- 1920\,\beta\,\%1^3\,\pi^4\cos\left(\frac{1}{2}\,\%1\right)\sin\left(\frac{1}{2}\,\%1\right) - 768\,\beta^3\,\%1^4\,\lambda^2\,\pi^2\,\mu\cos\left(\frac{1}{2}\,\%1\right)^2$$

$$- 1920\,\beta^3\,\%1^2\,\pi^4\cos\left(\frac{1}{2}\,\%1\right)^2 + 144\,\%1^6\,\lambda^4\,\beta^2\cos\left(\frac{1}{2}\,\%1\right)^2$$

$$+ 3840\,\%1^2\,\pi^4\,\beta^2\cos\left(\frac{1}{2}\,\%1\right)^2 - 72\,\beta^3\,\%1^6\,\lambda^4\cos\left(\frac{1}{2}\,\%1\right)^2 + 384\,\beta^3\,\%1^2\,\pi^4\cos\left(\frac{1}{2}\,\%1\right)^4$$

$$- 768\,\%1^2\,\pi^4\,\beta^2\cos\left(\frac{1}{2}\,\%1\right)^4 + 72\,\beta^3\,\%1^6\,\lambda^4\cos\left(\frac{1}{2}\,\%1\right)^4$$

$$+ 384\,\%1^4\,\lambda^2\,\pi^2\,\beta^2\cos\left(\frac{1}{2}\,\%1\right)^4 - 144\,\%1^6\,\lambda^4\,\beta^2\cos\left(\frac{1}{2}\,\%1\right)^4$$

$$
\begin{aligned}
&- 48 \sin\left(\frac{1}{2}\%1\right)\%1^7\lambda^4\cos\left(\frac{1}{2}\%1\right)^3 + 384\sin\left(\frac{1}{2}\%1\right)\%1^3\pi^2\lambda^2\mu\beta^2\cos\left(\frac{1}{2}\%1\right)^3 \\
&+ 384\beta^3\%1^4\pi^2\lambda^2\mu\cos\left(\frac{1}{2}\%1\right)^4 - 192\beta^3\%1^4\lambda^2\pi^2\cos\left(\frac{1}{2}\%1\right)^4 \\
&+ 768\beta^2\%1^5\lambda^2\pi^2\mu\cos\left(\frac{1}{2}\%1\right)\sin\left(\frac{1}{2}\%1\right) \\
&- 768\beta^2\%1^5\lambda^2\pi^2\mu\cos\left(\frac{1}{2}\%1\right)^3\sin\left(\frac{1}{2}\%1\right) + 48\beta^3\sin\left(\frac{1}{2}\%1\right)\%1^7\lambda^4\cos\left(\frac{1}{2}\%1\right)^3 \\
&- 128\beta^3\sin\left(\frac{1}{2}\%1\right)\%1^5\lambda^2\pi^2\cos\left(\frac{1}{2}\%1\right)^3 - 256\sin\left(\frac{1}{2}\%1\right)\%1^3\pi^4\cos\left(\frac{1}{2}\%1\right)^3 \\
&+ 256\beta^3\sin\left(\frac{1}{2}\%1\right)\%1^3\pi^4\cos\left(\frac{1}{2}\%1\right)^3 + 384\sin\left(\frac{1}{2}\%1\right)\%1\,\pi^4\beta^2\cos\left(\frac{1}{2}\%1\right)^3 \\
&- 768\%1^4\pi^2\lambda^2\mu\beta^2\cos\left(\frac{1}{2}\%1\right)^4 - 72\beta^3\sin\left(\frac{1}{2}\%1\right)\%1^5\lambda^4\cos\left(\frac{1}{2}\%1\right)^3 \\
&+ 768\beta\sin\left(\frac{1}{2}\%1\right)\%1^3\pi^4\cos\left(\frac{1}{2}\%1\right)^3 - 384\beta\sin\left(\frac{1}{2}\%1\right)\%1^5\lambda^2\pi^2\cos\left(\frac{1}{2}\%1\right)^3 \\
&- 384\beta^3\sin\left(\frac{1}{2}\%1\right)\%1^3\pi^2\lambda^2\mu\cos\left(\frac{1}{2}\%1\right)^3 - 144\beta^2\sin\left(\frac{1}{2}\%1\right)\%1^7\lambda^4\cos\left(\frac{1}{2}\%1\right)^3 \\
&+ 72\sin\left(\frac{1}{2}\%1\right)\%1^5\lambda^4\beta^2\cos\left(\frac{1}{2}\%1\right)^3 - 192\sin\left(\frac{1}{2}\%1\right)\%1^3\pi^2\lambda^2\beta^2\cos\left(\frac{1}{2}\%1\right)^3 \\
&- 960\%1^3\pi^2\lambda^2\mu\beta^2\cos\left(\frac{1}{2}\%1\right)\sin\left(\frac{1}{2}\%1\right) - 64\%1^5\lambda^2\pi^2\cos\left(\frac{1}{2}\%1\right)\sin\left(\frac{1}{2}\%1\right) \\
&+ 192\beta^3\%1^4\lambda^2\pi^2\cos\left(\frac{1}{2}\%1\right)^2 + 1536\%1^4\lambda^2\pi^2\mu\beta^2\cos\left(\frac{1}{2}\%1\right)^2 \\
&- 192\beta^2\%1^5\lambda^2\pi^2\cos\left(\frac{1}{2}\%1\right)\sin\left(\frac{1}{2}\%1\right) + 96\%1^3\pi^2\lambda^2\beta^2\cos\left(\frac{1}{2}\%1\right)\sin\left(\frac{1}{2}\%1\right) \\
&+ 3264\beta^3\pi^4\cos\left(\frac{1}{2}\%1\right)^2 - 192\pi^4\beta^3\cos\left(\frac{1}{2}\%1\right)^4 \\
&- 768\beta\%1^5\lambda^2\pi^2\mu\cos\left(\frac{1}{2}\%1\right)\sin\left(\frac{1}{2}\%1\right) + 768\beta\%1^5\lambda^2\pi^2\mu\cos\left(\frac{1}{2}\%1\right)^3\sin\left(\frac{1}{2}\%1\right) \\
&- 36\%1^5\lambda^4\beta^2\cos\left(\frac{1}{2}\%1\right)\sin\left(\frac{1}{2}\%1\right) + 144\beta\sin\left(\frac{1}{2}\%1\right)\%1^7\lambda^4\cos\left(\frac{1}{2}\%1\right)^3
\end{aligned}
$$

$$+ 36\,\beta^3\,\lambda^4\,\%1^4\cos\left(\frac{1}{2}\,\%1\right)^2 - 36\cos\left(\frac{1}{2}\,\%1\right)^4\beta^3\,\lambda^4\,\%1^4$$

$$- 384\,\beta^3\sin\left(\frac{1}{2}\,\%1\right)\%1\,\pi^4\cos\left(\frac{1}{2}\,\%1\right)^3 + 192\,\beta^3\sin\left(\frac{1}{2}\,\%1\right)\%1^3\,\pi^2\,\lambda^2\cos\left(\frac{1}{2}\,\%1\right)^3$$

$$+ 128\sin\left(\frac{1}{2}\,\%1\right)\%1^5\,\lambda^2\,\pi^2\cos\left(\frac{1}{2}\,\%1\right)^3 - 768\,\beta^2\sin\left(\frac{1}{2}\,\%1\right)\%1^3\,\pi^4\cos\left(\frac{1}{2}\,\%1\right)^3$$

$$+ 384\,\beta^2\sin\left(\frac{1}{2}\,\%1\right)\%1^5\,\lambda^2\,\pi^2\cos\left(\frac{1}{2}\,\%1\right)^3 + 960\,\beta^3\,\%1^3\,\pi^2\,\lambda^2\,\mu\cos\left(\frac{1}{2}\,\%1\right)\sin\left(\frac{1}{2}\,\%1\right)$$

$$- 96\,\beta^3\,\%1^3\,\pi^2\,\lambda^2\cos\left(\frac{1}{2}\,\%1\right)\sin\left(\frac{1}{2}\,\%1\right) + 3264\,\beta^3\,\%1\,\pi^4\cos\left(\frac{1}{2}\,\%1\right)\sin\left(\frac{1}{2}\,\%1\right)$$

$$+ 18\,\beta\,\%1^8\,\lambda^4 - 72\,\beta\,\lambda^4\,\%1^6\cos\left(\frac{1}{2}\,\%1\right)^2 + 72\cos\left(\frac{1}{2}\,\%1\right)^4\beta\,\lambda^4\,\%1^6 + 3\,\beta^3\,\%1^8\,\lambda^4$$

$$+ 48\,\beta^3\,\%1^4\,\pi^4 + 9\,\beta^3\,\%1^6\,\lambda^4 + 816\,\beta^3\,\%1^2\,\pi^4 - 24\,\beta^3\,\%1^7\,\lambda^4\cos\left(\frac{1}{2}\,\%1\right)\sin\left(\frac{1}{2}\,\%1\right)$$

$$- 768\,\pi^2\,\beta^3\,\lambda^2\,\%1^2\,\mu + 1536\,\pi^4\,\beta\,\%1^2 - 32\,\beta^2\,\%1^6\,\lambda^2\,\pi^2 - 480\,\%1^4\,\pi^2\,\lambda^2\,\mu\,\beta^2$$

$$- 32\,\%1^6\,\lambda^2\,\pi^2 - 18\,\%1^6\,\lambda^4\,\beta^2 + 48\,\%1^4\,\lambda^2\,\pi^2\,\beta^2 + 384\,\pi^2\,\beta\,\lambda^2\,\%1^4\,\mu - 12\,\beta^2\,\%1^8\,\lambda^4$$

$$- 192\,\beta^2\,\%1^4\,\pi^4 - 1632\,\%1^2\,\pi^4\,\beta^2 + 24\,\%1^7\,\lambda^4\cos\left(\frac{1}{2}\,\%1\right)\sin\left(\frac{1}{2}\,\%1\right) + 288\,\beta\,\%1^4\,\pi^4$$

$$- 1920\,\beta\,\pi^4\,\%1^2\cos\left(\frac{1}{2}\,\%1\right)^2 + 8\,\beta^3\,\%1^6\,\lambda^2\,\pi^2 + 48\,\beta\,\%1^6\,\lambda^2\,\pi^2 + 240\,\beta^3\,\%1^4\,\pi^2\,\lambda^2\,\mu$$

$$- 24\,\beta^3\,\%1^4\,\lambda^2\,\pi^2 + 64\,\beta^3\,\%1^5\,\lambda^2\,\pi^2\cos\left(\frac{1}{2}\,\%1\right)\sin\left(\frac{1}{2}\,\%1\right)$$

$$+ 960\,\beta^3\,\pi^2\,\lambda^2\,\%1^2\,\mu\cos\left(\frac{1}{2}\,\%1\right)^2 - 192\,\pi^2\,\beta^3\,\lambda^2\,\%1^2\,\mu\cos\left(\frac{1}{2}\,\%1\right)^4$$

$$- 768\cos\left(\frac{1}{2}\,\%1\right)^2\pi^2\,\beta\,\lambda^2\,\%1^4\,\mu + 384\,\pi^2\,\beta\,\lambda^2\,\%1^4\,\mu\cos\left(\frac{1}{2}\,\%1\right)^4$$

$$- 256\,\beta^3\,\%1^5\,\lambda^2\,\pi^2\,\mu\cos\left(\frac{1}{2}\,\%1\right)\sin\left(\frac{1}{2}\,\%1\right)$$

$$+ 256\,\beta^3\,\%1^5\,\lambda^2\,\pi^2\,\mu\cos\left(\frac{1}{2}\,\%1\right)^3\sin\left(\frac{1}{2}\,\%1\right) - 192\cos\left(\frac{1}{2}\,\%1\right)^4\beta\,\lambda^2\,\pi^2\,\%1^4$$

$$- 96\,\beta^3\,\pi^2\,\lambda^2\,\%1^2\cos\left(\frac{1}{2}\,\%1\right)^2 + 96\cos\left(\frac{1}{2}\,\%1\right)^4\beta^3\,\pi^2\,\lambda^2\,\%1^2$$

$$+ 192\,\beta\,\lambda^2\,\pi^2\,\%1^4\cos\left(\frac{1}{2}\,\%1\right)^2 - 72\,\beta\,\%1^7\,\lambda^4\cos\left(\frac{1}{2}\,\%1\right)\sin\left(\frac{1}{2}\,\%1\right)$$

$$- 3264\,\%1\,\pi^4\,\beta^2\cos\left(\frac{1}{2}\,\%1\right)\sin\left(\frac{1}{2}\,\%1\right) + 640\,\%1^3\,\pi^4\cos\left(\frac{1}{2}\,\%1\right)\sin\left(\frac{1}{2}\,\%1\right)$$

$$+ 384\,\pi^4\,\beta\,\%1^2\cos\left(\frac{1}{2}\,\%1\right)^4 - 256\,\%1^5\,\lambda^2\,\pi^2\,\mu\cos\left(\frac{1}{2}\,\%1\right)^3\sin\left(\frac{1}{2}\,\%1\right)$$

$$+ 256\,\%1^5\,\lambda^2\,\pi^2\,\mu\cos\left(\frac{1}{2}\,\%1\right)\sin\left(\frac{1}{2}\,\%1\right) - 640\,\beta^3\,\%1^3\,\pi^4\cos\left(\frac{1}{2}\,\%1\right)\sin\left(\frac{1}{2}\,\%1\right)$$

$$+ 192\,\beta\,\%1^5\,\lambda^2\,\pi^2\cos\left(\frac{1}{2}\,\%1\right)\sin\left(\frac{1}{2}\,\%1\right) + 1920\,\beta^2\,\%1^3\,\pi^4\cos\left(\frac{1}{2}\,\%1\right)\sin\left(\frac{1}{2}\,\%1\right)$$

$$- 3072\,\pi^4\,\beta^3 - 192\,\%1^4\,\pi^4 - 12\,\%1^8\,\lambda^4 + 36\,\beta^3\,\%1^5\,\lambda^4\cos\left(\frac{1}{2}\,\%1\right)\sin\left(\frac{1}{2}\,\%1\right)\Bigg) \Bigg/ \Bigg(\pi^4\,\lambda^2$$

$$\%1^2\left(-20\,\%1\,\beta\cos\left(\frac{1}{2}\,\%1\right)\sin\left(\frac{1}{2}\,\%1\right) + 8\,\%1\,\beta\sin\left(\frac{1}{2}\,\%1\right)\cos\left(\frac{1}{2}\,\%1\right)^3\right.$$

$$- 8\,\%1\sin\left(\frac{1}{2}\,\%1\right)\cos\left(\frac{1}{2}\,\%1\right)^3 + 3\,\beta\,\%1^2 + 16\,\beta - 20\,\beta\cos\left(\frac{1}{2}\,\%1\right)^2 + 4\cos\left(\frac{1}{2}\,\%1\right)^4\beta$$

$$\left.- 6\,\%1^2 + 20\,\%1\cos\left(\frac{1}{2}\,\%1\right)\sin\left(\frac{1}{2}\,\%1\right)\right)\Bigg)$$

$$\%1 := \arccos\left(\frac{1}{2}\,\frac{\mu}{-1+\mu}\right)$$

> save 'z1.m';

> mu:=1/3; beta:=0;Km1:=simplify(K1);

$$\mu := \frac{1}{3}$$

$$\beta := 0$$

$$Km1 := \frac{1}{12}\left(144\cos(\%1)^3\,\lambda^4\,\pi\arccos\left(\frac{1}{4}\right)^3\sin(\%1) - 216\cos(\%1)^3\,\lambda^4\,\pi^2\arccos\left(\frac{1}{4}\right)^2\sin(\%1)\right.$$

$$+ 144\cos(\%1)^3\,\lambda^4\,\pi^3\arccos\left(\frac{1}{4}\right)\sin(\%1) - 192\cos(\%1)^3\,\pi^4\sin(\%1)$$

$$\left.+ 32\cos(\%1)^3\,\lambda^2\,\pi^2\arccos\left(\frac{1}{4}\right)^2\sin(\%1) - 36\cos(\%1)^3\,\lambda^4\,\pi^4\sin(\%1)\right)$$

$$
\begin{aligned}
&- 36\cos(\%1)^3\lambda^4\arccos\left(\frac{1}{4}\right)^4\sin(\%1) - 64\cos(\%1)^3\lambda^2\pi^3\arccos\left(\frac{1}{4}\right)\sin(\%1)\\
&+ 32\cos(\%1)^3\lambda^2\pi^4\sin(\%1) - 90\lambda^4\pi^2\arccos\left(\frac{1}{4}\right)^3 + 90\lambda^4\pi^3\arccos\left(\frac{1}{4}\right)^2\\
&- 288\pi^4\sin(\%1)\cos(\%1) - 72\lambda^2\pi^4\arccos\left(\frac{1}{4}\right) + 72\lambda^2\pi^3\arccos\left(\frac{1}{4}\right)^2\\
&- 24\lambda^2\pi^2\arccos\left(\frac{1}{4}\right)^3 - 48\lambda^2\pi^4\sin(\%1)\cos(\%1)\\
&+ 96\lambda^2\pi^3\sin(\%1)\cos(\%1)\arccos\left(\frac{1}{4}\right) - 48\lambda^2\pi^2\sin(\%1)\cos(\%1)\arccos\left(\frac{1}{4}\right)^2\\
&+ 45\lambda^4\pi\arccos\left(\frac{1}{4}\right)^4 + 18\lambda^4\sin(\%1)\cos(\%1)\arccos\left(\frac{1}{4}\right)^4\\
&+ 18\lambda^4\sin(\%1)\cos(\%1)\pi^4 - 72\lambda^4\sin(\%1)\cos(\%1)\pi^3\arccos\left(\frac{1}{4}\right)\\
&+ 108\lambda^4\sin(\%1)\cos(\%1)\pi^2\arccos\left(\frac{1}{4}\right)^2 - 72\lambda^4\sin(\%1)\cos(\%1)\pi\arccos\left(\frac{1}{4}\right)^3\\
&- 45\lambda^4\pi^4\arccos\left(\frac{1}{4}\right) - 144\pi^4\arccos\left(\frac{1}{4}\right) - 9\lambda^4\arccos\left(\frac{1}{4}\right)^5 + 24\lambda^2\pi^5 + 9\lambda^4\pi^5 + 144\pi^5\\
&\Big)\Big/\left(\lambda^2\pi^4\left(-6\sin(\%1)\cos(\%1) - 4\cos(\%1)^3\sin(\%1) + 3\pi - 3\arccos\left(\frac{1}{4}\right)\right)\right)
\end{aligned}
$$

$$\%1 := \frac{1}{2}\arccos\left(\frac{1}{4}\right)$$

> KH:=4/lambda^2+0.0993*lambda^2+0.624;

$$KH := 4\frac{1}{\lambda^2} + .0993\lambda^2 + .624$$

> evalf(Km1);

$$.0006311849085\,\frac{157.3581196\lambda^4 + 991.338665\lambda^2 + 6337.28714}{\lambda^2}$$

> expand(");

$$.09932207032\lambda^2 + .6257180046 + 4.000000004\frac{1}{\lambda^2}$$

Appendix D

Derivation of rectangular plate buckling

(m=2)

> a:=lambda*b; n:=arccos(mu/2/(-1+mu)); m:=2;

$$a := \lambda\, b$$

$$n := \arccos\left(\frac{1}{2}\,\frac{\mu}{-1+\mu}\right)$$

$$m := 2$$

> w:=sin(Pi*x/a)*A*sin(m*Pi*x/a)*(1-cos(n*y/b));

$$w := \sin\left(\frac{\pi\, x}{\lambda\, b}\right) A \sin\left(2\,\frac{\pi\, x}{\lambda\, b}\right)\left(1 - \cos\left(\frac{\arccos\left(\frac{1}{2}\,\frac{\mu}{-1+\mu}\right) y}{b}\right)\right)$$

> DE:=(diff(w,x,x)+diff(w,y,y))^2-2*(1-mu)*(diff(w,x,x)*diff(w,y,y)-(diff(w,x,y))^2);

$$DE := \left(-5\,\frac{\sin\left(\frac{\pi\, x}{\lambda\, b}\right)\pi^2 A\, \%2\left(1 - \cos\left(\frac{\%1\, y}{b}\right)\right)}{\lambda^2 b^2} + 4\,\frac{\cos\left(\frac{\pi\, x}{\lambda\, b}\right)\pi^2 A \cos\left(2\,\frac{\pi\, x}{\lambda\, b}\right)\left(1 - \cos\left(\frac{\%1\, y}{b}\right)\right)}{\lambda^2 b^2} + \frac{\sin\left(\frac{\pi\, x}{\lambda\, b}\right) A\, \%2 \cos\left(\frac{\%1\, y}{b}\right)\%1^2}{b^2}\right)^2$$

$$- 2\,(1-\mu)\left(\left(-5\,\frac{\sin\left(\frac{\pi\, x}{\lambda\, b}\right)\pi^2 A\, \%2\left(1 - \cos\left(\frac{\%1\, y}{b}\right)\right)}{\lambda^2 b^2} + 4\,\frac{\cos\left(\frac{\pi\, x}{\lambda\, b}\right)\pi^2 A \cos\left(2\,\frac{\pi\, x}{\lambda\, b}\right)\left(1 - \cos\left(\frac{\%1\, y}{b}\right)\right)}{\lambda^2 b^2}\right)\sin\left(\frac{\pi\, x}{\lambda\, b}\right) A\, \%2 \cos\left(\frac{\%1\, y}{b}\right)\%1^2 / b^2$$

$$- \left(\frac{\cos\left(\frac{\pi\, x}{\lambda\, b}\right)\pi\, A\, \%2 \sin\left(\frac{\%1\, y}{b}\right)\%1}{\lambda\, b^2} + 2\,\frac{\sin\left(\frac{\pi\, x}{\lambda\, b}\right) A \cos\left(2\,\frac{\pi\, x}{\lambda\, b}\right)\pi \sin\left(\frac{\%1\, y}{b}\right)\%1}{\lambda\, b^2}\right)^2\Bigg)$$

$$\%1 := \arccos\left(\frac{1}{2}\,\frac{\mu}{-1+\mu}\right)$$

$$\%2 := \sin\left(2\,\frac{\pi\, x}{\lambda\, b}\right)$$

> Z1:=int(DE, x=0..a);

$$ZI := \frac{1}{192} A^2 \left(984\,\pi^5 \cos\left(2\,\frac{\%1\,y}{b}\right) + 480\,\pi^3\,\%1^2\,\lambda^2 + 24\,\%1^4\,\lambda^4\,\pi - 3\,\%11\,\lambda^4\,\%1^4 \right.$$

$$- 3\sin(2\,\%4)\,\lambda^4\,\%1^4 + 2952\,\pi^5 - 3936\,\pi^5 \cos\left(\frac{\%1\,y}{b}\right) - 27\sin(2\,\%5)\,\pi^4 + 81\,\%9\,\pi^4$$

$$- 27\sin(2\,\%4)\,\pi^4 - 51\,\%7\,\pi^4 + 108\,\%8\,\pi^4 - 51\,\%11\,\pi^4 + 204\sin(\%4)\,\pi^4 - 324\,\%2\,\pi^4$$

$$+ 81\,\%10\,\pi^4 + 204\sin(\%5)\,\pi^4 - 324\,\%3\,\pi^4 + 108\,\%6\,\pi^4 + 24\,\%1^4 \cos\left(2\,\frac{\%1\,y}{b}\right)\lambda^4\,\pi$$

$$- 36\,\pi^2\,\%1^2\,\lambda^2 \cos\left(\frac{\%1\,y}{b}\right)\%2 + 108\sin(\%4)\,\pi^2\,\%1^2\,\lambda^2$$

$$+ 108\,\pi^2\,\%1^2\,\lambda^2 \cos\left(\frac{\%1\,y}{b}\right)\sin(\%5) + 36\,\%10\,\pi^2\,\%1^2\,\lambda^2 - 42\,\%11\,\pi^2\,\%1^2\,\lambda^2\,\mu$$

$$+ 108\sin(\%5)\,\pi^2\,\%1^2\,\lambda^2 - 12\,\%11\,\pi^2\,\%1^2\,\lambda^2 + 18\sin(2\,\%4)\,\pi^2\,\%1^2\,\lambda^2\,\mu$$

$$+ 18\sin(2\,\%5)\,\pi^2\,\%1^2\,\lambda^2\,\mu - 36\,\pi^2\,\%1^2\,\lambda^2 \cos\left(\frac{\%1\,y}{b}\right)\%3$$

$$+ 60\,\pi^2\,\%1^2\,\lambda^2 \cos\left(\frac{\%1\,y}{b}\right)\%8 + 60\,\pi^2\,\%1^2\,\lambda^2 \cos\left(\frac{\%1\,y}{b}\right)\%6 - 36\,\%3\,\pi^2\,\%1^2\,\lambda^2$$

$$- 12\,\%7\,\pi^2\,\%1^2\,\lambda^2 - 480\,\pi^3\,\%1^2\,\lambda^2 \cos\left(\frac{\%1\,y}{b}\right)^2 - 240\,\pi^3\,\%1^2\,\lambda^2\,\mu$$

$$+ 480\,\pi^3\,\%1^2\,\lambda^2 \cos\left(\frac{\%1\,y}{b}\right)^2\mu + 240\,\pi^3\,\%1^2\,\lambda^2 \cos\left(2\,\frac{\%1\,y}{b}\right)\mu$$

$$- 480\,\pi^3\,\%1^2\,\lambda^2 \cos\left(\frac{\%1\,y}{b}\right)\mu + \%9\,\lambda^4\,\%1^4 + \%10\,\lambda^4\,\%1^4 - 3\sin(2\,\%5)\,\lambda^4\,\%1^4$$

$$- 3\,\%7\,\lambda^4\,\%1^4 - 48\sin(2\,\%4)\,\pi^2\,\%1^2\,\lambda^2 + 60\,\%8\,\pi^2\,\%1^2\,\lambda^2 + 60\,\%6\,\pi^2\,\%1^2\,\lambda^2$$

$$+ 36\,\%9\,\pi^2\,\%1^2\,\lambda^2 - 48\sin(2\,\%5)\,\pi^2\,\%1^2\,\lambda^2 - 36\,\%2\,\pi^2\,\%1^2\,\lambda^2 - 18\,\%10\,\pi^2\,\%1^2\,\lambda^2\,\mu$$

$$- 18\,\%9\,\pi^2\,\%1^2\,\lambda^2\,\mu - 60\,\pi^2\,\%1^2\,\lambda^2 \cos\left(\frac{\%1\,y}{b}\right)\%8\,\mu$$

$$+ 108\,\pi^2\,\%1^2\,\lambda^2 \cos\left(\frac{\%1\,y}{b}\right)\sin(\%4) - 42\,\%7\,\pi^2\,\%1^2\,\lambda^2\,\mu$$

$$- 60\,\pi^2\,\%1^2\,\lambda^2 \cos\left(\frac{\%1\,y}{b}\right)\%6\,\mu - 108\,\pi^2\,\%1^2\,\lambda^2 \cos\left(\frac{\%1\,y}{b}\right)\sin(\%5)\,\mu$$

$$- 108\,\pi^2\,\%1^2\,\lambda^2 \cos\left(\frac{\%1\,y}{b}\right)\sin(\%4)\,\mu + 36\,\pi^2\,\%1^2\,\lambda^2 \cos\left(\frac{\%1\,y}{b}\right)\%3\,\mu$$

$$+ 36\,\pi^2\,\%1^2\,\lambda^2\cos\left(\frac{\%1\,y}{b}\right)\%2\,\mu\Bigg)\Big/\left(\lambda^3\,b^3\,\pi\right)$$

$$\%1 := \arccos\left(\frac{1}{2}\,\frac{\mu}{-1+\mu}\right)$$

$$\%2 := \sin\left(\frac{6\,\pi\,b + \%1\,y}{b}\right)$$

$$\%3 := \sin\left(\frac{6\,\pi\,b - \%1\,y}{b}\right)$$

$$\%4 := \frac{\%1\,y + 2\,\pi\,b}{b}$$

$$\%5 := \frac{-\%1\,y + 2\,\pi\,b}{b}$$

$$\%6 := \sin\left(\frac{\%1\,y + 4\,\pi\,b}{b}\right)$$

$$\%7 := \sin\left(2\,\frac{\pi\,b + \%1\,y}{b}\right)$$

$$\%8 := \sin\left(\frac{-\%1\,y + 4\,\pi\,b}{b}\right)$$

$$\%9 := \sin\left(2\,\frac{\%1\,y + 3\,\pi\,b}{b}\right)$$

$$\%10 := \sin\left(2\,\frac{-\%1\,y + 3\,\pi\,b}{b}\right)$$

$$\%11 := \sin\left(2\,\frac{\pi\,b - \%1\,y}{b}\right)$$

> expand(Z1);

$$\frac{5}{2}\frac{A^2\pi^2\,\%1^2}{\lambda\,b^3}+\frac{41}{4}\frac{A^2\pi^4\cos\left(\frac{\%1\,y}{b}\right)^2}{\lambda^3 b^3}+\frac{1}{4}\frac{A^2\lambda\,\%1^4\cos\left(\frac{\%1\,y}{b}\right)^2}{b^3}+\frac{41}{4}\frac{A^2\pi^4}{\lambda^3 b^3}$$

$$-\frac{41}{2}\frac{A^2\pi^4\cos\left(\frac{\%1\,y}{b}\right)}{\lambda^3 b^3}-\frac{5}{2}\frac{A^2\pi^2\,\%1^2\cos\left(\frac{\%1\,y}{b}\right)^2}{\lambda\,b^3}-\frac{5}{2}\frac{A^2\pi^2\,\%1^2\,\mu}{\lambda\,b^3}$$

$$+5\frac{A^2\pi^2\,\%1^2\cos\left(\frac{\%1\,y}{b}\right)^2\mu}{\lambda\,b^3}-\frac{5}{2}\frac{A^2\pi^2\,\%1^2\cos\left(\frac{\%1\,y}{b}\right)\mu}{\lambda\,b^3}$$

$$\%1 := \arccos\left(\frac{1}{2}\frac{\mu}{-1+\mu}\right)$$

> Z2:=int("*(1-beta*y/b)^3, y=0..b);

$$Z2 := -\frac{1}{32}A^2\left(-6\,\%1^6\lambda^4\beta^2+123\,\beta^3\tan\left(\frac{1}{2}\%1\right)^4\%1^4\pi^4+10\,\beta^3\tan\left(\frac{1}{2}\%1\right)^4\%1^6\lambda^2\pi^2\right.$$

$$+\beta^3\tan\left(\frac{1}{2}\%1\right)^4\%1^8\lambda^4+246\,\beta^3\tan\left(\frac{1}{2}\%1\right)^2\%1^4\pi^4+20\,\beta^3\tan\left(\frac{1}{2}\%1\right)^2\%1^6\lambda^2\pi^2$$

$$+2\,\beta^3\tan\left(\frac{1}{2}\%1\right)^2\%1^8\lambda^4-492\,\beta^2\%1^4\pi^4-4\,\beta^2\%1^8\lambda^4+360\,\%1^4\pi^2\lambda^2\mu\,\beta^2$$

$$+60\tan\left(\frac{1}{2}\%1\right)^4\%1^4\lambda^2\pi^2\beta^2-4182\tan\left(\frac{1}{2}\%1\right)^4\%1^2\pi^4\beta^2-40\tan\left(\frac{1}{2}\%1\right)^4\%1^6\lambda^2\pi^2$$

$$-40\,\beta^2\%1^6\lambda^2\pi^2+60\,\%1^4\lambda^2\pi^2\beta^2-180\,\beta^3\%1^4\pi^2\lambda^2\mu-492\,\%1^4\pi^4+123\,\beta^3\%1^4\pi^4$$

$$+\beta^3\%1^8\lambda^4+6\,\beta\%1^8\lambda^4+1476\tan\left(\frac{1}{2}\%1\right)^2\%1^2\pi^4\beta^2-7380\tan\left(\frac{1}{2}\%1\right)\%1\,\pi^4\beta^2$$

$$+3\,\beta^3\tan\left(\frac{1}{2}\%1\right)^4\%1^6\lambda^4-720\tan\left(\frac{1}{2}\%1\right)\%1^3\lambda^2\pi^2\mu\,\beta^2+24\,\beta\tan\left(\frac{1}{2}\%1\right)\%1^7\lambda^4$$

$$+60\,\beta\tan\left(\frac{1}{2}\%1\right)^4\%1^6\lambda^2\pi^2+240\,\beta^2\tan\left(\frac{1}{2}\%1\right)\%1^5\lambda^2\pi^2$$

$$+2091\,\beta^3\tan\left(\frac{1}{2}\%1\right)^4\%1^2\pi^4+300\,\beta^3\tan\left(\frac{1}{2}\%1\right)^4\%1^4\lambda^2\pi^2\mu$$

$$-492\,\beta^2\tan\left(\frac{1}{2}\%1\right)^4\%1^4\pi^4+80\tan\left(\frac{1}{2}\%1\right)\%1^5\lambda^2\pi^2+120\tan\left(\frac{1}{2}\%1\right)^3\%1^3\lambda^2\pi^2\beta^2$$

$$+ 7380\,\beta^3 \tan\left(\frac{1}{2}\%1\right)\%1\,\pi^4 - 738\,\beta^3 \tan\left(\frac{1}{2}\%1\right)^2 \%1^2\,\pi^4 + 120\,\beta \tan\left(\frac{1}{2}\%1\right)^2 \%1^6\,\lambda^2\,\pi^2$$

$$+ 180\,\beta^3 \tan\left(\frac{1}{2}\%1\right)^2 \%1^4\,\pi^2\,\lambda^2 - 360\,\beta^3 \tan\left(\frac{1}{2}\%1\right)^2 \%1^4\,\pi^2\,\lambda^2\,\mu$$

$$- 12 \tan\left(\frac{1}{2}\%1\right)^3 \%1^5\,\lambda^4\,\beta^2 - 80 \tan\left(\frac{1}{2}\%1\right)^3 \%1^5\,\lambda^2\,\pi^2 + 738\,\beta \tan\left(\frac{1}{2}\%1\right)^4 \%1^4\,\pi^4$$

$$- 4\,\beta^2 \tan\left(\frac{1}{2}\%1\right)^4 \%1^8\,\lambda^4 - 40\,\beta^2 \tan\left(\frac{1}{2}\%1\right)^4 \%1^6\,\lambda^2\,\pi^2 + 984 \tan\left(\frac{1}{2}\%1\right)\%1^3\,\pi^4$$

$$- 24\,\beta^2 \tan\left(\frac{1}{2}\%1\right)\%1^7\,\lambda^4 - 8\,\beta^2 \tan\left(\frac{1}{2}\%1\right)^2 \%1^8\,\lambda^4 + 6\,\beta \tan\left(\frac{1}{2}\%1\right)^4 \%1^8\,\lambda^4$$

$$- 18\,\beta^3 \tan\left(\frac{1}{2}\%1\right)^2 \%1^6\,\lambda^4 + 960\,\beta^2 \tan\left(\frac{1}{2}\%1\right)^3 \%1^5\,\lambda^2\,\pi^2\,\mu - 12\,\beta^3 \tan\left(\frac{1}{2}\%1\right)\%1^5\,\lambda^4$$

$$- 2952\,\beta \tan\left(\frac{1}{2}\%1\right)\%1^3\,\pi^4 + 720\,\beta^3 \tan\left(\frac{1}{2}\%1\right)\%1^3\,\pi^2\,\lambda^2\,\mu$$

$$- 240\,\beta \tan\left(\frac{1}{2}\%1\right)\%1^5\,\lambda^2\,\pi^2 - 120\,\beta^3 \tan\left(\frac{1}{2}\%1\right)^2 \pi^2\,\lambda^2\,\%1^2 - 24\,\beta \tan\left(\frac{1}{2}\%1\right)^2 \lambda^4\,\%1^6$$

$$+ 36 \tan\left(\frac{1}{2}\%1\right)^2 \%1^6\,\lambda^4\,\beta^2 + 240\,\beta \tan\left(\frac{1}{2}\%1\right)^2 \lambda^2\,\pi^2\,\%1^4$$

$$- 1200 \tan\left(\frac{1}{2}\%1\right)^3 \%1^3\,\lambda^2\,\pi^2\,\mu\,\beta^2 - 120 \tan\left(\frac{1}{2}\%1\right)\%1^3\,\lambda^2\,\pi^2\,\beta^2$$

$$+ 120\,\beta^3 \tan\left(\frac{1}{2}\%1\right)\%1^3\,\pi^2\,\lambda^2 + 320 \tan\left(\frac{1}{2}\%1\right)^3 \%1^5\,\lambda^2\,\pi^2\,\mu$$

$$+ 1200\,\beta^3 \tan\left(\frac{1}{2}\%1\right)^2 \pi^2\,\lambda^2\,\%1^2\,\mu - 960\,\beta \tan\left(\frac{1}{2}\%1\right)^2 \lambda^2\,\pi^2\,\%1^4\,\mu$$

$$- 8364 \tan\left(\frac{1}{2}\%1\right)^3 \%1\,\pi^4\,\beta^2 + 12\,\beta^3 \tan\left(\frac{1}{2}\%1\right)^2 \lambda^4\,\%1^4 + 12 \tan\left(\frac{1}{2}\%1\right)\%1^5\,\lambda^4\,\beta^2$$

$$- 600 \tan\left(\frac{1}{2}\%1\right)^4 \%1^4\,\lambda^2\,\pi^2\,\mu\,\beta^2 + 1476\,\beta \tan\left(\frac{1}{2}\%1\right)^2 \%1^4\,\pi^4$$

$$- 4920\,\beta \tan\left(\frac{1}{2}\%1\right)^2 \pi^4\,\%1^2 + 12\,\beta \tan\left(\frac{1}{2}\%1\right)^2 \%1^8\,\lambda^4 - 80\,\beta^2 \tan\left(\frac{1}{2}\%1\right)^2 \%1^6\,\lambda^2\,\pi^2$$

$$- 240\,\beta^2 \tan\left(\frac{1}{2}\%1\right)^3 \%1^5\,\lambda^2\,\pi^2 + 12\,\beta^3 \tan\left(\frac{1}{2}\%1\right)^3 \%1^5\,\lambda^4 - 1845\,\beta^3\,\%1^2\,\pi^4$$

$$
- 8 \tan\left(\frac{1}{2}\,\%1\right)^2 \%1^8\,\lambda^4 - 8 \tan\left(\frac{1}{2}\,\%1\right)\%1^7\,\lambda^4 + 8 \tan\left(\frac{1}{2}\,\%1\right)^3 \%1^7\,\lambda^4
$$

$$
+ 1640 \tan\left(\frac{1}{2}\,\%1\right)^3 \%1^3\,\pi^4 - 984 \tan\left(\frac{1}{2}\,\%1\right)^2 \%1^4\,\pi^4 - 492 \tan\left(\frac{1}{2}\,\%1\right)^4 \%1^4\,\pi^4
$$

$$
+ 8364\,\beta^3 \tan\left(\frac{1}{2}\,\%1\right)^2 \pi^4 - 4 \tan\left(\frac{1}{2}\,\%1\right)^4 \%1^8\,\lambda^4 + 10\,\beta^3\,\%1^6\,\lambda^2\,\pi^2
$$

$$
- 1640\,\beta^3 \tan\left(\frac{1}{2}\,\%1\right)^3 \%1^3\,\pi^4 - 984\,\beta^2 \tan\left(\frac{1}{2}\,\%1\right)^2 \%1^4\,\pi^4 - 8\,\beta^3 \tan\left(\frac{1}{2}\,\%1\right)^3 \%1^7\,\lambda^4
$$

$$
+ 24\,\beta^2 \tan\left(\frac{1}{2}\,\%1\right)^3 \%1^7\,\lambda^4 + 4920\,\beta^2 \tan\left(\frac{1}{2}\,\%1\right)^3 \%1^3\,\pi^4 + 960\,\beta^3\,\pi^2\,\lambda^2\,\%1^2\,\mu
$$

$$
+ 60\,\beta\,\%1^6\,\lambda^2\,\pi^2 - 480\,\beta\,\pi^2\,\lambda^2\,\%1^4\,\mu - 6 \tan\left(\frac{1}{2}\,\%1\right)^4 \%1^6\,\lambda^4\,\beta^2 - 40\,\%1^6\,\lambda^2\,\pi^2
$$

$$
- 3936\,\beta\,\pi^4\,\%1^2 + 738\,\beta\,\%1^4\,\pi^4 + 1200\,\beta^3 \tan\left(\frac{1}{2}\,\%1\right)^3 \%1^3\,\lambda^2\,\pi^2\,\mu
$$

$$
- 320\,\beta^3 \tan\left(\frac{1}{2}\,\%1\right)^3 \%1^5\,\pi^2\,\lambda^2\,\mu - 120\,\beta^3 \tan\left(\frac{1}{2}\,\%1\right)^3 \%1^3\,\lambda^2\,\pi^2
$$

$$
+ 2952\,\beta^2 \tan\left(\frac{1}{2}\,\%1\right)\%1^3\,\pi^4 + 8\,\beta^3 \tan\left(\frac{1}{2}\,\%1\right)\%1^7\,\lambda^4 - 984\,\beta^3 \tan\left(\frac{1}{2}\,\%1\right)\%1^3\,\pi^4
$$

$$
+ 7872\,\beta^3\,\pi^4 - 4920\,\beta \tan\left(\frac{1}{2}\,\%1\right)^3 \%1^3\,\pi^4 - 24\,\beta \tan\left(\frac{1}{2}\,\%1\right)^3 \%1^7\,\lambda^4
$$

$$
+ 240\,\beta \tan\left(\frac{1}{2}\,\%1\right)^3 \%1^5\,\lambda^2\,\pi^2 - 30\,\beta^3 \tan\left(\frac{1}{2}\,\%1\right)^4 \%1^4\,\lambda^2\,\pi^2
$$

$$
+ 80\,\beta^3 \tan\left(\frac{1}{2}\,\%1\right)^3 \%1^5\,\pi^2\,\lambda^2 + 8364\,\beta^3 \tan\left(\frac{1}{2}\,\%1\right)^3 \%1\,\pi^4
$$

$$
- 960\,\beta \tan\left(\frac{1}{2}\,\%1\right)^3 \%1^5\,\lambda^2\,\pi^2\,\mu - 4\,\%1^8\,\lambda^4 - 30\,\beta^3\,\%1^4\,\lambda^2\,\pi^2 + 3\,\beta^3\,\%1^6\,\lambda^4
$$

$$
+ 3690\,\%1^2\,\pi^4\,\beta^2 - 80\,\beta^3 \tan\left(\frac{1}{2}\,\%1\right)\%1^5\,\lambda^2\,\pi^2 + 720 \tan\left(\frac{1}{2}\,\%1\right)^2 \%1^4\,\pi^2\,\lambda^2\,\mu\,\beta^2
$$

$$
- 80 \tan\left(\frac{1}{2}\,\%1\right)^2 \%1^6\,\lambda^2\,\pi^2 - 360 \tan\left(\frac{1}{2}\,\%1\right)^2 \%1^4\,\pi^2\,\lambda^2\,\beta^2 \Bigg) \Bigg/ \Bigg(b^2\,\lambda^3\,\%1^4
$$

$$\left(1+\tan\left(\frac{1}{2}\,\%1\right)^2\right)^2\Bigg)-3\,\frac{A^2\,\beta\,\pi^2\left(41\,\%1^2\,\pi^2-82\,\pi^2\,\beta^2-10\,\lambda^2\,\%1^2\,\mu\,\beta^2+5\,\lambda^2\,\%1^4\,\mu\right)}{b^2\,\%1^4\,\lambda^3}$$

$$\%1 := \arccos\left(\frac{1}{2}\,\frac{\mu}{-1+\mu}\right)$$

> int(diff(w,x)^2,x=0..a);

$$-\frac{1}{64}\,\pi\,A^2\Bigg(160\,\pi\cos\left(\frac{\%1\,y}{b}\right)-28\sin\left(\frac{-\%1\,y+2\,\pi\,b}{b}\right)-120\,\pi-28\sin\left(\frac{\%1\,y+2\,\pi\,b}{b}\right)$$
$$+12\sin\left(\frac{-\%1\,y+4\,\pi\,b}{b}\right)-3\sin\left(2\,\frac{\%1\,y+2\,\pi\,b}{b}\right)+12\sin\left(\frac{\%1\,y+4\,\pi\,b}{b}\right)$$
$$-40\,\pi\cos\left(2\,\frac{\%1\,y}{b}\right)-12\sin\left(\frac{6\,\pi\,b+\%1\,y}{b}\right)+3\sin\left(2\,\frac{\%1\,y+3\,\pi\,b}{b}\right)$$
$$-12\sin\left(\frac{6\,\pi\,b-\%1\,y}{b}\right)+3\sin\left(2\,\frac{-\%1\,y+3\,\pi\,b}{b}\right)+7\sin\left(2\,\frac{\pi\,b+\%1\,y}{b}\right)$$
$$+7\sin\left(2\,\frac{\pi\,b-\%1\,y}{b}\right)-3\sin\left(2\,\frac{-\%1\,y+2\,\pi\,b}{b}\right)\Bigg)\Big/(\lambda\,b)$$

$$\%1 := \arccos\left(\frac{1}{2}\,\frac{\mu}{-1+\mu}\right)$$

> expand(");

$$-\frac{5}{2}\,\frac{\pi^2\,A^2\cos\left(\dfrac{\arccos\left(\frac{1}{2}\,\frac{\mu}{-1+\mu}\right)y}{b}\right)}{\lambda\,b}+\frac{5}{4}\,\frac{\pi^2\,A^2}{\lambda\,b}+\frac{5}{4}\,\frac{\pi^2\,A^2\cos\left(\dfrac{\arccos\left(\frac{1}{2}\,\frac{\mu}{-1+\mu}\right)y}{b}\right)^2}{\lambda\,b}$$

> Z3:=int((1-beta*y/b)*",y=0..b);

$$Z3 := -\frac{5}{16}\,\pi^2\,A^2\Bigg(-6\tan\left(\frac{1}{2}\,\%1\right)^4\%1^2-20\,\beta\tan\left(\frac{1}{2}\,\%1\right)^3\%1-12\tan\left(\frac{1}{2}\,\%1\right)^2\%1^2$$
$$+12\,\beta\tan\left(\frac{1}{2}\,\%1\right)^2+3\,\beta\,\%1^2+20\tan\left(\frac{1}{2}\,\%1\right)^3\%1-6\,\%1^2+12\tan\left(\frac{1}{2}\,\%1\right)\%1$$
$$-12\,\beta\tan\left(\frac{1}{2}\,\%1\right)\%1+16\,\beta\tan\left(\frac{1}{2}\,\%1\right)^4+6\,\beta\tan\left(\frac{1}{2}\,\%1\right)^2\%1^2+3\,\beta\tan\left(\frac{1}{2}\,\%1\right)^4\%1^2\Bigg)$$
$$\Big/\left(\lambda\,\%1^2\left(1+\tan\left(\frac{1}{2}\,\%1\right)^2\right)^2\right)$$

$$\%1 := \arccos\left(\frac{1}{2}\,\frac{\mu}{-1+\mu}\right)$$

> U:=simplify((Z2-X*Z3)/A^2);

$$U := -\frac{1}{32}\left(200\,X\,\pi^2\,b^2\,\lambda^2\,\%1^3\,\beta\cos\left(\frac{1}{2}\%1\right)\sin\left(\frac{1}{2}\%1\right) - 6\,\%1^6\,\lambda^4\,\beta^2 - 492\,\beta^2\,\%1^4\,\pi^4\right.$$
$$- 4\,\beta^2\,\%1^8\,\lambda^4 - 600\,\%1^4\,\pi^2\,\lambda^2\,\mu\,\beta^2 - 40\,\beta^2\,\%1^6\,\lambda^2\,\pi^2 + 60\,\%1^4\,\lambda^2\,\pi^2\,\beta^2$$
$$+ 300\,\beta^3\,\%1^4\,\pi^2\,\lambda^2\,\mu - 492\,\%1^4\,\pi^4 + 123\,\beta^3\,\%1^4\,\pi^4 + \beta^3\,\%1^8\,\lambda^4 + 6\,\beta\,\%1^8\,\lambda^4$$
$$+ 60\,X\,\pi^2\,b^2\,\lambda^2\,\%1^4 + 2091\,\beta^3\,\%1^2\,\pi^4 + 10\,\beta^3\,\%1^6\,\lambda^2\,\pi^2 - 960\,\beta^3\,\pi^2\,\lambda^2\,\%1^2\,\mu$$
$$+ 60\,\beta\,\%1^6\,\lambda^2\,\pi^2 + 480\,\beta\,\pi^2\,\lambda^2\,\%1^4\,\mu - 40\,\%1^6\,\lambda^2\,\pi^2 + 3936\,\beta\,\pi^4\,\%1^2 + 738\,\beta\,\%1^4\,\pi^4$$
$$- 7872\,\beta^3\,\pi^4 - 4\,\%1^8\,\lambda^4 - 30\,\beta^3\,\%1^4\,\lambda^2\,\pi^2 + 3\,\beta^3\,\%1^6\,\lambda^4 - 4182\,\%1^2\,\pi^4\,\beta^2$$
$$- 80\,X\,\pi^2\,b^2\,\lambda^2\,\%1^3\,\beta\sin\left(\frac{1}{2}\%1\right)\cos\left(\frac{1}{2}\%1\right)^3$$
$$+ 80\,X\,\pi^2\,b^2\,\lambda^2\,\%1^3\sin\left(\frac{1}{2}\%1\right)\cos\left(\frac{1}{2}\%1\right)^3 + 984\,\beta^3\,\%1^2\,\pi^4\cos\left(\frac{1}{2}\%1\right)^4$$
$$- 240\,\beta^3\,\%1^4\,\lambda^2\,\pi^2\cos\left(\frac{1}{2}\%1\right)^4 + 480\,\%1^4\,\lambda^2\,\pi^2\,\beta^2\cos\left(\frac{1}{2}\%1\right)^4$$
$$+ 480\,\beta^3\,\%1^4\,\pi^2\,\lambda^2\,\mu\cos\left(\frac{1}{2}\%1\right)^4 - 960\,\%1^4\,\pi^2\,\lambda^2\,\mu\,\beta^2\cos\left(\frac{1}{2}\%1\right)^4$$
$$+ 24\,\beta^3\,\%1^6\,\lambda^4\cos\left(\frac{1}{2}\%1\right)^4 - 1968\,\%1^2\,\pi^4\,\beta^2\cos\left(\frac{1}{2}\%1\right)^4$$
$$+ 160\sin\left(\frac{1}{2}\%1\right)\%1^5\,\lambda^2\,\pi^2\cos\left(\frac{1}{2}\%1\right)^3 - 656\sin\left(\frac{1}{2}\%1\right)\%1^3\,\pi^4\cos\left(\frac{1}{2}\%1\right)^3$$
$$+ 16\,\beta^3\sin\left(\frac{1}{2}\%1\right)\%1^7\,\lambda^4\cos\left(\frac{1}{2}\%1\right)^3 - 1968\,\beta^2\sin\left(\frac{1}{2}\%1\right)\%1^3\,\pi^4\cos\left(\frac{1}{2}\%1\right)^3$$
$$+ 656\,\beta^3\sin\left(\frac{1}{2}\%1\right)\%1^3\,\pi^4\cos\left(\frac{1}{2}\%1\right)^3 + 24\sin\left(\frac{1}{2}\%1\right)\%1^5\,\lambda^4\,\beta^2\cos\left(\frac{1}{2}\%1\right)^3$$
$$+ 240\,\beta^3\sin\left(\frac{1}{2}\%1\right)\%1^3\,\pi^2\,\lambda^2\cos\left(\frac{1}{2}\%1\right)^3 - 48\,\beta^2\sin\left(\frac{1}{2}\%1\right)\%1^7\,\lambda^4\cos\left(\frac{1}{2}\%1\right)^3$$
$$- 480\,\beta^3\sin\left(\frac{1}{2}\%1\right)\%1^3\,\pi^2\,\lambda^2\,\mu\cos\left(\frac{1}{2}\%1\right)^3 - 480\,\beta\sin\left(\frac{1}{2}\%1\right)\%1^5\,\lambda^2\,\pi^2\cos\left(\frac{1}{2}\%1\right)^3$$

$$
\begin{aligned}
&- 240 \sin\left(\frac{1}{2}\%1\right)\%1^3 \lambda^2 \pi^2 \beta^2 \cos\left(\frac{1}{2}\%1\right)^3 + 1968 \beta \sin\left(\frac{1}{2}\%1\right)\%1^3 \pi^4 \cos\left(\frac{1}{2}\%1\right)^3 \\
&+ 480 \beta^2 \sin\left(\frac{1}{2}\%1\right)\%1^5 \lambda^2 \pi^2 \cos\left(\frac{1}{2}\%1\right)^3 - 24 \beta^3 \sin\left(\frac{1}{2}\%1\right)\%1^5 \lambda^4 \cos\left(\frac{1}{2}\%1\right)^3 \\
&- 16 \sin\left(\frac{1}{2}\%1\right)\%1^7 \lambda^4 \cos\left(\frac{1}{2}\%1\right)^3 - 984 \beta^3 \sin\left(\frac{1}{2}\%1\right)\%1 \pi^4 \cos\left(\frac{1}{2}\%1\right)^3 \\
&+ 48 \beta \sin\left(\frac{1}{2}\%1\right)\%1^7 \lambda^4 \cos\left(\frac{1}{2}\%1\right)^3 + 480 \sin\left(\frac{1}{2}\%1\right)\%1^3 \lambda^2 \pi^2 \mu \beta^2 \cos\left(\frac{1}{2}\%1\right)^3 \\
&+ 984 \sin\left(\frac{1}{2}\%1\right)\%1 \pi^4 \beta^2 \cos\left(\frac{1}{2}\%1\right)^3 - 160 \beta^3 \sin\left(\frac{1}{2}\%1\right)\%1^5 \lambda^2 \pi^2 \cos\left(\frac{1}{2}\%1\right)^3 \\
&- 48 \%1^6 \lambda^4 \beta^2 \cos\left(\frac{1}{2}\%1\right)^4 - 30 X \pi^2 b^2 \lambda^2 \%1^4 \beta + 8364 \beta^3 \pi^4 \cos\left(\frac{1}{2}\%1\right)^2 \\
&- 492 \beta^3 \pi^4 \cos\left(\frac{1}{2}\%1\right)^4 - 160 X \pi^2 b^2 \lambda^2 \%1^2 \beta - 960 \cos\left(\frac{1}{2}\%1\right)^2 \beta \pi^2 \lambda^2 \%1^4 \mu \\
&+ 480 \beta \pi^2 \lambda^2 \%1^4 \mu \cos\left(\frac{1}{2}\%1\right)^4 - 4920 \beta \pi^4 \%1^2 \cos\left(\frac{1}{2}\%1\right)^2 \\
&+ 984 \beta \pi^4 \%1^2 \cos\left(\frac{1}{2}\%1\right)^4 + 1200 \beta^3 \pi^2 \lambda^2 \%1^2 \mu \cos\left(\frac{1}{2}\%1\right)^2 \\
&- 240 \beta^3 \pi^2 \lambda^2 \%1^2 \mu \cos\left(\frac{1}{2}\%1\right)^4 - 200 X \pi^2 b^2 \lambda^2 \%1^3 \cos\left(\frac{1}{2}\%1\right)\sin\left(\frac{1}{2}\%1\right) \\
&+ 200 X \pi^2 b^2 \lambda^2 \%1^2 \beta \cos\left(\frac{1}{2}\%1\right)^2 - 40 \cos\left(\frac{1}{2}\%1\right)^4 X \pi^2 b^2 \lambda^2 \%1^2 \beta \\
&+ 24 \beta^2 \%1^7 \lambda^4 \cos\left(\frac{1}{2}\%1\right)\sin\left(\frac{1}{2}\%1\right) + 4920 \beta^2 \%1^3 \pi^4 \cos\left(\frac{1}{2}\%1\right)\sin\left(\frac{1}{2}\%1\right) \\
&- 1640 \beta^3 \%1^3 \pi^4 \cos\left(\frac{1}{2}\%1\right)\sin\left(\frac{1}{2}\%1\right) + 320 \%1^5 \lambda^2 \pi^2 \mu \cos\left(\frac{1}{2}\%1\right)\sin\left(\frac{1}{2}\%1\right) \\
&- 320 \%1^5 \lambda^2 \pi^2 \mu \cos\left(\frac{1}{2}\%1\right)^3 \sin\left(\frac{1}{2}\%1\right) - 240 \beta^2 \%1^5 \lambda^2 \pi^2 \cos\left(\frac{1}{2}\%1\right)\sin\left(\frac{1}{2}\%1\right) \\
&+ 12 \beta^3 \lambda^4 \%1^4 \cos\left(\frac{1}{2}\%1\right)^2 - 12 \cos\left(\frac{1}{2}\%1\right)^4 \beta^3 \lambda^4 \%1^4 \\
&- 1200 \%1^3 \lambda^2 \pi^2 \mu \beta^2 \cos\left(\frac{1}{2}\%1\right)\sin\left(\frac{1}{2}\%1\right) + 240 \beta \lambda^2 \pi^2 \%1^4 \cos\left(\frac{1}{2}\%1\right)^2
\end{aligned}
$$

$$
\begin{aligned}
&- 240 \cos\left(\frac{1}{2}\%1\right)^4 \beta \lambda^2 \pi^2 \%1^4 - 24 \beta \lambda^4 \%1^6 \cos\left(\frac{1}{2}\%1\right)^2 + 24 \cos\left(\frac{1}{2}\%1\right)^4 \beta \lambda^4 \%1^6 \\
&+ 240 \beta^3 \%1^4 \pi^2 \lambda^2 \cos\left(\frac{1}{2}\%1\right)^2 - 120 \beta^3 \pi^2 \lambda^2 \%1^2 \cos\left(\frac{1}{2}\%1\right)^2 \\
&+ 120 \cos\left(\frac{1}{2}\%1\right)^4 \beta^3 \pi^2 \lambda^2 \%1^2 + 960 \beta^2 \%1^5 \lambda^2 \pi^2 \mu \cos\left(\frac{1}{2}\%1\right) \sin\left(\frac{1}{2}\%1\right) \\
&- 960 \beta^2 \%1^5 \lambda^2 \pi^2 \mu \cos\left(\frac{1}{2}\%1\right)^3 \sin\left(\frac{1}{2}\%1\right) - 80 \%1^5 \lambda^2 \pi^2 \cos\left(\frac{1}{2}\%1\right) \sin\left(\frac{1}{2}\%1\right) \\
&- 12 \%1^5 \lambda^4 \beta^2 \cos\left(\frac{1}{2}\%1\right) \sin\left(\frac{1}{2}\%1\right) - 4920 \beta^3 \%1^2 \pi^4 \cos\left(\frac{1}{2}\%1\right)^2 \\
&- 24 \beta^3 \%1^6 \lambda^4 \cos\left(\frac{1}{2}\%1\right)^2 + 12 \beta^3 \%1^5 \lambda^4 \cos\left(\frac{1}{2}\%1\right) \sin\left(\frac{1}{2}\%1\right) \\
&- 8364 \%1 \pi^4 \beta^2 \cos\left(\frac{1}{2}\%1\right) \sin\left(\frac{1}{2}\%1\right) + 1640 \%1^3 \pi^4 \cos\left(\frac{1}{2}\%1\right) \sin\left(\frac{1}{2}\%1\right) \\
&+ 1200 \beta^3 \%1^3 \lambda^2 \pi^2 \mu \cos\left(\frac{1}{2}\%1\right) \sin\left(\frac{1}{2}\%1\right) - 120 \beta^3 \%1^3 \lambda^2 \pi^2 \cos\left(\frac{1}{2}\%1\right) \sin\left(\frac{1}{2}\%1\right) \\
&+ 8 \%1^7 \lambda^4 \cos\left(\frac{1}{2}\%1\right) \sin\left(\frac{1}{2}\%1\right) + 240 \beta \%1^5 \lambda^2 \pi^2 \cos\left(\frac{1}{2}\%1\right) \sin\left(\frac{1}{2}\%1\right) \\
&- 4920 \beta \%1^3 \pi^4 \cos\left(\frac{1}{2}\%1\right) \sin\left(\frac{1}{2}\%1\right) - 320 \beta^3 \%1^5 \pi^2 \lambda^2 \mu \cos\left(\frac{1}{2}\%1\right) \sin\left(\frac{1}{2}\%1\right) \\
&+ 320 \beta^3 \%1^5 \pi^2 \lambda^2 \mu \cos\left(\frac{1}{2}\%1\right)^3 \sin\left(\frac{1}{2}\%1\right) - 8 \beta^3 \%1^7 \lambda^4 \cos\left(\frac{1}{2}\%1\right) \sin\left(\frac{1}{2}\%1\right) \\
&- 24 \beta \%1^7 \lambda^4 \cos\left(\frac{1}{2}\%1\right) \sin\left(\frac{1}{2}\%1\right) + 48 \%1^6 \lambda^4 \beta^2 \cos\left(\frac{1}{2}\%1\right)^2 \\
&+ 120 \%1^3 \lambda^2 \pi^2 \beta^2 \cos\left(\frac{1}{2}\%1\right) \sin\left(\frac{1}{2}\%1\right) - 960 \beta \%1^5 \lambda^2 \pi^2 \mu \cos\left(\frac{1}{2}\%1\right) \sin\left(\frac{1}{2}\%1\right) \\
&+ 960 \beta \%1^5 \lambda^2 \pi^2 \mu \cos\left(\frac{1}{2}\%1\right)^3 \sin\left(\frac{1}{2}\%1\right) + 8364 \beta^3 \%1 \pi^4 \cos\left(\frac{1}{2}\%1\right) \sin\left(\frac{1}{2}\%1\right) \\
&- 960 \beta^3 \%1^4 \pi^2 \lambda^2 \mu \cos\left(\frac{1}{2}\%1\right)^2 + 80 \beta^3 \%1^5 \pi^2 \lambda^2 \cos\left(\frac{1}{2}\%1\right) \sin\left(\frac{1}{2}\%1\right) \\
&+ 9840 \%1^2 \pi^4 \beta^2 \cos\left(\frac{1}{2}\%1\right)^2 + 1920 \%1^4 \pi^2 \lambda^2 \mu \beta^2 \cos\left(\frac{1}{2}\%1\right)^2
\end{aligned}
$$

$$- 480\,\%1^4\,\pi^2\,\lambda^2\,\beta^2\cos\left(\frac{1}{2}\,\%1\right)^2\Bigg)\Big/\left(b^2\,\%1^4\,\lambda^3\right)$$

$$\%1 := \arccos\left(\frac{1}{2}\,\frac{\mu}{-1+\mu}\right)$$

> Z4:=solve(U, X);

$$Z4 := -\Bigg(-6\,\%1^6\,\lambda^4\,\beta^2 - 492\,\beta^2\,\%1^4\,\pi^4 - 4\,\beta^2\,\%1^8\,\lambda^4 - 600\,\%1^4\,\pi^2\,\lambda^2\,\mu\,\beta^2 - 40\,\beta^2\,\%1^6\,\lambda^2\,\pi^2$$
$$+ 60\,\%1^4\,\lambda^2\,\pi^2\,\beta^2 + 300\,\beta^3\,\%1^4\,\pi^2\,\lambda^2\,\mu - 492\,\%1^4\,\pi^4 + 123\,\beta^3\,\%1^4\,\pi^4 + \beta^3\,\%1^8\,\lambda^4$$
$$+ 6\,\beta\,\%1^8\,\lambda^4 + 2091\,\beta^3\,\%1^2\,\pi^4 + 10\,\beta^3\,\%1^6\,\lambda^2\,\pi^2 - 960\,\beta^3\,\pi^2\,\lambda^2\,\%1^2\,\mu + 60\,\beta\,\%1^6\,\lambda^2\,\pi^2$$
$$+ 480\,\beta\,\pi^2\,\lambda^2\,\%1^4\,\mu - 40\,\%1^6\,\lambda^2\,\pi^2 + 3936\,\beta\,\pi^4\,\%1^2 + 738\,\beta\,\%1^4\,\pi^4 - 7872\,\beta^3\,\pi^4$$
$$- 4\,\%1^8\,\lambda^4 - 30\,\beta^3\,\%1^4\,\lambda^2\,\pi^2 + 3\,\beta^3\,\%1^6\,\lambda^4 - 4182\,\%1^2\,\pi^4\,\beta^2$$
$$+ 984\,\beta^3\,\%1^2\,\pi^4\cos\left(\frac{1}{2}\,\%1\right)^4 - 240\,\beta^3\,\%1^4\,\lambda^2\,\pi^2\cos\left(\frac{1}{2}\,\%1\right)^4$$
$$+ 480\,\%1^4\,\lambda^2\,\pi^2\,\beta^2\cos\left(\frac{1}{2}\,\%1\right)^4 + 480\,\beta^3\,\%1^4\,\pi^2\,\lambda^2\,\mu\cos\left(\frac{1}{2}\,\%1\right)^4$$
$$- 960\,\%1^4\,\pi^2\,\lambda^2\,\mu\,\beta^2\cos\left(\frac{1}{2}\,\%1\right)^4 + 24\,\beta^3\,\%1^6\,\lambda^4\cos\left(\frac{1}{2}\,\%1\right)^4$$
$$- 1968\,\%1^2\,\pi^4\,\beta^2\cos\left(\frac{1}{2}\,\%1\right)^4 + 160\sin\left(\frac{1}{2}\,\%1\right)\%1^5\,\lambda^2\,\pi^2\cos\left(\frac{1}{2}\,\%1\right)^3$$
$$- 656\sin\left(\frac{1}{2}\,\%1\right)\%1^3\,\pi^4\cos\left(\frac{1}{2}\,\%1\right)^3 + 16\,\beta^3\sin\left(\frac{1}{2}\,\%1\right)\%1^7\,\lambda^4\cos\left(\frac{1}{2}\,\%1\right)^3$$
$$- 1968\,\beta^2\sin\left(\frac{1}{2}\,\%1\right)\%1^3\,\pi^4\cos\left(\frac{1}{2}\,\%1\right)^3 + 656\,\beta^3\sin\left(\frac{1}{2}\,\%1\right)\%1^3\,\pi^4\cos\left(\frac{1}{2}\,\%1\right)^3$$
$$+ 24\sin\left(\frac{1}{2}\,\%1\right)\%1^5\,\lambda^4\,\beta^2\cos\left(\frac{1}{2}\,\%1\right)^3 + 240\,\beta^3\sin\left(\frac{1}{2}\,\%1\right)\%1^3\,\pi^2\,\lambda^2\cos\left(\frac{1}{2}\,\%1\right)^3$$
$$- 48\,\beta^2\sin\left(\frac{1}{2}\,\%1\right)\%1^7\,\lambda^4\cos\left(\frac{1}{2}\,\%1\right)^3 - 480\,\beta^3\sin\left(\frac{1}{2}\,\%1\right)\%1^3\,\pi^2\,\lambda^2\,\mu\cos\left(\frac{1}{2}\,\%1\right)^3$$
$$- 480\,\beta\sin\left(\frac{1}{2}\,\%1\right)\%1^5\,\lambda^2\,\pi^2\cos\left(\frac{1}{2}\,\%1\right)^3 - 240\sin\left(\frac{1}{2}\,\%1\right)\%1^3\,\lambda^2\,\pi^2\,\beta^2\cos\left(\frac{1}{2}\,\%1\right)^3$$
$$+ 1968\,\beta\sin\left(\frac{1}{2}\,\%1\right)\%1^3\,\pi^4\cos\left(\frac{1}{2}\,\%1\right)^3 + 480\,\beta^2\sin\left(\frac{1}{2}\,\%1\right)\%1^5\,\lambda^2\,\pi^2\cos\left(\frac{1}{2}\,\%1\right)^3$$

$$
\begin{aligned}
&- 24\,\beta^3 \sin\left(\frac{1}{2}\,\%1\right) \%1^5\,\lambda^4 \cos\left(\frac{1}{2}\,\%1\right)^3 - 16 \sin\left(\frac{1}{2}\,\%1\right) \%1^7\,\lambda^4 \cos\left(\frac{1}{2}\,\%1\right)^3 \\
&- 984\,\beta^3 \sin\left(\frac{1}{2}\,\%1\right) \%1\,\pi^4 \cos\left(\frac{1}{2}\,\%1\right)^3 + 48\,\beta \sin\left(\frac{1}{2}\,\%1\right) \%1^7\,\lambda^4 \cos\left(\frac{1}{2}\,\%1\right)^3 \\
&+ 480 \sin\left(\frac{1}{2}\,\%1\right) \%1^3\,\lambda^2\,\pi^2\,\mu\,\beta^2 \cos\left(\frac{1}{2}\,\%1\right)^3 + 984 \sin\left(\frac{1}{2}\,\%1\right) \%1\,\pi^4\,\beta^2 \cos\left(\frac{1}{2}\,\%1\right)^3 \\
&- 160\,\beta^3 \sin\left(\frac{1}{2}\,\%1\right) \%1^5\,\lambda^2\,\pi^2 \cos\left(\frac{1}{2}\,\%1\right)^3 - 48\,\%1^6\,\lambda^4\,\beta^2 \cos\left(\frac{1}{2}\,\%1\right)^4 \\
&+ 8364\,\beta^3\,\pi^4 \cos\left(\frac{1}{2}\,\%1\right)^2 - 492\,\beta^3\,\pi^4 \cos\left(\frac{1}{2}\,\%1\right)^4 - 960 \cos\left(\frac{1}{2}\,\%1\right)^2 \beta\,\pi^2\,\lambda^2\,\%1^4\,\mu \\
&+ 480\,\beta\,\pi^2\,\lambda^2\,\%1^4\,\mu \cos\left(\frac{1}{2}\,\%1\right)^4 - 4920\,\beta\,\pi^4\,\%1^2 \cos\left(\frac{1}{2}\,\%1\right)^2 \\
&+ 984\,\beta\,\pi^4\,\%1^2 \cos\left(\frac{1}{2}\,\%1\right)^4 + 1200\,\beta^3\,\pi^2\,\lambda^2\,\%1^2\,\mu \cos\left(\frac{1}{2}\,\%1\right)^2 \\
&- 240\,\beta^3\,\pi^2\,\lambda^2\,\%1^2\,\mu \cos\left(\frac{1}{2}\,\%1\right)^4 + 24\,\beta^2\,\%1^7\,\lambda^4 \cos\left(\frac{1}{2}\,\%1\right) \sin\left(\frac{1}{2}\,\%1\right) \\
&+ 4920\,\beta^2\,\%1^3\,\pi^4 \cos\left(\frac{1}{2}\,\%1\right) \sin\left(\frac{1}{2}\,\%1\right) - 1640\,\beta^3\,\%1^3\,\pi^4 \cos\left(\frac{1}{2}\,\%1\right) \sin\left(\frac{1}{2}\,\%1\right) \\
&+ 320\,\%1^5\,\lambda^2\,\pi^2\,\mu \cos\left(\frac{1}{2}\,\%1\right) \sin\left(\frac{1}{2}\,\%1\right) - 320\,\%1^5\,\lambda^2\,\pi^2\,\mu \cos\left(\frac{1}{2}\,\%1\right)^3 \sin\left(\frac{1}{2}\,\%1\right) \\
&- 240\,\beta^2\,\%1^5\,\lambda^2\,\pi^2 \cos\left(\frac{1}{2}\,\%1\right) \sin\left(\frac{1}{2}\,\%1\right) + 12\,\beta^3\,\lambda^4\,\%1^4 \cos\left(\frac{1}{2}\,\%1\right)^2 \\
&- 12 \cos\left(\frac{1}{2}\,\%1\right)^4 \beta^3\,\lambda^4\,\%1^4 - 1200\,\%1^3\,\lambda^2\,\pi^2\,\mu\,\beta^2 \cos\left(\frac{1}{2}\,\%1\right) \sin\left(\frac{1}{2}\,\%1\right) \\
&+ 240\,\beta\,\lambda^2\,\pi^2\,\%1^4 \cos\left(\frac{1}{2}\,\%1\right)^2 - 240 \cos\left(\frac{1}{2}\,\%1\right)^4 \beta\,\lambda^2\,\pi^2\,\%1^4 - 24\,\beta\,\lambda^4\,\%1^6 \cos\left(\frac{1}{2}\,\%1\right)^2 \\
&+ 24 \cos\left(\frac{1}{2}\,\%1\right)^4 \beta\,\lambda^4\,\%1^6 + 240\,\beta^3\,\%1^4\,\pi^2\,\lambda^2 \cos\left(\frac{1}{2}\,\%1\right)^2 \\
&- 120\,\beta^3\,\pi^2\,\lambda^2\,\%1^2 \cos\left(\frac{1}{2}\,\%1\right)^2 + 120 \cos\left(\frac{1}{2}\,\%1\right)^4 \beta^3\,\pi^2\,\lambda^2\,\%1^2 \\
&+ 960\,\beta^2\,\%1^5\,\lambda^2\,\pi^2\,\mu \cos\left(\frac{1}{2}\,\%1\right) \sin\left(\frac{1}{2}\,\%1\right)
\end{aligned}
$$

$$
\begin{aligned}
&- 960\,\beta^2\,\%1^5\,\lambda^2\,\pi^2\,\mu\cos\left(\frac{1}{2}\%1\right)^3\sin\left(\frac{1}{2}\%1\right) - 80\,\%1^5\,\lambda^2\,\pi^2\cos\left(\frac{1}{2}\%1\right)\sin\left(\frac{1}{2}\%1\right)\\
&- 12\,\%1^5\,\lambda^4\,\beta^2\cos\left(\frac{1}{2}\%1\right)\sin\left(\frac{1}{2}\%1\right) - 4920\,\beta^3\,\%1^2\,\pi^4\cos\left(\frac{1}{2}\%1\right)^2\\
&- 24\,\beta^3\,\%1^6\,\lambda^4\cos\left(\frac{1}{2}\%1\right)^2 + 12\,\beta^3\,\%1^5\,\lambda^4\cos\left(\frac{1}{2}\%1\right)\sin\left(\frac{1}{2}\%1\right)\\
&- 8364\,\%1\,\pi^4\,\beta^2\cos\left(\frac{1}{2}\%1\right)\sin\left(\frac{1}{2}\%1\right) + 1640\,\%1^3\,\pi^4\cos\left(\frac{1}{2}\%1\right)\sin\left(\frac{1}{2}\%1\right)\\
&+ 1200\,\beta^3\,\%1^3\,\lambda^2\,\pi^2\,\mu\cos\left(\frac{1}{2}\%1\right)\sin\left(\frac{1}{2}\%1\right) - 120\,\beta^3\,\%1^3\,\lambda^2\,\pi^2\cos\left(\frac{1}{2}\%1\right)\sin\left(\frac{1}{2}\%1\right)\\
&+ 8\,\%1^7\,\lambda^4\cos\left(\frac{1}{2}\%1\right)\sin\left(\frac{1}{2}\%1\right) + 240\,\beta\,\%1^5\,\lambda^2\,\pi^2\cos\left(\frac{1}{2}\%1\right)\sin\left(\frac{1}{2}\%1\right)\\
&- 4920\,\beta\,\%1^3\,\pi^4\cos\left(\frac{1}{2}\%1\right)\sin\left(\frac{1}{2}\%1\right) - 320\,\beta^3\,\%1^5\,\pi^2\,\lambda^2\,\mu\cos\left(\frac{1}{2}\%1\right)\sin\left(\frac{1}{2}\%1\right)\\
&+ 320\,\beta^3\,\%1^5\,\pi^2\,\lambda^2\,\mu\cos\left(\frac{1}{2}\%1\right)^3\sin\left(\frac{1}{2}\%1\right) - 8\,\beta^3\,\%1^7\,\lambda^4\cos\left(\frac{1}{2}\%1\right)\sin\left(\frac{1}{2}\%1\right)\\
&- 24\,\beta\,\%1^7\,\lambda^4\cos\left(\frac{1}{2}\%1\right)\sin\left(\frac{1}{2}\%1\right) + 48\,\%1^6\,\lambda^4\,\beta^2\cos\left(\frac{1}{2}\%1\right)^2\\
&+ 120\,\%1^3\,\lambda^2\,\pi^2\,\beta^2\cos\left(\frac{1}{2}\%1\right)\sin\left(\frac{1}{2}\%1\right) - 960\,\beta\,\%1^5\,\lambda^2\,\pi^2\,\mu\cos\left(\frac{1}{2}\%1\right)\sin\left(\frac{1}{2}\%1\right)\\
&+ 960\,\beta\,\%1^5\,\lambda^2\,\pi^2\,\mu\cos\left(\frac{1}{2}\%1\right)^3\sin\left(\frac{1}{2}\%1\right) + 8364\,\beta^3\,\%1\,\pi^4\cos\left(\frac{1}{2}\%1\right)\sin\left(\frac{1}{2}\%1\right)\\
&- 960\,\beta^3\,\%1^4\,\pi^2\,\lambda^2\,\mu\cos\left(\frac{1}{2}\%1\right)^2 + 80\,\beta^3\,\%1^5\,\pi^2\,\lambda^2\cos\left(\frac{1}{2}\%1\right)\sin\left(\frac{1}{2}\%1\right)\\
&+ 9840\,\%1^2\,\pi^4\,\beta^2\cos\left(\frac{1}{2}\%1\right)^2 + 1920\,\%1^4\,\pi^2\,\lambda^2\,\mu\,\beta^2\cos\left(\frac{1}{2}\%1\right)^2\\
&- 480\,\%1^4\,\pi^2\,\lambda^2\,\beta^2\cos\left(\frac{1}{2}\%1\right)^2\Bigg)\Bigg/\Bigg(200\,\pi^2\,b^2\,\lambda^2\,\%1^3\,\beta\cos\left(\frac{1}{2}\%1\right)\sin\left(\frac{1}{2}\%1\right)\\
&+ 60\,\pi^2\,b^2\,\lambda^2\,\%1^4 - 80\,\pi^2\,b^2\,\lambda^2\,\%1^3\,\beta\sin\left(\frac{1}{2}\%1\right)\cos\left(\frac{1}{2}\%1\right)^3\\
&+ 80\,\pi^2\,b^2\,\lambda^2\,\%1^3\sin\left(\frac{1}{2}\%1\right)\cos\left(\frac{1}{2}\%1\right)^3 - 30\,\pi^2\,b^2\,\lambda^2\,\%1^4\,\beta - 160\,\pi^2\,b^2\,\lambda^2\,\%1^2\,\beta
\end{aligned}
$$

$$- 200\,\pi^2 b^2 \lambda^2 \%1^3 \cos\left(\frac{1}{2}\%1\right)\sin\left(\frac{1}{2}\%1\right) + 200\,\pi^2 b^2 \lambda^2 \%1^2 \beta \cos\left(\frac{1}{2}\%1\right)^2$$

$$- 40\cos\left(\frac{1}{2}\%1\right)^4 \pi^2 b^2 \lambda^2 \%1^2 \beta\Bigg)$$

$$\%1 := \arccos\left(\frac{1}{2}\,\frac{\mu}{-1+\mu}\right)$$

> X1:=simplify(Z4);

$$X1 := \frac{1}{10}\Bigg(-6\,\%1^6 \lambda^4 \beta^2 - 492\,\beta^2 \%1^4 \pi^4 - 4\,\beta^2 \%1^8 \lambda^4 - 600\,\%1^4 \pi^2 \lambda^2 \mu\,\beta^2 - 40\,\beta^2 \%1^6 \lambda^2 \pi^2$$

$$+ 60\,\%1^4 \lambda^2 \pi^2 \beta^2 + 300\,\beta^3 \%1^4 \pi^2 \lambda^2 \mu - 492\,\%1^4 \pi^4 + 123\,\beta^3 \%1^4 \pi^4 + \beta^3 \%1^8 \lambda^4$$

$$+ 6\,\beta \%1^8 \lambda^4 + 2091\,\beta^3 \%1^2 \pi^4 + 10\,\beta^3 \%1^6 \lambda^2 \pi^2 - 960\,\beta^3 \pi^2 \lambda^2 \%1^2 \mu + 60\,\beta \%1^6 \lambda^2 \pi^2$$

$$+ 480\,\beta \pi^2 \lambda^2 \%1^4 \mu - 40\,\%1^6 \lambda^2 \pi^2 + 3936\,\beta \pi^4 \%1^2 + 738\,\beta \%1^4 \pi^4 - 7872\,\beta^3 \pi^4$$

$$- 4\,\%1^8 \lambda^4 - 30\,\beta^3 \%1^4 \lambda^2 \pi^2 + 3\,\beta^3 \%1^6 \lambda^4 - 4182\,\%1^2 \pi^4 \beta^2$$

$$+ 984\,\beta^3 \%1^2 \pi^4 \cos\left(\frac{1}{2}\%1\right)^4 - 240\,\beta^3 \%1^4 \lambda^2 \pi^2 \cos\left(\frac{1}{2}\%1\right)^4$$

$$+ 480\,\%1^4 \lambda^2 \pi^2 \beta^2 \cos\left(\frac{1}{2}\%1\right)^4 + 480\,\beta^3 \%1^4 \pi^2 \lambda^2 \mu \cos\left(\frac{1}{2}\%1\right)^4$$

$$- 960\,\%1^4 \pi^2 \lambda^2 \mu\,\beta^2 \cos\left(\frac{1}{2}\%1\right)^4 + 24\,\beta^3 \%1^6 \lambda^4 \cos\left(\frac{1}{2}\%1\right)^4$$

$$- 1968\,\%1^2 \pi^4 \beta^2 \cos\left(\frac{1}{2}\%1\right)^4 + 160 \sin\left(\frac{1}{2}\%1\right)\%1^5 \lambda^2 \pi^2 \cos\left(\frac{1}{2}\%1\right)^3$$

$$- 656 \sin\left(\frac{1}{2}\%1\right)\%1^3 \pi^4 \cos\left(\frac{1}{2}\%1\right)^3 + 16\,\beta^3 \sin\left(\frac{1}{2}\%1\right)\%1^7 \lambda^4 \cos\left(\frac{1}{2}\%1\right)^3$$

$$- 1968\,\beta^2 \sin\left(\frac{1}{2}\%1\right)\%1^3 \pi^4 \cos\left(\frac{1}{2}\%1\right)^3 + 656\,\beta^3 \sin\left(\frac{1}{2}\%1\right)\%1^3 \pi^4 \cos\left(\frac{1}{2}\%1\right)^3$$

$$+ 24 \sin\left(\frac{1}{2}\%1\right)\%1^5 \lambda^4 \beta^2 \cos\left(\frac{1}{2}\%1\right)^3 + 240\,\beta^3 \sin\left(\frac{1}{2}\%1\right)\%1^3 \pi^2 \lambda^2 \cos\left(\frac{1}{2}\%1\right)^3$$

$$- 48\,\beta^2 \sin\left(\frac{1}{2}\%1\right)\%1^7 \lambda^4 \cos\left(\frac{1}{2}\%1\right)^3 - 480\,\beta^3 \sin\left(\frac{1}{2}\%1\right)\%1^3 \pi^2 \lambda^2 \mu \cos\left(\frac{1}{2}\%1\right)^3$$

$$- 480\,\beta \sin\left(\frac{1}{2}\%1\right)\%1^5 \lambda^2 \pi^2 \cos\left(\frac{1}{2}\%1\right)^3 - 240 \sin\left(\frac{1}{2}\%1\right)\%1^3 \lambda^2 \pi^2 \beta^2 \cos\left(\frac{1}{2}\%1\right)^3$$

$$+ 1968\,\beta \sin\left(\frac{1}{2}\,\%1\right)\%1^3\,\pi^4 \cos\left(\frac{1}{2}\,\%1\right)^3 + 480\,\beta^2 \sin\left(\frac{1}{2}\,\%1\right)\%1^5\,\lambda^2\,\pi^2 \cos\left(\frac{1}{2}\,\%1\right)^3$$

$$- 24\,\beta^3 \sin\left(\frac{1}{2}\,\%1\right)\%1^5\,\lambda^4 \cos\left(\frac{1}{2}\,\%1\right)^3 - 16 \sin\left(\frac{1}{2}\,\%1\right)\%1^7\,\lambda^4 \cos\left(\frac{1}{2}\,\%1\right)^3$$

$$- 984\,\beta^3 \sin\left(\frac{1}{2}\,\%1\right)\%1\,\pi^4 \cos\left(\frac{1}{2}\,\%1\right)^3 + 48\,\beta \sin\left(\frac{1}{2}\,\%1\right)\%1^7\,\lambda^4 \cos\left(\frac{1}{2}\,\%1\right)^3$$

$$+ 480 \sin\left(\frac{1}{2}\,\%1\right)\%1^3\,\lambda^2\,\pi^2\,\mu\,\beta^2 \cos\left(\frac{1}{2}\,\%1\right)^3 + 984 \sin\left(\frac{1}{2}\,\%1\right)\%1\,\pi^4\,\beta^2 \cos\left(\frac{1}{2}\,\%1\right)^3$$

$$- 160\,\beta^3 \sin\left(\frac{1}{2}\,\%1\right)\%1^5\,\lambda^2\,\pi^2 \cos\left(\frac{1}{2}\,\%1\right)^3 - 48\,\%1^6\,\lambda^4\,\beta^2 \cos\left(\frac{1}{2}\,\%1\right)^4$$

$$+ 8364\,\beta^3\,\pi^4 \cos\left(\frac{1}{2}\,\%1\right)^2 - 492\,\beta^3\,\pi^4 \cos\left(\frac{1}{2}\,\%1\right)^4 - 960 \cos\left(\frac{1}{2}\,\%1\right)^2 \beta\,\pi^2\,\lambda^2\,\%1^4\,\mu$$

$$+ 480\,\beta\,\pi^2\,\lambda^2\,\%1^4\,\mu \cos\left(\frac{1}{2}\,\%1\right)^4 - 4920\,\beta\,\pi^4\,\%1^2 \cos\left(\frac{1}{2}\,\%1\right)^2$$

$$+ 984\,\beta\,\pi^4\,\%1^2 \cos\left(\frac{1}{2}\,\%1\right)^4 + 1200\,\beta^3\,\pi^2\,\lambda^2\,\%1^2\,\mu \cos\left(\frac{1}{2}\,\%1\right)^2$$

$$- 240\,\beta^3\,\pi^2\,\lambda^2\,\%1^2\,\mu \cos\left(\frac{1}{2}\,\%1\right)^4 + 24\,\beta^2\,\%1^7\,\lambda^4 \cos\left(\frac{1}{2}\,\%1\right)\sin\left(\frac{1}{2}\,\%1\right)$$

$$+ 4920\,\beta^2\,\%1^3\,\pi^4 \cos\left(\frac{1}{2}\,\%1\right)\sin\left(\frac{1}{2}\,\%1\right) - 1640\,\beta^3\,\%1^3\,\pi^4 \cos\left(\frac{1}{2}\,\%1\right)\sin\left(\frac{1}{2}\,\%1\right)$$

$$+ 320\,\%1^5\,\lambda^2\,\pi^2\,\mu \cos\left(\frac{1}{2}\,\%1\right)\sin\left(\frac{1}{2}\,\%1\right) - 320\,\%1^5\,\lambda^2\,\pi^2\,\mu \cos\left(\frac{1}{2}\,\%1\right)^3 \sin\left(\frac{1}{2}\,\%1\right)$$

$$- 240\,\beta^2\,\%1^5\,\lambda^2\,\pi^2 \cos\left(\frac{1}{2}\,\%1\right)\sin\left(\frac{1}{2}\,\%1\right) + 12\,\beta^3\,\lambda^4\,\%1^4 \cos\left(\frac{1}{2}\,\%1\right)^2$$

$$- 12 \cos\left(\frac{1}{2}\,\%1\right)^4 \beta^3\,\lambda^4\,\%1^4 - 1200\,\%1^3\,\lambda^2\,\pi^2\,\mu\,\beta^2 \cos\left(\frac{1}{2}\,\%1\right)\sin\left(\frac{1}{2}\,\%1\right)$$

$$+ 240\,\beta\,\lambda^2\,\pi^2\,\%1^4 \cos\left(\frac{1}{2}\,\%1\right)^2 - 240 \cos\left(\frac{1}{2}\,\%1\right)^4 \beta\,\lambda^2\,\pi^2\,\%1^4 - 24\,\beta\,\lambda^4\,\%1^6 \cos\left(\frac{1}{2}\,\%1\right)^2$$

$$+ 24 \cos\left(\frac{1}{2}\,\%1\right)^4 \beta\,\lambda^4\,\%1^6 + 240\,\beta^3\,\%1^4\,\pi^2\,\lambda^2 \cos\left(\frac{1}{2}\,\%1\right)^2$$

$$- 120\,\beta^3\,\pi^2\,\lambda^2\,\%1^2 \cos\left(\frac{1}{2}\,\%1\right)^2 + 120 \cos\left(\frac{1}{2}\,\%1\right)^4 \beta^3\,\pi^2\,\lambda^2\,\%1^2$$

$$+ 960\,\beta^2\,\%1^5\,\lambda^2\,\pi^2\,\mu\cos\left(\frac{1}{2}\%1\right)\sin\left(\frac{1}{2}\%1\right)$$

$$- 960\,\beta^2\,\%1^5\,\lambda^2\,\pi^2\,\mu\cos\left(\frac{1}{2}\%1\right)^3\sin\left(\frac{1}{2}\%1\right) - 80\,\%1^5\,\lambda^2\,\pi^2\cos\left(\frac{1}{2}\%1\right)\sin\left(\frac{1}{2}\%1\right)$$

$$- 12\,\%1^5\,\lambda^4\,\beta^2\cos\left(\frac{1}{2}\%1\right)\sin\left(\frac{1}{2}\%1\right) - 4920\,\beta^3\,\%1^2\,\pi^4\cos\left(\frac{1}{2}\%1\right)^2$$

$$- 24\,\beta^3\,\%1^6\,\lambda^4\cos\left(\frac{1}{2}\%1\right)^2 + 12\,\beta^3\,\%1^5\,\lambda^4\cos\left(\frac{1}{2}\%1\right)\sin\left(\frac{1}{2}\%1\right)$$

$$- 8364\,\%1\,\pi^4\,\beta^2\cos\left(\frac{1}{2}\%1\right)\sin\left(\frac{1}{2}\%1\right) + 1640\,\%1^3\,\pi^4\cos\left(\frac{1}{2}\%1\right)\sin\left(\frac{1}{2}\%1\right)$$

$$+ 1200\,\beta^3\,\%1^3\,\lambda^2\,\pi^2\,\mu\cos\left(\frac{1}{2}\%1\right)\sin\left(\frac{1}{2}\%1\right) - 120\,\beta^3\,\%1^3\,\lambda^2\,\pi^2\cos\left(\frac{1}{2}\%1\right)\sin\left(\frac{1}{2}\%1\right)$$

$$+ 8\,\%1^7\,\lambda^4\cos\left(\frac{1}{2}\%1\right)\sin\left(\frac{1}{2}\%1\right) + 240\,\beta\,\%1^5\,\lambda^2\,\pi^2\cos\left(\frac{1}{2}\%1\right)\sin\left(\frac{1}{2}\%1\right)$$

$$- 4920\,\beta\,\%1^3\,\pi^4\cos\left(\frac{1}{2}\%1\right)\sin\left(\frac{1}{2}\%1\right) - 320\,\beta^3\,\%1^5\,\pi^2\,\lambda^2\,\mu\cos\left(\frac{1}{2}\%1\right)\sin\left(\frac{1}{2}\%1\right)$$

$$+ 320\,\beta^3\,\%1^5\,\pi^2\,\lambda^2\,\mu\cos\left(\frac{1}{2}\%1\right)^3\sin\left(\frac{1}{2}\%1\right) - 8\,\beta^3\,\%1^7\,\lambda^4\cos\left(\frac{1}{2}\%1\right)\sin\left(\frac{1}{2}\%1\right)$$

$$- 24\,\beta\,\%1^7\,\lambda^4\cos\left(\frac{1}{2}\%1\right)\sin\left(\frac{1}{2}\%1\right) + 48\,\%1^6\,\lambda^4\,\beta^2\cos\left(\frac{1}{2}\%1\right)^2$$

$$+ 120\,\%1^3\,\lambda^2\,\pi^2\,\beta^2\cos\left(\frac{1}{2}\%1\right)\sin\left(\frac{1}{2}\%1\right) - 960\,\beta\,\%1^5\,\lambda^2\,\pi^2\,\mu\cos\left(\frac{1}{2}\%1\right)\sin\left(\frac{1}{2}\%1\right)$$

$$+ 960\,\beta\,\%1^5\,\lambda^2\,\pi^2\,\mu\cos\left(\frac{1}{2}\%1\right)^3\sin\left(\frac{1}{2}\%1\right) + 8364\,\beta^3\,\%1\,\pi^4\cos\left(\frac{1}{2}\%1\right)\sin\left(\frac{1}{2}\%1\right)$$

$$- 960\,\beta^3\,\%1^4\,\pi^2\,\lambda^2\,\mu\cos\left(\frac{1}{2}\%1\right)^2 + 80\,\beta^3\,\%1^5\,\pi^2\,\lambda^2\cos\left(\frac{1}{2}\%1\right)\sin\left(\frac{1}{2}\%1\right)$$

$$+ 9840\,\%1^2\,\pi^4\,\beta^2\cos\left(\frac{1}{2}\%1\right)^2 + 1920\,\%1^4\,\pi^2\,\lambda^2\,\mu\,\beta^2\cos\left(\frac{1}{2}\%1\right)^2$$

$$- 480\,\%1^4\,\pi^2\,\lambda^2\,\beta^2\cos\left(\frac{1}{2}\%1\right)^2\Bigg) \Bigg/ \Bigg(\pi^2\,b^2\,\lambda^2\,\%1^2\left(-20\,\%1\,\beta\cos\left(\frac{1}{2}\%1\right)\sin\left(\frac{1}{2}\%1\right)\right.$$

$$\left. - 6\,\%1^2 + 8\,\%1\,\beta\sin\left(\frac{1}{2}\%1\right)\cos\left(\frac{1}{2}\%1\right)^3 - 8\,\%1\sin\left(\frac{1}{2}\%1\right)\cos\left(\frac{1}{2}\%1\right)^3 + 3\,\beta\,\%1^2\right.$$

$$+ 16\beta + 20\,\%1\cos\left(\frac{1}{2}\%1\right)\sin\left(\frac{1}{2}\%1\right) - 20\beta\cos\left(\frac{1}{2}\%1\right)^2 + 4\cos\left(\frac{1}{2}\%1\right)^4\beta\Bigg)\Bigg)$$

$$\%1 := \arccos\left(\frac{1}{2}\,\frac{\mu}{-1+\mu}\right)$$

> X2:=collect(X1, [sin(n/2), cos(n/2)], distributed, factor);

$$X2 := \frac{1}{10}\Bigg(-6\,\%1^6\lambda^4\beta^2 - 492\,\beta^2\%1^4\pi^4 - 4\,\beta^2\%1^8\lambda^4 - 600\,\%1^4\pi^2\lambda^2\mu\beta^2 - 40\,\beta^2\%1^6\lambda^2\pi^2$$
$$+ 60\,\%1^4\lambda^2\pi^2\beta^2 + 300\,\beta^3\%1^4\pi^2\lambda^2\mu - 492\,\%1^4\pi^4 + 123\,\beta^3\%1^4\pi^4 + \beta^3\%1^8\lambda^4$$
$$+ 6\,\beta\%1^8\lambda^4 + 2091\,\beta^3\%1^2\pi^4 + 10\,\beta^3\%1^6\lambda^2\pi^2 - 960\,\beta^3\pi^2\lambda^2\%1^2\mu + 60\,\beta\%1^6\lambda^2\pi^2$$
$$+ 480\,\beta\pi^2\lambda^2\%1^4\mu - 40\,\%1^6\lambda^2\pi^2 + 3936\,\beta\pi^4\%1^2 + 738\,\beta\%1^4\pi^4 - 7872\,\beta^3\pi^4$$
$$- 4\,\%1^8\lambda^4 - 30\,\beta^3\%1^4\lambda^2\pi^2 + 3\,\beta^3\%1^6\lambda^4 - 4182\,\%1^2\pi^4\beta^2 + 8\,\%1\,(\beta-1)$$
$$\left(2\,\%1^2\beta^2 - 3\,\beta^2 - 4\,\beta\%1^2 + 2\,\%1^2\right)\left(\lambda^4\%1^4 - 10\,\pi^2\%1^2\lambda^2 + 20\,\pi^2\%1^2\lambda^2\mu + 41\,\pi^4\right)$$
$$\cos\left(\frac{1}{2}\%1\right)^3\sin\left(\frac{1}{2}\%1\right) + 12\left(2\,\%1^2\beta^2 + 2\,\%1^2 - 4\,\beta\%1^2 - \beta^2\right)\beta$$
$$\left(\lambda^4\%1^4 - 10\,\pi^2\%1^2\lambda^2 + 20\,\pi^2\%1^2\lambda^2\mu + 41\,\pi^4\right)\cos\left(\frac{1}{2}\%1\right)^4 - 12\,\beta\left(80\,\%1^4\pi^2\lambda^2\mu\beta^2\right.$$
$$- 100\,\pi^2\lambda^2\%1^2\mu\beta^2 - 697\,\pi^4\beta^2 - \lambda^4\%1^4\beta^2 + 2\,\%1^6\lambda^4\beta^2 + 410\,\%1^2\pi^4\beta^2$$
$$+ 10\,\lambda^2\pi^2\%1^2\beta^2 - 20\,\%1^4\lambda^2\pi^2\beta^2 + 40\,\beta\lambda^2\pi^2\%1^4 - 160\,\beta\pi^2\lambda^2\%1^4\mu - 4\,\beta\lambda^4\%1^6$$
$$\left.- 820\,\beta\pi^4\%1^2 + 2\,\lambda^4\%1^6 + 80\,\lambda^2\pi^2\%1^4\mu + 410\,\pi^4\%1^2 - 20\,\lambda^2\pi^2\%1^4\right)\cos\left(\frac{1}{2}\%1\right)^2$$
$$- 4\,(\beta-1)\,\%1\left(2\,\%1^6\lambda^4\beta^2 - 4\,\beta\lambda^4\%1^6 + 2\,\lambda^4\%1^6 - 20\,\%1^4\lambda^2\pi^2\beta^2 - 3\,\lambda^4\%1^4\beta^2\right.$$
$$+ 80\,\%1^4\pi^2\lambda^2\mu\beta^2 - 160\,\beta\pi^2\lambda^2\%1^4\mu + 40\,\beta\lambda^2\pi^2\%1^4 - 20\,\lambda^2\pi^2\%1^4$$
$$+ 80\,\lambda^2\pi^2\%1^4\mu + 30\,\lambda^2\pi^2\%1^2\beta^2 + 410\,\%1^2\pi^4\beta^2 - 300\,\pi^2\lambda^2\%1^2\mu\beta^2$$
$$\left.- 820\,\beta\pi^4\%1^2 + 410\,\pi^4\%1^2 - 2091\,\pi^4\beta^2\right)\sin\left(\frac{1}{2}\%1\right)\cos\left(\frac{1}{2}\%1\right)\Bigg)\Bigg/\Bigg(\pi^2 b^2\lambda^2\%1^2\Bigg($$
$$3\,\beta\%1^2 - 6\,\%1^2 + 16\,\beta - 20\,\beta\cos\left(\frac{1}{2}\%1\right)^2 + 4\cos\left(\frac{1}{2}\%1\right)^4\beta$$
$$+ 8\,(\beta-1)\,\%1\cos\left(\frac{1}{2}\%1\right)^3\sin\left(\frac{1}{2}\%1\right) - 20\,(\beta-1)\,\%1\sin\left(\frac{1}{2}\%1\right)\cos\left(\frac{1}{2}\%1\right)\Bigg)\Bigg)$$

$$\%1 := \arccos\left(\frac{1}{2}\,\frac{\mu}{-1+\mu}\right)$$

> K2:=simplify(X2*b^2/Pi^2);

$$K2 := \frac{1}{10}\Bigg(-6\,\%1^6\lambda^4\beta^2 - 492\,\beta^2\,\%1^4\pi^4 - 4\,\beta^2\,\%1^8\lambda^4 - 600\,\%1^4\pi^2\lambda^2\mu\,\beta^2 - 40\,\beta^2\,\%1^6\lambda^2\pi^2$$
$$+ 60\,\%1^4\lambda^2\pi^2\beta^2 + 300\,\beta^3\,\%1^4\pi^2\lambda^2\mu - 492\,\%1^4\pi^4 + 123\,\beta^3\,\%1^4\pi^4 + \beta^3\,\%1^8\lambda^4$$
$$+ 6\,\beta\,\%1^8\lambda^4 + 2091\,\beta^3\,\%1^2\pi^4 + 10\,\beta^3\,\%1^6\lambda^2\pi^2 - 960\,\beta^3\pi^2\lambda^2\,\%1^2\mu + 60\,\beta\,\%1^6\lambda^2\pi^2$$
$$+ 480\,\beta\,\pi^2\lambda^2\,\%1^4\mu - 40\,\%1^6\lambda^2\pi^2 + 3936\,\beta\,\pi^4\,\%1^2 + 738\,\beta\,\%1^4\pi^4 - 7872\,\beta^3\pi^4$$
$$- 4\,\%1^8\lambda^4 - 30\,\beta^3\,\%1^4\lambda^2\pi^2 + 3\,\beta^3\,\%1^6\lambda^4 - 4182\,\%1^2\pi^4\beta^2$$
$$+ 984\,\beta^3\,\%1^2\pi^4\cos\left(\frac{1}{2}\%1\right)^4 - 240\,\beta^3\,\%1^4\lambda^2\pi^2\cos\left(\frac{1}{2}\%1\right)^4$$
$$+ 480\,\%1^4\lambda^2\pi^2\beta^2\cos\left(\frac{1}{2}\%1\right)^4 + 480\,\beta^3\,\%1^4\pi^2\lambda^2\mu\cos\left(\frac{1}{2}\%1\right)^4$$
$$- 960\,\%1^4\pi^2\lambda^2\mu\,\beta^2\cos\left(\frac{1}{2}\%1\right)^4 + 24\,\beta^3\,\%1^6\lambda^4\cos\left(\frac{1}{2}\%1\right)^4$$
$$- 1968\,\%1^2\pi^4\beta^2\cos\left(\frac{1}{2}\%1\right)^4 + 160\sin\left(\frac{1}{2}\%1\right)\%1^5\lambda^2\pi^2\cos\left(\frac{1}{2}\%1\right)^3$$
$$- 656\sin\left(\frac{1}{2}\%1\right)\%1^3\pi^4\cos\left(\frac{1}{2}\%1\right)^3 + 16\,\beta^3\sin\left(\frac{1}{2}\%1\right)\%1^7\lambda^4\cos\left(\frac{1}{2}\%1\right)^3$$
$$- 1968\,\beta^2\sin\left(\frac{1}{2}\%1\right)\%1^3\pi^4\cos\left(\frac{1}{2}\%1\right)^3 + 656\,\beta^3\sin\left(\frac{1}{2}\%1\right)\%1^3\pi^4\cos\left(\frac{1}{2}\%1\right)^3$$
$$+ 24\sin\left(\frac{1}{2}\%1\right)\%1^5\lambda^4\beta^2\cos\left(\frac{1}{2}\%1\right)^3 + 240\,\beta^3\sin\left(\frac{1}{2}\%1\right)\%1^3\pi^2\lambda^2\cos\left(\frac{1}{2}\%1\right)^3$$
$$- 48\,\beta^2\sin\left(\frac{1}{2}\%1\right)\%1^7\lambda^4\cos\left(\frac{1}{2}\%1\right)^3 - 480\,\beta^3\sin\left(\frac{1}{2}\%1\right)\%1^3\pi^2\lambda^2\mu\cos\left(\frac{1}{2}\%1\right)^3$$
$$- 480\,\beta\sin\left(\frac{1}{2}\%1\right)\%1^5\lambda^2\pi^2\cos\left(\frac{1}{2}\%1\right)^3 - 240\sin\left(\frac{1}{2}\%1\right)\%1^3\lambda^2\pi^2\beta^2\cos\left(\frac{1}{2}\%1\right)^3$$
$$+ 1968\,\beta\sin\left(\frac{1}{2}\%1\right)\%1^3\pi^4\cos\left(\frac{1}{2}\%1\right)^3 + 480\,\beta^2\sin\left(\frac{1}{2}\%1\right)\%1^5\lambda^2\pi^2\cos\left(\frac{1}{2}\%1\right)^3$$
$$- 24\,\beta^3\sin\left(\frac{1}{2}\%1\right)\%1^5\lambda^4\cos\left(\frac{1}{2}\%1\right)^3 - 16\sin\left(\frac{1}{2}\%1\right)\%1^7\lambda^4\cos\left(\frac{1}{2}\%1\right)^3$$

$$
\begin{aligned}
&- 984\,\beta^3 \sin\left(\frac{1}{2}\%1\right)\%1\,\pi^4 \cos\left(\frac{1}{2}\%1\right)^3 + 48\,\beta \sin\left(\frac{1}{2}\%1\right)\%1^7\,\lambda^4 \cos\left(\frac{1}{2}\%1\right)^3 \\
&+ 480 \sin\left(\frac{1}{2}\%1\right)\%1^3\,\lambda^2\,\pi^2\,\mu\,\beta^2 \cos\left(\frac{1}{2}\%1\right)^3 + 984 \sin\left(\frac{1}{2}\%1\right)\%1\,\pi^4\,\beta^2 \cos\left(\frac{1}{2}\%1\right)^3 \\
&- 160\,\beta^3 \sin\left(\frac{1}{2}\%1\right)\%1^5\,\lambda^2\,\pi^2 \cos\left(\frac{1}{2}\%1\right)^3 - 48\,\%1^6\,\lambda^4\,\beta^2 \cos\left(\frac{1}{2}\%1\right)^4 \\
&+ 8364\,\beta^3\,\pi^4 \cos\left(\frac{1}{2}\%1\right)^2 - 492\,\beta^3\,\pi^4 \cos\left(\frac{1}{2}\%1\right)^4 - 960 \cos\left(\frac{1}{2}\%1\right)^2 \beta\,\pi^2\,\lambda^2\,\%1^4\,\mu \\
&+ 480\,\beta\,\pi^2\,\lambda^2\,\%1^4\,\mu \cos\left(\frac{1}{2}\%1\right)^4 - 4920\,\beta\,\pi^4\,\%1^2 \cos\left(\frac{1}{2}\%1\right)^2 \\
&+ 984\,\beta\,\pi^4\,\%1^2 \cos\left(\frac{1}{2}\%1\right)^4 + 1200\,\beta^3\,\pi^2\,\lambda^2\,\%1^2\,\mu \cos\left(\frac{1}{2}\%1\right)^2 \\
&- 240\,\beta^3\,\pi^2\,\lambda^2\,\%1^2\,\mu \cos\left(\frac{1}{2}\%1\right)^4 + 24\,\beta^2\,\%1^7\,\lambda^4 \cos\left(\frac{1}{2}\%1\right)\sin\left(\frac{1}{2}\%1\right) \\
&+ 4920\,\beta^2\,\%1^3\,\pi^4 \cos\left(\frac{1}{2}\%1\right)\sin\left(\frac{1}{2}\%1\right) - 1640\,\beta^3\,\%1^3\,\pi^4 \cos\left(\frac{1}{2}\%1\right)\sin\left(\frac{1}{2}\%1\right) \\
&+ 320\,\%1^5\,\lambda^2\,\pi^2\,\mu \cos\left(\frac{1}{2}\%1\right)\sin\left(\frac{1}{2}\%1\right) - 320\,\%1^5\,\lambda^2\,\pi^2\,\mu \cos\left(\frac{1}{2}\%1\right)^3 \sin\left(\frac{1}{2}\%1\right) \\
&- 240\,\beta^2\,\%1^5\,\lambda^2\,\pi^2 \cos\left(\frac{1}{2}\%1\right)\sin\left(\frac{1}{2}\%1\right) + 12\,\beta^3\,\lambda^4\,\%1^4 \cos\left(\frac{1}{2}\%1\right)^2 \\
&- 12 \cos\left(\frac{1}{2}\%1\right)^4 \beta^3\,\lambda^4\,\%1^4 - 1200\,\%1^3\,\lambda^2\,\pi^2\,\mu\,\beta^2 \cos\left(\frac{1}{2}\%1\right)\sin\left(\frac{1}{2}\%1\right) \\
&+ 240\,\beta\,\lambda^2\,\pi^2\,\%1^4 \cos\left(\frac{1}{2}\%1\right)^2 - 240 \cos\left(\frac{1}{2}\%1\right)^4 \beta\,\lambda^2\,\pi^2\,\%1^4 - 24\,\beta\,\lambda^4\,\%1^6 \cos\left(\frac{1}{2}\%1\right)^2 \\
&+ 24 \cos\left(\frac{1}{2}\%1\right)^4 \beta\,\lambda^4\,\%1^6 + 240\,\beta^3\,\%1^4\,\pi^2\,\lambda^2 \cos\left(\frac{1}{2}\%1\right)^2 \\
&- 120\,\beta^3\,\pi^2\,\lambda^2\,\%1^2 \cos\left(\frac{1}{2}\%1\right)^2 + 120 \cos\left(\frac{1}{2}\%1\right)^4 \beta^3\,\pi^2\,\lambda^2\,\%1^2 \\
&+ 960\,\beta^2\,\%1^5\,\lambda^2\,\pi^2\,\mu \cos\left(\frac{1}{2}\%1\right)\sin\left(\frac{1}{2}\%1\right) \\
&- 960\,\beta^2\,\%1^5\,\lambda^2\,\pi^2\,\mu \cos\left(\frac{1}{2}\%1\right)^3 \sin\left(\frac{1}{2}\%1\right) - 80\,\%1^5\,\lambda^2\,\pi^2 \cos\left(\frac{1}{2}\%1\right)\sin\left(\frac{1}{2}\%1\right)
\end{aligned}
$$

$$
\begin{aligned}
&- 12\,\%1^5\,\lambda^4\,\beta^2\cos\left(\frac{1}{2}\%1\right)\sin\left(\frac{1}{2}\%1\right) - 4920\,\beta^3\,\%1^2\,\pi^4\cos\left(\frac{1}{2}\%1\right)^2 \\
&- 24\,\beta^3\,\%1^6\,\lambda^4\cos\left(\frac{1}{2}\%1\right)^2 + 12\,\beta^3\,\%1^5\,\lambda^4\cos\left(\frac{1}{2}\%1\right)\sin\left(\frac{1}{2}\%1\right) \\
&- 8364\,\%1\,\pi^4\,\beta^2\cos\left(\frac{1}{2}\%1\right)\sin\left(\frac{1}{2}\%1\right) + 1640\,\%1^3\,\pi^4\cos\left(\frac{1}{2}\%1\right)\sin\left(\frac{1}{2}\%1\right) \\
&+ 1200\,\beta^3\,\%1^3\,\lambda^2\,\pi^2\,\mu\cos\left(\frac{1}{2}\%1\right)\sin\left(\frac{1}{2}\%1\right) - 120\,\beta^3\,\%1^3\,\lambda^2\,\pi^2\cos\left(\frac{1}{2}\%1\right)\sin\left(\frac{1}{2}\%1\right) \\
&+ 8\,\%1^7\,\lambda^4\cos\left(\frac{1}{2}\%1\right)\sin\left(\frac{1}{2}\%1\right) + 240\,\beta\,\%1^5\,\lambda^2\,\pi^2\cos\left(\frac{1}{2}\%1\right)\sin\left(\frac{1}{2}\%1\right) \\
&- 4920\,\beta\,\%1^3\,\pi^4\cos\left(\frac{1}{2}\%1\right)\sin\left(\frac{1}{2}\%1\right) - 320\,\beta^3\,\%1^5\,\pi^2\,\lambda^2\,\mu\cos\left(\frac{1}{2}\%1\right)\sin\left(\frac{1}{2}\%1\right) \\
&+ 320\,\beta^3\,\%1^5\,\pi^2\,\lambda^2\,\mu\cos\left(\frac{1}{2}\%1\right)^3\sin\left(\frac{1}{2}\%1\right) - 8\,\beta^3\,\%1^7\,\lambda^4\cos\left(\frac{1}{2}\%1\right)\sin\left(\frac{1}{2}\%1\right) \\
&- 24\,\beta\,\%1^7\,\lambda^4\cos\left(\frac{1}{2}\%1\right)\sin\left(\frac{1}{2}\%1\right) + 48\,\%1^6\,\lambda^4\,\beta^2\cos\left(\frac{1}{2}\%1\right)^2 \\
&+ 120\,\%1^3\,\lambda^2\,\pi^2\,\beta^2\cos\left(\frac{1}{2}\%1\right)\sin\left(\frac{1}{2}\%1\right) - 960\,\beta\,\%1^5\,\lambda^2\,\pi^2\,\mu\cos\left(\frac{1}{2}\%1\right)\sin\left(\frac{1}{2}\%1\right) \\
&+ 960\,\beta\,\%1^5\,\lambda^2\,\pi^2\,\mu\cos\left(\frac{1}{2}\%1\right)^3\sin\left(\frac{1}{2}\%1\right) + 8364\,\beta^3\,\%1\,\pi^4\cos\left(\frac{1}{2}\%1\right)\sin\left(\frac{1}{2}\%1\right) \\
&- 960\,\beta^3\,\%1^4\,\pi^2\,\lambda^2\,\mu\cos\left(\frac{1}{2}\%1\right)^2 + 80\,\beta^3\,\%1^5\,\pi^2\,\lambda^2\cos\left(\frac{1}{2}\%1\right)\sin\left(\frac{1}{2}\%1\right) \\
&+ 9840\,\%1^2\,\pi^4\,\beta^2\cos\left(\frac{1}{2}\%1\right)^2 + 1920\,\%1^4\,\pi^2\,\lambda^2\,\mu\,\beta^2\cos\left(\frac{1}{2}\%1\right)^2 \\
&- 480\,\%1^4\,\pi^2\,\lambda^2\,\beta^2\cos\left(\frac{1}{2}\%1\right)^2\Bigg) \Bigg/ \Bigg(\pi^4\,\lambda^2\,\%1^2\left(-20\,\%1\,\beta\cos\left(\frac{1}{2}\%1\right)\sin\left(\frac{1}{2}\%1\right)\right. \\
&- 6\,\%1^2 + 8\,\%1\,\beta\sin\left(\frac{1}{2}\%1\right)\cos\left(\frac{1}{2}\%1\right)^3 - 8\,\%1\sin\left(\frac{1}{2}\%1\right)\cos\left(\frac{1}{2}\%1\right)^3 + 3\,\beta\,\%1^2 \\
&\left.\left. + 16\,\beta + 20\,\%1\cos\left(\frac{1}{2}\%1\right)\sin\left(\frac{1}{2}\%1\right) - 20\,\beta\cos\left(\frac{1}{2}\%1\right)^2 + 4\cos\left(\frac{1}{2}\%1\right)^4\beta\right)\right)
\end{aligned}
$$

$$\%1 := \arccos\left(\frac{1}{2}\,\frac{\mu}{-1+\mu}\right)$$

> save 'z2.m';

> mu:=1/3; beta:=0;Km2:=simplify(K2);

$$\mu := \frac{1}{3}$$

$$\beta := 0$$

$$Km2 := \frac{1}{15}\left(-369\,\pi^5 - 3\,\lambda^4\,\pi^5 + 3\,\lambda^4 \arccos\left(\frac{1}{4}\right)^5 + 369\,\pi^4 \arccos\left(\frac{1}{4}\right) - 30\,\lambda^2\,\pi^5 \right.$$

$$+ 738\,\pi^4 \sin(\%1)\cos(\%1) + 90\,\lambda^2\,\pi^4 \arccos\left(\frac{1}{4}\right) - 90\,\lambda^2\,\pi^3 \arccos\left(\frac{1}{4}\right)^2$$

$$+ 30\,\lambda^2\,\pi^2 \arccos\left(\frac{1}{4}\right)^3 + 15\,\lambda^4\,\pi^4 \arccos\left(\frac{1}{4}\right) + 24\,\lambda^4 \sin(\%1)\cos(\%1)\,\pi^3 \arccos\left(\frac{1}{4}\right)$$

$$- 36\,\lambda^4 \sin(\%1)\cos(\%1)\,\pi^2 \arccos\left(\frac{1}{4}\right)^2 + 24\,\lambda^4 \sin(\%1)\cos(\%1)\,\pi \arccos\left(\frac{1}{4}\right)^3$$

$$- 6\,\lambda^4 \sin(\%1)\cos(\%1) \arccos\left(\frac{1}{4}\right)^4 - 15\,\lambda^4\,\pi \arccos\left(\frac{1}{4}\right)^4 - 6\,\lambda^4 \sin(\%1)\cos(\%1)\,\pi^4$$

$$+ 60\,\lambda^2\,\pi^4 \sin(\%1)\cos(\%1) - 120\,\lambda^2\,\pi^3 \sin(\%1)\cos(\%1) \arccos\left(\frac{1}{4}\right)$$

$$- 30\,\lambda^4\,\pi^3 \arccos\left(\frac{1}{4}\right)^2 + 60\,\lambda^2\,\pi^2 \sin(\%1)\cos(\%1) \arccos\left(\frac{1}{4}\right)^2 + 30\,\lambda^4\,\pi^2 \arccos\left(\frac{1}{4}\right)^3$$

$$- 48\cos(\%1)^3\,\lambda^4\,\pi^3 \arccos\left(\frac{1}{4}\right)\sin(\%1) - 40\cos(\%1)^3\,\lambda^2\,\pi^2 \arccos\left(\frac{1}{4}\right)^2 \sin(\%1)$$

$$+ 492\cos(\%1)^3\,\pi^4 \sin(\%1) - 40\cos(\%1)^3\,\lambda^2\,\pi^4 \sin(\%1)$$

$$+ 80\cos(\%1)^3\,\lambda^2\,\pi^3 \arccos\left(\frac{1}{4}\right)\sin(\%1) + 72\cos(\%1)^3\,\lambda^4\,\pi^2 \arccos\left(\frac{1}{4}\right)^2 \sin(\%1)$$

$$- 48\cos(\%1)^3\,\lambda^4\,\pi \arccos\left(\frac{1}{4}\right)^3 \sin(\%1) + 12\cos(\%1)^3\,\lambda^4\,\pi^4 \sin(\%1)$$

$$\left. + 12\cos(\%1)^3\,\lambda^4 \arccos\left(\frac{1}{4}\right)^4 \sin(\%1) \right) \Big/ \left(\lambda^2\,\pi^4 \right.$$

$$\left. \left(-3\,\pi + 3 \arccos\left(\frac{1}{4}\right) + 6 \sin(\%1)\cos(\%1) + 4\cos(\%1)^3 \sin(\%1) \right) \right)$$

$$\%1 := \frac{1}{2} \arccos\left(\frac{1}{4}\right)$$

> evalf(");

$$-.0005049479268\,\frac{-16239.29831 - 52.4527063\,\lambda^4 - 1239.173324\,\lambda^2}{\lambda^2}$$

> expand(");

$$8.200000014\,\frac{1}{\lambda^2} + .02648588530\,\lambda^2 + .6257180009$$

> save Km2, 'Km.m';

>

Appendix E

Derivation of rectangular plate buckling

(m=3)

> a:=lambda*b; n:=arccos(mu/2/(-1+mu)); m:=3;

$$a := \lambda\, b$$

$$n := \arccos\left(\frac{1}{2}\,\frac{\mu}{-1+\mu}\right)$$

$$m := 3$$

> w:=sin(Pi*x/a)*A*sin(m*Pi*x/a)*(1-cos(n*y/b));

$$w := \sin\left(\frac{\pi\, x}{\lambda\, b}\right) A \sin\left(3\,\frac{\pi\, x}{\lambda\, b}\right)\left(1 - \cos\left(\frac{\arccos\left(\frac{1}{2}\,\frac{\mu}{-1+\mu}\right) y}{b}\right)\right)$$

> DE:=(diff(w,x,x)+diff(w,y,y))^2-2*(1-mu)*(diff(w,x,x)*diff(w,y,y)-(diff(w,x,y))^2);

$$DE := \left(-10\,\frac{\sin\left(\frac{\pi\, x}{\lambda\, b}\right)\pi^2 A\, \%2\left(1 - \cos\left(\frac{\%1\, y}{b}\right)\right)}{\lambda^2 b^2} + 6\,\frac{\cos\left(\frac{\pi\, x}{\lambda\, b}\right)\pi^2 A \cos\left(3\,\frac{\pi\, x}{\lambda\, b}\right)\left(1 - \cos\left(\frac{\%1\, y}{b}\right)\right)}{\lambda^2 b^2} + \frac{\sin\left(\frac{\pi\, x}{\lambda\, b}\right) A\, \%2 \cos\left(\frac{\%1\, y}{b}\right)\%1^2}{b^2}\right)^2$$

$$- 2\,(1-\mu)\left(\left(-10\,\frac{\sin\left(\frac{\pi\, x}{\lambda\, b}\right)\pi^2 A\, \%2\left(1 - \cos\left(\frac{\%1\, y}{b}\right)\right)}{\lambda^2 b^2} + 6\,\frac{\cos\left(\frac{\pi\, x}{\lambda\, b}\right)\pi^2 A \cos\left(3\,\frac{\pi\, x}{\lambda\, b}\right)\left(1 - \cos\left(\frac{\%1\, y}{b}\right)\right)}{\lambda^2 b^2}\right)\sin\left(\frac{\pi\, x}{\lambda\, b}\right) A\, \%2 \cos\left(\frac{\%1\, y}{b}\right)\%1^2 \Big/ b^2$$

$$- \left(\frac{\cos\left(\frac{\pi\, x}{\lambda\, b}\right)\pi\, A\, \%2 \sin\left(\frac{\%1\, y}{b}\right)\%1}{\lambda\, b^2} + 3\,\frac{\sin\left(\frac{\pi\, x}{\lambda\, b}\right) A \cos\left(3\,\frac{\pi\, x}{\lambda\, b}\right)\pi \sin\left(\frac{\%1\, y}{b}\right)\%1}{\lambda\, b^2}\right)^2\Bigg)$$

$$\%1 := \arccos\left(\frac{1}{2}\,\frac{\mu}{-1+\mu}\right)$$

$$\%2 := \sin\left(3\,\frac{\pi\, x}{\lambda\, b}\right)$$

> Z1:=int(DE, x=0..a);

$$Z1 := \frac{1}{768} A^2 \left(24\ \%11\ \lambda^4\ \%1^4 - 2048\ \%5\ \pi^4 + 96 \sin(2\ \%6)\ \pi^4 - 3072\ \%4\ \pi^4 \right.$$

$$+ 768 \sin(2\ \%9)\ \pi^4 + 3 \sin(2\ \%9)\ \lambda^4\ \%1^4 + 6 \sin(2\ \%6)\ \lambda^4\ \%1^4 - 6144 \sin(\%8)\ \pi^4$$

$$- 96 \sin(2\ \%8)\ \pi^4 + 1536\ \%11\ \pi^4 - 8\ \%7\ \lambda^4\ \%1^4 - 512\ \%7\ \pi^4$$

$$- 96\ \pi^2\ \%1^2\ \lambda^2 \cos\left(\frac{\%1\ y}{b}\right) \sin(\%3)\ \mu - 192\ \pi^2\ \%1^2\ \lambda^2 \cos\left(\frac{\%1\ y}{b}\right) \%2\ \mu$$

$$+ 192\ \pi^2\ \%1^2\ \lambda^2 \cos\left(\frac{\%1\ y}{b}\right) \%2 - 3840\ \pi^3\ \%1^2\ \lambda^2 \cos\left(\frac{\%1\ y}{b}\right) \mu$$

$$+ 96\ \pi^2\ \%1^2\ \lambda^2 \cos\left(\frac{\%1\ y}{b}\right) \sin(\%3) + 96\ \%1^4 \cos\left(2\ \frac{\%1\ y}{b}\right) \lambda^4\ \pi + 288\ \%12\ \pi^2\ \%1^2\ \lambda^2$$

$$+ 3840\ \pi^3\ \%1^2\ \lambda^2 + 3840\ \pi^3\ \%1^2\ \lambda^2 \cos\left(\frac{\%1\ y}{b}\right)^2 \mu + 320\ \pi^2\ \%1^2\ \lambda^2 \cos\left(\frac{\%1\ y}{b}\right) \%5\ \mu$$

$$- 1536\ \%13\ \pi^4 - 768 \sin(2\ \%3)\ \pi^4 - 52224\ \pi^5 \cos\left(\frac{\%1\ y}{b}\right) + 512\ \%12\ \pi^4$$

$$+ 13056\ \pi^5 \cos\left(2\ \frac{\%1\ y}{b}\right) - 96 \sin(2\ \%9)\ \pi^2\ \%1^2\ \lambda^2\ \mu + 96 \sin(2\ \%6)\ \pi^2\ \%1^2\ \lambda^2$$

$$- 96\ \%13\ \pi^2\ \%1^2\ \lambda^2 - 24\ \%13\ \lambda^4\ \%1^4 - 6 \sin(2\ \%8)\ \lambda^4\ \%1^4 + 8\ \%12\ \lambda^4\ \%1^4$$

$$+ 96\ \%1^4\ \lambda^4\ \pi - 960\ \pi^2\ \%1^2\ \lambda^2 \cos\left(\frac{\%1\ y}{b}\right) \sin(\%6)\ \mu - 48 \sin(2\ \%6)\ \pi^2\ \%1^2\ \lambda^2\ \mu$$

$$- 384\ \%13\ \pi^2\ \%1^2\ \lambda^2\ \mu + 192 \sin(2\ \%9)\ \pi^2\ \%1^2\ \lambda^2 - 3 \sin(2\ \%3)\ \lambda^4\ \%1^4$$

$$+ 6144 \sin(\%6)\ \pi^4 - 960 \sin(\%8)\ \pi^2\ \%1^2\ \lambda^2 - 96\ \pi^2\ \%1^2\ \lambda^2 \cos\left(\frac{\%1\ y}{b}\right) \sin(\%9)$$

$$- 1920\ \pi^3\ \%1^2\ \lambda^2\ \mu - 3840\ \pi^3\ \%1^2\ \lambda^2 \cos\left(\frac{\%1\ y}{b}\right)^2 - 192\ \pi^2\ \%1^2\ \lambda^2 \cos\left(\frac{\%1\ y}{b}\right) \%4$$

$$+ 384\ \%11\ \pi^2\ \%1^2\ \lambda^2\ \mu - 192 \sin(2\ \%3)\ \pi^2\ \%1^2\ \lambda^2 + 48 \sin(2\ \%8)\ \pi^2\ \%1^2\ \lambda^2\ \mu$$

$$- 128\ \%12\ \pi^2\ \%1^2\ \lambda^2\ \mu - 96 \sin(\%9)\ \pi^2\ \%1^2\ \lambda^2 + 96\ \%11\ \pi^2\ \%1^2\ \lambda^2$$

$$- 320\ \pi^2\ \%1^2\ \lambda^2 \cos\left(\frac{\%1\ y}{b}\right) \%10\ \mu - 96 \sin(2\ \%8)\ \pi^2\ \%1^2\ \lambda^2$$

$$+ 96\ \pi^2\ \%1^2\ \lambda^2 \cos\left(\frac{\%1\ y}{b}\right) \sin(\%9)\ \mu + 320\ \pi^2\ \%1^2\ \lambda^2 \cos\left(\frac{\%1\ y}{b}\right) \%10$$

$$- 320\ \pi^2\ \%1^2\ \lambda^2 \cos\left(\frac{\%1\ y}{b}\right) \%5 + 1920\ \pi^3\ \%1^2\ \lambda^2 \cos\left(2\ \frac{\%1\ y}{b}\right) \mu$$

$$+ 128\,\%7\,\pi^2\,\%1^2\,\lambda^2\,\mu + 960\,\pi^2\,\%1^2\,\lambda^2\cos\left(\frac{\%1\,y}{b}\right)\sin(\%6) + 320\,\%10\,\pi^2\,\%1^2\,\lambda^2$$

$$+ 2048\,\%10\,\pi^4 - 384\sin(\%9)\,\pi^4 + 960\,\pi^2\,\%1^2\,\lambda^2\cos\left(\frac{\%1\,y}{b}\right)\sin(\%8)\,\mu$$

$$+ 96\sin(\%3)\,\pi^2\,\%1^2\,\lambda^2 + 192\,\%2\,\pi^2\,\%1^2\,\lambda^2 - 960\,\pi^2\,\%1^2\,\lambda^2\cos\left(\frac{\%1\,y}{b}\right)\sin(\%8)$$

$$- 192\,\%4\,\pi^2\,\%1^2\,\lambda^2 - 288\,\%7\,\pi^2\,\%1^2\,\lambda^2 + 96\sin(2\,\%3)\,\pi^2\,\%1^2\,\lambda^2\,\mu$$

$$+ 960\sin(\%6)\,\pi^2\,\%1^2\,\lambda^2 - 320\,\%5\,\pi^2\,\%1^2\,\lambda^2 + 192\,\pi^2\,\%1^2\,\lambda^2\cos\left(\frac{\%1\,y}{b}\right)\%4\,\mu$$

$$+ 39168\,\pi^5 + 384\sin(\%3)\,\pi^4 + 3072\,\%2\,\pi^4\Bigg)\Big/\left(\lambda^3\,b^3\,\pi\right)$$

$$\%1 := \arccos\left(\frac{1}{2}\,\frac{\mu}{-1+\mu}\right)$$

$$\%2 := \sin\left(\frac{-8\,\pi\,b + \%1\,y}{b}\right)$$

$$\%3 := \frac{-4\,\pi\,b + \%1\,y}{b}$$

$$\%4 := \sin\left(\frac{8\,\pi\,b + \%1\,y}{b}\right)$$

$$\%5 := \sin\left(\frac{\%1\,y - 6\,\pi\,b}{b}\right)$$

$$\%6 := \frac{\%1\,y + 2\,\pi\,b}{b}$$

$$\%7 := \sin\left(2\,\frac{3\,\pi\,b + \%1\,y}{b}\right)$$

$$\%8 := \frac{\%1\,y - 2\,\pi\,b}{b}$$

$$\%9 := \frac{4\,\pi\,b + \%1\,y}{b}$$

$$\%10 := \sin\left(\frac{\%1\,y + 6\,\pi\,b}{b}\right)$$

$$\%11 := \sin\left(2\,\frac{-\pi\,b + \%1\,y}{b}\right)$$

$$\%12 := \sin\left(2\,\frac{-3\,\pi\,b + \%1\,y}{b}\right)$$

$$\%13 := \sin\left(2\,\frac{\pi\,b + \%1\,y}{b}\right)$$

> expand(Z1);

$$-5\,\frac{A^2\,\pi^2\,\%1^2\cos\left(\frac{\%1\,y}{b}\right)\mu}{\lambda\,b^3} + 5\,\frac{A^2\,\pi^2\,\%1^2}{\lambda\,b^3} + 10\,\frac{A^2\,\pi^2\,\%1^2\cos\left(\frac{\%1\,y}{b}\right)^2\mu}{\lambda\,b^3}$$

$$- 68\,\frac{A^2\,\pi^4\cos\left(\frac{\%1\,y}{b}\right)}{\lambda^3\,b^3} - 5\,\frac{A^2\,\pi^2\,\%1^2\,\mu}{\lambda\,b^3} - 5\,\frac{A^2\,\pi^2\,\%1^2\cos\left(\frac{\%1\,y}{b}\right)^2}{\lambda\,b^3} + 34\,\frac{A^2\,\pi^4}{\lambda^3\,b^3}$$

$$+\frac{1}{4}\,\frac{A^2\,\lambda\,\%1^4\cos\left(\frac{\%1\,y}{b}\right)^2}{b^3} + 34\,\frac{A^2\,\pi^4\cos\left(\frac{\%1\,y}{b}\right)^2}{\lambda^3\,b^3}$$

$$\%1 := \arccos\left(\frac{1}{2}\,\frac{\mu}{-1+\mu}\right)$$

> Z2:=int("*(1-beta*y/b)^3, y=0..b);

$$Z2 := -\frac{1}{32}\,A^2\left(-60\,\beta^3\,\%1^4\,\lambda^2\,\pi^2 - 360\,\beta^3\,\%1^4\,\pi^2\,\lambda^2\,\mu - 18\,\beta^3\tan\left(\frac{1}{2}\,\%1\right)^2\%1^6\,\lambda^4\right.$$

$$- 8\tan\left(\frac{1}{2}\,\%1\right)^2\%1^8\,\lambda^4 + 40\,\beta^3\tan\left(\frac{1}{2}\,\%1\right)^2\%1^6\,\lambda^2\,\pi^2 + 816\,\beta^3\tan\left(\frac{1}{2}\,\%1\right)^2\%1^4\,\pi^4$$

$$\left.+\,\beta^3\tan\left(\frac{1}{2}\,\%1\right)^4\%1^8\,\lambda^4 + 2\,\beta^3\tan\left(\frac{1}{2}\,\%1\right)^2\%1^8\,\lambda^4 + 20\,\beta^3\tan\left(\frac{1}{2}\,\%1\right)^4\%1^6\,\lambda^2\,\pi^2\right.$$

$$+ 408\,\beta^3 \tan\left(\frac{1}{2}\%1\right)^4 \%1^4\,\pi^4 - 6\,\%1^6\,\lambda^4\,\beta^2 - 80\,\beta^2\,\%1^6\,\lambda^2\,\pi^2$$

$$+ 4896\,\beta \tan\left(\frac{1}{2}\%1\right)^2 \%1^4\,\pi^4 - 60\,\beta^3 \tan\left(\frac{1}{2}\%1\right)^4 \%1^4\,\pi^2\,\lambda^2$$

$$+ 600\,\beta^3 \tan\left(\frac{1}{2}\%1\right)^4 \%1^4\,\pi^2\,\lambda^2\,\mu - 3264 \tan\left(\frac{1}{2}\%1\right)^2 \%1^4\,\pi^4 - 24480\,\beta^3 \tan\left(\frac{1}{2}\%1\right)^2 \pi^4$$

$$- 4 \tan\left(\frac{1}{2}\%1\right)^4 \%1^8\,\lambda^4 + 8 \tan\left(\frac{1}{2}\%1\right)^3 \%1^7\,\lambda^4 - 8 \tan\left(\frac{1}{2}\%1\right) \%1^7\,\lambda^4$$

$$+ 5440 \tan\left(\frac{1}{2}\%1\right)^3 \%1^3\,\pi^4 + 720\,\%1^4\,\pi^2\,\lambda^2\,\mu\,\beta^2 - 1440 \tan\left(\frac{1}{2}\%1\right) \%1^3\,\lambda^2\,\pi^2\,\mu\,\beta^2$$

$$- 240 \tan\left(\frac{1}{2}\%1\right) \%1^3\,\lambda^2\,\pi^2\,\beta^2 + 6\,\beta\,\%1^8\,\lambda^4 + 3\,\beta^3\,\%1^6\,\lambda^4 + 2448\,\beta\,\%1^4\,\pi^4$$

$$- 26112\,\pi^4\,\beta^3 \tan\left(\frac{1}{2}\%1\right)^4 + 360\,\beta^3 \tan\left(\frac{1}{2}\%1\right)^2 \%1^4\,\lambda^2\,\pi^2 + 12\,\beta \tan\left(\frac{1}{2}\%1\right)^2 \%1^8\,\lambda^4$$

$$+ 20\,\beta^3\,\%1^6\,\lambda^2\,\pi^2 - 1632\,\beta^2\,\%1^4\,\pi^4 + 12240\,\%1^2\,\pi^4\,\beta^2 - 80\,\%1^6\,\lambda^2\,\pi^2$$

$$+ 3264 \tan\left(\frac{1}{2}\%1\right) \%1^3\,\pi^4 - 4\,\beta^2\,\%1^8\,\lambda^4 - 1920\,\pi^2\,\beta^3 \tan\left(\frac{1}{2}\%1\right)^4 \lambda^2\,\%1^2\,\mu$$

$$- 8\,\beta^2 \tan\left(\frac{1}{2}\%1\right)^2 \%1^8\,\lambda^4 - 24\,\beta \tan\left(\frac{1}{2}\%1\right)^2 \lambda^4\,\%1^6 + 1440 \tan\left(\frac{1}{2}\%1\right)^2 \%1^4\,\lambda^2\,\pi^2\,\mu\,\beta^2$$

$$- 80\,\beta^2 \tan\left(\frac{1}{2}\%1\right)^4 \%1^6\,\lambda^2\,\pi^2 - 4\,\beta^2 \tan\left(\frac{1}{2}\%1\right)^4 \%1^8\,\lambda^4 - 1632\,\beta^2 \tan\left(\frac{1}{2}\%1\right)^4 \%1^4\,\pi^4$$

$$+ 1920\,\beta^2 \tan\left(\frac{1}{2}\%1\right)^3 \%1^5\,\pi^2\,\lambda^2\,\mu - 24\,\beta \tan\left(\frac{1}{2}\%1\right)^3 \%1^7\,\lambda^4$$

$$- 1920\,\beta \tan\left(\frac{1}{2}\%1\right)^3 \%1^5\,\lambda^2\,\pi^2\,\mu + 12\,\beta^3 \tan\left(\frac{1}{2}\%1\right)^2 \lambda^4\,\%1^4$$

$$+ 24\,\beta^2 \tan\left(\frac{1}{2}\%1\right)^3 \%1^7\,\lambda^4 - 12\,\beta^3 \tan\left(\frac{1}{2}\%1\right) \%1^5\,\lambda^4 - 240\,\beta^3 \tan\left(\frac{1}{2}\%1\right)^3 \%1^3\,\lambda^2\,\pi^2$$

$$- 160\,\beta^3 \tan\left(\frac{1}{2}\%1\right) \%1^5\,\lambda^2\,\pi^2 - 480\,\beta \tan\left(\frac{1}{2}\%1\right) \%1^5\,\lambda^2\,\pi^2 + 24\,\beta \tan\left(\frac{1}{2}\%1\right) \%1^7\,\lambda^4$$

$$- 240\,\beta^3 \tan\left(\frac{1}{2}\%1\right)^2 \pi^2\,\lambda^2\,\%1^2 + 480\,\beta \tan\left(\frac{1}{2}\%1\right)^2 \lambda^2\,\pi^2\,\%1^4$$

$$+ 27744\,\beta^3 \tan\left(\frac{1}{2}\%1\right)^3 \%1\,\pi^4 - 9792\,\beta \tan\left(\frac{1}{2}\%1\right)\%1^3\,\pi^4 + 9792\,\beta \tan\left(\frac{1}{2}\%1\right)^2 \pi^4\,\%1^2$$

$$- 16320\,\beta \tan\left(\frac{1}{2}\%1\right)^3 \%1^3\,\pi^4 + 24480\,\beta^3 \tan\left(\frac{1}{2}\%1\right)\%1\,\pi^4$$

$$- 480\,\beta^2 \tan\left(\frac{1}{2}\%1\right)^3 \%1^5\,\pi^2\,\lambda^2 + 2400\,\beta^3 \tan\left(\frac{1}{2}\%1\right)^3 \%1^3\,\lambda^2\,\pi^2\,\mu$$

$$+ 16320\,\beta^2 \tan\left(\frac{1}{2}\%1\right)^3 \%1^3\,\pi^4 + 2448\,\beta \tan\left(\frac{1}{2}\%1\right)^4 \%1^4\,\pi^4$$

$$+ 6936\,\beta^3 \tan\left(\frac{1}{2}\%1\right)^4 \%1^2\,\pi^4 + 9792\,\beta^2 \tan\left(\frac{1}{2}\%1\right)\%1^3\,\pi^4$$

$$- 640\,\beta^3 \tan\left(\frac{1}{2}\%1\right)^3 \%1^5\,\lambda^2\,\pi^2\,\mu - 720\,\beta^3 \tan\left(\frac{1}{2}\%1\right)^2 \%1^4\,\lambda^2\,\pi^2\,\mu$$

$$- 3264\,\beta^3 \tan\left(\frac{1}{2}\%1\right)\%1^3\,\pi^4 + 12 \tan\left(\frac{1}{2}\%1\right)\%1^5\,\lambda^4\,\beta^2 - 24\,\beta^2 \tan\left(\frac{1}{2}\%1\right)\%1^7\,\lambda^4$$

$$- 27744 \tan\left(\frac{1}{2}\%1\right)^3 \%1\,\pi^4\,\beta^2 - 160 \tan\left(\frac{1}{2}\%1\right)^3 \%1^5\,\lambda^2\,\pi^2$$

$$+ 240\,\beta^3 \tan\left(\frac{1}{2}\%1\right)\%1^3\,\pi^2\,\lambda^2 + 1440\,\beta^3 \tan\left(\frac{1}{2}\%1\right)\%1^3\,\pi^2\,\lambda^2\,\mu$$

$$- 3264\,\beta^2 \tan\left(\frac{1}{2}\%1\right)^2 \%1^4\,\pi^4 + 12\,\beta^3 \tan\left(\frac{1}{2}\%1\right)^3 \%1^5\,\lambda^4$$

$$+ 160\,\beta^3 \tan\left(\frac{1}{2}\%1\right)^3 \%1^5\,\lambda^2\,\pi^2 + 4896 \tan\left(\frac{1}{2}\%1\right)^2 \%1^2\,\pi^4\,\beta^2$$

$$+ 120\,\beta \tan\left(\frac{1}{2}\%1\right)^4 \%1^6\,\lambda^2\,\pi^2 - 1440\,\beta^3 \tan\left(\frac{1}{2}\%1\right)^2 \pi^2\,\lambda^2\,\%1^2\,\mu$$

$$- 160\,\beta^2 \tan\left(\frac{1}{2}\%1\right)^2 \%1^6\,\lambda^2\,\pi^2 + 480\,\beta \tan\left(\frac{1}{2}\%1\right)^3 \%1^5\,\lambda^2\,\pi^2$$

$$- 5440\,\beta^3 \tan\left(\frac{1}{2}\%1\right)^3 \%1^3\,\pi^4 + 8\,\beta^3 \tan\left(\frac{1}{2}\%1\right)\%1^7\,\lambda^4 + 240 \tan\left(\frac{1}{2}\%1\right)^3 \%1^3\,\lambda^2\,\pi^2\,\beta^2$$

$$- 12 \tan\left(\frac{1}{2}\%1\right)^3 \%1^5\,\lambda^4\,\beta^2 - 8\,\beta^3 \tan\left(\frac{1}{2}\%1\right)^3 \%1^7\,\lambda^4 + 480\,\beta^2 \tan\left(\frac{1}{2}\%1\right)\%1^5\,\lambda^2\,\pi^2$$

$$+ 3\,\beta^3 \tan\left(\frac{1}{2}\%1\right)^4 \%1^6\,\lambda^4 + 36 \tan\left(\frac{1}{2}\%1\right)^2 \%1^6\,\lambda^4\,\beta^2 - 720 \tan\left(\frac{1}{2}\%1\right)^2 \%1^4\,\lambda^2\,\pi^2\,\beta^2$$

$$- 160 \tan\left(\frac{1}{2}\,\%1\right)^2 \%1^6 \lambda^2 \pi^2 - 1200 \tan\left(\frac{1}{2}\,\%1\right)^4 \%1^4 \lambda^2 \pi^2 \mu \beta^2$$

$$+ 240 \beta \tan\left(\frac{1}{2}\,\%1\right)^2 \%1^6 \lambda^2 \pi^2 + 13056 \pi^4 \beta \tan\left(\frac{1}{2}\,\%1\right)^4 \%1^2 - 6120 \beta^3 \%1^2 \pi^4$$

$$- 80 \tan\left(\frac{1}{2}\,\%1\right)^4 \%1^6 \lambda^2 \pi^2 + 120 \tan\left(\frac{1}{2}\,\%1\right)^4 \%1^4 \lambda^2 \pi^2 \beta^2 - 6 \tan\left(\frac{1}{2}\,\%1\right)^4 \%1^6 \lambda^4 \beta^2$$

$$- 2400 \tan\left(\frac{1}{2}\,\%1\right)^3 \%1^3 \lambda^2 \pi^2 \mu \beta^2 - 1632 \tan\left(\frac{1}{2}\,\%1\right)^4 \%1^4 \pi^4$$

$$- 24480 \tan\left(\frac{1}{2}\,\%1\right) \%1 \pi^4 \beta^2 + 160 \tan\left(\frac{1}{2}\,\%1\right) \%1^5 \lambda^2 \pi^2 + 6 \beta \tan\left(\frac{1}{2}\,\%1\right)^4 \%1^8 \lambda^4$$

$$- 2448 \beta^3 \tan\left(\frac{1}{2}\,\%1\right)^2 \%1^2 \pi^4 - 13872 \tan\left(\frac{1}{2}\,\%1\right)^4 \%1^2 \pi^4 \beta^2 - 4\,\%1^8 \lambda^4$$

$$+ 640 \tan\left(\frac{1}{2}\,\%1\right)^3 \%1^5 \lambda^2 \pi^2 \mu + 120\,\%1^4 \lambda^2 \pi^2 \beta^2 - 1632\,\%1^4 \pi^4$$

$$+ 960 \pi^2 \beta \tan\left(\frac{1}{2}\,\%1\right)^4 \lambda^2 \%1^4 \mu + 120 \beta \%1^6 \lambda^2 \pi^2 + \beta^3 \%1^8 \lambda^4 + 408 \beta^3 \%1^4 \pi^4 \Bigg) \Bigg/ \Bigg(.$$

$$b^2 \%1^4 \lambda^3 \left(1 + \tan\left(\frac{1}{2}\,\%1\right)^2\right)^2 \Bigg)$$

$$\%1 := \arccos\left(\frac{1}{2}\,\frac{\mu}{-1+\mu}\right)$$

> int(diff(w,x)^2,x=0..a);

$$\frac{1}{96} \pi A^2 \Bigg(120 \pi \cos\left(2\,\frac{\%1\, y}{b}\right) - 32 \sin\left(\frac{-\%1\, y + 6 \pi b}{b}\right) - 6 \sin\left(2\,\frac{4 \pi b - \%1\, y}{b}\right)$$

$$- 32 \sin\left(\frac{\%1\, y + 6 \pi b}{b}\right) + 8 \sin\left(2\,\frac{3 \pi b - \%1\, y}{b}\right) + 12 \sin\left(\frac{4 \pi b + \%1\, y}{b}\right)$$

$$- 6 \sin\left(2\,\frac{4 \pi b + \%1\, y}{b}\right) - 24 \sin\left(2\,\frac{\pi b - \%1\, y}{b}\right) + 96 \sin\left(\frac{\%1\, y + 2 \pi b}{b}\right)$$

$$- 480 \pi \cos\left(\frac{\%1\, y}{b}\right) + 8 \sin\left(2\,\frac{3 \pi b + \%1\, y}{b}\right) - 3 \sin\left(2\,\frac{\%1\, y + 2 \pi b}{b}\right)$$

$$+ 24 \sin\left(\frac{8 \pi b + \%1\, y}{b}\right) + 96 \sin\left(\frac{-\%1\, y + 2 \pi b}{b}\right) - 3 \sin\left(2\,\frac{-\%1\, y + 2 \pi b}{b}\right) + 360 \pi$$

$$- 24 \sin\left(2 \frac{\pi b + \%1\, y}{b} \right) + 12 \sin\left(\frac{4 \pi b - \%1\, y}{b} \right) + 24 \sin\left(\frac{8 \pi b - \%1\, y}{b} \right) \Big) / (\lambda b)$$

$$\%1 := \arccos\left(\frac{1}{2} \frac{\mu}{-1 + \mu} \right)$$

> expand(");

$$\frac{5}{2} \frac{\pi^2 A^2 \cos\left(\frac{\arccos\left(\frac{1}{2} \frac{\mu}{-1+\mu} \right) y}{b} \right)^2}{\lambda b} + \frac{5}{2} \frac{\pi^2 A^2}{\lambda b} - 5 \frac{\pi^2 A^2 \cos\left(\frac{\arccos\left(\frac{1}{2} \frac{\mu}{-1+\mu} \right) y}{b} \right)}{\lambda b}$$

> Z3:=int((1-beta*y/b)*",y=0..b);

$$Z3 := -\frac{5}{8} \pi^2 A^2 \left(20 \tan\left(\frac{1}{2} \%1 \right)^3 \%1 - 20 \beta \tan\left(\frac{1}{2} \%1 \right)^3 \%1 + 12 \tan\left(\frac{1}{2} \%1 \right) \%1 \right.$$
$$+ 12 \beta \tan\left(\frac{1}{2} \%1 \right)^2 - 12 \beta \tan\left(\frac{1}{2} \%1 \right) \%1 + 6 \beta \tan\left(\frac{1}{2} \%1 \right)^2 \%1^2 + 3 \beta \%1^2$$
$$- 12 \tan\left(\frac{1}{2} \%1 \right)^2 \%1^2 - 6 \%1^2 + 3 \beta \tan\left(\frac{1}{2} \%1 \right)^4 \%1^2 - 6 \tan\left(\frac{1}{2} \%1 \right)^4 \%1^2$$
$$\left. + 16 \beta \tan\left(\frac{1}{2} \%1 \right)^4 \right) \Big/ \left(\lambda \%1^2 \left(1 + \tan\left(\frac{1}{2} \%1 \right)^2 \right)^2 \right)$$

$$\%1 := \arccos\left(\frac{1}{2} \frac{\mu}{-1 + \mu} \right)$$

> U:=simplify((Z2-X*Z3)/A^2);

$$U := -\frac{1}{32} \left(-16320 \beta \%1^3 \pi^4 \cos\left(\frac{1}{2} \%1 \right) \sin\left(\frac{1}{2} \%1 \right) - 12 \beta^3 \lambda^4 \%1^4 \cos\left(\frac{1}{2} \%1 \right)^4 \right.$$
$$+ 12 \beta^3 \lambda^4 \%1^4 \cos\left(\frac{1}{2} \%1 \right)^2 + 24 \beta^2 \%1^7 \lambda^4 \cos\left(\frac{1}{2} \%1 \right) \sin\left(\frac{1}{2} \%1 \right)$$
$$+ 2400 \beta^3 \%1^3 \lambda^2 \pi^2 \mu \cos\left(\frac{1}{2} \%1 \right) \sin\left(\frac{1}{2} \%1 \right) - 5440 \beta^3 \%1^3 \pi^4 \cos\left(\frac{1}{2} \%1 \right) \sin\left(\frac{1}{2} \%1 \right)$$
$$- 240 \beta^3 \pi^2 \lambda^2 \%1^2 \cos\left(\frac{1}{2} \%1 \right)^2 + 240 \beta^3 \pi^2 \lambda^2 \%1^2 \cos\left(\frac{1}{2} \%1 \right)^4$$
$$\left. - 480 \sin\left(\frac{1}{2} \%1 \right) \%1^3 \lambda^2 \pi^2 \beta^2 \cos\left(\frac{1}{2} \%1 \right)^3 + 960 \sin\left(\frac{1}{2} \%1 \right) \%1^3 \lambda^2 \pi^2 \mu \beta^2 \cos\left(\frac{1}{2} \%1 \right)^3 \right.$$

$$+ 160\,X\,\pi^2\,b^2\,\%1^3\,\lambda^2\sin\left(\frac{1}{2}\%1\right)\cos\left(\frac{1}{2}\%1\right)^3 + 480\,\beta^3\sin\left(\frac{1}{2}\%1\right)\%1^3\,\pi^2\,\lambda^2\cos\left(\frac{1}{2}\%1\right)^3$$

$$- 960\,\beta^3\sin\left(\frac{1}{2}\%1\right)\%1^3\,\pi^2\,\lambda^2\,\mu\cos\left(\frac{1}{2}\%1\right)^3 + 960\,\beta^2\sin\left(\frac{1}{2}\%1\right)\%1^5\,\lambda^2\,\pi^2\cos\left(\frac{1}{2}\%1\right)^3$$

$$+ 24\sin\left(\frac{1}{2}\%1\right)\%1^5\,\lambda^4\,\beta^2\cos\left(\frac{1}{2}\%1\right)^3 + 960\,\%1^4\,\lambda^2\,\pi^2\,\beta^2\cos\left(\frac{1}{2}\%1\right)^4$$

$$- 1920\,\%1^4\,\pi^2\,\lambda^2\,\mu\,\beta^2\cos\left(\frac{1}{2}\%1\right)^4 - 6528\,\%1^2\,\pi^4\,\beta^2\cos\left(\frac{1}{2}\%1\right)^4$$

$$+ 3264\,\beta^3\,\%1^2\,\pi^4\cos\left(\frac{1}{2}\%1\right)^4 + 16320\,\beta^2\,\%1^3\,\pi^4\cos\left(\frac{1}{2}\%1\right)\sin\left(\frac{1}{2}\%1\right)$$

$$+ 24\,\beta^3\,\%1^6\,\lambda^4\cos\left(\frac{1}{2}\%1\right)^4 - 60\,\beta^3\,\%1^4\,\lambda^2\,\pi^2 + 600\,\beta^3\,\%1^4\,\pi^2\,\lambda^2\,\mu$$

$$+ 3264\sin\left(\frac{1}{2}\%1\right)\%1\,\pi^4\,\beta^2\cos\left(\frac{1}{2}\%1\right)^3 + 48\,\beta\sin\left(\frac{1}{2}\%1\right)\%1^7\,\lambda^4\cos\left(\frac{1}{2}\%1\right)^3$$

$$- 48\,\beta^2\sin\left(\frac{1}{2}\%1\right)\%1^7\,\lambda^4\cos\left(\frac{1}{2}\%1\right)^3 + 16\,\beta^3\sin\left(\frac{1}{2}\%1\right)\%1^7\,\lambda^4\cos\left(\frac{1}{2}\%1\right)^3$$

$$+ 2176\,\beta^3\sin\left(\frac{1}{2}\%1\right)\%1^3\,\pi^4\cos\left(\frac{1}{2}\%1\right)^3 - 480\,\beta\,\lambda^2\,\pi^2\,\%1^4\cos\left(\frac{1}{2}\%1\right)^4$$

$$+ 6528\,\beta\sin\left(\frac{1}{2}\%1\right)\%1^3\,\pi^4\cos\left(\frac{1}{2}\%1\right)^3 - 2176\sin\left(\frac{1}{2}\%1\right)\%1^3\,\pi^4\cos\left(\frac{1}{2}\%1\right)^3$$

$$- 320\,\beta^3\sin\left(\frac{1}{2}\%1\right)\%1^5\,\lambda^2\,\pi^2\cos\left(\frac{1}{2}\%1\right)^3 + 320\sin\left(\frac{1}{2}\%1\right)\%1^5\,\lambda^2\,\pi^2\cos\left(\frac{1}{2}\%1\right)^3$$

$$- 6528\,\beta^2\sin\left(\frac{1}{2}\%1\right)\%1^3\,\pi^4\cos\left(\frac{1}{2}\%1\right)^3 - 48\,\%1^6\,\lambda^4\,\beta^2\cos\left(\frac{1}{2}\%1\right)^4$$

$$+ 960\,\beta^3\,\%1^4\,\pi^2\,\lambda^2\,\mu\cos\left(\frac{1}{2}\%1\right)^4 - 480\,\beta^3\,\%1^4\,\lambda^2\,\pi^2\cos\left(\frac{1}{2}\%1\right)^4$$

$$- 160\,X\,\pi^2\,b^2\,\%1^3\,\lambda^2\,\beta\sin\left(\frac{1}{2}\%1\right)\cos\left(\frac{1}{2}\%1\right)^3 - 960\,\beta\sin\left(\frac{1}{2}\%1\right)\%1^5\,\lambda^2\,\pi^2\cos\left(\frac{1}{2}\%1\right)^3$$

$$- 16\sin\left(\frac{1}{2}\%1\right)\%1^7\,\lambda^4\cos\left(\frac{1}{2}\%1\right)^3 - 24\,\beta^3\sin\left(\frac{1}{2}\%1\right)\%1^5\,\lambda^4\cos\left(\frac{1}{2}\%1\right)^3$$

$$- 3264\,\beta^3\sin\left(\frac{1}{2}\%1\right)\%1\,\pi^4\cos\left(\frac{1}{2}\%1\right)^3 + 3264\,\beta\,\pi^4\,\%1^2\cos\left(\frac{1}{2}\%1\right)^4$$

$$- 16320\,\beta\,\pi^4\,\%1^2\cos\left(\frac{1}{2}\%1\right)^2 - 640\,\beta^3\,\%1^5\,\lambda^2\,\pi^2\,\mu\cos\left(\frac{1}{2}\%1\right)\sin\left(\frac{1}{2}\%1\right)$$

$$- 27744\,\%1\,\pi^4\,\beta^2\cos\left(\frac{1}{2}\%1\right)\sin\left(\frac{1}{2}\%1\right) - 1920\,\pi^2\,\beta^3\,\lambda^2\,\%1^2\,\mu$$

$$- 160\,\%1^5\,\lambda^2\,\pi^2\cos\left(\frac{1}{2}\%1\right)\sin\left(\frac{1}{2}\%1\right) - 16320\,\beta^3\,\%1^2\,\pi^4\cos\left(\frac{1}{2}\%1\right)^2 - 26112\,\pi^4\,\beta^3$$

$$+ 13056\,\pi^4\,\beta\,\%1^2 + 640\,\beta^3\,\%1^5\,\lambda^2\,\pi^2\,\mu\cos\left(\frac{1}{2}\%1\right)^3\sin\left(\frac{1}{2}\%1\right)$$

$$- 1920\,\beta^2\,\%1^5\,\pi^2\,\lambda^2\,\mu\cos\left(\frac{1}{2}\%1\right)^3\sin\left(\frac{1}{2}\%1\right)$$

$$+ 1920\,\beta^2\,\%1^5\,\pi^2\,\lambda^2\,\mu\cos\left(\frac{1}{2}\%1\right)\sin\left(\frac{1}{2}\%1\right) + 480\,\beta\,\lambda^2\,\pi^2\,\%1^4\cos\left(\frac{1}{2}\%1\right)^2$$

$$- 480\,\beta^2\,\%1^5\,\pi^2\,\lambda^2\cos\left(\frac{1}{2}\%1\right)\sin\left(\frac{1}{2}\%1\right) - 240\,\beta^3\,\%1^3\,\lambda^2\,\pi^2\cos\left(\frac{1}{2}\%1\right)\sin\left(\frac{1}{2}\%1\right)$$

$$- 1920\,\beta\,\%1^5\,\lambda^2\,\pi^2\,\mu\cos\left(\frac{1}{2}\%1\right)\sin\left(\frac{1}{2}\%1\right)$$

$$+ 1920\,\beta\,\%1^5\,\lambda^2\,\pi^2\,\mu\cos\left(\frac{1}{2}\%1\right)^3\sin\left(\frac{1}{2}\%1\right) - 60\,X\,\pi^2\,b^2\,\%1^4\,\lambda^2\,\beta$$

$$+ 640\,\%1^5\,\lambda^2\,\pi^2\,\mu\cos\left(\frac{1}{2}\%1\right)\sin\left(\frac{1}{2}\%1\right) - 24\,\beta\,\%1^7\,\lambda^4\cos\left(\frac{1}{2}\%1\right)\sin\left(\frac{1}{2}\%1\right)$$

$$+ 120\,X\,\pi^2\,b^2\,\%1^4\,\lambda^2 - 6\,\%1^6\,\lambda^4\,\beta^2 - 640\,\%1^5\,\lambda^2\,\pi^2\,\mu\cos\left(\frac{1}{2}\%1\right)^3\sin\left(\frac{1}{2}\%1\right)$$

$$- 80\,\beta^2\,\%1^6\,\lambda^2\,\pi^2 - 1200\,\%1^4\,\pi^2\,\lambda^2\,\mu\,\beta^2 + 6\,\beta\,\%1^8\,\lambda^4 + 3\,\beta^3\,\%1^6\,\lambda^4 + 2448\,\beta\,\%1^4\,\pi^4$$

$$+ 20\,\beta^3\,\%1^6\,\lambda^2\,\pi^2 - 1632\,\beta^2\,\%1^4\,\pi^4 - 13872\,\%1^2\,\pi^4\,\beta^2 - 80\,\%1^6\,\lambda^2\,\pi^2 - 4\,\beta^2\,\%1^8\,\lambda^4$$

$$+ 6936\,\beta^3\,\%1^2\,\pi^4 - 4\,\%1^8\,\lambda^4 + 120\,\%1^4\,\lambda^2\,\pi^2\,\beta^2 - 1632\,\%1^4\,\pi^4 + 120\,\beta\,\%1^6\,\lambda^2\,\pi^2$$

$$+ \beta^3\,\%1^8\,\lambda^4 + 408\,\beta^3\,\%1^4\,\pi^4 - 2400\,\%1^3\,\lambda^2\,\pi^2\,\mu\,\beta^2\cos\left(\frac{1}{2}\%1\right)\sin\left(\frac{1}{2}\%1\right)$$

$$+ 960\,\pi^2\,\beta\,\lambda^2\,\%1^4\,\mu - 1920\,\pi^2\,\beta\,\lambda^2\,\%1^4\,\mu\cos\left(\frac{1}{2}\%1\right)^2 + 960\,\pi^2\,\beta\,\lambda^2\,\%1^4\,\mu\cos\left(\frac{1}{2}\%1\right)^4$$

$$+ 27744\,\beta^3\,\%1\,\pi^4\cos\left(\frac{1}{2}\%1\right)\sin\left(\frac{1}{2}\%1\right) - 320\,X\,\pi^2\,b^2\,\%1^2\,\lambda^2\,\beta$$

$$+ 400\,X\,\pi^2\,b^2\,\%1^2\,\lambda^2\,\beta\cos\left(\frac{1}{2}\%1\right)^2 + 5440\,\%1^3\,\pi^4\cos\left(\frac{1}{2}\%1\right)\sin\left(\frac{1}{2}\%1\right)$$

$$+ 160\,\beta^3\,\%1^5\,\lambda^2\,\pi^2\cos\left(\frac{1}{2}\%1\right)\sin\left(\frac{1}{2}\%1\right) + 3840\,\%1^4\,\lambda^2\,\pi^2\,\mu\,\beta^2\cos\left(\frac{1}{2}\%1\right)^2$$

$$- 24\,\beta\,\lambda^4\,\%1^6\cos\left(\frac{1}{2}\%1\right)^2 + 24\,\beta\,\lambda^4\,\%1^6\cos\left(\frac{1}{2}\%1\right)^4 + 27744\,\beta^3\,\pi^4\cos\left(\frac{1}{2}\%1\right)^2$$

$$- 1632\,\beta^3\,\pi^4\cos\left(\frac{1}{2}\%1\right)^4 + 480\,\beta^3\,\%1^4\,\lambda^2\,\pi^2\cos\left(\frac{1}{2}\%1\right)^2 - 24\,\beta^3\,\%1^6\,\lambda^4\cos\left(\frac{1}{2}\%1\right)^2$$

$$- 80\,X\,\pi^2\,b^2\,\%1^2\,\lambda^2\,\beta\cos\left(\frac{1}{2}\%1\right)^4 - 400\,X\,\pi^2\,b^2\,\%1^3\,\lambda^2\cos\left(\frac{1}{2}\%1\right)\sin\left(\frac{1}{2}\%1\right)$$

$$+ 400\,X\,\pi^2\,b^2\,\%1^3\,\lambda^2\,\beta\cos\left(\frac{1}{2}\%1\right)\sin\left(\frac{1}{2}\%1\right) + 8\,\%1^7\,\lambda^4\cos\left(\frac{1}{2}\%1\right)\sin\left(\frac{1}{2}\%1\right)$$

$$+ 12\,\beta^3\,\%1^5\,\lambda^4\cos\left(\frac{1}{2}\%1\right)\sin\left(\frac{1}{2}\%1\right) + 480\,\beta\,\%1^5\,\lambda^2\,\pi^2\cos\left(\frac{1}{2}\%1\right)\sin\left(\frac{1}{2}\%1\right)$$

$$- 960\,\%1^4\,\lambda^2\,\pi^2\,\beta^2\cos\left(\frac{1}{2}\%1\right)^2 + 48\,\%1^6\,\lambda^4\,\beta^2\cos\left(\frac{1}{2}\%1\right)^2$$

$$+ 240\,\%1^3\,\lambda^2\,\pi^2\,\beta^2\cos\left(\frac{1}{2}\%1\right)\sin\left(\frac{1}{2}\%1\right) - 1920\,\beta^3\,\%1^4\,\lambda^2\,\pi^2\,\mu\cos\left(\frac{1}{2}\%1\right)^2$$

$$+ 32640\,\%1^2\,\pi^4\,\beta^2\cos\left(\frac{1}{2}\%1\right)^2 - 8\,\beta^3\,\%1^7\,\lambda^4\cos\left(\frac{1}{2}\%1\right)\sin\left(\frac{1}{2}\%1\right)$$

$$- 12\,\%1^5\,\lambda^4\,\beta^2\cos\left(\frac{1}{2}\%1\right)\sin\left(\frac{1}{2}\%1\right) + 2400\,\beta^3\,\pi^2\,\lambda^2\,\%1^2\,\mu\cos\left(\frac{1}{2}\%1\right)^2$$

$$- 480\,\beta^3\,\pi^2\,\lambda^2\,\%1^2\,\mu\cos\left(\frac{1}{2}\%1\right)^4\Big)\Big/\left(\lambda^3\,\%1^4\,b^2\right)$$

$$\%1 := \arccos\left(\frac{1}{2}\,\frac{\mu}{-1+\mu}\right)$$

> Z4:=solve(U, X);

$$Z4 := -\Big(-16320\,\beta\,\%1^3\,\pi^4\cos\left(\frac{1}{2}\%1\right)\sin\left(\frac{1}{2}\%1\right) - 12\,\beta^3\,\lambda^4\,\%1^4\cos\left(\frac{1}{2}\%1\right)^4$$

$$+ 12\,\beta^3\,\lambda^4\,\%1^4\cos\left(\frac{1}{2}\%1\right)^2 + 24\,\beta^2\,\%1^7\,\lambda^4\cos\left(\frac{1}{2}\%1\right)\sin\left(\frac{1}{2}\%1\right)$$

$$+ 2400\,\beta^3\,\%1^3\,\lambda^2\,\pi^2\,\mu\cos\left(\frac{1}{2}\%1\right)\sin\left(\frac{1}{2}\%1\right) - 5440\,\beta^3\,\%1^3\,\pi^4\cos\left(\frac{1}{2}\%1\right)\sin\left(\frac{1}{2}\%1\right)$$

$$- 240\,\beta^3\,\pi^2\,\lambda^2\,\%1^2\cos\left(\frac{1}{2}\%1\right)^2 + 240\,\beta^3\,\pi^2\,\lambda^2\,\%1^2\cos\left(\frac{1}{2}\%1\right)^4$$

$$- 480\sin\left(\frac{1}{2}\%1\right)\%1^3\,\lambda^2\,\pi^2\,\beta^2\cos\left(\frac{1}{2}\%1\right)^3 + 960\sin\left(\frac{1}{2}\%1\right)\%1^3\,\lambda^2\,\pi^2\,\mu\,\beta^2\cos\left(\frac{1}{2}\%1\right)^3$$

$$+ 480\,\beta^3\sin\left(\frac{1}{2}\%1\right)\%1^3\,\pi^2\,\lambda^2\cos\left(\frac{1}{2}\%1\right)^3 - 960\,\beta^3\sin\left(\frac{1}{2}\%1\right)\%1^3\,\pi^2\,\lambda^2\,\mu\cos\left(\frac{1}{2}\%1\right)^3$$

$$+ 960\,\beta^2\sin\left(\frac{1}{2}\%1\right)\%1^5\,\lambda^2\,\pi^2\cos\left(\frac{1}{2}\%1\right)^3 + 24\sin\left(\frac{1}{2}\%1\right)\%1^5\,\lambda^4\,\beta^2\cos\left(\frac{1}{2}\%1\right)^3$$

$$+ 960\,\%1^4\,\lambda^2\,\pi^2\,\beta^2\cos\left(\frac{1}{2}\%1\right)^4 - 1920\,\%1^4\,\pi^2\,\lambda^2\,\mu\,\beta^2\cos\left(\frac{1}{2}\%1\right)^4$$

$$- 6528\,\%1^2\,\pi^4\,\beta^2\cos\left(\frac{1}{2}\%1\right)^4 + 3264\,\beta^3\,\%1^2\,\pi^4\cos\left(\frac{1}{2}\%1\right)^4$$

$$+ 16320\,\beta^2\,\%1^3\,\pi^4\cos\left(\frac{1}{2}\%1\right)\sin\left(\frac{1}{2}\%1\right) + 24\,\beta^3\,\%1^6\,\lambda^4\cos\left(\frac{1}{2}\%1\right)^4 - 60\,\beta^3\,\%1^4\,\lambda^2\,\pi^2$$

$$+ 600\,\beta^3\,\%1^4\,\pi^2\,\lambda^2\,\mu + 3264\sin\left(\frac{1}{2}\%1\right)\%1\,\pi^4\,\beta^2\cos\left(\frac{1}{2}\%1\right)^3$$

$$+ 48\,\beta\sin\left(\frac{1}{2}\%1\right)\%1^7\,\lambda^4\cos\left(\frac{1}{2}\%1\right)^3 - 48\,\beta^2\sin\left(\frac{1}{2}\%1\right)\%1^7\,\lambda^4\cos\left(\frac{1}{2}\%1\right)^3$$

$$+ 16\,\beta^3\sin\left(\frac{1}{2}\%1\right)\%1^7\,\lambda^4\cos\left(\frac{1}{2}\%1\right)^3 + 2176\,\beta^3\sin\left(\frac{1}{2}\%1\right)\%1^3\,\pi^4\cos\left(\frac{1}{2}\%1\right)^3$$

$$- 480\,\beta\,\lambda^2\,\pi^2\,\%1^4\cos\left(\frac{1}{2}\%1\right)^4 + 6528\,\beta\sin\left(\frac{1}{2}\%1\right)\%1^3\,\pi^4\cos\left(\frac{1}{2}\%1\right)^3$$

$$- 2176\sin\left(\frac{1}{2}\%1\right)\%1^3\,\pi^4\cos\left(\frac{1}{2}\%1\right)^3 - 320\,\beta^3\sin\left(\frac{1}{2}\%1\right)\%1^5\,\lambda^2\,\pi^2\cos\left(\frac{1}{2}\%1\right)^3$$

$$+ 320\sin\left(\frac{1}{2}\%1\right)\%1^5\,\lambda^2\,\pi^2\cos\left(\frac{1}{2}\%1\right)^3 - 6528\,\beta^2\sin\left(\frac{1}{2}\%1\right)\%1^3\,\pi^4\cos\left(\frac{1}{2}\%1\right)^3$$

$$- 48\,\%1^6\,\lambda^4\,\beta^2\cos\left(\frac{1}{2}\%1\right)^4 + 960\,\beta^3\,\%1^4\,\pi^2\,\lambda^2\,\mu\cos\left(\frac{1}{2}\%1\right)^4$$

$$- 480\,\beta^3\,\%1^4\,\lambda^2\,\pi^2\cos\left(\frac{1}{2}\%1\right)^4 - 960\,\beta\sin\left(\frac{1}{2}\%1\right)\%1^5\,\lambda^2\,\pi^2\cos\left(\frac{1}{2}\%1\right)^3$$

$$
\begin{aligned}
&- 16 \sin\left(\frac{1}{2}\%1\right)\%1^7\lambda^4\cos\left(\frac{1}{2}\%1\right)^3 - 24\beta^3\sin\left(\frac{1}{2}\%1\right)\%1^5\lambda^4\cos\left(\frac{1}{2}\%1\right)^3 \\
&- 3264\beta^3\sin\left(\frac{1}{2}\%1\right)\%1\,\pi^4\cos\left(\frac{1}{2}\%1\right)^3 + 3264\beta\pi^4\%1^2\cos\left(\frac{1}{2}\%1\right)^4 \\
&- 16320\beta\pi^4\%1^2\cos\left(\frac{1}{2}\%1\right)^2 - 640\beta^3\%1^5\lambda^2\pi^2\mu\cos\left(\frac{1}{2}\%1\right)\sin\left(\frac{1}{2}\%1\right) \\
&- 27744\%1\,\pi^4\beta^2\cos\left(\frac{1}{2}\%1\right)\sin\left(\frac{1}{2}\%1\right) - 1920\pi^2\beta^3\lambda^2\%1^2\mu \\
&- 160\%1^5\lambda^2\pi^2\cos\left(\frac{1}{2}\%1\right)\sin\left(\frac{1}{2}\%1\right) - 16320\beta^3\%1^2\pi^4\cos\left(\frac{1}{2}\%1\right)^2 - 26112\pi^4\beta^3 \\
&+ 13056\pi^4\beta\%1^2 + 640\beta^3\%1^5\lambda^2\pi^2\mu\cos\left(\frac{1}{2}\%1\right)^3\sin\left(\frac{1}{2}\%1\right) \\
&- 1920\beta^2\%1^5\pi^2\lambda^2\mu\cos\left(\frac{1}{2}\%1\right)^3\sin\left(\frac{1}{2}\%1\right) \\
&+ 1920\beta^2\%1^5\pi^2\lambda^2\mu\cos\left(\frac{1}{2}\%1\right)\sin\left(\frac{1}{2}\%1\right) + 480\beta\lambda^2\pi^2\%1^4\cos\left(\frac{1}{2}\%1\right)^2 \\
&- 480\beta^2\%1^5\pi^2\lambda^2\cos\left(\frac{1}{2}\%1\right)\sin\left(\frac{1}{2}\%1\right) - 240\beta^3\%1^3\lambda^2\pi^2\cos\left(\frac{1}{2}\%1\right)\sin\left(\frac{1}{2}\%1\right) \\
&- 1920\beta\%1^5\lambda^2\pi^2\mu\cos\left(\frac{1}{2}\%1\right)\sin\left(\frac{1}{2}\%1\right) \\
&+ 1920\beta\%1^5\lambda^2\pi^2\mu\cos\left(\frac{1}{2}\%1\right)^3\sin\left(\frac{1}{2}\%1\right) + 640\%1^5\lambda^2\pi^2\mu\cos\left(\frac{1}{2}\%1\right)\sin\left(\frac{1}{2}\%1\right) \\
&- 24\beta\%1^7\lambda^4\cos\left(\frac{1}{2}\%1\right)\sin\left(\frac{1}{2}\%1\right) - 6\%1^6\lambda^4\beta^2 \\
&- 640\%1^5\lambda^2\pi^2\mu\cos\left(\frac{1}{2}\%1\right)^3\sin\left(\frac{1}{2}\%1\right) - 80\beta^2\%1^6\lambda^2\pi^2 - 1200\%1^4\pi^2\lambda^2\mu\beta^2 \\
&+ 6\beta\%1^8\lambda^4 + 3\beta^3\%1^6\lambda^4 + 2448\beta\%1^4\pi^4 + 20\beta^3\%1^6\lambda^2\pi^2 - 1632\beta^2\%1^4\pi^4 \\
&- 13872\%1^2\pi^4\beta^2 - 80\%1^6\lambda^2\pi^2 - 4\beta^2\%1^8\lambda^4 + 6936\beta^3\%1^2\pi^4 - 4\%1^8\lambda^4 \\
&+ 120\%1^4\lambda^2\pi^2\beta^2 - 1632\%1^4\pi^4 + 120\beta\%1^6\lambda^2\pi^2 + \beta^3\%1^8\lambda^4 + 408\beta^3\%1^4\pi^4 \\
&- 2400\%1^3\lambda^2\pi^2\mu\beta^2\cos\left(\frac{1}{2}\%1\right)\sin\left(\frac{1}{2}\%1\right) + 960\pi^2\beta\lambda^2\%1^4\mu
\end{aligned}
$$

$$
\begin{aligned}
&- 1920\,\pi^2\,\beta\,\lambda^2\,\%1^4\,\mu\cos\left(\frac{1}{2}\%1\right)^2 + 960\,\pi^2\,\beta\,\lambda^2\,\%1^4\,\mu\cos\left(\frac{1}{2}\%1\right)^4 \\
&+ 27744\,\beta^3\,\%1\,\pi^4\cos\left(\frac{1}{2}\%1\right)\sin\left(\frac{1}{2}\%1\right) + 5440\,\%1^3\,\pi^4\cos\left(\frac{1}{2}\%1\right)\sin\left(\frac{1}{2}\%1\right) \\
&+ 160\,\beta^3\,\%1^5\,\lambda^2\,\pi^2\cos\left(\frac{1}{2}\%1\right)\sin\left(\frac{1}{2}\%1\right) + 3840\,\%1^4\,\lambda^2\,\pi^2\,\mu\,\beta^2\cos\left(\frac{1}{2}\%1\right)^2 \\
&- 24\,\beta\,\lambda^4\,\%1^6\cos\left(\frac{1}{2}\%1\right)^2 + 24\,\beta\,\lambda^4\,\%1^6\cos\left(\frac{1}{2}\%1\right)^4 + 27744\,\beta^3\,\pi^4\cos\left(\frac{1}{2}\%1\right)^2 \\
&- 1632\,\beta^3\,\pi^4\cos\left(\frac{1}{2}\%1\right)^4 + 480\,\beta^3\,\%1^4\,\lambda^2\,\pi^2\cos\left(\frac{1}{2}\%1\right)^2 - 24\,\beta^3\,\%1^6\,\lambda^4\cos\left(\frac{1}{2}\%1\right)^2 \\
&+ 8\,\%1^7\,\lambda^4\cos\left(\frac{1}{2}\%1\right)\sin\left(\frac{1}{2}\%1\right) + 12\,\beta^3\,\%1^5\,\lambda^4\cos\left(\frac{1}{2}\%1\right)\sin\left(\frac{1}{2}\%1\right) \\
&+ 480\,\beta\,\%1^5\,\lambda^2\,\pi^2\cos\left(\frac{1}{2}\%1\right)\sin\left(\frac{1}{2}\%1\right) - 960\,\%1^4\,\lambda^2\,\pi^2\,\beta^2\cos\left(\frac{1}{2}\%1\right)^2 \\
&+ 48\,\%1^6\,\lambda^4\,\beta^2\cos\left(\frac{1}{2}\%1\right)^2 + 240\,\%1^3\,\lambda^2\,\pi^2\,\beta^2\cos\left(\frac{1}{2}\%1\right)\sin\left(\frac{1}{2}\%1\right) \\
&- 1920\,\beta^3\,\%1^4\,\lambda^2\,\pi^2\,\mu\cos\left(\frac{1}{2}\%1\right)^2 + 32640\,\%1^2\,\pi^4\,\beta^2\cos\left(\frac{1}{2}\%1\right)^2 \\
&- 8\,\beta^3\,\%1^7\,\lambda^4\cos\left(\frac{1}{2}\%1\right)\sin\left(\frac{1}{2}\%1\right) - 12\,\%1^5\,\lambda^4\,\beta^2\cos\left(\frac{1}{2}\%1\right)\sin\left(\frac{1}{2}\%1\right) \\
&+ 2400\,\beta^3\,\pi^2\,\lambda^2\,\%1^2\,\mu\cos\left(\frac{1}{2}\%1\right)^2 - 480\,\beta^3\,\pi^2\,\lambda^2\,\%1^2\,\mu\cos\left(\frac{1}{2}\%1\right)^4\Bigg)\Bigg/\Bigg(\\
&160\,\pi^2\,b^2\,\%1^3\,\lambda^2\sin\left(\frac{1}{2}\%1\right)\cos\left(\frac{1}{2}\%1\right)^3 - 160\,\pi^2\,b^2\,\%1^3\,\lambda^2\,\beta\sin\left(\frac{1}{2}\%1\right)\cos\left(\frac{1}{2}\%1\right)^3 \\
&- 60\,\pi^2\,b^2\,\%1^4\,\lambda^2\,\beta + 120\,\pi^2\,b^2\,\%1^4\,\lambda^2 - 320\,\pi^2\,b^2\,\%1^2\,\lambda^2\,\beta \\
&+ 400\,\pi^2\,b^2\,\%1^2\,\lambda^2\,\beta\cos\left(\frac{1}{2}\%1\right)^2 - 80\,\pi^2\,b^2\,\%1^2\,\lambda^2\,\beta\cos\left(\frac{1}{2}\%1\right)^4 \\
&- 400\,\pi^2\,b^2\,\%1^3\,\lambda^2\cos\left(\frac{1}{2}\%1\right)\sin\left(\frac{1}{2}\%1\right) + 400\,\pi^2\,b^2\,\%1^3\,\lambda^2\,\beta\cos\left(\frac{1}{2}\%1\right)\sin\left(\frac{1}{2}\%1\right)\Bigg)
\end{aligned}
$$

$$\%1 := \arccos\left(\frac{1}{2}\,\frac{\mu}{-1+\mu}\right)$$

> X1:=simplify(Z4);

$$XI := \frac{1}{20}\left(-16320\,\beta\,\%1^3\,\pi^4\cos\left(\frac{1}{2}\%1\right)\sin\left(\frac{1}{2}\%1\right) - 12\,\beta^3\,\lambda^4\,\%1^4\cos\left(\frac{1}{2}\%1\right)^4 \right.$$

$$+ 12\,\beta^3\,\lambda^4\,\%1^4\cos\left(\frac{1}{2}\%1\right)^2 + 24\,\beta^2\,\%1^7\,\lambda^4\cos\left(\frac{1}{2}\%1\right)\sin\left(\frac{1}{2}\%1\right)$$

$$+ 2400\,\beta^3\,\%1^3\,\lambda^2\,\pi^2\,\mu\cos\left(\frac{1}{2}\%1\right)\sin\left(\frac{1}{2}\%1\right) - 5440\,\beta^3\,\%1^3\,\pi^4\cos\left(\frac{1}{2}\%1\right)\sin\left(\frac{1}{2}\%1\right)$$

$$- 240\,\beta^3\,\pi^2\,\lambda^2\,\%1^2\cos\left(\frac{1}{2}\%1\right)^2 + 240\,\beta^3\,\pi^2\,\lambda^2\,\%1^2\cos\left(\frac{1}{2}\%1\right)^4$$

$$- 480\sin\left(\frac{1}{2}\%1\right)\%1^3\,\lambda^2\,\pi^2\,\beta^2\cos\left(\frac{1}{2}\%1\right)^3 + 960\sin\left(\frac{1}{2}\%1\right)\%1^3\,\lambda^2\,\pi^2\,\mu\,\beta^2\cos\left(\frac{1}{2}\%1\right)^3$$

$$+ 480\,\beta^3\sin\left(\frac{1}{2}\%1\right)\%1^3\,\pi^2\,\lambda^2\cos\left(\frac{1}{2}\%1\right)^3 - 960\,\beta^3\sin\left(\frac{1}{2}\%1\right)\%1^3\,\pi^2\,\lambda^2\,\mu\cos\left(\frac{1}{2}\%1\right)^3$$

$$+ 960\,\beta^2\sin\left(\frac{1}{2}\%1\right)\%1^5\,\lambda^2\,\pi^2\cos\left(\frac{1}{2}\%1\right)^3 + 24\sin\left(\frac{1}{2}\%1\right)\%1^5\,\lambda^4\,\beta^2\cos\left(\frac{1}{2}\%1\right)^3$$

$$+ 960\,\%1^4\,\lambda^2\,\pi^2\,\beta^2\cos\left(\frac{1}{2}\%1\right)^4 - 1920\,\%1^4\,\pi^2\,\lambda^2\,\mu\,\beta^2\cos\left(\frac{1}{2}\%1\right)^4$$

$$- 6528\,\%1^2\,\pi^4\,\beta^2\cos\left(\frac{1}{2}\%1\right)^4 + 3264\,\beta^3\,\%1^2\,\pi^4\cos\left(\frac{1}{2}\%1\right)^4$$

$$+ 16320\,\beta^2\,\%1^3\,\pi^4\cos\left(\frac{1}{2}\%1\right)\sin\left(\frac{1}{2}\%1\right) + 24\,\beta^3\,\%1^6\,\lambda^4\cos\left(\frac{1}{2}\%1\right)^4 - 60\,\beta^3\,\%1^4\,\lambda^2\,\pi^2$$

$$+ 600\,\beta^3\,\%1^4\,\pi^2\,\lambda^2\,\mu + 3264\sin\left(\frac{1}{2}\%1\right)\%1\,\pi^4\,\beta^2\cos\left(\frac{1}{2}\%1\right)^3$$

$$+ 48\,\beta\sin\left(\frac{1}{2}\%1\right)\%1^7\,\lambda^4\cos\left(\frac{1}{2}\%1\right)^3 - 48\,\beta^2\sin\left(\frac{1}{2}\%1\right)\%1^7\,\lambda^4\cos\left(\frac{1}{2}\%1\right)^3$$

$$+ 16\,\beta^3\sin\left(\frac{1}{2}\%1\right)\%1^7\,\lambda^4\cos\left(\frac{1}{2}\%1\right)^3 + 2176\,\beta^3\sin\left(\frac{1}{2}\%1\right)\%1^3\,\pi^4\cos\left(\frac{1}{2}\%1\right)^3$$

$$- 480\,\beta\,\lambda^2\,\pi^2\,\%1^4\cos\left(\frac{1}{2}\%1\right)^4 + 6528\,\beta\sin\left(\frac{1}{2}\%1\right)\%1^3\,\pi^4\cos\left(\frac{1}{2}\%1\right)^3$$

$$- 2176\sin\left(\frac{1}{2}\%1\right)\%1^3\,\pi^4\cos\left(\frac{1}{2}\%1\right)^3 - 320\,\beta^3\sin\left(\frac{1}{2}\%1\right)\%1^5\,\lambda^2\,\pi^2\cos\left(\frac{1}{2}\%1\right)^3$$

$$+ 320\sin\left(\frac{1}{2}\%1\right)\%1^5\,\lambda^2\,\pi^2\cos\left(\frac{1}{2}\%1\right)^3 - 6528\,\beta^2\sin\left(\frac{1}{2}\%1\right)\%1^3\,\pi^4\cos\left(\frac{1}{2}\%1\right)^3$$

$$
\begin{aligned}
&- 48\,\%1^6\,\lambda^4\,\beta^2\cos\left(\frac{1}{2}\,\%1\right)^4 + 960\,\beta^3\,\%1^4\,\pi^2\,\lambda^2\,\mu\cos\left(\frac{1}{2}\,\%1\right)^4 \\
&- 480\,\beta^3\,\%1^4\,\lambda^2\,\pi^2\cos\left(\frac{1}{2}\,\%1\right)^4 - 960\,\beta\sin\left(\frac{1}{2}\,\%1\right)\%1^5\,\lambda^2\,\pi^2\cos\left(\frac{1}{2}\,\%1\right)^3 \\
&- 16\sin\left(\frac{1}{2}\,\%1\right)\%1^7\,\lambda^4\cos\left(\frac{1}{2}\,\%1\right)^3 - 24\,\beta^3\sin\left(\frac{1}{2}\,\%1\right)\%1^5\,\lambda^4\cos\left(\frac{1}{2}\,\%1\right)^3 \\
&- 3264\,\beta^3\sin\left(\frac{1}{2}\,\%1\right)\%1\,\pi^4\cos\left(\frac{1}{2}\,\%1\right)^3 + 3264\,\beta\,\pi^4\,\%1^2\cos\left(\frac{1}{2}\,\%1\right)^4 \\
&- 16320\,\beta\,\pi^4\,\%1^2\cos\left(\frac{1}{2}\,\%1\right)^2 - 640\,\beta^3\,\%1^5\,\lambda^2\,\pi^2\,\mu\cos\left(\frac{1}{2}\,\%1\right)\sin\left(\frac{1}{2}\,\%1\right) \\
&- 27744\,\%1\,\pi^4\,\beta^2\cos\left(\frac{1}{2}\,\%1\right)\sin\left(\frac{1}{2}\,\%1\right) - 1920\,\pi^2\,\beta^3\,\lambda^2\,\%1^2\,\mu \\
&- 160\,\%1^5\,\lambda^2\,\pi^2\cos\left(\frac{1}{2}\,\%1\right)\sin\left(\frac{1}{2}\,\%1\right) - 16320\,\beta^3\,\%1^2\,\pi^4\cos\left(\frac{1}{2}\,\%1\right)^2 - 26112\,\pi^4\,\beta^3 \\
&+ 13056\,\pi^4\,\beta\,\%1^2 + 640\,\beta^3\,\%1^5\,\lambda^2\,\pi^2\,\mu\cos\left(\frac{1}{2}\,\%1\right)^3\sin\left(\frac{1}{2}\,\%1\right) \\
&- 1920\,\beta^2\,\%1^5\,\pi^2\,\lambda^2\,\mu\cos\left(\frac{1}{2}\,\%1\right)^3\sin\left(\frac{1}{2}\,\%1\right) \\
&+ 1920\,\beta^2\,\%1^5\,\pi^2\,\lambda^2\,\mu\cos\left(\frac{1}{2}\,\%1\right)\sin\left(\frac{1}{2}\,\%1\right) + 480\,\beta\,\lambda^2\,\pi^2\,\%1^4\cos\left(\frac{1}{2}\,\%1\right)^2 \\
&- 480\,\beta^2\,\%1^5\,\pi^2\,\lambda^2\cos\left(\frac{1}{2}\,\%1\right)\sin\left(\frac{1}{2}\,\%1\right) - 240\,\beta^3\,\%1^3\,\lambda^2\,\pi^2\cos\left(\frac{1}{2}\,\%1\right)\sin\left(\frac{1}{2}\,\%1\right) \\
&- 1920\,\beta\,\%1^5\,\lambda^2\,\pi^2\,\mu\cos\left(\frac{1}{2}\,\%1\right)\sin\left(\frac{1}{2}\,\%1\right) \\
&+ 1920\,\beta\,\%1^5\,\lambda^2\,\pi^2\,\mu\cos\left(\frac{1}{2}\,\%1\right)^3\sin\left(\frac{1}{2}\,\%1\right) + 640\,\%1^5\,\lambda^2\,\pi^2\,\mu\cos\left(\frac{1}{2}\,\%1\right)\sin\left(\frac{1}{2}\,\%1\right) \\
&- 24\,\beta\,\%1^7\,\lambda^4\cos\left(\frac{1}{2}\,\%1\right)\sin\left(\frac{1}{2}\,\%1\right) - 6\,\%1^6\,\lambda^4\,\beta^2 \\
&- 640\,\%1^5\,\lambda^2\,\pi^2\,\mu\cos\left(\frac{1}{2}\,\%1\right)^3\sin\left(\frac{1}{2}\,\%1\right) - 80\,\beta^2\,\%1^6\,\lambda^2\,\pi^2 - 1200\,\%1^4\,\pi^2\,\lambda^2\,\mu\,\beta^2 \\
&+ 6\,\beta\,\%1^8\,\lambda^4 + 3\,\beta^3\,\%1^6\,\lambda^4 + 2448\,\beta\,\%1^4\,\pi^4 + 20\,\beta^3\,\%1^6\,\lambda^2\,\pi^2 - 1632\,\beta^2\,\%1^4\,\pi^4 \\
&- 13872\,\%1^2\,\pi^4\,\beta^2 - 80\,\%1^6\,\lambda^2\,\pi^2 - 4\,\beta^2\,\%1^8\,\lambda^4 + 6936\,\beta^3\,\%1^2\,\pi^4 - 4\,\%1^8\,\lambda^4
\end{aligned}
$$

$$+ 120\,\%1^4\,\lambda^2\,\pi^2\,\beta^2 - 1632\,\%1^4\,\pi^4 + 120\,\beta\,\%1^6\,\lambda^2\,\pi^2 + \beta^3\,\%1^8\,\lambda^4 + 408\,\beta^3\,\%1^4\,\pi^4$$

$$- 2400\,\%1^3\,\lambda^2\,\pi^2\,\mu\,\beta^2\cos\left(\frac{1}{2}\,\%1\right)\sin\left(\frac{1}{2}\,\%1\right) + 960\,\pi^2\,\beta\,\lambda^2\,\%1^4\,\mu$$

$$- 1920\,\pi^2\,\beta\,\lambda^2\,\%1^4\,\mu\cos\left(\frac{1}{2}\,\%1\right)^2 + 960\,\pi^2\,\beta\,\lambda^2\,\%1^4\,\mu\cos\left(\frac{1}{2}\,\%1\right)^4$$

$$+ 27744\,\beta^3\,\%1\,\pi^4\cos\left(\frac{1}{2}\,\%1\right)\sin\left(\frac{1}{2}\,\%1\right) + 5440\,\%1^3\,\pi^4\cos\left(\frac{1}{2}\,\%1\right)\sin\left(\frac{1}{2}\,\%1\right)$$

$$+ 160\,\beta^3\,\%1^5\,\lambda^2\,\pi^2\cos\left(\frac{1}{2}\,\%1\right)\sin\left(\frac{1}{2}\,\%1\right) + 3840\,\%1^4\,\lambda^2\,\pi^2\,\mu\,\beta^2\cos\left(\frac{1}{2}\,\%1\right)^2$$

$$- 24\,\beta\,\lambda^4\,\%1^6\cos\left(\frac{1}{2}\,\%1\right)^2 + 24\,\beta\,\lambda^4\,\%1^6\cos\left(\frac{1}{2}\,\%1\right)^4 + 27744\,\beta^3\,\pi^4\cos\left(\frac{1}{2}\,\%1\right)^2$$

$$- 1632\,\beta^3\,\pi^4\cos\left(\frac{1}{2}\,\%1\right)^4 + 480\,\beta^3\,\%1^4\,\lambda^2\,\pi^2\cos\left(\frac{1}{2}\,\%1\right)^2 - 24\,\beta^3\,\%1^6\,\lambda^4\cos\left(\frac{1}{2}\,\%1\right)^2$$

$$+ 8\,\%1^7\,\lambda^4\cos\left(\frac{1}{2}\,\%1\right)\sin\left(\frac{1}{2}\,\%1\right) + 12\,\beta^3\,\%1^5\,\lambda^4\cos\left(\frac{1}{2}\,\%1\right)\sin\left(\frac{1}{2}\,\%1\right)$$

$$+ 480\,\beta\,\%1^5\,\lambda^2\,\pi^2\cos\left(\frac{1}{2}\,\%1\right)\sin\left(\frac{1}{2}\,\%1\right) - 960\,\%1^4\,\lambda^2\,\pi^2\,\beta^2\cos\left(\frac{1}{2}\,\%1\right)^2$$

$$+ 48\,\%1^6\,\lambda^4\,\beta^2\cos\left(\frac{1}{2}\,\%1\right)^2 + 240\,\%1^3\,\lambda^2\,\pi^2\,\beta^2\cos\left(\frac{1}{2}\,\%1\right)\sin\left(\frac{1}{2}\,\%1\right)$$

$$- 1920\,\beta^3\,\%1^4\,\lambda^2\,\pi^2\,\mu\cos\left(\frac{1}{2}\,\%1\right)^2 + 32640\,\%1^2\,\pi^4\,\beta^2\cos\left(\frac{1}{2}\,\%1\right)^2$$

$$- 8\,\beta^3\,\%1^7\,\lambda^4\cos\left(\frac{1}{2}\,\%1\right)\sin\left(\frac{1}{2}\,\%1\right) - 12\,\%1^5\,\lambda^4\,\beta^2\cos\left(\frac{1}{2}\,\%1\right)\sin\left(\frac{1}{2}\,\%1\right)$$

$$+ 2400\,\beta^3\,\pi^2\,\lambda^2\,\%1^2\,\mu\cos\left(\frac{1}{2}\,\%1\right)^2 - 480\,\beta^3\,\pi^2\,\lambda^2\,\%1^2\,\mu\cos\left(\frac{1}{2}\,\%1\right)^4\Bigg) \Bigg/ \Bigg(\pi^2\,b^2\,\%1^2\,\lambda^2$$

$$\left(-8\sin\left(\frac{1}{2}\,\%1\right)\%1\cos\left(\frac{1}{2}\,\%1\right)^3 + 8\,\%1\,\beta\sin\left(\frac{1}{2}\,\%1\right)\cos\left(\frac{1}{2}\,\%1\right)^3 + 3\,\beta\,\%1^2 - 6\,\%1^2\right.$$

$$+ 16\,\beta - 20\,\beta\cos\left(\frac{1}{2}\,\%1\right)^2 + 4\,\beta\cos\left(\frac{1}{2}\,\%1\right)^4 + 20\,\%1\cos\left(\frac{1}{2}\,\%1\right)\sin\left(\frac{1}{2}\,\%1\right)$$

$$\left.\left. - 20\,\%1\,\beta\cos\left(\frac{1}{2}\,\%1\right)\sin\left(\frac{1}{2}\,\%1\right)\right)\right)\Bigg)$$

$$\%1 := \arccos\left(\frac{1}{2}\,\frac{\mu}{-1+\mu}\right)$$

> X2:=collect(X1, [sin(n/2), cos(n/2)], distributed, factor);

$$X2 := \frac{1}{20}\Bigg(-4\,(-1+\beta)\,\%1\,\Big(2\,\%1^6\,\lambda^4\,\beta^2 - 40\,\%1^4\,\lambda^2\,\pi^2\,\beta^2 + 160\,\%1^4\,\pi^2\,\lambda^2\,\mu\,\beta^2 - 3\,\lambda^4\,\%1^4\,\beta^2$$
$$+ 1360\,\%1^2\,\pi^4\,\beta^2 + 60\,\lambda^2\,\pi^2\,\%1^2\,\beta^2 - 600\,\pi^2\,\lambda^2\,\%1^2\,\mu\,\beta^2 - 6936\,\pi^4\,\beta^2 + 80\,\beta\,\lambda^2\,\pi^2\,\%1^4$$
$$- 320\,\pi^2\,\beta\,\lambda^2\,\%1^4\,\mu - 2720\,\pi^4\,\beta\,\%1^2 - 4\,\beta\,\lambda^4\,\%1^6 + 160\,\pi^2\,\lambda^2\,\%1^4\,\mu - 40\,\lambda^2\,\pi^2\,\%1^4$$
$$+ 2\,\lambda^4\,\%1^6 + 1360\,\pi^4\,\%1^2\Big)\sin\left(\frac{1}{2}\%1\right)\cos\left(\frac{1}{2}\%1\right) - 60\,\beta^3\,\%1^4\,\lambda^2\,\pi^2$$
$$+ 600\,\beta^3\,\%1^4\,\pi^2\,\lambda^2\,\mu - 1920\,\pi^2\,\beta^3\,\lambda^2\,\%1^2\,\mu + 8\,(-1+\beta)\,\%1$$
$$\left(2\,\%1^2\,\beta^2 - 3\,\beta^2 - 4\,\beta\,\%1^2 + 2\,\%1^2\right)\left(\lambda^4\,\%1^4 - 20\,\pi^2\,\%1^2\,\lambda^2 + 40\,\pi^2\,\%1^2\,\lambda^2\,\mu + 136\,\pi^4\right)$$
$$\cos\left(\frac{1}{2}\%1\right)^3\sin\left(\frac{1}{2}\%1\right) - 26112\,\pi^4\,\beta^3 + 13056\,\pi^4\,\beta\,\%1^2 + 12$$
$$\left(2\,\%1^2\,\beta^2 + 2\,\%1^2 - 4\,\beta\,\%1^2 - \beta^2\right)\beta\left(\lambda^4\,\%1^4 - 20\,\pi^2\,\%1^2\,\lambda^2 + 40\,\pi^2\,\%1^2\,\lambda^2\,\mu + 136\,\pi^4\right)$$
$$\cos\left(\frac{1}{2}\%1\right)^4 - 12\,\beta\,\Big(-2312\,\pi^4\,\beta^2 + 20\,\lambda^2\,\pi^2\,\%1^2\,\beta^2 - 200\,\pi^2\,\lambda^2\,\%1^2\,\mu\,\beta^2$$
$$+ 160\,\%1^4\,\pi^2\,\lambda^2\,\mu\,\beta^2 - \lambda^4\,\%1^4\,\beta^2 + 2\,\%1^6\,\lambda^4\,\beta^2 + 1360\,\%1^2\,\pi^4\,\beta^2 - 40\,\%1^4\,\lambda^2\,\pi^2\,\beta^2$$
$$+ 80\,\beta\,\lambda^2\,\pi^2\,\%1^4 - 320\,\pi^2\,\beta\,\lambda^2\,\%1^4\,\mu - 2720\,\pi^4\,\beta\,\%1^2 - 4\,\beta\,\lambda^4\,\%1^6 + 160\,\pi^2\,\lambda^2\,\%1^4\,\mu$$
$$- 40\,\lambda^2\,\pi^2\,\%1^4 + 2\,\lambda^4\,\%1^6 + 1360\,\pi^4\,\%1^2\Big)\cos\left(\frac{1}{2}\%1\right)^2 - 6\,\%1^6\,\lambda^4\,\beta^2 - 80\,\beta^2\,\%1^6\,\lambda^2\,\pi^2$$
$$- 1200\,\%1^4\,\pi^2\,\lambda^2\,\mu\,\beta^2 + 6\,\beta\,\%1^8\,\lambda^4 + 3\,\beta^3\,\%1^6\,\lambda^4 + 2448\,\beta\,\%1^4\,\pi^4 + 20\,\beta^3\,\%1^6\,\lambda^2\,\pi^2$$
$$- 1632\,\beta^2\,\%1^4\,\pi^4 - 13872\,\%1^2\,\pi^4\,\beta^2 - 80\,\%1^6\,\lambda^2\,\pi^2 - 4\,\beta^2\,\%1^8\,\lambda^4 + 6936\,\beta^3\,\%1^2\,\pi^4$$
$$- 4\,\%1^8\,\lambda^4 + 120\,\%1^4\,\lambda^2\,\pi^2\,\beta^2 - 1632\,\%1^4\,\pi^4 + 120\,\beta\,\%1^6\,\lambda^2\,\pi^2 + \beta^3\,\%1^8\,\lambda^4$$
$$+ 408\,\beta^3\,\%1^4\,\pi^4 + 960\,\pi^2\,\beta\,\lambda^2\,\%1^4\,\mu\Big)\Big/\Big(\pi^2\,b^2\,\%1^2\,\lambda^2\Big(16\,\beta + 3\,\beta\,\%1^2 - 6\,\%1^2$$
$$- 20\,\beta\cos\left(\frac{1}{2}\%1\right)^2 + 4\,\beta\cos\left(\frac{1}{2}\%1\right)^4 - 20\,(-1+\beta)\,\%1\sin\left(\frac{1}{2}\%1\right)\cos\left(\frac{1}{2}\%1\right)$$
$$+ 8\,(-1+\beta)\,\%1\cos\left(\frac{1}{2}\%1\right)^3\sin\left(\frac{1}{2}\%1\right)\Big)\Big)\Bigg)$$

$$\%1 := \arccos\left(\frac{1}{2}\,\frac{\mu}{-1+\mu}\right)$$

> **K3:=simplify(X2*b^2/Pi^2);**

$$K3 := \frac{1}{20}\left(-16320\,\beta\,\%1^3\,\pi^4\cos\left(\frac{1}{2}\%1\right)\sin\left(\frac{1}{2}\%1\right) - 12\,\beta^3\,\lambda^4\,\%1^4\cos\left(\frac{1}{2}\%1\right)^4 \right.$$

$$+ 12\,\beta^3\,\lambda^4\,\%1^4\cos\left(\frac{1}{2}\%1\right)^2 + 24\,\beta^2\,\%1^7\,\lambda^4\cos\left(\frac{1}{2}\%1\right)\sin\left(\frac{1}{2}\%1\right)$$

$$+ 2400\,\beta^3\,\%1^3\,\lambda^2\,\pi^2\,\mu\cos\left(\frac{1}{2}\%1\right)\sin\left(\frac{1}{2}\%1\right) - 5440\,\beta^3\,\%1^3\,\pi^4\cos\left(\frac{1}{2}\%1\right)\sin\left(\frac{1}{2}\%1\right)$$

$$- 240\,\beta^3\,\pi^2\,\lambda^2\,\%1^2\cos\left(\frac{1}{2}\%1\right)^2 + 240\,\beta^3\,\pi^2\,\lambda^2\,\%1^2\cos\left(\frac{1}{2}\%1\right)^4$$

$$- 480\sin\left(\frac{1}{2}\%1\right)\%1^3\,\lambda^2\,\pi^2\,\beta^2\cos\left(\frac{1}{2}\%1\right)^3 + 960\sin\left(\frac{1}{2}\%1\right)\%1^3\,\lambda^2\,\pi^2\,\mu\,\beta^2\cos\left(\frac{1}{2}\%1\right)^3$$

$$+ 480\,\beta^3\sin\left(\frac{1}{2}\%1\right)\%1^3\,\pi^2\,\lambda^2\cos\left(\frac{1}{2}\%1\right)^3 - 960\,\beta^3\sin\left(\frac{1}{2}\%1\right)\%1^3\,\pi^2\,\lambda^2\,\mu\cos\left(\frac{1}{2}\%1\right)^3$$

$$+ 960\,\beta^2\sin\left(\frac{1}{2}\%1\right)\%1^5\,\lambda^2\,\pi^2\cos\left(\frac{1}{2}\%1\right)^3 + 24\sin\left(\frac{1}{2}\%1\right)\%1^5\,\lambda^4\,\beta^2\cos\left(\frac{1}{2}\%1\right)^3$$

$$+ 960\,\%1^4\,\lambda^2\,\pi^2\,\beta^2\cos\left(\frac{1}{2}\%1\right)^4 - 1920\,\%1^4\,\pi^2\,\lambda^2\,\mu\,\beta^2\cos\left(\frac{1}{2}\%1\right)^4$$

$$- 6528\,\%1^2\,\pi^4\,\beta^2\cos\left(\frac{1}{2}\%1\right)^4 + 3264\,\beta^3\,\%1^2\,\pi^4\cos\left(\frac{1}{2}\%1\right)^4$$

$$+ 16320\,\beta^2\,\%1^3\,\pi^4\cos\left(\frac{1}{2}\%1\right)\sin\left(\frac{1}{2}\%1\right) + 24\,\beta^3\,\%1^6\,\lambda^4\cos\left(\frac{1}{2}\%1\right)^4 - 60\,\beta^3\,\%1^4\,\lambda^2\,\pi^2$$

$$+ 600\,\beta^3\,\%1^4\,\pi^2\,\lambda^2\,\mu + 3264\sin\left(\frac{1}{2}\%1\right)\%1\,\pi^4\,\beta^2\cos\left(\frac{1}{2}\%1\right)^3$$

$$+ 48\,\beta\sin\left(\frac{1}{2}\%1\right)\%1^7\,\lambda^4\cos\left(\frac{1}{2}\%1\right)^3 - 48\,\beta^2\sin\left(\frac{1}{2}\%1\right)\%1^7\,\lambda^4\cos\left(\frac{1}{2}\%1\right)^3$$

$$+ 16\,\beta^3\sin\left(\frac{1}{2}\%1\right)\%1^7\,\lambda^4\cos\left(\frac{1}{2}\%1\right)^3 + 2176\,\beta^3\sin\left(\frac{1}{2}\%1\right)\%1^3\,\pi^4\cos\left(\frac{1}{2}\%1\right)^3$$

$$- 480\,\beta\,\lambda^2\,\pi^2\,\%1^4\cos\left(\frac{1}{2}\%1\right)^4 + 6528\,\beta\sin\left(\frac{1}{2}\%1\right)\%1^3\,\pi^4\cos\left(\frac{1}{2}\%1\right)^3$$

$$- 2176\sin\left(\frac{1}{2}\%1\right)\%1^3\,\pi^4\cos\left(\frac{1}{2}\%1\right)^3 - 320\,\beta^3\sin\left(\frac{1}{2}\%1\right)\%1^5\,\lambda^2\,\pi^2\cos\left(\frac{1}{2}\%1\right)^3$$

$$+ 320 \sin\left(\frac{1}{2}\%1\right)\%1^5 \lambda^2 \pi^2 \cos\left(\frac{1}{2}\%1\right)^3 - 6528 \beta^2 \sin\left(\frac{1}{2}\%1\right)\%1^3 \pi^4 \cos\left(\frac{1}{2}\%1\right)^3$$

$$- 48 \%1^6 \lambda^4 \beta^2 \cos\left(\frac{1}{2}\%1\right)^4 + 960 \beta^3 \%1^4 \pi^2 \lambda^2 \mu \cos\left(\frac{1}{2}\%1\right)^4$$

$$- 480 \beta^3 \%1^4 \lambda^2 \pi^2 \cos\left(\frac{1}{2}\%1\right)^4 - 960 \beta \sin\left(\frac{1}{2}\%1\right)\%1^5 \lambda^2 \pi^2 \cos\left(\frac{1}{2}\%1\right)^3$$

$$- 16 \sin\left(\frac{1}{2}\%1\right)\%1^7 \lambda^4 \cos\left(\frac{1}{2}\%1\right)^3 - 24 \beta^3 \sin\left(\frac{1}{2}\%1\right)\%1^5 \lambda^4 \cos\left(\frac{1}{2}\%1\right)^3$$

$$- 3264 \beta^3 \sin\left(\frac{1}{2}\%1\right)\%1 \pi^4 \cos\left(\frac{1}{2}\%1\right)^3 + 3264 \beta \pi^4 \%1^2 \cos\left(\frac{1}{2}\%1\right)^4$$

$$- 16320 \beta \pi^4 \%1^2 \cos\left(\frac{1}{2}\%1\right)^2 - 640 \beta^3 \%1^5 \lambda^2 \pi^2 \mu \cos\left(\frac{1}{2}\%1\right)\sin\left(\frac{1}{2}\%1\right)$$

$$- 27744 \%1 \pi^4 \beta^2 \cos\left(\frac{1}{2}\%1\right)\sin\left(\frac{1}{2}\%1\right) - 1920 \pi^2 \beta^3 \lambda^2 \%1^2 \mu$$

$$- 160 \%1^5 \lambda^2 \pi^2 \cos\left(\frac{1}{2}\%1\right)\sin\left(\frac{1}{2}\%1\right) - 16320 \beta^3 \%1^2 \pi^4 \cos\left(\frac{1}{2}\%1\right)^2 - 26112 \pi^4 \beta^3$$

$$+ 13056 \pi^4 \beta \%1^2 + 640 \beta^3 \%1^5 \lambda^2 \pi^2 \mu \cos\left(\frac{1}{2}\%1\right)^3 \sin\left(\frac{1}{2}\%1\right)$$

$$- 1920 \beta^2 \%1^5 \pi^2 \lambda^2 \mu \cos\left(\frac{1}{2}\%1\right)^3 \sin\left(\frac{1}{2}\%1\right)$$

$$+ 1920 \beta^2 \%1^5 \pi^2 \lambda^2 \mu \cos\left(\frac{1}{2}\%1\right)\sin\left(\frac{1}{2}\%1\right) + 480 \beta \lambda^2 \pi^2 \%1^4 \cos\left(\frac{1}{2}\%1\right)^2$$

$$- 480 \beta^2 \%1^5 \pi^2 \lambda^2 \cos\left(\frac{1}{2}\%1\right)\sin\left(\frac{1}{2}\%1\right) - 240 \beta^3 \%1^3 \lambda^2 \pi^2 \cos\left(\frac{1}{2}\%1\right)\sin\left(\frac{1}{2}\%1\right)$$

$$- 1920 \beta \%1^5 \lambda^2 \pi^2 \mu \cos\left(\frac{1}{2}\%1\right)\sin\left(\frac{1}{2}\%1\right)$$

$$+ 1920 \beta \%1^5 \lambda^2 \pi^2 \mu \cos\left(\frac{1}{2}\%1\right)^3 \sin\left(\frac{1}{2}\%1\right) + 640 \%1^5 \lambda^2 \pi^2 \mu \cos\left(\frac{1}{2}\%1\right)\sin\left(\frac{1}{2}\%1\right)$$

$$- 24 \beta \%1^7 \lambda^4 \cos\left(\frac{1}{2}\%1\right)\sin\left(\frac{1}{2}\%1\right) - 6 \%1^6 \lambda^4 \beta^2$$

$$- 640 \%1^5 \lambda^2 \pi^2 \mu \cos\left(\frac{1}{2}\%1\right)^3 \sin\left(\frac{1}{2}\%1\right) - 80 \beta^2 \%1^6 \lambda^2 \pi^2 - 1200 \%1^4 \pi^2 \lambda^2 \mu \beta^2$$

$$+ 6\,\beta\,\%1^8\,\lambda^4 + 3\,\beta^3\,\%1^6\,\lambda^4 + 2448\,\beta\,\%1^4\,\pi^4 + 20\,\beta^3\,\%1^6\,\lambda^2\,\pi^2 - 1632\,\beta^2\,\%1^4\,\pi^4$$
$$- 13872\,\%1^2\,\pi^4\,\beta^2 - 80\,\%1^6\,\lambda^2\,\pi^2 - 4\,\beta^2\,\%1^8\,\lambda^4 + 6936\,\beta^3\,\%1^2\,\pi^4 - 4\,\%1^8\,\lambda^4$$
$$+ 120\,\%1^4\,\lambda^2\,\pi^2\,\beta^2 - 1632\,\%1^4\,\pi^4 + 120\,\beta\,\%1^6\,\lambda^2\,\pi^2 + \beta^3\,\%1^8\,\lambda^4 + 408\,\beta^3\,\%1^4\,\pi^4$$
$$- 2400\,\%1^3\,\lambda^2\,\pi^2\,\mu\,\beta^2\cos\left(\frac{1}{2}\%1\right)\sin\left(\frac{1}{2}\%1\right) + 960\,\pi^2\,\beta\,\lambda^2\,\%1^4\,\mu$$
$$- 1920\,\pi^2\,\beta\,\lambda^2\,\%1^4\,\mu\cos\left(\frac{1}{2}\%1\right)^2 + 960\,\pi^2\,\beta\,\lambda^2\,\%1^4\,\mu\cos\left(\frac{1}{2}\%1\right)^4$$
$$+ 27744\,\beta^3\,\%1\,\pi^4\cos\left(\frac{1}{2}\%1\right)\sin\left(\frac{1}{2}\%1\right) + 5440\,\%1^3\,\pi^4\cos\left(\frac{1}{2}\%1\right)\sin\left(\frac{1}{2}\%1\right)$$
$$+ 160\,\beta^3\,\%1^5\,\lambda^2\,\pi^2\cos\left(\frac{1}{2}\%1\right)\sin\left(\frac{1}{2}\%1\right) + 3840\,\%1^4\,\lambda^2\,\pi^2\,\mu\,\beta^2\cos\left(\frac{1}{2}\%1\right)^2$$
$$- 24\,\beta\,\lambda^4\,\%1^6\cos\left(\frac{1}{2}\%1\right)^2 + 24\,\beta\,\lambda^4\,\%1^6\cos\left(\frac{1}{2}\%1\right)^4 + 27744\,\beta^3\,\pi^4\cos\left(\frac{1}{2}\%1\right)^2$$
$$- 1632\,\beta^3\,\pi^4\cos\left(\frac{1}{2}\%1\right)^4 + 480\,\beta^3\,\%1^4\,\lambda^2\,\pi^2\cos\left(\frac{1}{2}\%1\right)^2 - 24\,\beta^3\,\%1^6\,\lambda^4\cos\left(\frac{1}{2}\%1\right)^2$$
$$+ 8\,\%1^7\,\lambda^4\cos\left(\frac{1}{2}\%1\right)\sin\left(\frac{1}{2}\%1\right) + 12\,\beta^3\,\%1^5\,\lambda^4\cos\left(\frac{1}{2}\%1\right)\sin\left(\frac{1}{2}\%1\right)$$
$$+ 480\,\beta\,\%1^5\,\lambda^2\,\pi^2\cos\left(\frac{1}{2}\%1\right)\sin\left(\frac{1}{2}\%1\right) - 960\,\%1^4\,\lambda^2\,\pi^2\,\beta^2\cos\left(\frac{1}{2}\%1\right)^2$$
$$+ 48\,\%1^6\,\lambda^4\,\beta^2\cos\left(\frac{1}{2}\%1\right)^2 + 240\,\%1^3\,\lambda^2\,\pi^2\,\beta^2\cos\left(\frac{1}{2}\%1\right)\sin\left(\frac{1}{2}\%1\right)$$
$$- 1920\,\beta^3\,\%1^4\,\lambda^2\,\pi^2\,\mu\cos\left(\frac{1}{2}\%1\right)^2 + 32640\,\%1^2\,\pi^4\,\beta^2\cos\left(\frac{1}{2}\%1\right)^2$$
$$- 8\,\beta^3\,\%1^7\,\lambda^4\cos\left(\frac{1}{2}\%1\right)\sin\left(\frac{1}{2}\%1\right) - 12\,\%1^5\,\lambda^4\,\beta^2\cos\left(\frac{1}{2}\%1\right)\sin\left(\frac{1}{2}\%1\right)$$
$$+ 2400\,\beta^3\,\pi^2\,\lambda^2\,\%1^2\,\mu\cos\left(\frac{1}{2}\%1\right)^2 - 480\,\beta^3\,\pi^2\,\lambda^2\,\%1^2\,\mu\cos\left(\frac{1}{2}\%1\right)^4\Bigg)\Bigg/\Bigg(\pi^4\,\%1^2\,\lambda^2\Bigg($$
$$-8\sin\left(\frac{1}{2}\%1\right)\%1\cos\left(\frac{1}{2}\%1\right)^3 + 8\,\%1\,\beta\sin\left(\frac{1}{2}\%1\right)\cos\left(\frac{1}{2}\%1\right)^3 + 3\,\beta\,\%1^2 - 6\,\%1^2$$
$$+ 16\,\beta - 20\,\beta\cos\left(\frac{1}{2}\%1\right)^2 + 4\,\beta\cos\left(\frac{1}{2}\%1\right)^4 + 20\,\%1\cos\left(\frac{1}{2}\%1\right)\sin\left(\frac{1}{2}\%1\right)$$

$$- 20\ \%1\ \beta \cos\left(\frac{1}{2}\%1\right)\sin\left(\frac{1}{2}\%1\right)\Big)\Big)$$

$$\%1 := \arccos\left(\frac{1}{2}\frac{\mu}{-1+\mu}\right)$$

> save 'z3.m';

> mu:=1/3; beta:=0;Km3:=simplify(K3);

$$\mu := \frac{1}{3}$$

$$\beta := 0$$

$$Km3 := \frac{1}{30}\Bigg(-1224\,\pi^5 - 36\,\lambda^4 \sin(\%1)\cos(\%1)\,\pi^2 \arccos\left(\frac{1}{4}\right)^2$$

$$+ 24\,\lambda^4 \sin(\%1)\cos(\%1)\,\pi \arccos\left(\frac{1}{4}\right)^3 - 6\,\lambda^4 \sin(\%1)\cos(\%1) \arccos\left(\frac{1}{4}\right)^4$$

$$+ 120\,\lambda^2 \pi^4 \sin(\%1)\cos(\%1) - 240\,\lambda^2 \pi^3 \sin(\%1)\cos(\%1) \arccos\left(\frac{1}{4}\right)$$

$$- 6\,\lambda^4 \sin(\%1)\cos(\%1)\,\pi^4 + 24\,\lambda^4 \sin(\%1)\cos(\%1)\,\pi^3 \arccos\left(\frac{1}{4}\right)$$

$$+ 120\,\lambda^2 \pi^2 \sin(\%1)\cos(\%1) \arccos\left(\frac{1}{4}\right)^2 + 1224\,\pi^4 \arccos\left(\frac{1}{4}\right) - 3\,\lambda^4 \pi^5$$

$$+ 3\,\lambda^4 \arccos\left(\frac{1}{4}\right)^5 - 60\,\lambda^2 \pi^5 - 180\,\lambda^2 \pi^3 \arccos\left(\frac{1}{4}\right)^2 + 60\,\lambda^2 \pi^2 \arccos\left(\frac{1}{4}\right)^3$$

$$- 30\,\lambda^4 \pi^3 \arccos\left(\frac{1}{4}\right)^2 + 30\,\lambda^4 \pi^2 \arccos\left(\frac{1}{4}\right)^3 - 15\,\lambda^4 \pi \arccos\left(\frac{1}{4}\right)^4 + 15\,\lambda^4 \pi^4 \arccos\left(\frac{1}{4}\right)$$

$$+ 2448\,\pi^4 \sin(\%1)\cos(\%1) + 180\,\lambda^2 \pi^4 \arccos\left(\frac{1}{4}\right) + 12\cos(\%1)^3 \lambda^4 \pi^4 \sin(\%1)$$

$$- 48\cos(\%1)^3 \lambda^4 \pi^3 \arccos\left(\frac{1}{4}\right)\sin(\%1) + 12\cos(\%1)^3 \lambda^4 \arccos\left(\frac{1}{4}\right)^4 \sin(\%1)$$

$$- 80\cos(\%1)^3 \lambda^2 \pi^2 \arccos\left(\frac{1}{4}\right)^2 \sin(\%1) - 80\cos(\%1)^3 \lambda^2 \pi^4 \sin(\%1)$$

$$- 48\cos(\%1)^3 \lambda^4 \pi \arccos\left(\frac{1}{4}\right)^3 \sin(\%1) + 72\cos(\%1)^3 \lambda^4 \pi^2 \arccos\left(\frac{1}{4}\right)^2 \sin(\%1)$$

$$+ 1632 \cos(\%1)^3 \pi^4 \sin(\%1) + 160 \cos(\%1)^3 \lambda^2 \pi^3 \arccos\left(\frac{1}{4}\right) \sin(\%1) \Big) \Big/ \Big(\lambda^2 \pi^4 \left(6 \sin(\%1) \cos(\%1) + 4 \cos(\%1)^3 \sin(\%1) - 3 \pi + 3 \arccos\left(\frac{1}{4}\right) \right) \Big)$$

$$\%1 := \frac{1}{2} \arccos\left(\frac{1}{4}\right)$$

> evalf(");

$$-.0002524739634 \frac{-52.45270589 \lambda^4 - 2478.346672 \lambda^2 - 53866.94061}{\lambda^2}$$

> expand(");

$$.01324294255 \lambda^2 + .6257180070 + 13.59999999 \frac{1}{\lambda^2}$$

>

Appendix F

Tensile strain along free edge of buckled stable flap

Fig. 4-4 shows one wave length of a buckled stable flap. By using $y = H$ in Eq. (4-24), the arc length, L, at the free edge of stable flap can be derived as follows:

$$L = \int_0^l \sqrt{1 + (y'')^2}\, dx = \int_0^l \sqrt{1 + \left[\frac{w_o \pi}{l} \cos\left(\frac{\pi x}{l}\right)\right]^2}\, dx \,. \tag{F-1}$$

The tensile strain along the arc length, L, is defined as

$$\varepsilon = \frac{1}{2} \cdot \left[1 - \left(\frac{l}{L}\right)^2\right], \tag{F-2}$$

where l is the original plate length. This strain definition takes into account the geometric non-linearity effect due to the plate large deflection. Note that Eq. (F-2) only provides an average strain measurement, which neglects the non-uniform strain distribution actually exists along the arc length (refer Section 4.2. for detail).

Fig. F-1 plots the tensile strain ε calculated from Eq. (F-2) *vs.* the normalized out-of-plane deflection w_o/l. This curve has a similar shape as a parabolic curve so that curve fitting is done to simplify Eq. (F-2). It is found that the strain equation can be approximately expressed as follows:

$$\varepsilon \approx 2.2\left(\frac{w_o}{l}\right)^2. \tag{F-3}$$

This is a very simple and useful equation which has a good accuracy for the strain range interested, i.e. for strain values less than 5%.

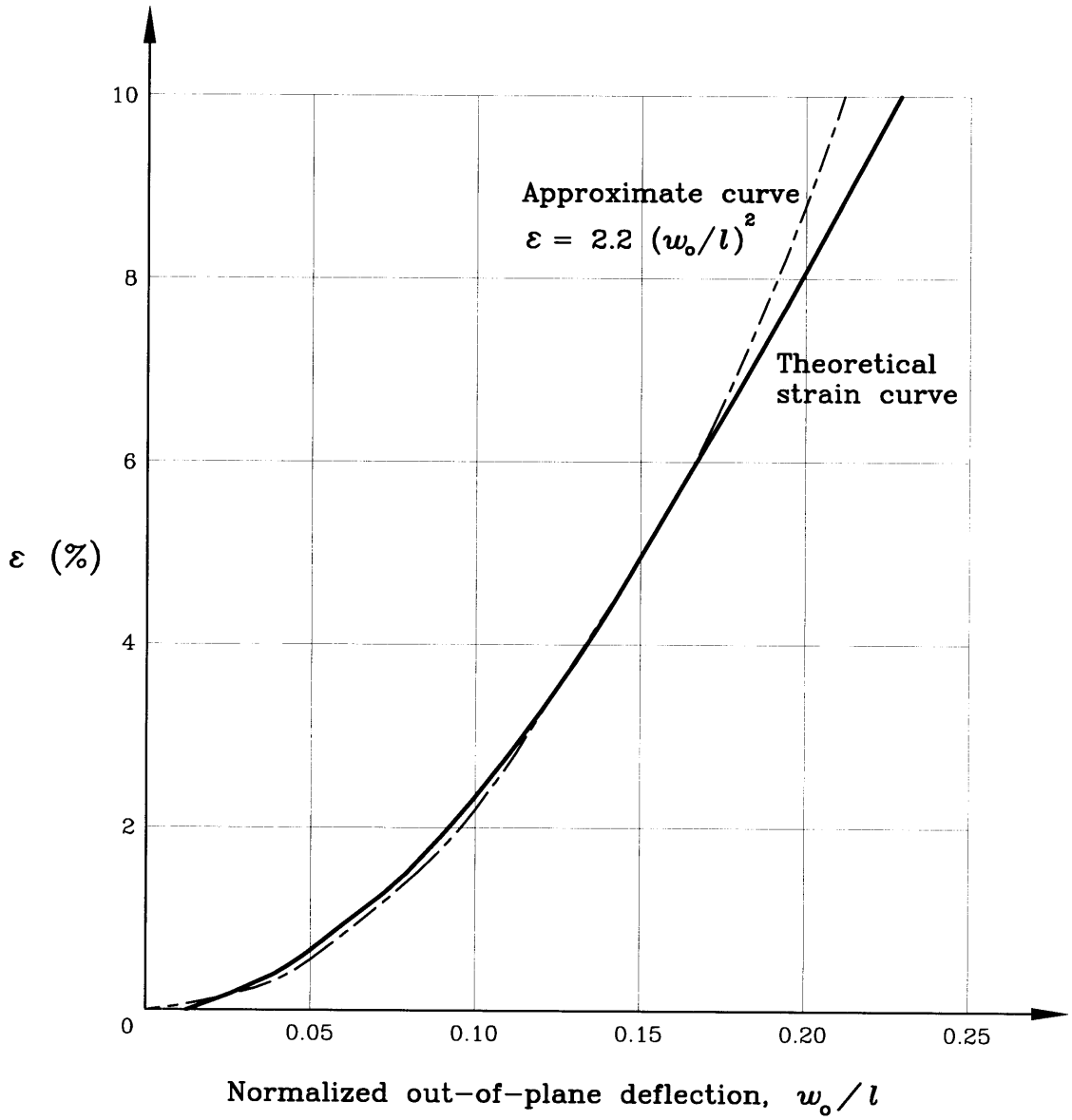

Fig. F-1 Plot of strain *vs.* normalized out-of-plane deflection

Zi-Ming Zheng, P.E.

Current Address

60 Wadsworth St., Apt. 10D
Cambridge, MA 02142
(617) 374-9261

Home Address

54 Second St., Apt. 2N
Raritan, N.J. 08869
(908) 231-1852

Objective

Autobiography for the Ph.D. dissertation.

Education

Massachusetts Institute of Technology Cambridge, MA
Ph.D. candidate, graduation expected in September, 1994. Thesis supervised by Professor T. Wierzbicki of Ocean Engineering Department on "Theoretical Analysis of Wedge Cutting Through Metal Plates" simulating oil tanker grounding damage scenario. GPA=5/5.

Massachusetts Institute of Technology Cambridge, MA
Civil Engineer and Master of Science in Civil Engineering degrees, June, 1991. Thesis supervised by Professor J. J. Connor of Civil Engineering Department on "Theoretical Study of Post-buckling Behaviors of Simply-supported Rectangular Plates". Background in structural mechanics, design, and computer applications. GPA=5/5.

Jiao Tong University Shanghai, China
Master of Science in Mechanical Engineering, May, 1985. Major research in theoretical and experimental studies of post-buckling behaviors of simply-supported rectangular plates under combined in-plane loads.

Tong Ji University Shanghai, China
Bachelor of Science in Engineering Mechanics, January, 1982. Majoring theoretical and experimental structure mechanics. Bachelor thesis topic: "Solution of Nonlinear Vibration Problem of Multi-degree-of-freedom Dynamic Systems by Using Perturbation Methods".

Computer Skills

Computer programming using C, FORTRAN 77 languages. Fluent in computer software such as FrameMaker, Lotus, AutoCAD, MAPLE, MathCAD, and structural analysis & design packages, such as ADAPT, ETABS, MATS, STAAD III, etc.

Experience

Weidlinger Associates, Inc. Cambridge, MA
January, 1992–Present. Structural engineer designing residential, underground, and infra structures using ACI, AISC, AASHTO, and UBC codes. Fluent in structural analysis and design software.

MIT, Mechanical Engineering Department Cambridge, MA
September, 1989–January, 1992. Research assistant concentrated in submarine shell tearing mechanism and prediction using plasticity theory and exper-

imental methods. Having general structural laboratory knowledge including testing machine operation, material hardness testing, and heat treatment. With sound background on FEM and BEM and familiar with ADINA FEM software.

MIT, Civil Engineering Department Cambridge, MA
February, 1989–May, 1989. Teaching assistant under Prof. J. Connor for course 1.122: "Finite and Boundary Element Methods".

Shanghai Metallurgical Institute of Technology Shanghai, China
June, 1985–August, 1988. Lecturer teaching structural mechanics in Mechanical Engineering Department. Also participated many steel and concrete structure design projects.

East China Survey & Design Institute Hangzhou, China
February, 1982–August, 1982. Structural engineer performing structural analysis and design. Projects participated including finite element analysis of dam structures in a hydro-electric power station, and design of a power plant building.

Background

U.S. citizen. Professional Engineer in structural engineering with an Engineer-in-Training certificate. Fluent in Chinese language. Enjoy traveling, photography, and videotaping.

Publications

McClintock, F.M. and Zheng, Z.M., *Ductile Fracture before Localized Necking in a Strip under Tension,* International Journal of Fracture, Vol. 64, December 1993, pp 191-200.

McClintock, F.M. and Zheng, Z.M., *Ductile Fracture in Sheets under Transverse Strain Gradients,* International Journal of Fracture, Vol. 64, December 1993, pp 321-337.

Zheng, Z.M. and Wierzbicki, T., *Theoretical Study on the Steady-state Wedge Cutting Force through Thin Metal Plates,* Joint MIT-Industry Program on Tanker Safety, Report No. 19, Department of Ocean Engineering, M.I.T. (1994).